MICROBIOTECHNOLOGY TOOLS FOR WASTEWATER CLEANUP AND ORGANIC SOLIDS REDUCTION

EDITED BY: Mayur B. Kurade, Mukesh Kumar Awasthi, Sanjay Prabhu Govindwar, Byong-Hun Jeon and Dayanand Kalyani

PUBLISHED IN: Frontiers in Microbiology

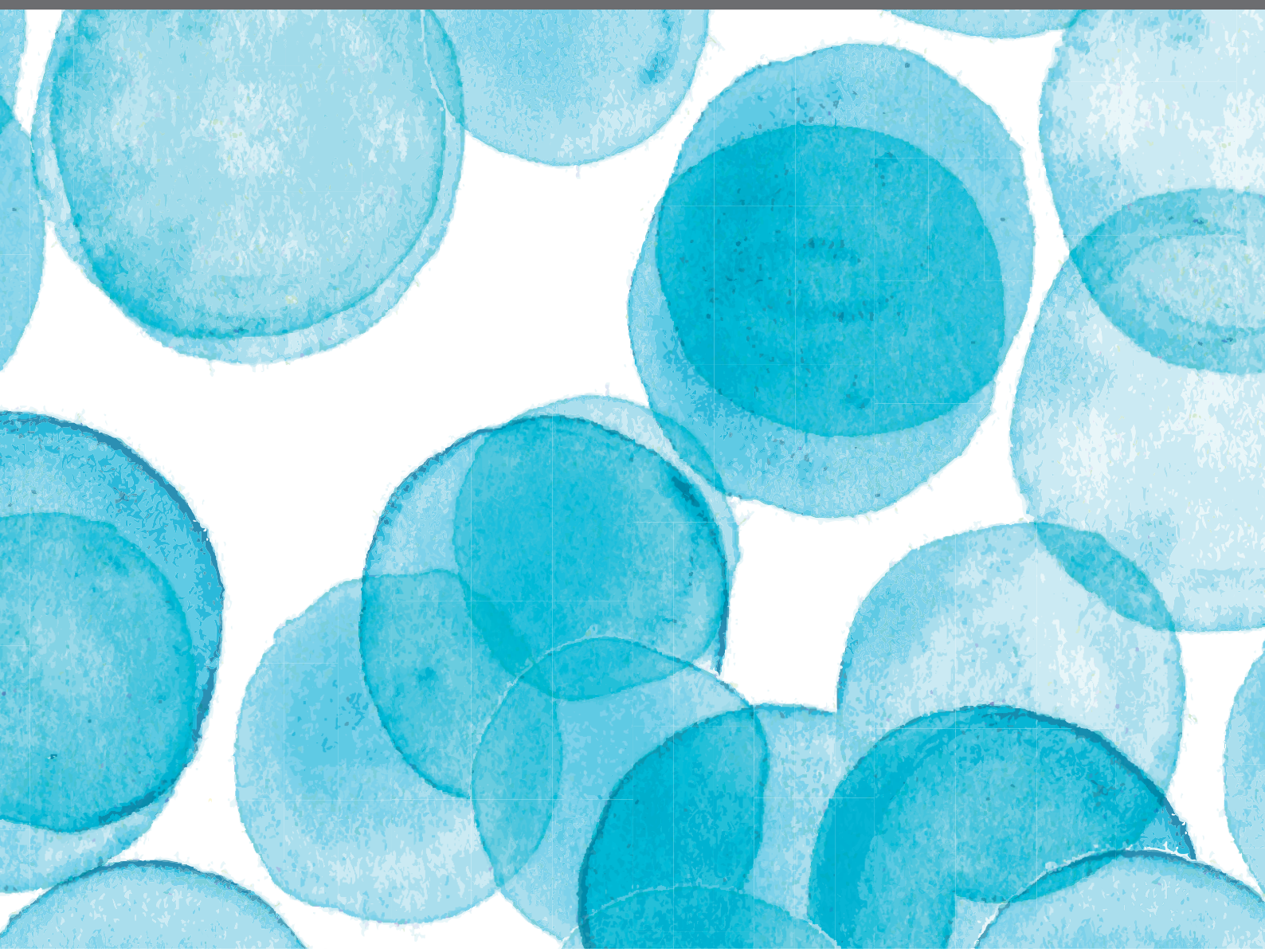

frontiers Research Topics

frontiers

ISSN 1664-8714
ISBN 978-2-88966-631-7
DOI 10.3389/978-2-88966-631-7

About Frontiers

Frontiers is more than just an open-access publisher of scholarly articles: it is a pioneering approach to the world of academia, radically improving the way scholarly research is managed. The grand vision of Frontiers is a world where all people have an equal opportunity to seek, share and generate knowledge. Frontiers provides immediate and permanent online open access to all its publications, but this alone is not enough to realize our grand goals.

Frontiers Journal Series

The Frontiers Journal Series is a multi-tier and interdisciplinary set of open-access, online journals, promising a paradigm shift from the current review, selection and dissemination processes in academic publishing. All Frontiers journals are driven by researchers for researchers; therefore, they constitute a service to the scholarly community. At the same time, the Frontiers Journal Series operates on a revolutionary invention, the tiered publishing system, initially addressing specific communities of scholars, and gradually climbing up to broader public understanding, thus serving the interests of the lay society, too.

Dedication to Quality

Each Frontiers article is a landmark of the highest quality, thanks to genuinely collaborative interactions between authors and review editors, who include some of the world's best academicians. Research must be certified by peers before entering a stream of knowledge that may eventually reach the public - and shape society; therefore, Frontiers only applies the most rigorous and unbiased reviews.
Frontiers revolutionizes research publishing by freely delivering the most outstanding research, evaluated with no bias from both the academic and social point of view. By applying the most advanced information technologies, Frontiers is catapulting scholarly publishing into a new generation.

What are Frontiers Research Topics?

Frontiers Research Topics are very popular trademarks of the Frontiers Journals Series: they are collections of at least ten articles, all centered on a particular subject. With their unique mix of varied contributions from Original Research to Review Articles, Frontiers Research Topics unify the most influential researchers, the latest key findings and historical advances in a hot research area! Find out more on how to host your own Frontiers Research Topic or contribute to one as an author by contacting the Frontiers Editorial Office: frontiersin.org/about/contact

MICROBIOTECHNOLOGY TOOLS FOR WASTEWATER CLEANUP AND ORGANIC SOLIDS REDUCTION

Topic Editors:
Mayur B. Kurade, Hanyang University, South Korea
Mukesh Kumar Awasthi, Northwest A&F University, China
Sanjay Prabhu Govindwar, Shivaji University, India
Byong-Hun Jeon, Hanyang University, South Korea
Dayanand Kalyani, Royal Institute of Technology, Sweden

Topic Editor Byong-Hun Jeon has patents related to the Research Topic. All other topic editors declare no competing interests with regard to the Research Topic subject.

Citation: Kurade, M. B., Awasthi, M. K., Govindwar, S. P., Jeon, B.-H., Kalyani, D., eds. (2021). Microbiotechnology Tools for Wastewater Cleanup and Organic Solids Reduction. Lausanne: Frontiers Media SA. doi: 10.3389/978-2-88966-631-7

Table of Contents

frontiers in Microbiology

EDITORIAL
published: 18 February 2021
doi: 10.3389/fmicb.2021.631506

Editorial: Microbiotechnology Tools for Wastewater Cleanup and Organic Solids Reduction

Mayur B. Kurade[1]*, *Mukesh Kumar Awasthi*[2], *Sanjay P. Govindwar*[1], *Byong-Hun Jeon*[1]* *and Dayanand Kalyani*[3]

[1] Department of Earth Resources and Environmental Engineering, Hanyang University, Seoul, South Korea, [2] College of Natural Resources and Environment, Northwest A&F University, Yangling, China, [3] School of Industrial Biotechnology, Royal Institute of Technology, Stockholm, Sweden

Keywords: emerging contaminants (ECs), wastewater treatment, phytoremediation, phycoremedation, nutrient removal, biodegradation, bioremediation

Editorial on the Research Topic

Microbiotechnology Tools for Wastewater Cleanup and Organic Solids Reduction

OPEN ACCESS

Edited by:
Sanket J. Joshi,
Sultan Qaboos University, Oman

Reviewed by:
Seung Gu Shin,
Pohang University of Science and Technology, South Korea

***Correspondence:**
Mayur B. Kurade
mayurkurade@hanyang.ac.kr
Byong-Hun Jeon
bhjeon@hanyang.ac.kr

Specialty section:
This article was submitted to Microbiotechnology, a section of the journal Frontiers in Microbiology

Received: *20 November 2020*
Accepted: *28 January 2021*
Published: *18 February 2021*

Citation:
Kurade MB, Awasthi MK, Govindwar SP, Jeon B-H and Kalyani D (2021) Editorial: Microbiotechnology Tools for Wastewater Cleanup and Organic Solids Reduction. Front. Microbiol. 12:631506. doi: 10.3389/fmicb.2021.631506

Millions of people around the world lack access to safe water and suffer the consequences of unacceptable sanitary conditions due to contamination of water resources with various synthetic and geogenic compounds, which are being leached from agricultural, industrial, and domestic activities (Kurade et al., 2019; Xiong et al., 2021). The primary objective of a wastewater treatment plant is to reduce the concentrations of the pollutants to the level at which the discharge of the effluent will not adversely affect the environment or pose a health threat. Treatment of wastewater using bioremedial tools is an attractive approach because of their cost-effective and environmentally friendly properties. The modifications and improvements of existing biological treatment systems and/or addition of advanced technologies into wastewater treatment plants (WWTPs) is important to maximize the treatment efficiency. Along with the bacterial-mediated wastewater treatment, microalgae- and plant- based remediation is also of growing scientific interest (Rane et al., 2016; Huang et al., 2017; Vila-Costa et al., 2017). This Research Topic aims to gather the current advancements in microbial biotechnologies for wastewater treatment and biosolids reduction from urban and industrial wastewater. It includes eight original research articles that deal with related topics, ranging from novel methodology in quantifying the wastewater processes to the biologically facilitated removal and degradation of a diverse class of water pollutants.

The activated sludge process is a widely employed biological treatment of industrial and municipal wastewater. To achieve the highest treatment efficiency, it is important to monitor and maintain the optimum biomass concentration. Asgharnejad and Sarrafzadeh, proposed a cost-effective, high-throughput and errorless methodology of image processing and Red Green Blue (RGB) analysis for the quantification of activated sludge. Several essential parameters required for the deployment of such a method at large-scale industrial conditions are addressed.

The contamination of water resources with pharmaceutical contaminants has become a serious environmental problem in recent times. Xiong et al., utilized a green microalga, *Scenedesmus obliquus*, for the treatment of wastewater contaminated with doxylamine. Doxylamine exhibited negligible effect on *S. obliquus* and its biochemical characteristics, including pigments. As a result, *S. obliquus* exhibited the effective removal of doxylamine, chemical oxygen demand, and nutrients from the wastewater. Authors have shown the feasibility of using microalgae-based biotechnologies for wastewater treatment, but concluded that pilot-scale studies are needed for its implementation.

Swine wastewater has detrimental effects on the water quality and aquatic ecosystem due to the presence of high concentrations of organic compounds, nutrients, heavy metals, and antibiotics. Therefore, Dan et al., investigated an intermittent cycle extended aeration system (ICEAS) for the removal of nutrients from anaerobically digested swine wastewater. Authors observed that the performance of the ICEAS was superior to conventional sequencing batch reactor technology in terms of nutrient removal, and the effluent quality was within the discharge standard, suggesting that ICEAS is a promising technology for wastewater treatment.

Water pollution created by colored wastewater is a serious issue as it leads to ecological disturbances and reduces the aesthetic value of water resources. It is immensely important to eliminate the xenobiotic compounds responsible for coloration before they are released into the environment. In this view, two original research articles in this article collection emphasized the application of bacterial-mediated remediation of two different kinds of colored wastewaters. Amin et al., improved the decolorization of a model, textile azo dye, Direct Red 81, under microaerophilic conditions by optimizing the nutritional and environmental parameters through statistical models. They explored the metabolic pathway and the active involvement of laccase and azoreductase in dye degradation and confirmed that the retrieved products were non-toxic. The contribution of Abdulsalam et al., focused on the decolorization of palm oil mill effluent using bacterial treatment. The treatment of palm oil mill effluent has been a challenge due to its intense brownish color due to excessive concentrations of tannins, melanoidin, and lignin compounds. Authors optimized the influential parameters of decolorization, including inoculum size, initial color concentration, and treatment time, using Response Surface Methodology.

The contribution of Thongpitak et al. outlined the treatment of a herbicide- paraquat contaminated waters using biologically synthesized manganese oxide considering its widespread contamination throughout the globe in soil and water, including rivers and surface waters, and its further accumulation in the food chain. The manganese oxide synthesized from microalga, *Pediastrum duplex,* performed Fenton-like reactions to deliver 50% degradation of paraquat within three days. It indicates that biosynthesized manganese oxide is an environmentally friendly alternative catalyst that can be effectively applied in wastewater treatment systems.

Phenol is a ubiquitous pollutant that is frequently observed in wastewater. Biological treatment of phenol-containing wastewater is an effective approach, however the toxicity of phenol on microorganisms hinders the process efficiency. Wang et al. explored the phenol tolerance mechanism of *Candida tropicalis* through transcriptomic analysis and showed that *C. tropicalis* prevented cell damage through improvement of cell wall resistance, maintenance of intracellular protein homeostasis, high-fidelity DNA replication, and organelle integrity. The outcomes of this study would help in the genetic modification of yeast for improving their efficiency of phenol degradation.

The utilization of *Dendrobium* plants for the phytoremediation of wastewater are highlighted due to their cost-effectivity and ecological advantages. *Dendrobium nobile* is the only plant that can produce the natural bioactive compound dendrobine, which has potential medical significance. The article by Sarsaiya et al., determined the presence of an endophytic fungal strain in *D. nobile*, and evaluated the production of endophyte and dendrobine using the molecular method and analytical characterization, respectively. The potential dendrobine producer strain in *D. nobile* was identified to be *Trichoderma longibrachiatum*, which exhibited strong bactericidal activity against common pathogens, indicating its potential in microbiotechnology fields.

With this Research Topic, we presented some newly developed techniques to deal with pollutants in wastewaters with a consideration of a broad readership with interest in the bioremediation of wastewater. Although the provided technologies are very attractive in terms of their efficiency, further in-depth investigations are needed to implement these technologies at an engineered scale. The inclusion of the existing research gaps and recommendations for future research in this Research Topic will ensure a productive progression toward a bright future of bioremediation.

AUTHOR CONTRIBUTIONS

All the authors of this editorial article have made a significant, direct and intellectual contribution to the work, and approved it for publication.

FUNDING

The theme of this Research Topic is based on the research projects received from the National Research Foundation of Korea (NRF), Ministry of Education, Science, and Technology (MEST) of the South Korean government (NRF-No. 2019R1I1A1A01063318 and No. 2019R1F1A1064379).

ACKNOWLEDGMENTS

This Research Topic was initiated to update the current progress of research in the field of bioremediation of waste. There is a total of eight manuscripts accepted for publication in this Research Topic that were contributed by 52 authors residing in several countries including Sweden, Malaysia, India, China, Netherlands, Iran, Nigeria, Vietnam, and Thailand. We would like to gratefully acknowledge all the research contributors for their invaluable work to this topic and encouraging the scientific community across the globe to become more involved in this research area. The editors would like to extend their gratitude toward the expert reviewers for their precious time given for the respected criticism meant to improve the quality and standards of the manuscripts.

REFERENCES

Huang, X., Zheng, J. L., Liu, C. X., Liu, L., Liu, Y. H., Fan, H. Y., et al. (2017). Performance and bacterial community dynamics of vertical flow constructed wetlands during the treatment of antibiotics-enriched swine wastewater. *Chem. Eng. J.* 316, 727–735. doi: 10.1016/j.cej.2017.02.029

Kurade, M. B., Xiong, J. Q., Govindwar, S. P., Roh, H. S., Saratale, G. D., Jeon, B. H., et al. (2019). Uptake and biodegradation of emerging contaminant sulfamethoxazole from aqueous phase using *Ipomoea aquatica*. *Chemosphere* 225, 696–704. doi: 10.1016/j. chemosphere.2019.03.086

Rane, N. R., Patil, S. M., Chandanshive, V. V., Kadam, S. K., Khandare, R. V., Jadhav, J. P., et al. (2016). *Ipomoea hederifolia* rooted soil bed and *Ipomoea aquatica* rhizofiltration coupled phytoreactors for efficient treatment of textile wastewater. *Water Res.* 96, 1–11. doi: 10.1016/j. watres.2016.03.029

Vila-Costa, M., Gioia, R., Acena, J., Perez, S., Casamayor, E. O., and Dachs, J. (2017). Degradation of sulfonamides as a microbial resistance mechanism. *Water Res.* 115, 309–317. doi: 10.1016/j. watres.2017.03.007

Xiong, J. Q., Cui, P., Ru, S., Govindwar, S. P., Kurade, M. B., Jang, M., et al. (2021). Unravelling metabolism and microbial community of a phytobed co-planted with *Typha angustifolia* and *Ipomoea aquatica* for biodegradation of doxylamine from wastewater. *J. Hazard. Mat.* 401:123404. doi: 10.1016/j. jhazmat.2020.123404

Conflict of Interest: The authors declare that the research was conducted in the absence of any commercial or financial relationships that could be construed as a potential conflict of interest.

frontiers in Microbiology

ORIGINAL RESEARCH
published: 12 March 2020
doi: 10.3389/fmicb.2020.00337

New Insights Into Detection of a Dendrobine Compound From a Novel Endophytic *Trichoderma longibrachiatum* Strain and Its Toxicity Against Phytopathogenic Bacteria

Surendra Sarsaiya[1,2,3†], Archana Jain[1,2†], Xiaokuan Fan[4], Qi Jia[3], Quan Xu[4], Fuxing Shu[3], Qinian Zhou[3], Jingshan Shi[1] and Jishuang Chen[1,2,3,4*]*

[1] Key Laboratory of Basic Pharmacology of Ministry of Education, Zunyi Medical University, Zunyi, China, [2] Joint International Research Laboratory of Ethnomedicine of Ministry of Education, Zunyi Medical University, Zunyi, China, [3] Bioresource Institute for Healthy Utilization, Zunyi Medical University, Zunyi, China, [4] College of Biotechnology and Pharmaceutical Engineering, Nanjing Tech University, Nanjing, China

OPEN ACCESS

Edited by:
Sanjay Prabhu Govindwar,
Shivaji University, India

Reviewed by:
Rajendra Prasad Singh,
Southeast University, China
Vijai K. Gupta,
Tallinn University of Technology, Estonia
Jiao Li,
Northwest A&F University, China

***Correspondence:**
Jingshan Shi
shijs@zmu.edu.cn
Jishuang Chen
bihu_zmu@zmu.edu.cn

[†] These authors share first authorship

Specialty section:
This article was submitted to Microbiotechnology, a section of the journal Frontiers in Microbiology

Received: 03 January 2020
Accepted: 17 February 2020
Published: 12 March 2020

Citation:
Sarsaiya S, Jain A, Fan X, Jia Q, Xu Q, Shu F, Zhou Q, Shi J and Chen J (2020) New Insights Into Detection of a Dendrobine Compound From a Novel Endophytic Trichoderma longibrachiatum Strain and Its Toxicity Against Phytopathogenic Bacteria. Front. Microbiol. 11:337. doi: 10.3389/fmicb.2020.00337

Dendrobium nobile is the only plant that could produce the natural bioactive dendrobine. No other source of dendrobine has been found to date except from *D. nobile* and via chemical synthesis. In this study, we aimed to examine the potential fungal endophyte isolated from *D. nobile* stem segments using the molecular method and to detect dendrobine compound through high-performance liquid chromatography (HPLC), gas chromatography–mass spectrometry (GC-MS), and liquid chromatography with tandem mass spectrometry (LC-MS/MS) and their metabolite for their antibacterial activity. The potential dendrobine producer strain was recognized as *Trichoderma longibrachiatum* based on molecular DNA sequencing and GenBank databases. The *T. longibrachiatum* MD33 produced dendrobine and other compounds in a potato dextrose medium (PDM), as confirmed by HPLC retention time peak analysis. The HPLC results revealed that *T. longibrachiatum* MD33 biomass showed a peak retention time of 5.28 ± 0.2 min, similar to wild *D. nobile* stem dendrobine (5.32 ± 0.2 min) and standard chemical reference dendrobine (5.30 ± 0.2 min), indicating the presence of dendrobine in the fungal biomass. Results of GC-MS and LC-MS analysis revealed that *T. longibrachiatum* MD33 produced the same molecular weight (263 in GC-MS and 264.195 in LC-MS) of dendrobine as compared with standard chemical reference dendrobine and *D. nobile* dendrobine. Antibacterial activity data revealed that *T. longibrachiatum* MD33 produced the strongest bactericidal activity against *Bacillus subtilis*, *Bacillus mycoides*, and *Staphylococcus* species, and the diameter of the bacterial growth inhibition zone was 12 ± 0.2, 9 ± 0.2, and 8 ± 0.2 mm, respectively. To the best of our knowledge,

this was the first study to investigate *T. longibrachiatum* as a dendrobine producer, and the results revealed that *T. longibrachiatum* was directly involved in the potential production of a similar bioactive compound to *D. nobile* (dendrobine). In addition, the *T. longibrachiatum* metabolite exhibited potent antibacterial activity and can be a potential strain for medical and industrial purposes.

Keywords: chromatography, dendrobine, *Dendrobium nobile*, endophytic fungi, phytopathogenic bacteria, *Trichoderma longibrachiatum*

INTRODUCTION

Plant tissues are intracellularly colonized by a complex group of endophytic microbial species, where they play a vital role in plant development, health, and protection. These endophytic microbes, especially fungi, have the ability to promote plant development via indirect and direct mechanisms. Endophytic fungi can directly help host plants through the production of several plant development regulators and by enabling nutrient uptake. In addition, they can keep the host plant healthy through indirect responses by producing substances such as antibiotics and siderophores to inhibit phytopathogens (Bahroun et al., 2018). Recently, the medicinal plant-based wastewater remediation approaches are highlighted due to their being comparatively cheap and ecologically advantageous, compared to other common technological approaches. There are several medicinal plants species known for their phytoremediative abilities (Hegazy et al., 2011; Santal et al., 2019). The *Dendrobium* phytoremediation potentials of plant species have been considered in many previous researches (Sarawaneeyaruk et al., 2014; Sutantoa et al., 2016; Santal et al., 2019).

Owing to health hazards and harmful effects associated with the indiscriminate use of artificial drugs and antibiotics, there has been growing attention to the practice of biomedicine. In the past 20 years, more than half of the market drugs were developed from bioresources (Pham et al., 2019). *Dendrobium* plants belonging to the Orchidaceae family have been attributed as earliest sources of medicine over extended periods in Asia, Australia, and Europe. More than 1100 species were testified worldwide and have been verified to be an upright source of bioactive metabolites (Khamchatra et al., 2016). The orchid family, Orchidaceae, represents earlier branches of the evolutionary tree and is possibly 120 million years old. It is one of the earlier families of angiosperms in which majority of plants are composed of highly evolved flowering plants, with approximately 25,000 to 35,000 species belonging to 750 to 900 genera (Lam et al., 2015; Sarsaiya et al., 2019b, 2020).

Dendrobium, referred to as Shihu in traditional Chinese medicine, is widely distributed throughout China and includes 78 species. Approximately 30 species (of 78 species) have been used as chief medicinal agents and food, such as tea or soup ingredients, for many centuries (Deng et al., 2018). The compounds found in *Dendrobium,* including dendrobine and related compounds, can boost human immunity besides preventing and improving metastatic cancer and have shown promising therapeutic effects on Alzheimer's disease (Nie et al., 2016). This medicinal plant has been used to prevent or treat illnesses owing to the presence of bioactive compounds in their cells and have been added to drugs since ancient times (Elgorban et al., 2019). However, dendrobine is not produced in large quantities by the *D. nobile* plant species because of its slow growth. The quantity of *D. nobile* dendrobine is low to fulfill the current industrial and research requirements (Jiang et al., 2018; Zhang et al., 2018).

Endophytic fungus has also been described to produce active enzymes and metabolites, which may be used to produce pharmaceutical products. Endophytic fungus can form a consortium of unstable carbon-based complexes (aldehydes, ketones, hydrocarbons, alcohols, heterocycles, thioesters, thioalcohols, phenols, and their byproducts) through substantial antimicrobial actions counter to plants and human pathogens (Manganyi et al., 2018; Jain et al., 2019). Most researchers are investigating the diversity and functional characteristics of fungal endophytes as biocontrol. They have focused on economically imperative crops or indigenous herbal class. The dynamic relationship between the host and its fungal endophytes has not been fully understood to date. However, a few endophytic fungi are recognized and categorized based on their molecular characteristics (Singh et al., 2017; Hoysted et al., 2018). To the best of our knowledge, this is the first study in China to analyze endophytic fungal diversity in *Dendrobium nobile* and to identify fungal metabolites, such as dendrobine and similar compounds, for the development of pharmacologically and industrially imperative bioactive compounds.

Some fungal endophytes are known to produce bioactive metabolites, and these metabolites may be similar to those produced by the host. For example, *Taxomyces andreanae,* a paclitaxel-producing fungal endophyte, was effectively recovered from the yew tree *Taxus brevifolia*. A study using a *Chaetomium* sp. reported the possible industrial production of paclitaxel (1124.34 μg/L) under optimized fermentation conditions. A gibberellin-producing *Penicillium commune* strain has been recovered from the *Sesamum indicum* plant (Elgorban et al., 2019). Many fungal endophytes have the potential to biosynthesize numerous bioactive natural compounds that may indirectly or directly be applied as therapeutic mediators in the treatment of various diseases. Fungal endophytes that produce the host herbal secondary metabolites with beneficial value or potential have been discovered (Dey et al., 2017). The detection

Abbreviations: ANOVA, analysis of variance; BLAST, Basic Local Alignment Search Tool; GC-MS, gas chromatography–mass spectrometry; HPLC, high-performance liquid chromatography; ITS, internal transcribed spacer; LC-MS/MS, liquid chromatography with tandem mass spectrometry; NCBI, National Center for Biotechnology Information; PCR, polymerase chain reaction; PDA, potato dextrose agar; PDM, potato dextrose medium; S.D., standard deviation.

of bioactive metabolites produced by fungal endophytes by using compounds simulated to resemble associated host herbal metabolites is important for both industrial and educational purposes (Kusari et al., 2012; Yu et al., 2017). In contrast, fewer efforts have been made to explore bioactive compounds similar to plant compounds produced by fungal endophytes (Raghavendra et al., 2017). Bacterial contaminations constitute a major plant health problem due to wastewater in developing and developed countries, which directly or indirectly influence growth. In recent years, the change of resistance of bacterial pathogens against natural compounds has become a problematic issue caused by the unselective use of natural compounds. Natural compounds have been called miracle natural active substances, but for more than 60 years of use, the efficacy of current natural active substances has been reduced due to the continuing emergence of natural active substance-resistant bacterial population in wastewater and the adaptations by bacterial pathogens to commonly used antibacterial compounds (Donga et al., 2017). Due to such issues, it is important to explore novel natural compounds, which have the ability to show effective antibacterial activity.

The present study was therefore performed to determine the presence of *Trichoderma longibrachiatum* endophytic fungal strain in *D. nobile* plants from Chishui, Guizhou, China. In addition, we aimed to assess the potential of the fungi to produce dendrobine compounds through HPLC, gas chromatography–mass spectrometry (GC-MS), and liquid chromatography with tandem mass spectrometry (LC-MS/MS) analysis and to determine the antibacterial effects of its metabolite against phytopathogenic bacteria.

MATERIALS AND METHODS

Processing of Samples for the Isolation of Endophytic Fungi

The endophytic fungi were isolated from the stem segments of single wild *D. nobile*, which was collected from the native agricultural farm area of Jinshishi, Chishui, China, and processed in the Bioresource Institute for Health Utilization, Zunyi Medical University, Zunyi, China. The processing of samples was performed according to the previous process of Sarsaiya et al. (2019a) and Sarsaiya et al. (2020). The stem samples of wild *D. nobile* were considered for processing and isolation. The samples (1.5 cm per piece) were inoculated onto PDA media plates. The plates were placed in an incubator at 25°C for 5 days. After 5-day incubation, the fungal hyphal growths emerged from the plant samples (**Figure 1**). These were recovered and purified by sub-culturing from growing hyphal tips.

Identification of Plant Endophytic Fungi

The potential dendrobine producing endophytic fungal genus was identified by using lactophenol cotton blue staining and microscopic observations (Ellis, 1976; Barnett and Hunter, 1998). For molecular identification, the DNA was extracted and polymerase chain reaction (PCR) was performed to amplify the internal transcribed spacer (ITS) regions for endophytes using a standard protocol (Manganyi et al., 2018).

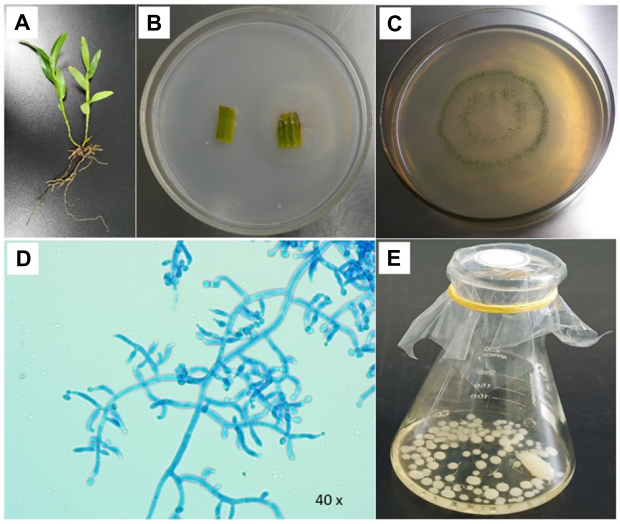

FIGURE 1 | Examination of *Trichoderma longibrachiatum* MD33 isolated from wild *Dendrobium nobile* stem segment. **(A)** Wild *D. nobile* plant. **(B)** Endophytic fungal culture emerge from stem. **(C)** Pure culture of *T. longibrachiatum* MD33. **(D)** Microscopic characteristics of *T. longibrachiatum* MD33. **(E)** *T. longibrachiatum* MD33 mycelial growth in the potato dextrose liquid medium.

Sequence Analysis of PCR Products

The amplified ITS regions of PCR samples were sequenced by Tsingke, Beijing, China. Sequence data were analyzed by using the BLAST (basic local alignment search tool) Web Tool on the NCBI (National Center for Biological Information)[1] to validate the similarity of species of the amplified sequences as compared with NCBI reference sequence. MEGA (molecular evolutionary genetics analysis) 7.0 software was used for phylogeny tree study.

Screening Medium for the Detection of Dendrobine Compounds

Potato dextrose medium was used for the synthesis of dendrobine compounds from the isolated endophytic fungi. Erlenmeyer flasks (250 ml) contained 100 ml of PDM in triplicate (initial pH 6.4). Two disks of 5-day-old fungal culture were inoculated separately on PDM and incubated at 25 ± 2°C for 14 days. The fungal culture biomass and metabolites were tested for the presence of dendrobine compounds through HPLC. The culture biomass and metabolite have shown dendrobine peak, which was further analyzed by using the GC-MS and LC-MS/MS analysis. Sample processing for the dendrobine detection through HPLC, GC-MS, and LC-MS/MS analysis is as follows:

HPLC Analysis for the Detection of Dendrobine Compounds

Preparation of Standard Dendrobine

Oven-dried powder of *D. nobile* stem was used for the extraction of dendrobine alkaloids. The powder was mixed

[1]http://blast.ncbi.nlm.nih.gov/Blast.cgi

with absolute ethanol and boiled at 90°C for 2 h. After extraction, the contents were filtered through Whatman filter paper, and the filtrate was transferred to sample tubes for HPLC analysis by comparing with the peak retention time of standard chemical reference dendrobine (purchased from Chengdu DeSiTe Biological Technology Co., Ltd., Chengdu, China, with purity greater than 99%).

Separation of Fungal Biomass and Metabolite

The endophytic fungal biomass and metabolite were separated from the Erlenmeyer flask by using the Water-Circulation Multifunction Vacuum Pump (Zhengzhou Greatwall Scientific Industrial and Trade Co., Ltd, Henan, China).

Freeze Drying of Fungal Biomass Samples

The test endophytic fungal biomass, after the separation through a Water Circulation Multifunction Vacuum Pump, was freeze dried at −40°C at 669 mbar for 10 h by using a ModulyoD-230 Freeze Dryer (Thermo Electron Corporation, Milford, MA, United States).

HPLC Analysis

The freeze-dried biomass (100 mg power of biomass used) and metabolite samples were mixed separately with 600 μl of acetonitrile in a 1.5-ml centrifuge tube. The tubes were vortex mixed for 1 min and centrifuged at 15,000 rpm (20,627 × *g*) for 15 min. Dendrobine and related compounds were analyzed using HPLC Agilent 1100 (United States) equipped with a C18 column (150 × 4.6 mm, 5 μm) maintained at 35°C. The mobile phase comprised 0.1% formic acid and acetonitrile with gradient elution at a flow rate of 1 ml/min. The injection volume was 20 μl. The ultraviolet (UV) wavelength was 205 nm. The retention peak time of dendrobine and its related compounds was calculated for all the trials through chromatograms.

Detection of Dendrobine by GC-MS

The following conditions were maintained in the GC-MS for the detection of dendrobine: Instrument: Agilent Technologies 6890N Network GC system; 5973 Network Mass selective detector; 7683B series Injector; Column: Capillary column Agilent 190915-433 HP-5MS (30.0 M × 250 μm × 0.25 μm); Initial temperature 150°C, keep 5 min, 10°C min^{-1}, Temperature-programed 250°C, keep 5 min; Inlet temperature of 250°C, detector temperature of 250°C; carrier: N_2, Flow rate: 1 ml min^{-1}, sample volume 1 μl.

Detection of Dendrobine by LC-MS/MS

Intracellular Dendrobine Extraction From Fungal Biomass

For the extraction of dendrobine from fungal biomass, the 100 mg of dry biomass was powdered in a mortar pestle, soaked with 50 ml of chloroform into the 50-ml centrifuge tube for 12 h at 180 rpm. From the mixture, the 40-ml liquid part was extracted by using the 5-ml Eppendorf micropipette. The plant dendrobine was also processed the same as the intracellular dendrobine extraction process. The chloroform phase was separated by evaporation at 35°C under a rotary evaporator (Rotary Evaporator N-1300V-W, EYELA, United States). After evaporation, the remaining residue was re-dissolved in 5 ml of chloroform and filtered through a 0.22-mm filter prior to analysis.

D. nobile Dendrobine Extraction

For the extraction of dendrobine from *D. nobile*, the freeze-dried stem sample (100 mg) of *D. nobile* was powdered after freeze drying (ModulyoD-230 Freeze Dryer; Thermo Electron Corporation, Milford, MA, United States) in a mortar pestle, soaked with 50 ml of chloroform for 12 h at 180 rpm. From the mixture, the 40-ml liquid part was separated. The chloroform phase was separated from the aqueous phase and evaporated at 35°C under a rotary evaporator. The remaining residue was re-dissolved in 5 ml of chloroform and filtered through a 0.22-mm filter prior to analysis.

Standard Dendrobine Solution Preparation

The stock solution of dendrobine (20.0 μg/ml) was prepared in chloroform. The 20, 80 ng/ml, and 20.0 μg/ml working standard solutions of the dendrobine were prepared from the dendrobine stock solution by dilution with chloroform. The dendrobine standard was purchased from Chengdu DeSiTe Biological Technology Co., Ltd., Chengdu, China, with a purity greater than 99%.

Detection of Dendrobine by LC-MS/MS

LC-MS is used for non-volatile and thermally fragile molecules. The detection of dendrobine was performed via the UHPLC system (Thermo Scientific DionexUltiMate 3000, Golden Valley, Minnesota, United States) with a column (150 × 2.1 mm) and a mobile phase consisting of 0.1% formic acid:acetonitrile at 95:5 (v/v) with a flow rate of 0.3 ml/min, a sheath gas flow rate of 35 arbitrary units, an auxiliary gas flow rate of 15 arbitrary units, a spray voltage of 3.5 kV, a capillary temperature of 350°C, and an aux gas heater temperature of 400°C. Identification of dendrobine was accomplished by comparison of retention times, molecular weight (264.195), and LC-MS fragmentation patterns with authentic chemical reference standard (dendrobine standard was purchased from Chengdu DeSiTe Biological Technology Co., Ltd., Chengdu, China, with a purity greater than 99%) and *D. nobile* plant stem dendrobine.

Toxicological Bioassay of Fungal Metabolite Against Plant Pathogenic Bacteria

Toxicological bioassay used in this research was performed as per the standard procedure (Bahroun et al., 2018). The pure pathogenic identified cultures of *Bacillus subtilis*, *Bacillus mycoides*, and *Staphylococcus* sp. strains were obtained from the Bioresource Institute for Health Utilization, Zunyi Medical University, Zunyi, China, for antibacterial study of fungal metabolite. A fresh culture of these selected pathogenic strains was transferred into 1 ml of sterile H_2O, and a 100-μl portion was spread over solidified PDA plates. Five-millimeter-diameter filter paper disks immersed in fungal metabolite were placed at equal

distances on the inoculated PDA plates. All bacterial isolations were done in triplicate and transferred to an incubator for 1 h incubation at 4°C to ensure diffusion of compounds from the fungal metabolite disks. Then, the test plates were incubated at 25°C for 24 h in a bacteriological incubator. The size of the bacterial growth inhibition zone was calculated in millimeters (mm). The standard formula (Balouiri et al., 2016) was applied to the inhibition zone size.

Inhibition zone = average diameter of the colony−5 mm (diameter).

Statistical Analysis

All data were expressed as means ± standard deviation (S.D.). The comparison between different treatments was performed by a one-way ANOVA using SPSS version 20.0 software. A value of $p < 0.05$ was considered statistically significant.

RESULTS

Endophytic Fungus Isolation and Identification

The *Trichoderma* was isolated and identified through ITS sequencing. It was confirmed from the NCBI web tool that the isolated fungi had maximum homology with *T. longibrachiatum,* and the investigated organism was confirmed to be *T. longibrachiatum*. The *Trichoderma* species was identified as *longibrachiatum* based on sequence identities of ≥100% with GenBank references, which belong to order Hypocreales and family Hypocreaceae. On the other hand, the *T. longibrachiatum* MD33 was identified at the species level based on sequence identities of ≥100% with its neighboring GenBank match. BLAST analysis showed that the isolated ITS sequence had 99% similarity with the ITS sequence of *T. longibrachiatum* (Accession no. NR_120298.1).

Screening for the Detection of Dendrobine Compounds Through HPLC

The secondary metabolite of the *T. longibrachiatum* MD33 strain was assessed by metabolite analysis through HPLC investigation to detect dendrobine compounds. The endophytic fungi were recovered from wild *D. nobile* stem segments and have shown great potential to release bioactive compounds through submerged fermentation and were, therefore, commonly used to produce natural active compounds. Based on the screening of all endophytic fungi for dendrobine and other related compounds, it was observed that *T. longibrachiatum* MD33 biomass samples showed the ability to produce compounds similar to dendrobine as compared with reference peaks and other related compounds. The fungal dry biomass of *T. longibrachiatum* was 1.36 ± 0.2 g after 14 days of incubation. Only *T. longibrachiatum* MD33 strain showed dendrobine peak as compared with standard chemical reference dendrobine and wild *D. nobile* stem dendrobine. HPLC analysis data of *T. longibrachiatum* MD33-fermented metabolites did not show any dendrobine peaks. The results revealed that the *T. longibrachiatum* MD33 biomass sample shared similar peak retention time to standard chemical reference dendrobine and *D. nobile* stem alkaloid (**Figure 2** and **Table 1**). Dendrobine of *T. longibrachiatum* MD33 fungal endophyte and *D. nobile* stem alkaloid samples were identified based on peak retention time relative to that of the reference standard (dendrobine; >99% purity). The retention time of dendrobine was 5.28 ± 0.2 min and that of other compounds was 1.36 ± 0.2, 3.02 ± 0.2, and 4.28 ± 0.2 min. Many other peaks were also recorded at retention times of 3.02 ± 0.2, 4.28 ± 0.2, and 5.28 ± 0.2 min compared with the standard dendrobine, while dendrobine peak in both showed the same retention time (5.28 ± 0.2 min; **Figure 2**). Furthermore, the peak retention time of *D. nobile* stem alkaloid was similar to that of fungal metabolite (retention time 1.32 ± 0.2, 3.21 ± 0.2, and 5.32 ± 0.2 min). The retention time of 5.28 ± 0.2 min was similar in all HPLC chromatograms (**Figure 2** and **Table 1**), indicating the presence of dendrobine compounds in the fungal metabolite.

Detection of Dendrobine by GC-MS Analysis

The GC-MS analysis of the fungal biomass of *T. longibrachiatum* MD33 revealed the presence of dendrobine bioactive volatile compounds. The *T. longibrachiatum* MD33 was found strongly to produce dendrobine as compared with standard chemical reference dendrobine and *D. nobile* stem dendrobine. The mass spectrum of the *T. longibrachiatum* MD33 biomass dendrobine along with *D. nobile* stem dendrobine and chemical reference standard dendrobine showed dendrobine molecular weight at 263 with a peak retention time of 14.96 ± 0.01, respectively (**Figure 3** and **Table 1**). Other compounds produced by *T. longibrachiatum* MD33 were **(1)** 1-Decene, 8- methyl-, **(2)** Benzene, 2-ethyl-1,4- dimethyl-, **(3)** Ethane, hexachloro- (CAS); Hexachloroethane; Egitol; Phenohep; Distopan; Distopin; Falkitol; Distokal; Avlothane; Fasciolin; Mottenhexe; Perchloroethane; Hexachlorethane; Hexachloroethylene; Carbon hexachloride; Ethane hexachloride; 1,1,1,2,2,2-Hexachloro, **(4)** Benzene, 1,2,4,5-tetramethyl-; Durene; Durol; 1,2,4,5-Tetramethylbenzene, **(5)** Benzene, 1,2,3,4-tetramethyl- (CAS); Prehnitol; 1,2,3,4-Tetramethylbenzene; Prehnitene; 1,2,3,4-Tetramethylbenzene (Prehnitene), **(6)** Dodecane, **(7)** Dodecane, 4,6- dimethyl-, **(8)** Benzene, 1,3-bis(1,1-dimethylethyl)-, **(9)** Eicosane, **(10)** Hexane, 2,3,4- trimethyl-, **(11)** 2-Undecene, 4,5- dimethyl-, [R*,S*-(Z)]-, **(12)** Hexane, 2,3,4- trimethyl-, **(13)** Tetradecane (CAS); n-Tetradecane; Isotetradecane, **(14)** Ethanone, 1,1′-(1,4-phenylene)bis-; Benzene, p-diacetyl-; p-Acetylacetophenone; p-Diacetylbenzene; 1,4-Diacetylbenzene, **(15)** Tridecane, 1- iodo-, **(16)** Pentadecane, **(17)** Phenol, 2,4-bis(1,1-dimethylethyl)-, **(18)** Pyridine-3-carboxamide, oxime, N-(2-trifluoromethylphenyl)-, **(19)** Sulfurous acid, octadecyl 2-propyl ester, **(20)** Cyclohexane, 1,2,4- trimethyl-, **(21)** Hexadecane, **(22)** Heptadecane, **(23)** Octadecane (CAS); n-Octadecane; Octadecan, **(24)** 2-Isopropyl-5-methyl-1-heptanol, **(25)** Eicosane, **(26)** Nonadecane, **(27)** Octadecane (CAS); n-Octadecane; Octadecan, **(28)** Hexadecane, 3-methyl-; 3-Methylhexadecane, **(29)** Heptadecane, **(30)** Hexadecanoic acid (CAS); Palmitic acid; Palmitinic acid; n-Hexadecoic

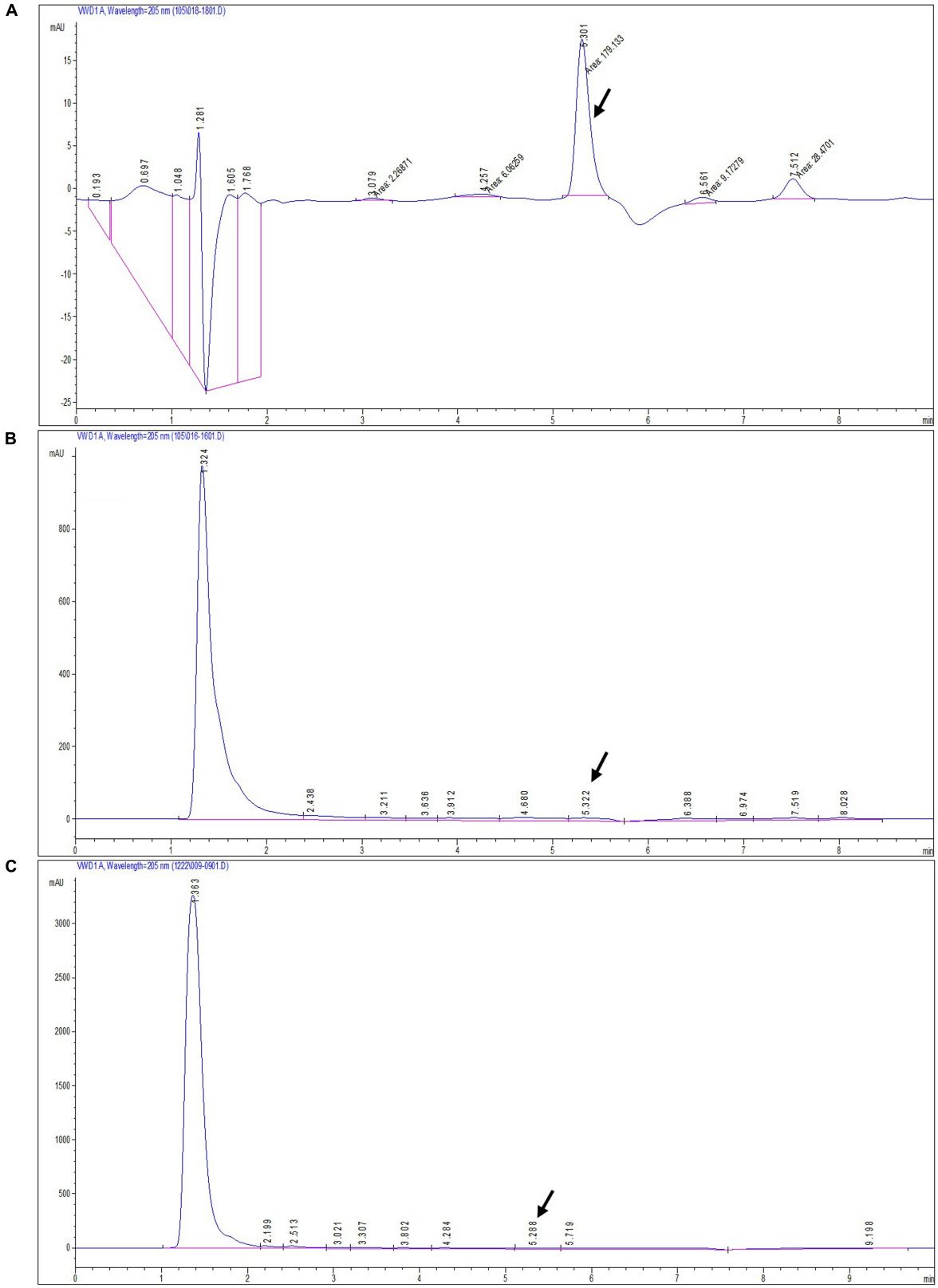

FIGURE 2 | HPLC chromatograms of standard dendrobine **(A)**, *D. nobile* plant alkaloid **(B)**, and fungal dendrobine and other related compounds **(C)**. Dendrobine-specific peak was observed at 5.3 ± 0.02.

TABLE 1 | Comparison of HPLC, GC-MS, and LC-MS/MS analysis for the dendrobine peak retention times and its molecular weight.

Sample type	Dendrobine peak retention time (min)		
	HPLC	GC-MS	LC-MS/MS
	5.30 ± 0.02	14.97 ± 0.02	7.51 ± 0.02
Trichoderma longibrachiatum MD33	5.28 ± 0.02	14.96 ± 0.02	7.51 ± 0.02
Chemical reference standard dendrobine	5.30 ± 0.02	14.96 ± 0.02	7.57 ± 0.02
Wild *Dendrobium nobile* stem dendrobine	5.32 ± 0.02	14.97 ± 0.02	7.48 ± 0.02
Dendrobine molecular weight	NA	263	264.195

All the values are the standard deviation of three replicates; NA: not available.

acid; n-Hexadecanoic acid; Pentadecanecarboxylic acid; 1-Pentadecanecarboxylic acid; Prifrac 2960; Coconut oil fatty acids; Cetylic acid; Emersol 140; Emersol 143; Hexadecylic acid; Hyd, **(31)** 1,2-Benzenedicarboxylic acid, ditridecyl ester, **(32)** Eicosane (CAS); n-Eicosane, **(33)** Heneicosane, **(34)** Heneicosane, **(35)** Oleic Acid; 9-Octadecenoic acid (Z)-;.delta.(Sup9)-*cis*-Oleic acid; *cis*-.delta.(Sup9)-Octadecenoic acid; *cis*-Oleic Acid; cis-9-Octadecenoic Acid; Emersol 211; Emersol 220 White Oleic Acid; Emersol 221 Low Titer White Oleic Acid; Oelsauere; Oleine 7503; Pa, **(36)** Oleic Acid; 9-Octadecenoic acid (Z)-;.delta.(Sup9)-*cis*-Oleic acid; *cis*-.delta.(Sup9)-Octadecenoic acid; *cis*-Oleic Acid; *cis*-9-Octadecenoic Acid; Emersol 211; Emersol 220 White Oleic Acid; Emersol 221 Low Titer White Oleic Acid; Oelsauere; Oleine 7503; Pa, **(37)** Thiosulfuric acid (H2S2O3), S-(2-aminoethyl) ester; Thiosulfuric acid, S-(2-aminoethyl) ester; Cysteamine, S-sulfo-; Cysteaminesulfonic acid; S-.beta.-Aminoethylthiosulfuric acid; S-(2-Aminoethyl) hydrogen thiosulfate; 2-Aminoethanethiol hydrogen sulfate, **(38)** Triacontane (CAS); n-Triacontane, **(39)** Tricosane (CAS); n-Tricosane, **(40)** Octadecane (CAS); n-Octadecane; Octadecan, **(41)** Phenol, 2,2′-methylenebis[6-(1,1-dimethylethyl)-4-methyl-(CAS); 2,2′-Methylenebis(4-methyl-6-tert-butylphenol); BKF; AO 1; S 67; CAO 5; CAO 14; CAO-14; AO 2246; A-22-46; NG 2246; A 22-46; MBP 5; 2,2′-METHYLENE-BIS(6-T-BUTYL-P-CRESOL); Anti Ox; Catolin 14, **(42)** Eicosane (CAS); n-Eicosane, **(43)** Nonadecane.

Detection of Dendrobine by LC-MS/MS Analysis

The LC-MS results revealed that standard chemical reference dendrobine was found at a retention time of 7.57 ± 0.1 and a molecular weight of 264.195. From the *D. nobile* stem dendrobine, it was found that the dendrobine peak was recorded at a retention time of 7.48 ± 0.1 with 264.195 molecular weight, which was nearly the same as the chemical standard dendrobine peak retention time and molecular weight. In case of intracellular dendrobine of *T. longibrachiatum* MD33, the dendrobine peak was recorded at 7.51 ± 0.1 with a dendrobine molecular weight of 264.195. The *T. longibrachiatum* MD33 was found to strongly produce dendrobine as compared with standard chemical reference dendrobine and *D. nobile* stem dendrobine in the LC-MS/MS analysis (**Figure 4** and **Table 1**).

Toxic Effect of Fungal Metabolite Against Phytopathogenic Bacteria

The *T. longibrachiatum* MD33 strain metabolite showed potent toxicity against all tested bacteria. The *T. longibrachiatum* MD33 exhibited the highest inhibition zone size of 12 ± 0.2 mm against *B. subtilis*, followed by *B. mycoides* and *Staphylococcus* sp. with inhibition zone sizes of 9 ± 0.2 and 8 ± 0.2 mm, respectively, indicating weaker effects. The findings are presented in **Table 2**. The results showed that *T. longibrachiatum* MD33 possessed potent toxic effects against plant pathogens such as *B. subtilis*, *B. mycoides*, and *Staphylococcus* sp. It was found that the *T. longibrachiatum* MD33 not only produced many bioactive compounds but also showed antibacterial activity of these natural compounds.

DISCUSSION

In this study, we aimed to determine the presence of *T. longibrachiatum* MD33 endophytic fungal strain in *D. nobile* stems, to assess the potential of the fungi to produce dendrobine compounds, and to determine the antibacterial effects of bioactive compounds against phytopathogenic bacteria. We found that *T. longibrachiatum* MD33 was involved in the production of a similar bioactive compound of *D. nobile* such as dendrobine. Moreover, dendrobine exhibited strong antibacterial activity against the bacterial strains tested. *D. nobile*, a medicinal plant, may harbor a complex group of endophytic fungi, and previous studies revealed that over 1 million fungi were associated with medicinal plants (Manganyi et al., 2018; Sarsaiya et al., 2020). When these endophytes exist in the internal tissues of medicinal plants, they can form and secrete secondary metabolites that may be of great value, especially in pharmaceutical and agricultural applications (Ghorbanpour et al., 2018). The current study was therefore designed to elucidate the *T. longibrachiatum* MD33 endophyte isolated from *D. nobile* segments and to screen the isolates for dendrobine compound and determine their antibacterial activities against plant pathogens. The fungal endophytes and inner herb tissues create a favorable environment for each other. The versatile synthesis capabilities of fungi are favored to their absorptive and heterotrophic mode of nutrition (Suryanarayanan et al., 2009; Sarsaiya et al., 2019b). This observation is in line with a previous research on endophytic fungi from plant segments (Kosawang et al., 2018).

In the current study, we found that endophytic fungal establishment upsurges in plant segments, because it depends on micro- and macronutrients and other climatic conditions. It was found that the colonization of *Trichoderma* endophytic fungi was higher in stem segments, indicating that the stem is more suitable for the colonization of *Trichoderma* as compared with other endophytic fungi. The outline of isolations and variations in fungal colonization according to plant segments validates that the community of endophytes in *D. nobile* herb is distributed on different segments of the host herb through spore dispersion in the environment. Henceforth, among other aspects, contact time, size of interaction surface, and the amount of natural intros in the

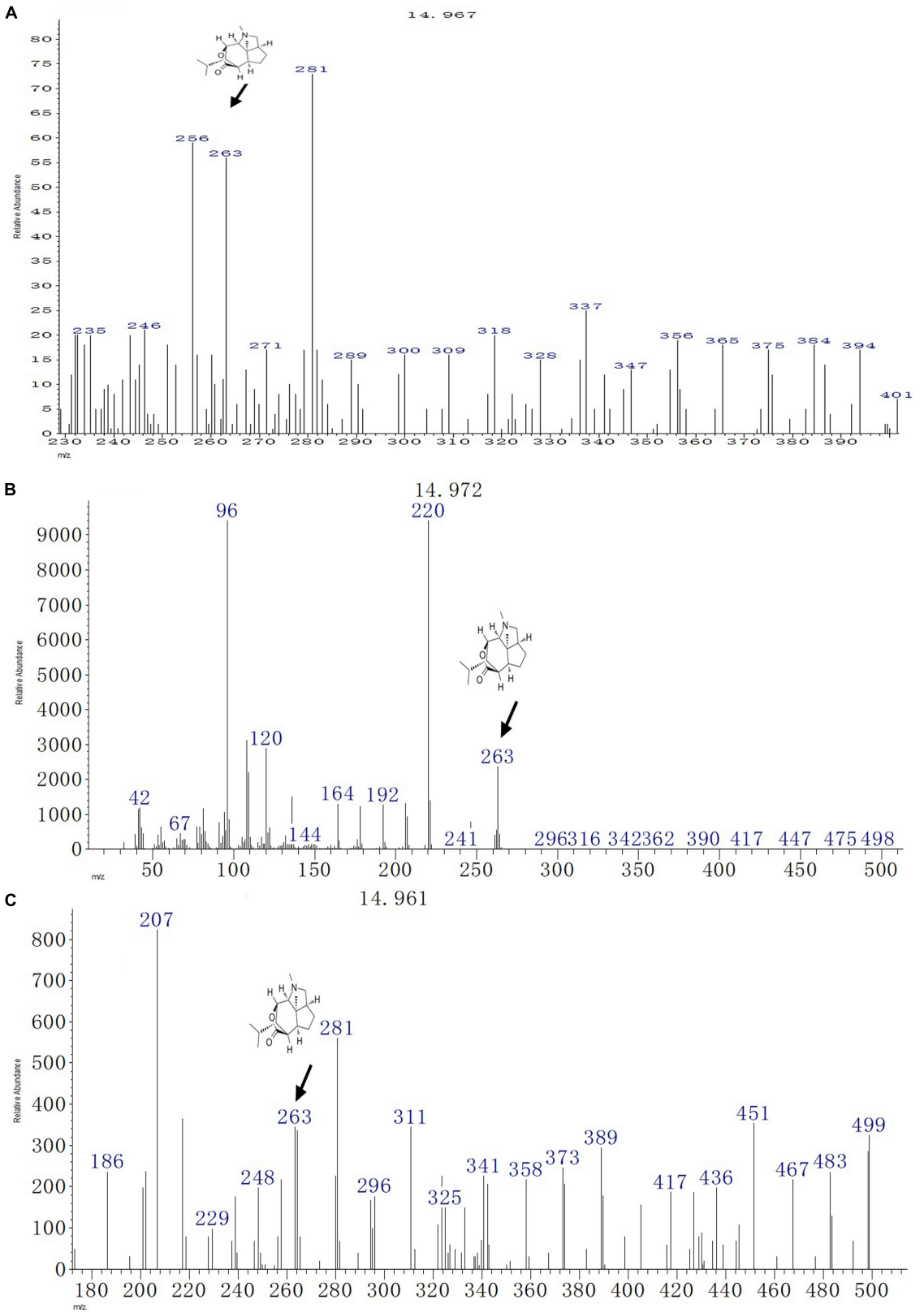

FIGURE 3 | GC-MS chromatographs for the detection of dendrobine (molecular weight: 263). **(A)** *T. longibrachiatum* MD33 dendrobine. **(B)** *Dendrobium nobile* stem dendrobine. **(C)** Chemical reference dendrobine standard.

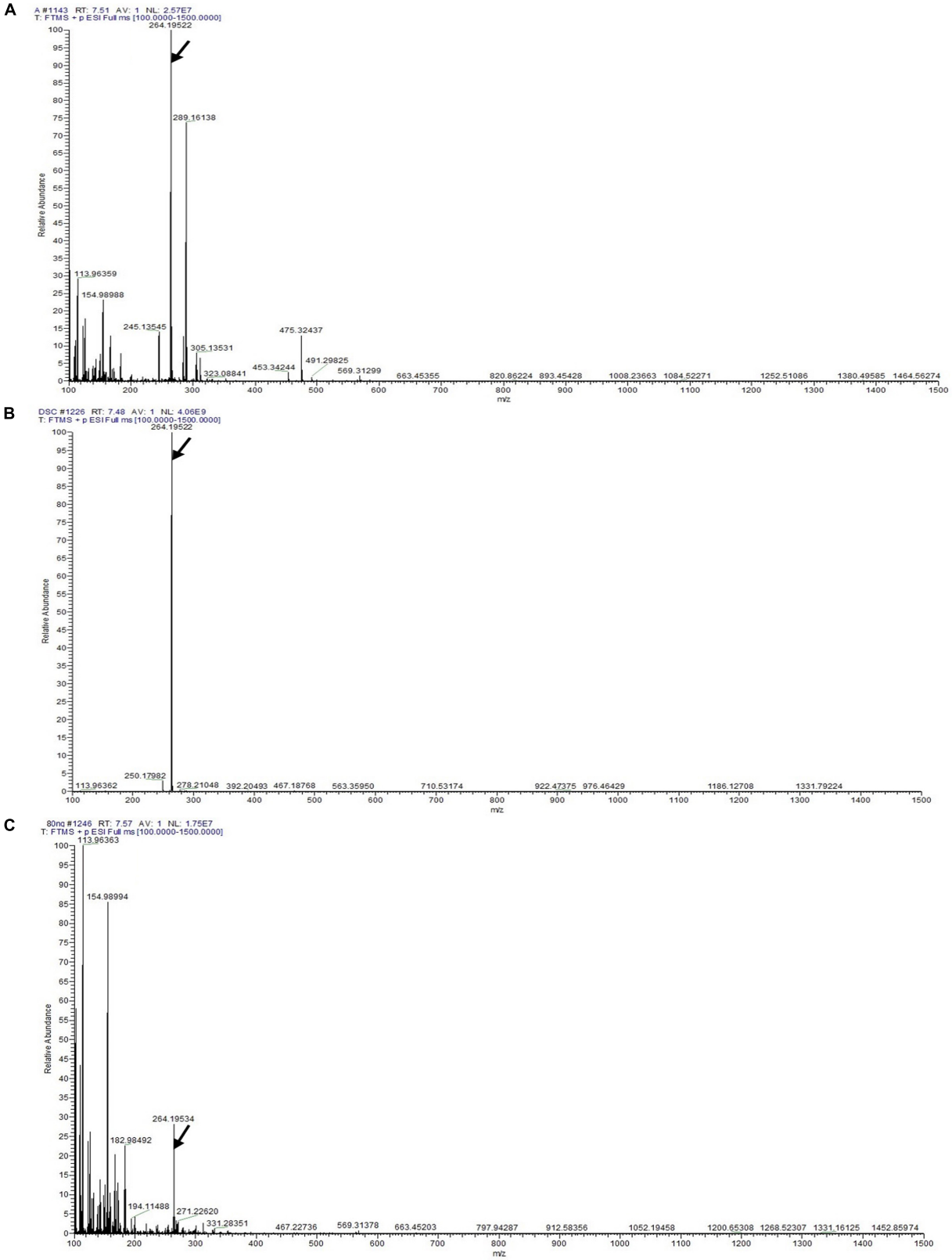

FIGURE 4 | LC-MS/MS chromatographs for the detection of dendrobine (molecular weight: 264.195). **(A)** *T. longibrachiatum* MD33 intracellular dendrobine. **(B)** *Dendrobium nobile* stem dendrobine. **(C)** Chemical reference dendrobine standard.

TABLE 2 | Toxicological effect of *Trichoderma longibrachiatum* metabolite against test pathogenic bacteria.

Phytopathogenic bacteria	Test fungi	Zone of inhibition	Zone (in mm)
Bacillus subtilis	*Trichoderma longibrachiatum*	+	12 ± 0.2 mm
Bacillus mycoides		+	9 ± 0.2 mm
Staphylococcus sp.		+	8 ± 0.2 mm

Values are presented as means ± standard deviation (S.D.); + = Produced inhibition zone; - No zone of inhibition.

plant tissue may impact the quantity of endophytic formations (Nascimento et al., 2015). Unlike bacteria, the identification and organization of fungi still rely mostly on morphological features and the use of light microscope relics to be dynamic in fungiform investigations. However, such identification techniques may be problematic and time-consuming as they may need specific proficiency to obtain consistent evidence (Ziaee et al., 2016). In the current research, both macroscopic features and microscopic practices were used to identify fungal isolate. The present study suggests that ITS sequencing provides an adequate resolution to identify endophytic fungi at least to the species level. The results showed that the isolated endophytic fungus from the stem segment of wild *D. nobile* was *T. longibrachiatum* MD33. Similarly, *Trichoderma viride* strain was reported from different medicinal plant segments previously (Nalini et al., 2014; Xiang et al., 2016).

Fungal endophytes from *D. nobile* are still a weakly investigated set of microorganisms, and their complex biological functions remain poorly elucidated (Zheng et al., 2017). *D. nobile* is a medicinal plant used widely in China. To date, there are no reports on dendrobine and related compound-producing endophytic fungi isolated from *D. nobile*; however, studies have focused on dendrobine produced by the herb (Li et al., 2017; Meng et al., 2017). *D. nobile* has attracted increasing attention in medical and chemical fields because of its active ingredients. However, the production of these ingredients in the plants is very low. A few endophytic fungi have the ability to produce substances similar to the host herb. Another research revealed that the taxol bioactive compound had been detected as an alternative source of natural compound (earlier obtained from Taxus plant) from endophytic fungal species, which has shown antimicrobial and anti-cancer activity (Somjaipeng et al., 2015). This attracted interest in the potential of endophytes isolated from *D. nobile* to produce a high value product such as dendrobine. Owing to the increasing global demand for anti-cancer drugs, the global market for dendrobine is increasing rapidly and is expected to cross the outer limit of other drugs. Thus, the demand for dendrobine will continue to increase (Li et al., 2017; Sarsaiya et al., 2019c). However, dendrobine is an expensive drug and, therefore, not easily accessible to many people worldwide. To our knowledge, no attempt has been made to isolate endophytes from *D. nobile* for possessing the ability to produce dendrobine in China and other countries. Through HPLC analysis, it was observed that *T. longibrachiatum* MD33 showed a peak retention time (5.28 ± 0.2 min) similar to the host plant (*D. nobile*) and standard chemical reference dendrobine. This finding suggested the possibility of finding alternative sources of dendrobine through fungal endophyte (*T. longibrachiatum* MD33). The GC-MS of the *T. longibrachiatum* MD33 biomass dendrobine along with *D. nobile* stem dendrobine and standard chemical reference dendrobine showed similar dendrobine (263 molecular weight and 14.96 ± 0.01 retention time). In the case of LC-MS/MS, the *T. longibrachiatum* MD33 was found strongly to produce dendrobine (264.195 molecular weight and 7.51 ± 0.1 retention time) as compared with standard chemical reference dendrobine and *D. nobile* stem dendrobine. Previous research on the metabolite profile of *D. nobile* has revealed that dendrobine, an alkaloid found in *D. nobile*, is a hydrophobic weak base, related to the picrotoxin family of natural products, and has a molecular weight of 263 in GC-MS (Yamamura and Hirata, 1964) and 264.195 in LC-MS, UHPLC system (Wang et al., 2016), with a chemical structure of $C_{16}H_{25}NO_2$. The findings of the present study will be an important research breakthrough to fulfill the market demands of dendrobine production in the future.

It is well known that endophytic fungi are considered "biofactories" of bioactive products for the development of natural products besides active biological mediators (ABMs) compared to phytopathogens, because they show beneficial functions on host herbs. In the present study, the biocontrol potential of cultivable endophytic fungi harbored in *D. nobile* was described. Furthermore, *Trichoderma* species are currently utilized as growth promoters or bio-fertilizers in the agricultural industry (Manganyi et al., 2018). Our present study showed that *T. longibrachiatum* MD33 strain was effective for growth mitigation of phytopathogenic bacteria found in the rhizospheric wastewater-contaminated soil. The *T. longibrachiatum* MD33 was effective for inhibiting the growth of most of the pathogenic bacteria tested (*B. subtilis*, *B. mycoides*, and *Staphylococcus* sp.). These findings are in accordance with the results of Nwakanma et al. (2016). The previous findings revealed that fungal endophytes belonging to *Aspergillus* (Mousavi et al., 2016) and *Penicillium* (Chowdhary et al., 2016) genus have shown antibacterial activity. Our study has also shown that *T. longibrachiatum* MD33 also contained compounds that were active against plant bacterial pathogens and rhizosphere soil-contaminated (wastewater) pathogenic microorganisms. We suggest that fungal endophytes can play important functions to support the survival of host herbs against development of phytobacterial diseases because the contaminated wastewater has favored the existence of pathogenic bacteria in the rhizosphere regions. The *T. longibrachiatum* MD33 metabolite can be used for the cleanup of pathogenic bacteria for plants as well as from the wastewater.

Finally, dendrobine, a major component of *D. nobile*, but now from *T. longibrachiatum* MD33 (as an alternative source of dendrobine), has caught the attention of researchers worldwide for its wide applications in the pharmaceutical and medical field. More importantly, the results provide valuable information on the full practical application of HPLC, GC-MS, and LC-MS/MS for the accurate detection of dendrobine as compared with *D. nobile* stem and standard chemical reference

dendrobine (**Figures 2–4**). Dendrobine was firstly extracted in 1932 (from *D. nobile* Lindl) through detection from the Chinese herb *D. nobile*. The chemical structural formula of dendrobine was $C_{16}H_{25}NO_2$, molecular weight 263, melting at 134–136°C, soluble in chloroform, and insoluble in ethanol and water (Yamamura and Hirata, 1964). However, there is still no report on the alternative production of dendrobine from fungal sources. In this study, we recognized a simple, accurate, and rapid method for the chloroform extraction and detection of dendrobine in *T. longibrachiatum* MD33 using HPLC, GC-MS, and LC-MS/MS. Chloroform is an active solvent for natural bioactive compounds in their base form and thus fungal material is regularly extracted with chloroform for bioactive compound investigation. Dendrobine bioactive compound is strictly hydrophobic. Chloroform extraction is used for extraction of dendrobine bioactive compound. Furthermore, HPLC was used for the preliminary detection of dendrobine, but for strong chemical and structural confirmation, the GC-MS (*T. longibrachiatum* MD33 dendrobine molecular weight 263) and LC-MS/MS (*T. longibrachiatum* MD33 dendrobine molecular weight 264.195) techniques gave clear evidence of *T. longibrachiatum* MD33 dendrobine, which was never seen in any science research database. In the future, the pure form of *T. longibrachiatum* MD33 dendrobine will be used for the determination of dendrobine function and applications for pharmacokinetic investigation, which will give more insights into the function and applicability of the *T. longibrachiatum* MD33 dendrobine.

In summary, the dendrobine produced by *T. longibrachiatum* MD33 endophytic fungi was reported for the first time. The characterization of *T. longibrachiatum* MD33 biomass using highly accurate HPLC, GC-MS, and LC-MS/MS analysis showed that the similar peak retention time and molecular weight of dendrobine were observed as compared with standard chemical reference dendrobine and *D. nobile* stem dendrobine, indicating the strong evidence of the presence of dendrobine. Furthermore, *T. longibrachiatum* MD33 endophytic fungi metabolite showed antibacterial effects against phytopathogenic bacteria. In conclusion, this study can lay the foundation for therapeutic application of an alternative source of dendrobine from *T. longibrachiatum* MD33 endophytic fungi in medical and biotechnology fields.

DATA AVAILABILITY STATEMENT

The datasets generated for this study are available on request to the corresponding author.

AUTHOR CONTRIBUTIONS

SS, JC, and JS conceived and designed the experiments. SS, AJ, and XF performed the experiments. SS and JC analyzed the data. QJ, FS, QZ, and QX contributed reagents, materials, and analysis tools. SS wrote and edited the manuscript.

FUNDING

The authors are grateful for the financial support from the Distinguished High-Level Talents Research Grant from a Guizhou Science and Technology Corporation Platform Talents Fund [Grant Nos. (2017)5733-001, and CK-1130-002] and Zunyi Medical University for their advance research facility.

ACKNOWLEDGMENTS

We thank all our laboratory colleagues especially Dr. Xiwu Pan, Mr. Chen Hong Bo, and Ms. Tingwang Xiong for their support.

REFERENCES

Bahroun, A., Jousset, A., Mhamdi, R., Mrabet, M., and Mhadhbi, H. (2018). Anti-fungal activity of bacterial endophytes associated with legumes against *Fusarium solani*: assessment of fungi soil suppressiveness and plant protection induction. *Appl. Soil Ecol.* 124, 131–140. doi: 10.1016/j.apsoil.2017.10.025

Balouiri, M., Sadiki, M., and Ibnsouda, S. K. (2016). Methods for in vitro evaluating antimicrobial activity. *J. Pharma. Analy.* 6, 71–79. doi: 10.1016/j.jpha.2015.11.005

Barnett, H. L., and Hunter, B. B. (1998). *Illustrated Genera of Imperfect Fungi*, 3rd Edn, Philippines: ABS Press.

Chowdhary, A., Agarwal, K., and Meis, J. F. (2016). Filamentous fungi in respiratory infections. What lies beyond *Aspergillosis* and *Mucormycosis*? *PLoS Pathog.* 12:e1005491. doi: 10.1371/journal.ppat.1005491

Deng, Y., Li, M., Chen, L. X., Chen, X. Q., Lu, J. H., Zhao, J., et al. (2018). Chemical characterization and immunomodulatory activity of acetylated polysaccharides from *Dendrobium devonianum*. *Carbohydr. Polym.* 180, 238–245. doi: 10.1016/j.carbpol.2017.10.026

Dey, A., Bhattacharya, R., Mukherjee, A., and Pandey, D. K. (2017). Natural products against Alzheimer's disease: pharmaco-therapeutics and biotechnological interventions. *Biotechnol. Adv.* 35, 178–216. doi: 10.1016/j.biotechadv.2016.12.005

Donga, S., Moteriya, P., and Chanda, S. (2017). Evaluation of antimicrobial and synergistic antimicrobial properties of *Pterocarpus santalinus*. *Asian J. Pharm. Clin. Res.* 10, 204–209.

Elgorban, A. M., Bahkali, A. H., and Wahab, M. A. A. (2019). Natural products of *Alternaria* sp., an endophytic fungus isolated from *Salvadora persica* from Saudi Arabia. *Saudi J. Biol. Sci.* 26, 1068–1077. doi: 10.1016/j.sjbs.2018.04.010

Ellis, M. B. (1976). *Dematiaceous Hyphomycetes*. Kew: International Mycological Institute.

Ghorbanpour, M., Omidvari, M., Dahaji, P. A., Omidvar, R., and Kariman, K. (2018). Mechanisms underlying the protective effects of beneficial fungi against plant diseases. *Biol. Control.* 117, 147–157. doi: 10.1016/j.biocontrol.2017.11.006

Hegazy, A. K., Abdel-Ghani, N. T., and El-Chaghaby, G. A. (2011). Phytoremediation of industrial wastewater potentiality by *Typha domingensis*. *Int. J. Environ. Sci.* 8, 639–648. doi: 10.1007/bf03326249

Hoysted, G. A., Kowal, J., Jacob, A., Rimington, W. R., Duckett, J. G., Pressel, S., et al. (2018). A mycorrhizal revolution. *Curr. Opin. Plant Biol.* 44, 1–6. doi: 10.1016/j.pbi.2017.12.004

Jain, A., Sarsaiya, S., Wu, Q., Lu, Y., and Shi, J. (2019). A review of plant leaf fungal diseases and its environment speciation. *Bioengineered* 10, 409–424. doi: 10.1080/21655979.2019.1649520

Jiang, C., Luo, Y., Yuan, Y., Dong, X., Zhao, Y., and Huang, L. (2018). Conventional octaplex PCR for the simultaneous identification of eight mainstream closely related *Dendrobium* species. *Ind. Crops Prod.* 112, 569–576. doi: 10.1016/j.indcrop.2017.12.048

Khamchatra, N. M., Dixon, K., Chayamarit, K., Apisitwanich, S., and Tantiwiwat, S. (2016). Using in situ seed baiting technique to isolate and identify endophytic and mycorrhizal fungi from seeds of a threatened epiphytic orchid, *Dendrobium friedericksianum* Rchb.f. (Orchidaceae). *Agri. Nat. Resour.* 50, 8–13. doi: 10.1016/j.anres.2016.01.002

Kosawang, C., Amby, D. B., Bussaban, B., McKinney, L. V., Xu, J., Kjær, E. D., et al. (2018). Fungal communities associated with species of *Fraxinus* tolerant to ash dieback, and their potential for biological control. *Fungal Biol.* 122, 110–120. doi: 10.1016/j.funbio.2017.11.002

Kusari, S., Hertweck, C., and Spiteller, M. (2012). Chemical ecology of endophytic fungi: origins of secondary metabolites. *Chem. Biol.* 19, 792–798. doi: 10.1016/j.chembiol.2012.06.004

Lam, Y., Ng, T. B., Yao, R. M., Shi, J., Xu, K., Sze, S. C. W., et al. (2015). Evaluation of chemical constituents and important mechanism of pharmacological biology in *Dendrobium* Plants. *J. Evid. Based Complement. Altern. Med.* 2015:841752. doi: 10.1155/2015/841752

Li, J. L., Zhao, Z., Liu, H. C., Luo, C. L., and Wang, H. L. (2017). Influence of light intensity and water content of medium on total dendrobine of *Dendrobium nobile* Lindl. *Asian Pac. J. Trop. Med.* 10, 1095–1100. doi: 10.1016/j.apjtm.2017.10.015

Manganyi, M. C., Regnier, T., Kumar, A., Bezuidenhout, C. C., and Ateba, C. N. (2018). Biodiversity and antibacterial screening of endophytic fungi isolated from *Pelargonium sidoides*. *South Afr. J. Bot.* 116, 192–199. doi: 10.1016/j.sajb.2018.03.016

Meng, C. W., He, Y. L., Peng, C., Ding, X. J., Guo, L., and Xiong, L. (2017). Picrotoxane sesquiterpenoids from the stems of *Dendrobium nobile* and their absolute configurations and angiogenesis effect. *Fitoterapia* 121, 206–211. doi: 10.1016/j.fitote.2017.07.017

Mousavi, B., Hedayati, M. T., Hedayati, N., Ilkit, M., and Syedmousavi, S. (2016). *Aspergillus* species in indoor environments and their possible occupational and public health hazards. *Curr. Med. Mycol.* 2, 36–42. doi: 10.18869/acadpub.cmm.2.1.36

Nalini, M. S., Sunayana, N., and Prakash, H. S. (2014). Endophytic fungal diversity in medicinal plants of Western Ghats, India. *Inter. J. Biodiver.* 9:494213. doi: 10.1155/2014/494213

Nascimento, T. L., Oki, Y., Lima, D. M. M., Almeida-Cortez, J. S., Fernandes, G. W., and Souza-Motta, C. M. (2015). Biodiversity of endophytic fungi in different leaf ages of *Calotropis procera* and their antimicrobial activity. *Fungal. Ecol.* 14, 79–86. doi: 10.1016/j.funeco.2014.10.004

Nie, J., Tian, Y., Zhang, Y., Lu, Y.-L., Li, L.-S., and Shi, J.-S. (2016). *Dendrobium* alkaloids prevent Aβ25–35-induced neuronal and synaptic loss via promoting neurotrophic factors expression in mice. *PeerJ* 4:e2739. doi: 10.7717/peerj.2739

Nwakanma, N., Njoku, E. N., and Pharamat, T. (2016). Antimicrobial activity of secondary metabolites of fungi isolated from leaves of bush mango. *J. Next Gen. Seq. Appl.* 3, 1–6. doi: 10.4172/2469-9853.1000135

Pham, J. V., Yilma, M. A., Feliz, A., Majid, M. T., Maffetone, N., Walker, J. R., et al. (2019). A review of the microbial production of bioactive natural products and biologics. *Front. Microbiol.* 10:1404. doi: 10.3389/fmicb.2019.01404

Raghavendra, A. K. H., Bissett, A. B., Thrall, P. H., Morin, L., Steinrucken, T. V., Galea, V. J., et al. (2017). Characterisation of above-ground endophytic and soil fungal communities associated with dieback-affected and healthy plants in five exotic invasive species. *Fungal Ecol.* 26, 114–124. doi: 10.1016/j.funeco.2017.01.003

Santal, A. R., Singh, N. P., and Singha, T. K. (2019). Characterization of extracellular polymeric substance producing isolates from wastewaters and their antibacterial prospective. *J. Appl. Biol. Biotech.* 7, 56–62. doi: 10.7324/JABB.2019.70609

Sarawaneeyaruk, S., Pringsulaka, O., Wichalek, S., Koto, R., and Sukkhum, S. (2014). The effect of domestic wastewater from Thailand's Saen Saeb canal on plant growth and rhizosphere microorganisms. *Songklanakarin J. Sci. Technol.* 36, 627–632.

Sarsaiya, S., Jain, A., Jia, Q., Fan, X., Shu, F., Chen, Z., et al. (2020). Molecular identification of endophytic fungi and their pathogenicity evaluation against *Dendrobium nobile* and *Dendrobium officinale*. *Int. J. Mol. Sci.* 21:316. doi: 10.3390/ijms21010316

Sarsaiya, S., Jia, Q., Fan, X., Jain, A., Shu, F., Lu, Y., et al. (2019a). First report of leaf black circular spots on *Dendrobium nobile* caused by *Trichoderma longibrachiatum* in Guizhou Province, China. *Plant Dis.* 103:3275. doi: 10.1094/pdis-03-19-0672-pdn

Sarsaiya, S., Shi, J., and Chen, J. (2019b). A comprehensive review on fungal endophytes and its dynamics on orchidaceae plants: current research, challenges, and future possibilities. *Bioengineered* 10, 316–334. doi: 10.1080/21655979.2019.1644854

Sarsaiya, S., Shi, J., and Chen, J. (2019c). Bioengineering tools for the production of pharmaceuticals: current perspective and future outlook. *Bioengineered* 10, 469–492. doi: 10.1080/21655979.2019.1682108

Singh, M., Kumar, A., Singh, R., and Pandey, K. D. (2017). Endophytic bacteria: a new source of bioactive compounds. *3 Biotech.* 7:315. doi: 10.1007/s13205-017-0942-z

Somjaipeng, S., Medina, A., Kwaśna, H., Ortiz, J. O., and Magan, N. (2015). Isolation, identification, and ecology of growth and taxol production by an endophytic strain of *Paraconiothyrium variabile* from English yew trees (*Taxus baccata*). *Fungal Biol.* 119, 1022–1031. doi: 10.1016/j.funbio.2015.07.007

Suryanarayanan, T. S., Thirunavukkarasu, N., Govindarajulu, M. B., Sasse, F., Jansen, R., and Murali, T. S. (2009). Fungal endophytes and bioprospecting. *Fungal Biol. Rev.* 23, 9–19. doi: 10.1016/j.fbr.2009.07.001

Sutantoa, A., Zena, S., and Nor, R. (2016). The formulation of pineapple liquid waste (PLW) as liquid organic fertilizer for agricultural crops. *Sci. J.* 3, 176–181.

Wang, Y. H., Avula, B., Abe, N., Wei, F., Wang, M., Ma, S. C., et al. (2016). Tandem mass spectrometry for structural identification of sesquiterpene alkaloids from the stems of *Dendrobium nobile* using LC-QToF. *Planta Med.* 82, 662–670. doi: 10.1055/s-0042-103031

Xiang, L., Gong, S., Yang, L., Hao, J., Xue, M. F., Zeng, F. S., et al. (2016). Biocontrol potential of endophytic fungi in medicinal plants from Wuhan Botanical Garden in China. *Biol. Control.* 94, 47–55. doi: 10.1016/j.biocontrol.2015.12.002

Yamamura, S., and Hirata, Y. (1964). Structures of nobiline and dendrobine. *Tetrahedron Lett.* 5, 79–87. doi: 10.1016/S0040-4039(00)90333-2

Yu, Y., Ma, B. J., Liu, J. S., Yue, J. Y., Chen, H. P., Liang, Y. M., et al. (2017). Two new alkaloid metabolites produced by endophytic fungus *Stagonosporopsis oculihominis* isolated from *Dendrobium huoshanense*. *Phytochem. Letters.* 19, 266–270. doi: 10.1016/j.phytol.2017.02.006

Zhang, Y., Wang, H., Mei, N., Ma, C., Lou, Z., and He, G. H. (2018). Protective effects of polysaccharide from *Dendrobium nobile* against ethanol-induced gastric damage in rats. *Inter. J. Biol. Macromol.* 107, 230–235. doi: 10.1016/j.ijbiomac.2017.08.175

Zheng, Y. K., Miao, C. P., Chen, H. H., Huang, F. F., Xia, Y. M., Chen, Y. W., et al. (2017). Endophytic fungi harbored in Panax notoginseng: diversity and potential as biological control agents against host plant pathogens of root-rot disease. *J. Ginseng Res.* 41, 353–360. doi: 10.1016/j.jgr.2016.07.005

Ziaee, A., Zia, M., Bayat, M., and Hashemi, J. (2016). Molecular identification of *Mucor* and *lichtheimia* species in pure cultures of zygomycetes. *Jundishapur J. Microbiol.* 9, 1–8. doi: 10.5812/jjm.35237

Conflict of Interest: The authors declare that the research was conducted in the absence of any commercial or financial relationships that could be construed as a potential conflict of interest.

frontiers in Microbiology

ORIGINAL RESEARCH
published: 15 April 2020
doi: 10.3389/fmicb.2020.00544

Cellular Analysis and Comparative Transcriptomics Reveal the Tolerance Mechanisms of *Candida tropicalis* Toward Phenol

Hanyu Wang[1†], Qian Li[1†], Yuanyuan Peng[1†], Zhengyue Zhang[1†], Xiaolin Kuang[1], Xiangdong Hu[1], Ellen Ayepa[1], Xuebing Han[1], Getachew Tafere Abrha[1], Quanju Xiang[2], Xiumei Yu[2], Ke Zhao[2], Likou Zou[2], Yunfu Gu[2], Xi Li[3], Xiaoying Li[4], Qiang Chen[2], Xiaoping Zhang[2], Beidong Liu[5,6] and Menggen Ma[1,2]**

[1] Institute of Resources and Geographic Information Technology, College of Resources, Sichuan Agricultural University, Chengdu, China, [2] Department of Applied Microbiology, College of Resources, Sichuan Agricultural University, Chengdu, China, [3] College of Landscape Architecture, Sichuan Agricultural University, Chengdu, China, [4] School of Forestry and Life Science, Chongqing University of Arts and Sciences, Chongqing, China, [5] Department of Chemistry and Molecular Biology, University of Gothenburg, Göteburg, Sweden, [6] State Key Laboratory of Subtropical Silviculture, School of Forestry and Biotechnology, Zhejiang A&F University, Hangzhou, China

OPEN ACCESS

Edited by:
Sanjay Prabhu Govindwar, Shivaji University, India

Reviewed by:
Vishwas Ananat Bapat, Shivaji University, India
Ashutosh Singh, University of Lucknow, India

***Correspondence:**
Beidong Liu
beidong.liu@cmb.gu.se
Menggen Ma
mgen@sicau.edu.cn

[†] These authors have contributed equally to this work

Specialty section:
This article was submitted to Microbiotechnology, a section of the journal Frontiers in Microbiology

Received: 21 January 2020
Accepted: 12 March 2020
Published: 15 April 2020

Citation:
Wang H, Li Q, Peng Y, Zhang Z, Kuang X, Hu X, Ayepa E, Han X, Abrha GT, Xiang Q, Yu X, Zhao K, Zou L, Gu Y, Li X, Li X, Chen Q, Zhang X, Liu B and Ma M (2020) Cellular Analysis and Comparative Transcriptomics Reveal the Tolerance Mechanisms of Candida tropicalis Toward Phenol. Front. Microbiol. 11:544. doi: 10.3389/fmicb.2020.00544

Phenol is a ubiquitous pollutant and can contaminate natural water resources. Hence, the removal of phenol from wastewater is of significant importance. A series of biological methods were used to remove phenol based on the natural ability of microorganisms to degrade phenol, but the tolerance mechanism of phenol-degraded strains to phenol are not very clear. Morphological observation on *Candida tropicalis* showed that phenol caused the reactive oxygen species (ROS) accumulation, damaging the mitochondrial and the endoplasmic reticulum. On the basis of transcriptome data and cell wall susceptibility analysis, it was found that *C. tropicalis* prevented phenol-caused cell damage through improvement of cell wall resistance, maintenance of high-fidelity DNA replication, intracellular protein homeostasis, organelle integrity, and kept the intracellular phenol concentration at a low level through cell-wall remodeling and removal of excess phenol via MDR/MXR transporters. The knowledge obtained will promote the genetic modification of yeast strains in general to tolerate the high concentrations of phenol and improve their efficiency of phenol degradation.

Keywords: *Candida tropicalis*, morphological observation, phenol, reactive oxygen species (ROS), tolerance mechanism, transcriptome

INTRODUCTION

Phenol, one of the aromatic compounds, is composed of the hydroxyl group and the benzene ring and is applied as the main material for the production of pesticides, antiseptics, slimicides, and medicinal preparations (Mishra and Kumar, 2017) but contaminate the natural water resources. It was found that the inhalation, skin contact, and ingestion of phenol can lead to damages of central nervous system (CNS) disorders and the kidneys (Mahgoub et al., 2014; Mishra and Kumar, 2017).

Hence, the removal of phenol from wastewater is quite important for environmental protection and for the human health. A series of physicochemical methods have been explored and applied to remove phenol from the wastewater (Pinto et al., 2005; Matjie and Engelbrecht, 2007; Busca et al., 2008). However, the energy consumption, high cost, hazardous byproducts production, and poor efficiency of these methods limited their widespread applications (Banerjee and Ghoshal, 2011). The natural ability of microorganisms to degrade phenol, and a few biological treatments of phenol are explored and found to be more efficient than physicochemical methods (Jiang et al., 2005; Banerjee and Ghoshal, 2011; Yoneda et al., 2016). It is a challenge for the wide applications of biological methods that these compounds are toxic to microbial cells, can prolong the lag phase, and reduce the phenol degradation efficiency (Heipieper et al., 1991). Additionally, phenol can penetrate the cellular membrane and cause the increased membrane permeability and decreased membrane lipid-to-protein ratios (Heipieper et al., 1991), and can cause dysfunction of organelles. The membrane disruption of mitochondria induced by phenol can induce the accumulation of excessive ROS (Klaunig et al., 2011), which interact with proteins, DNA, and lipids, and then result in damage of cytoskeleton, DNA mutagenesis, and the programmed cell death (Ibraheem and Ndimba, 2013). Hence, the phenol tolerance of microorganisms is vital to the effective degradation of phenol as well as screening and isolation of phenol-tolerant strains and deciphering of their tolerance mechanisms are immensely important.

Although recent studies found that chromatin remodeling, efflux of toxic compounds, and aggregation of lipopolysaccharides on the outer cell membrane could increase the resistance of microorganisms to phenolic aldehydes derived from lignocellulose pretreatment (Gu et al., 2015; Yi et al., 2015), a part of the above mechanisms might be associated with the aldehyde tolerance. Another study focused on *R. opacus* PD630 found that phenol tolerance mainly involved the import and degradation of extracellular phenol (Yoneda et al., 2016), but the understanding of the tolerance mechanisms, not degradation mechanisms, of strains to phenol is not very clear.

C. tropicalis can not only utilize a range of carbon sources but also produce a range of biological products, including bioethanol, xylitol, and long-chain dicarboxylic acids (Horitsu et al., 1992; Kurihara et al., 1992; Sampaio, 1999). Additionally, *C. tropicalis* can tolerate high concentrations of phenol, salts, heat, furfural, and acetic acid (Adav et al., 2007; Wang et al., 2015). The genome of *C. tropicalis* has been completely sequenced (Butler et al., 2009), enabling to explore the molecular mechanisms of *C. tropicalis* in different conditions and considered as one of the promising strains for deciphering the tolerance mechanisms of microorganisms to phenol. Previous studies on the tolerance mechanisms of *C. tropicalis* to phenol have been focused on the degradation of phenol by biodegradation (Jiang et al., 2005; Klaunig et al., 2011), but not the molecular and cellular mechanisms. In this study, pre-cultured cells of *C. tropicalis* strain SHC-03 were treated with phenol in order to explore the above mechanisms via fluorescence microscopy and comparative transcriptomics.

MATERIALS AND METHODS

Yeast Growth Conditions and Reagents

C. tropicalis SHC-03, isolated from a winery in She Hong, was grown in YPD medium (w/v, 1% yeast extract, 2% peptone, and 2% glucose) and in YPD medium supplemented with 0.5, 1.0, 2.0, and 3.0 g/L phenol with 200 rpm shaking at 30°C. The initial cell count in the culture was adjusted to ∼1.0 × absorbance value (optical density at 600 nm wavelength, OD_{600}). With non-phenol-treated culture as control, the pre-cultures were cultivated in YPD medium overnight, then harvested by centrifugation at 4,000 rpm for 3 min at 4°C, and inoculated into 50 mL flasks with phenol-added YPD medium. Aliquots of cells and supernatant were harvested for analysis at various time points from 0 to 72 h. Cell density (OD_{600}) of the cultures was determined by using a UV-2802 spectrophotometer (Unico, NJ, United States). Media ingredients were purchased from Sigma-Aldrich (St. Louis, MO, United States) or Sangon Biotech (Shanghai, China).

Determination of Phenol Degradation Rate

The concentration of residual phenol was determined by the 4-aminoantipyrine spectrophotometric method. The reaction among phenol, 4-aminoantipyrine and potassium ferricyanide will develop a red color under alkaline conditions which can be measured by reading the absorbance at 510 nm (OD_{510}).

qRT-PCR Assays

To confirm the accuracy of results from RNA-seq, the qRT-PCR assay of the isolated mRNA for RNA-seq were implemented on a Mastercycler® EP Realplex system (Eppendorf, Hamburg, Germany), using the procedures reported previously (Anders and Huber, 2010). A FastQuant RT Kit (With gDNase) and a Real Master Mix (SYBR Green) Kit (Tiangen Biotech Co., Ltd.) were respectively exploited to synthesize the first-strand cDNA and quantitative PCR reactions. Before qRT-PCR reactions were carried out, a calibrated messenger RNA (mRNA) control mix, which was gifted by Z. Lewis Liu (Bioenergy Research, NCAUR-ARS, US Department of Agriculture, Peoria, IL, United States), was integrated into the reaction system as a reference. Using online software of primer3[1], the primers of the selected genes were designed for qRT-PCR assay (**Supplementary Table S1**). In the qRT-PCR reactions, three biological replicates and three technical replicates were performed, and the acquired data was analyzed using the developed methods (Liu and Slininger, 2007).

RNA-Seq and Analysis

After the pre-cultured cells of *C. tropicalis* SHC-03 were transferred into the YPD mediums with different concentration of phenol, the phenol-treated cells and the non-phenol-treated cells were obtained at 3 h for RNA-Seq. RNA-Seq was conducted by Biomarker Technology Co. Ltd. (Beijing, China) with Hiseq-PE150 (Illumina, Inc., San Diego, CA United States). Based on the sequence of *C. tropicalis* MYA-3404 as reference genome,

[1]http://bioinfo.ut.ee/primer3-0.4.0/primer3/

we analyzed the raw data by the BMKCloud cloud server[2]. The gene expression levels were analyzed using fragments per kilobase of the transcript per million mapped (FPKM) method (Florea et al., 2013). Differential expression analysis of two samples with three biological replicates was performed using the DEGseq R package (Anders and Huber, 2010) in a threshold criterion of the value of $|\log_2(\text{fold change})| \geq 1$ (FDR < 0.05). The annotations of differentially expressed genes (DEGs) were performed by the GO (Ashburner et al., 2000) and KEGG (Kanehisa et al., 2004) databases. We performed the statistical tests to identify the DEGs enriched in different KEGG pathways using KOBAS software (Mao et al., 2005).

Fluorescence Microscopy and Cellular Analysis

The fluorescence microscopy, an Axio Imager A2 microscope (Carl Zeiss AG, Oberkochen, Germany) equipped with DIC, GFP, Rhod and DAPI filter lens, and different dyes, including 2′,7′-dichlorofluorescein diacetate (DCFH-DA), diaminophenylindole (DAPI), Mito Tracker™ Green FM, ER-Tracker™ Red, and Yeast Vacuole Membrane Marker MDY-64, were used to observe the integrity of the cellular structures to evaluate the accumulation of ROS, nuclear chromatin disorganization, mitochondrial membrane damage, endoplasmic reticulum membrane damage, and vacuole membrane damage. The processing procedure is carried out according to the corresponding experimental instruction, respectively (**Supplementary Material 2**). Before the harvested cells were stained by various dyes, all the reagents and buffers have been preheated at 30°C. To ensure the accuracy of experiment results, at least 100 cells were examined on each bright-field image.

Determination of Intracellular SOD, CTT, GPX, GLR Activity, and GSH Content

After the pre-cultured cells of *C. tropicalis* SHC-03 were transferred into the YPD mediums with different concentration of phenol, the phenol-treated cells and the non-phenol-treated cells were harvested at 3, 6, and 9 h for determination of intracellular SOD, GPX, CTT, GLR activity, and GSH content. The corresponding values was detected using SOD, GPX, CTT, GLR, and GSH assay kit purchased from Solarbio (Beijing, China) according to the manufacturer's instructions, respectively.

Cell Wall Susceptibility Analysis

To understand the structural changes of cell wall induced by phenol, we performed the lyticase-dependent susceptibility analysis (Teixeira et al., 2009). Lyticase, a β-1,3-glucanase from *Arthrobacter luteus*, was purchased from Sigma-Aldrich (St. Louis, MO, United States). 10^7 cells, harvested from different mediums with or without phenol, were washed twice with ultrapure water and resuspended in 2.0 mL PBS pH 7.0. Sixty microliters of a 2 mgmL lyticase was mixed into the cell suspensions, the decrease in the OD_{600} of each cell suspension was detected from 0 to 4 h.

[2]http://www.biocloud.net

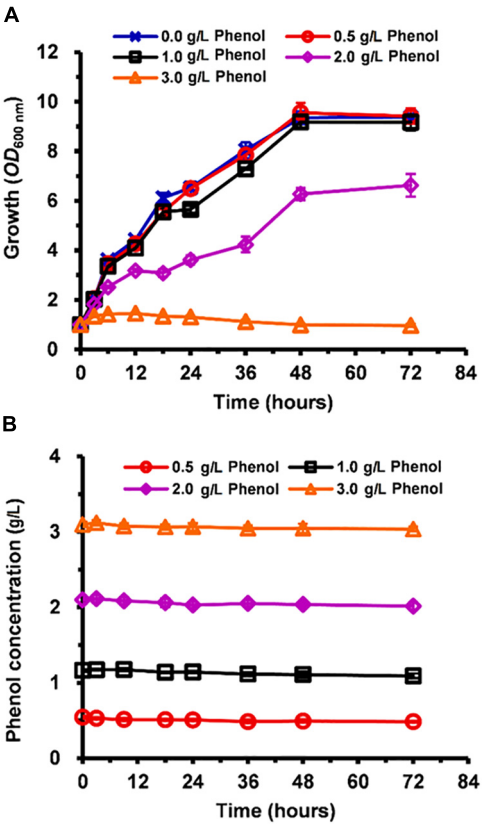

FIGURE 1 | Inhibition of *C. tropicalis* SHC-03 cell growth by different concentrations of phenol. **(A)** Cell growth as measured by reading absorbance at 600 nm (OD_{600}). **(B)** Phenol consumption.

RESULTS

Growth and Phenol Consumption in Phenol-Supplemented Medium

Compared with the non-phenol-treated culture, the cell growth of phenol-treated *C. tropicalis* SHC-03 was slightly inhibited when the media contained 0.5 and 1.0 g/L phenol (**Figure 1A**). However, in the presence of 2.0 and 3.0 g/L phenol, cell growth was hindered by ∼40 and 100%, respectively (**Figure 1A**). The growth rate of cells treated with 2.0 g/L phenol remained at a low level from 3 to 24 h, implying that phenol influenced cell growth (**Figure 1A**). However, the cells returned to normal levels of growth after treatment for 24 h in the presence of 2.0 g/L phenol. The 4-aminoantipyrine spectrophotometric method revealed no significant change in the concentration of phenol in any of the treatments at 0–72 h (**Figure 1B**), which indicated that the phenol degradation mechanism of *C. tropicalis* SHC-03 was not activated in these conditions. To summarize, a range of tolerance mechanisms for protecting cells from the toxic damage of phenol were activated during the lag phase and RNA-seq technology and cytological techniques demonstrated the potential tolerance mechanisms of *C. tropicalis* to phenol.

RNA-Seq, Transcriptomic Analysis, and qRT-PCR Assays

After incubation with or without phenol for 3 h, the cells were harvested for RNA-seq. Sequence reads data were archived at NCBI sequence read archive (SRA) with Accession Number PRJNA591802. The quality-control test results showed that the quality score (Q_{30}), clean data, and sequencing depth of each sample were, respectively, more than 94%, 4 Gb, and 675× (**Supplementary Table S2**), which indicated a high level of accuracy for the RNA-seq results. To mitigate errors induced by biological variability between the samples, three biological replicates were used for the RNA-seq. The classification of the groups receiving different concentrations of phenol have been illustrated in **Figure 2A**, the correlations between T01, T06, T09 and their corresponding biological replicates were relatively low. To guarantee reliability and accuracy of the results from the differential expression analysis, T01, T06, and T09 were eliminated (**Figure 2B**).

The expression pattern of the 0.5 g/L phenol group was highly consistent with that of the control group; only 39 genes and 40 genes showed up- and down-regulated expression, respectively, with twofold changes in the 0.5 g/L phenol group compared with the control (**Figures 2D,E**). In contrast, for the 1.0 and 2.0 g/L phenol groups, 353 and 1,985 genes showed altered expression levels, respectively (**Figure 2C**). Among these genes, 215 and 1,050 genes were identified as up-regulated genes in the 1.0 and 2.0 g/L phenol groups, respectively (**Figure 2D**), and 138 and 935 genes, respectively, were repressed by phenol (**Figure 2E**).

In this study, 21 differentially expressed genes in response to 1.0 g/L phenol were selected for the accuracy of the results from RNA-seq through a qRT-PCR assay. The criterion for gene selection was a combination of high-low gene expression level (FPKM) and absolute value of $\log_2$(fold change). Through comparison and analysis, the expression levels of 18 of 21 genes (∼85%) were consistent in the trend of up- and down-regulation (**Figure 2F**). Of the other three genes, inconsistent with the data from RNA-seq, two displayed lower absolute values of $\log_2$(fold change) (**Figure 2F**). The results from RNA-Seq showed high accuracy, which contributed to the exploration of the phenol tolerance mechanism utilized by *C. tropicalis*.

Accumulation and Scavenging of Reactive Oxygen Species (ROS) in Cells

In order of increasing damage, to phenol stress, mitochondrial membrane showed different types of morphologies these were: tubular, fragmented, aggregated shapes, and necrotic (**Figure 3A**). At 3 h, cells grown in media containing 0.0 and 0.5 g/L phenol displayed tubular and fragmented mitochondria, while cells grown in media containing 2.0 and 3.0 g/L phenol displayed aggregated and necrotic mitochondria (**Figure 3C**). In contrast, at 9 h, only 3% of the non-phenol-treated cells appeared to be necrotic. At the same time point, among cells grown in 0.5 g/L phenol, the percentage of cells with aggregated and necrotic mitochondria remained at a low level (**Figure 3C**). At 18 h, cells with tubular mitochondria were no longer seen in cells grown in media with or without phenol. In addition, compared with the results at 3 and 9 h, the distribution of cells containing aggregated mitochondria increased tremendously, with 95% of the yeast cells cultured in 1.0 g/L phenol showing aggregated mitochondria at 18 h. Furthermore, in cells cultured in 2.0 and 3.0 g/L phenol, the proportion of necrotic cells increased to 33 and 58% at 18 h, respectively (**Figure 3C**). In summary, the ratio of mitochondrial deformation increased with the elevation of phenol concentration and treatment duration.

As most of the exogenous ROS were produced by damaged mitochondria (Klaunig et al., 2011), ROS accumulation of the treated and untreated cells was detected. The percentage of cells staining positive for ROS was considered to be representative of severity of oxidative stress (**Figure 3B**). Cultures in media containing 2.5, 5.0, and 7.5 mM hydrogen peroxide served as the positive controls for ROS (**Figure 3D**). In the medium without phenol, at 3 and 9 h after treatment, 5.6 and 6.5% of the cells exhibited a positive ROS signal, respectively (**Figure 3D**). At 3 h, 9.1, 10.2, 30.3, and 42.1% of cells stained positive for ROS when 0.5, 1.0, 2.0, and 3.0 g/L phenol were present, respectively (**Figure 3D**), showing that the proportion of cells with ROS increased with increasing phenol concentration. At 9 h, the percent of cells staining positive for accumulated ROS was 5.7, 12.8, 11.6, and 100.0%, respectively (**Figure 3D**). The above results implied that the accumulation of ROS reached its peak 3 h after the treatment, while the accumulation of excessive ROS at this time might cause damage to DNA, proteins, and lipids (Gourlay and Ayscough, 2005; Perrone et al., 2008; Rowe et al., 2008), and that the intracellular ROS were eliminated by several molecular mechanisms between 3 and 9 h after the treatment.

Based on the transcriptome data, we found that the expression levels of most of these genes were not significantly up-regulated against 0.5, 1.0, and 2.0 g/L phenol (**Supplementary Table S3**). Among these genes, CTRG_04448, CTRG_04203, CTRG_01769, CTRG_00610, and CTRG_05111 exhibited 4.3-, 2.3-, 2.1-, 4.0-, and 3.2-fold down-regulation, and CTRG_03986, CTRG_00152, CTRG_06042, and CTRG_02189 displayed 3.0-, 2.5-, 2.1-, and 2.6-fold up-regulation when exposed to 2.0 g/L phenol (**Supplementary Table S3**). In addition, one of these genes, CTRG_00142, displayed 2.1-fold up-regulation when exposed to 1.0 g/L phenol. The transcriptome data demonstrated that the enzymatic antioxidant defense systems would not be significantly activated for scavenging excessive ROS at 3 h. In contrast, the above results from the determination of ROS showed that the excessive ROS in the phenol-treated cells were scavenged between 3 and 9 h (**Figure 3D**).

The enzyme activity assays was carried out for SOD, CTT, and GPX in the phenol-treated and non-phenol-treated cells which showed that, at 3 h, the enzyme activity of intracellular SOD increased dramatically along with increasing phenol concentration (**Figure 4B**). The SOD activity of cells treated with 2.0 g/L phenol was significantly higher after 6 h than that of the cells treated with 0.0, 0.5, and 1.0 g/L phenol, but the SOD activity in cells treated with 3.0 g/L phenol was considerably lower (**Figure 4B**). The SOD activities of all the treatments were lower at 6 h than those of the corresponding treatments at 3 h. A few samples exhibited any SOD activity at 9 h (**Figure 4B**). Since GPX and CTT are the key enzymes for the reduction of

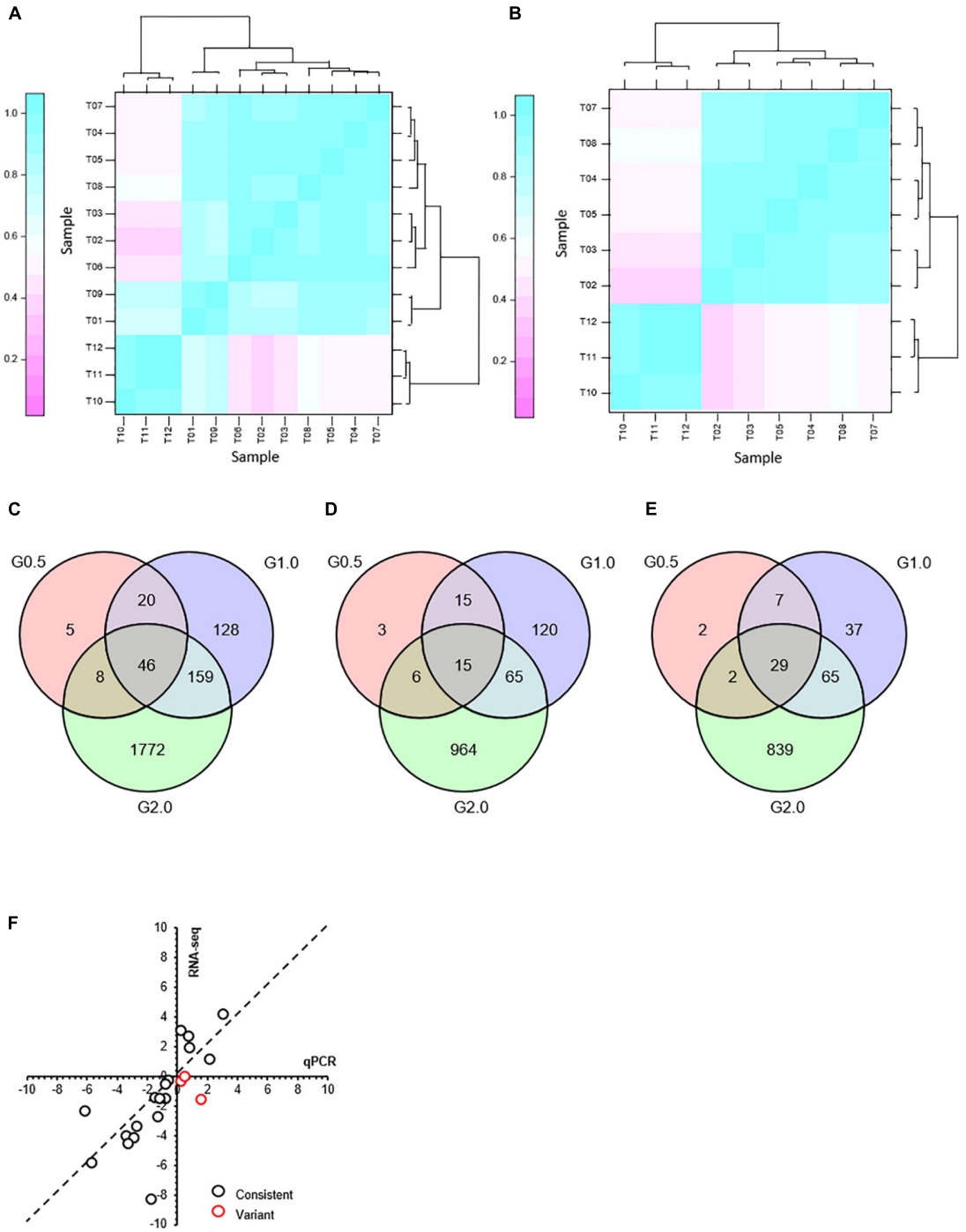

FIGURE 2 | Transcriptome response to phenol after treatment for 3 h and comparison of expression levels of the selected genes as determined by RNA-seq and qRT-PCR. **(A)** Hierarchical cluster analysis of all replications. Replications of each phenol treatment group analyzed for RNA transcription are labeled as follows: 0.0 g/L phenol (T01, T02, T03); 0.5 g/L phenol (T04, T05, T06); 1.0 g/L phenol (T07, T08, T09); 2.0 g/L phenol (T10, T11, T12). Given the $\log_2$(fold change), expression levels of genes were clustered. **(B)** Hierarchical cluster analysis of the replications that did not include samples T01, T06, and T09. After T01, T06, and T09 were eliminated as outliers, three Venn diagrams were created based on differentially expressed genes in response to 0.5 g/L phenol (G0.5), 1.0 g/L phenol (G1.0), and 2.0 g/L phenol (G2.0), compared with the control group. **(C)** Differential expression of all genes. **(D)** Differential expression of up-regulated genes. **(E)** Differential expression of down-regulated genes. **(F)** Comparison of expression levels of the selected genes between the RNA-seq and qRT-PCR. The gene expression ratios of RNA-seq and qRT-PCR for 21 genes in response to 1.0 g/L phenol were calculated according to the values of $\log_2$(fold change) (treatment/control). The 21 selected genes included CTRG_00166, CTRG_00173, CTRG_00423, CTRG_00627, CTRG_00770, CTRG_01068, CTRG_01142, CTRG_01327, CTRG_01443, CTRG_01732, CTRG_01733, CTRG_01777, CTRG_02090, CTRG_02168, CTRG_02702, CTRG_03102, CTRG_03235, CTRG_03453, CTRG_03911, CTRG_03917, and CTRG_03930. The primers for RT-PCR of these selected genes are listed in **Supplementary Table S1**.

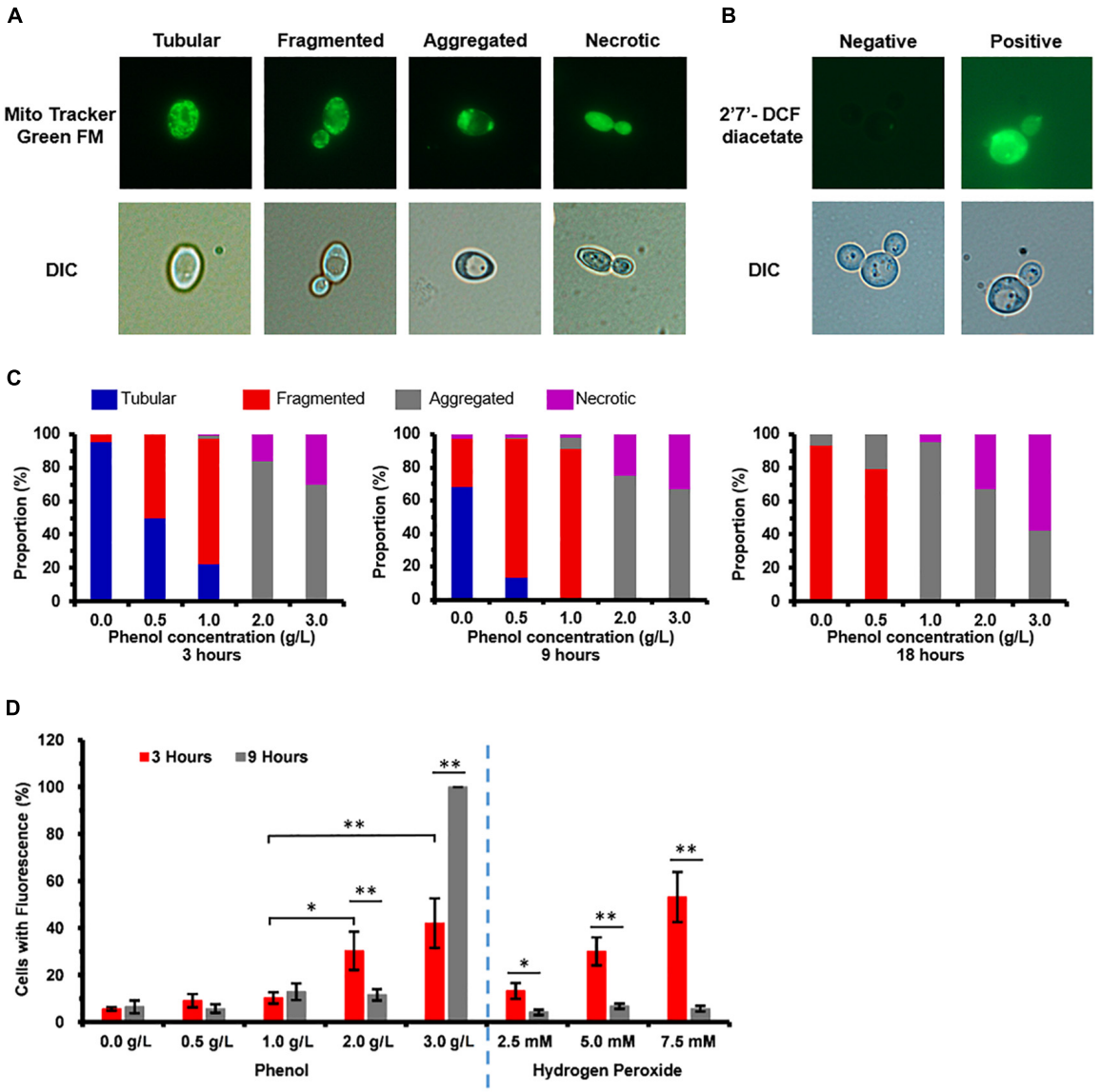

FIGURE 3 | Mitochondrial membrane damage and accumulation of reactive oxygen species (ROS) caused by phenol. Representative images of cells stained with the mitochondria-specific dye Mito Tracker^{TM} Green FM and ROS indicator dye 2′,7′-dichlorofluorescein diacetate (DCFH-DA) are shown in the top column, and images taken using a differential interference contrast (DIC) lens are shown in the bottom column. **(A)** Morphological structure analysis of mitochondria. **(B)** Accumulation analysis of ROS. **(C)** Percentage of cells at each concentration of phenol that displayed tubular, fragmented, and aggregated mitochondria, as well as necrotic, at 3, 9, and 18 h. **(D)** Percentage of cells at each concentration of phenol and hydrogen peroxide that stained positive for ROS by DCFH-DA at 3 and 9 h, with cultures in medium containing 2.5, 5.0, and 7.5 mM hydrogen peroxide as positive controls for ROS. $^{*}p < 0.05$; $^{**}p < 0.01$ indicates significant differences. The data represent averages of three experiments. At least 100 cells were examined on each bright-field image.

H_2O_2, activities of both of the two enzymes were assayed. We found no significant differences in GPX activity in any of the treatments at 3 h. However, cells treated with 1.0 g/L phenol exhibited an increase in GPX activity at 9 h, and cells treated with 2.0 g/L phenol exhibited an increase in GPX activity at 6 and 9 h. At both 6 and 9 h, cells treated with 3.0 g/L phenol had lost their GPX activity almost completely (**Figure 4C**). These results indicated that GPX activity significantly increased in cells treated with 1.0 and 2.0 g/L phenol after 6 and 9 h, but that the high concentration of phenol (3.0 g/L phenol) caused the loss of cellular GPX activity at 6 h. The enzyme activity assays demonstrated no CTT activity in either phenol-treated or non-phenol-treated cells at the different processing times (data not shown). In addition, it has been found that high GLR activity and high GSH content can support high catalytic efficiency of GPX, which could protect the cells against ROS (Gill et al., 2013). In the present study, the enzyme activity of intracellular GLR was found to increase with phenol concentration at different processing times, except in those cells treated with 3.0 g/L phenol, at 6 and 9 h (**Figure 4D**). From the viewpoint of processing time, the

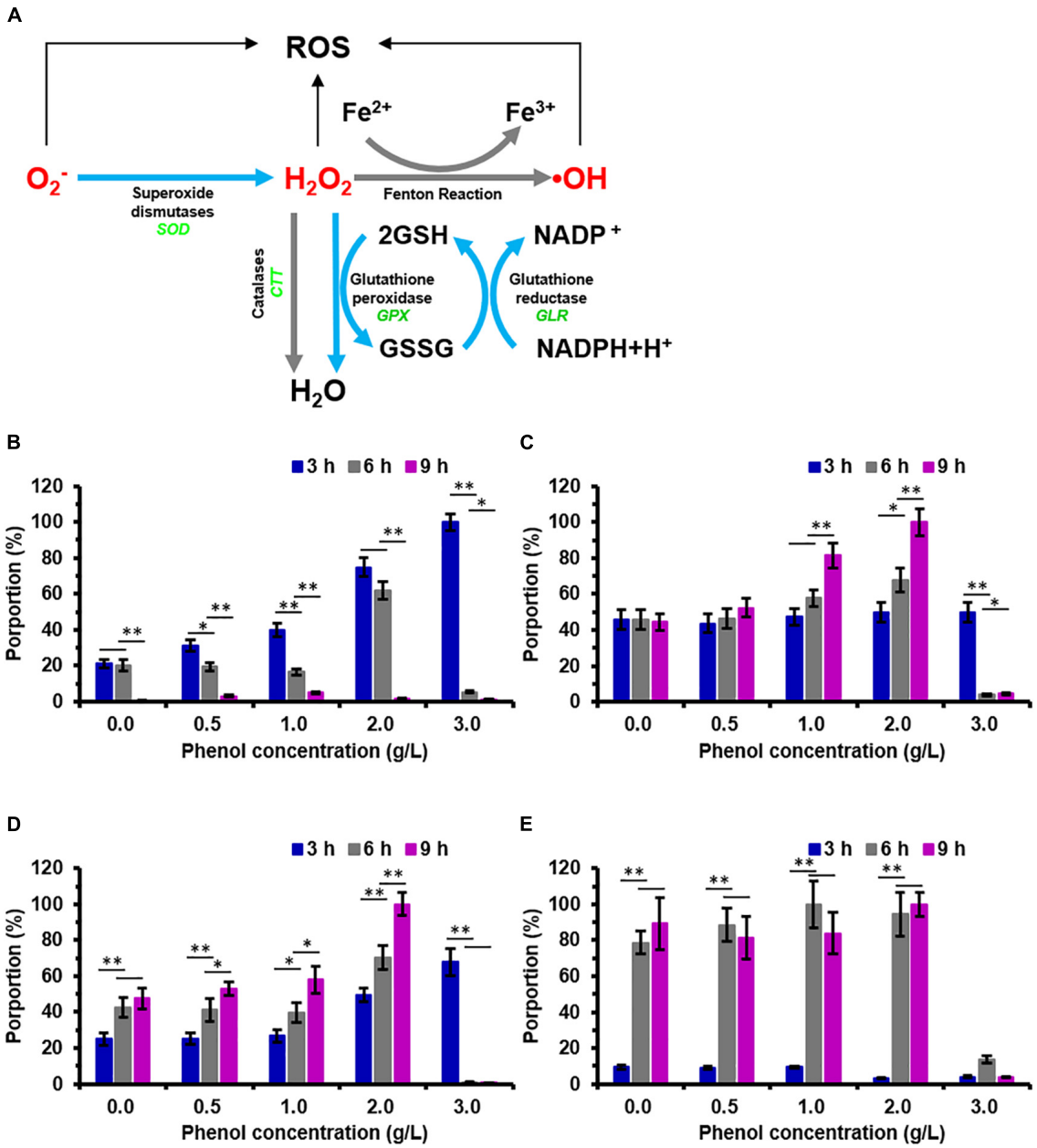

FIGURE 4 | Pathway for reactive oxygen species (ROS) scavenging in *C. tropicalis* SHC-03 and the change in activity of ROS-related enzymes after treatment with phenol. **(A)** The pathway shows the scavenging of reactive oxygen species (ROS) catalyzed by enzymatic antioxidant defense systems containing SOD, GPX, CTT, GLR, and GSH. **(B–E)** Activities of **(B)** SOD, **(C)** GPX, **(D)** GLR, and **(E)** GSH after treatments with 0.0–3.0 g/L phenol for 3, 6, and 9 h. $^{*}p < 0.05$; $^{**}p < 0.01$ indicates significant differences.

cellular GLR activity after treatment for 9 h was higher than that after 3 and 6 h in the presence of 0.0–2.0 g/L phenol. However, no GLR activity could be detected in cells treated with 3.0 g/L phenol, at either 6 or 9 h (**Figure 4D**). The GSH content of cells treated with 2.0 and 3.0 g/L phenol was lower than that in cells treated with less than 2.0 g/L phenol at 3 h. However, after 3 h, the GSH content of cells treated with 0.0–2.0 g/L phenol rose rapidly after 6 and 9 h, and remained at a high level (**Figure 4E**). The GSH content remained at the same level in the presence of different concentrations of phenol after treatment for 6 and 9 h, except in the 3.0 g/L phenol group (**Figure 4E**).

Damage to Chromatin and Protection of Chromosomal DNA

The investigation on the chromatin damage caused by phenol showed that the structurally abnormal nuclear chromatin appeared larger and more diffuse, while the normal chromatin

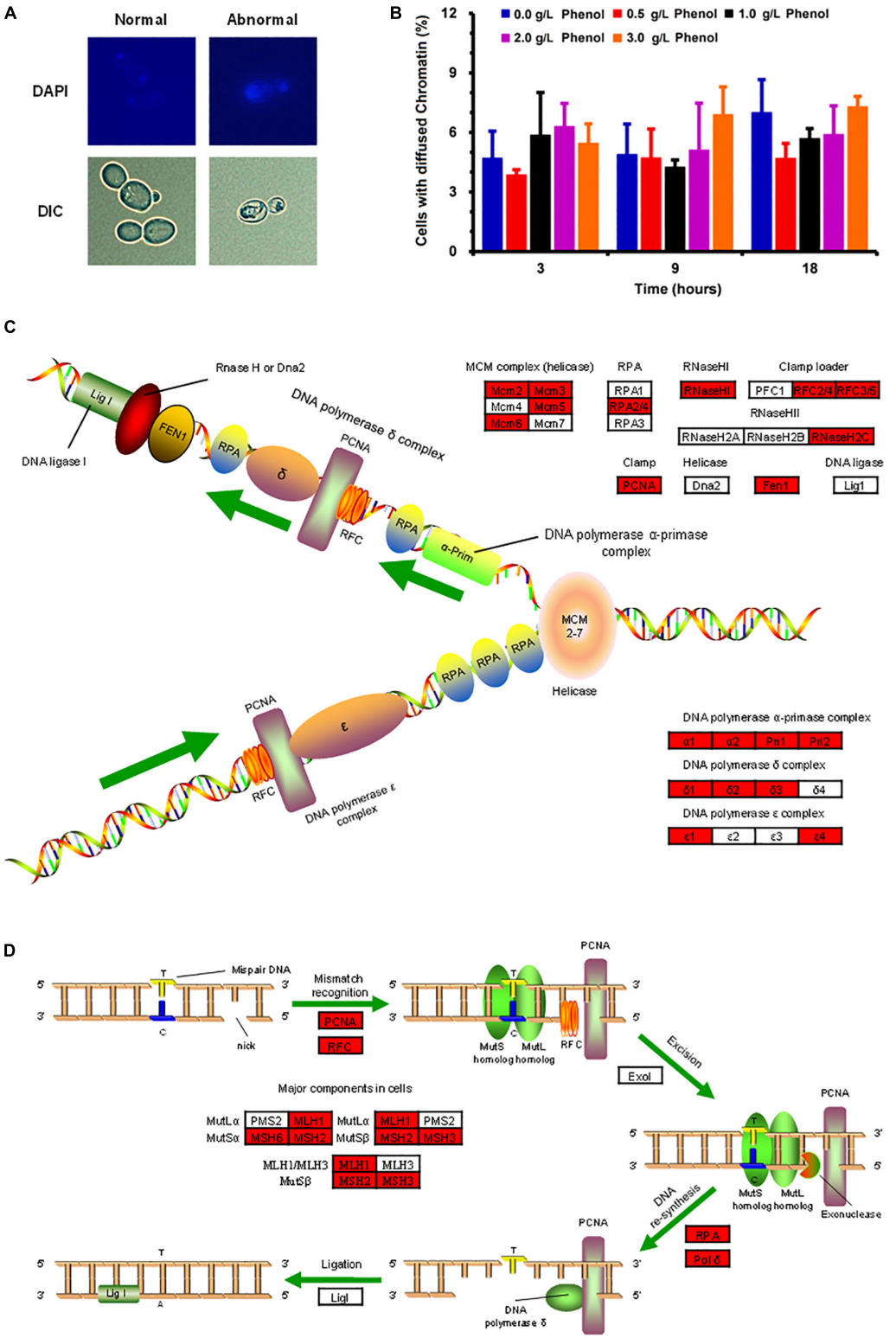

FIGURE 5 | Morphological change in nuclear chromatin caused by phenol and the protection of nuclear DNA. **(A)** Representative images of cells stained with the DNA specific dye diaminophenylindole (DAPI) are shown in the top column, and images taken by a differential interference contrast (DIC) lens are shown in the bottom column. **(B)** Percentage of cells containing abnormal chromatin in the presence of each concentration of phenol at 3, 9, and 18 h. Data represent averages of three experiments. At least 100 cells were examined on each bright-field image. **(C,D)** DNA replication **(C)** and DNA mismatch repair **(D)** pathways. *Red* genes were up-regulated by 2-fold in the presence of 2.0 g/L phenol and listed in **Supplementary Table S4**.

remained small and compacted (**Figure 5A**). The percentage of cells with abnormal diffuse nuclear chromatin was recorded in order to investigate the severity of nuclear chromatin damage. As illustrated in **Figure 5B**, the percentage of cells with nuclear chromatin disorganization remained at a low level (3.86–7.30%) when phenol was present or absent, which implied that 0.0–3.0 g/L phenol did not cause obvious damage to DNA and chromatin.

The transcriptome data indicated that most of the genes participating in DNA replication and DNA repair showed significant up-regulation in the presence of 2.0 g/L phenol (**Figures 5C,D** and **Supplementary Table S4**). Genes encoding ribonucleoside-diphosphate reductase subunit M2 (CTRG_01327 and CTRG_01698), as well as genes encoding ribonucleoside-diphosphate reductase subunit M1 (CTRG_01309), were highly expressed in cells exposed to 1.0 and 2.0 g/L phenol (**Supplementary Table S4**). The encoded proteins of the above genes are small and large subunits of ribonucleotide reductase (RNR), which plays a crucial role in dNTP production and DNA synthesis (Yao et al., 2003). Meanwhile, chromosome transmission fidelity protein 18 (CTRG_00975) was up-regulated by more than 4-fold in the presence of both 1.0 and 2.0 g/L phenol (Mayer et al., 2001; **Supplementary Table S4**).

Accumulation and Degradation of Unfolded and Misfolded Proteins

The ER structures of the viable cells were divided into three groups: normal (unfolded), abnormal shapes (folded and fragmented), and necrotic (**Figure 6A**). When cells were exposed to 0.0, 0.5, and 1.0 g/L phenol, normal and abnormal ER structures were distributed roughly 35 and 65% of cells at 3 h, respectively (**Figure 6C**). Under the same conditions, there was no significant change in the ratio of cells containing normal and abnormal ER structures from 3 to 9 h, but there was a slight increase in the proportion of cells containing abnormal ER at 18 h (**Figure 6C**). The necrotic cells and the cells containing abnormal ER accounted for a large share of the observed cells treated with high concentrations of phenol (2.0 and 3.0 g/L) at various time points (**Figure 6C**). These results demonstrated that ER was not significantly injured by phenol at low concentrations (0.5 and 1.0 g/L), but was markedly damaged by phenol at high concentrations (2.0 and 3.0 g/L). In contrast, the recovery of cell growth in cells exposed to 2.0 g/L phenol after 24 h suggested that certain mechanisms provided enough protein to retain homeostasis in the cells. Previous studies have demonstrated that, after the unfolded protein response (UPR) and autophagy, cells could recover homeostasis and normal ER function (Senft and Ronai, 2015). HSPs functioning as chaperones were implicated in the reversal of amino acid oxidation and refolding of denatured proteins resulting from the UPR (Doong et al., 2003; Obeng et al., 2006; Lanneau et al., 2010). The expression of a gene CTRG_01443, annotated as "small heat shock protein 21" (Hsp21), was up-regulated by 11. 3-, 64-, and 13.9-fold change in the presence of 0.5, 1.0, and 2.0 g/L phenol, respectively (**Supplementary Table S5**). Besides, the gene CTRG_04372, annotated as co-chaperones in the Hsp70/Hsp90 family, was significantly up-regulated in the presence of 2.0 g/L phenol (**Supplementary Table S5**). Autophagy, as a conserved trafficking pathway, delivered unfolded or misfolded proteins, components, and organelles from the cytoplasm to the vacuole for degradation and recycling (Senft and Ronai, 2015). Four pivotal steps, including the activation of autophagy, the formation of the autophagosome, the cytoplasm-to-vacuole targeting (CVT) pathway, and vacuole fusion, ensured the effective degradation of the contents by vacuole hydrolases (Oku et al., 2006; Suzuki and Ohsumi, 2007; Senft and Ronai, 2015). In the presence of 2.0 g/L phenol, it was found that the expression of genes *IRE1*, *ATG11*, *ATG23*, and *ATG25,* related to the activation of autophagy and the formation of the autophagosome, were up-regulated by more than 2-fold (**Supplementary Table S5**). However, *APE1* and *AMS1,* which are related to autophagy, showed down-regulation by twofold (**Supplementary Table S5**).

The vacuole plays a key role in autophagy for the degradation and recycling of unfolded or misfolded proteins (Suzuki and Ohsumi, 2007) and accordingly changes of vacuole morphology in the non-phenol-treated and phenol-treated cells were observed. The observation revealed vacuoles in different configurations that could be classified as follows: a single large vacuole, two to four medium-sized vacuoles, and massively fragmented vacuoles (**Figure 6B**). After treatment for 3 h, compared with the other treatments, 75% of cells treated with 0.5 g/L phenol contained a single large vacuole. A single large vacuole was also predominant in cells treated with 1.0 and 2.0 g/L phenol (71 and 68%, respectively) (**Figure 6D**). Similarly processing time, cells treated with non-lethal doses of phenol (0.5, 1.0, and 2.0 g/L) exhibited a lower proportion of fragmented vacuoles than untreated cells (**Figure 6D**). At 9 h after treatment, cells treated with 1.0 g/L phenol (49%) showed the highest proportion of single large vacuoles, followed by cells treated with 0.5 g/L phenol (40%) (**Figure 6D**). From these observations, we speculated that low concentrations of phenol suppressed the fragmentation of the cellular vacuole. However, the cells treated with 2.0 and 3.0 g/L phenol exhibited a higher proportion of fragmented vacuoles than the untreated cells, after treatment for both 9 and 18 h (**Figure 6D**). Since mutation of *VAC8* has been correlated with vacuole fragmentation (Oku et al., 2006), the above results might be related to down-regulation of *VAC8* (**Supplementary Table S5**).

Accumulation of Fatty Acid

The KEGG pathway enrichment analysis revealed down-regulation of 13 genes involved in fatty acid degradation (**Figure 7**). In this pathway, long-chain acyl-CoA synthetase (EC: 6.2.1.3) is responsible for the degradation of hexadecanoate (fatty acid), and the corresponding genes, CTRG_02563 and CTRG_05500, were down-regulated by 11.3- and 7-fold in response to 2.0 g/L phenol, respectively (**Figure 7**). When hexa-decanoyl-CoA was converted into trans-hexadec-2-enoyl-CoA, the expression of the corresponding genes (CTRG_02374, CTRG_02377, CTRG_02721, and CTRG_05958), annotated as acyl-CoA oxidase (EC: 1.3.3.6) and acyl-CoA dehydrogenase

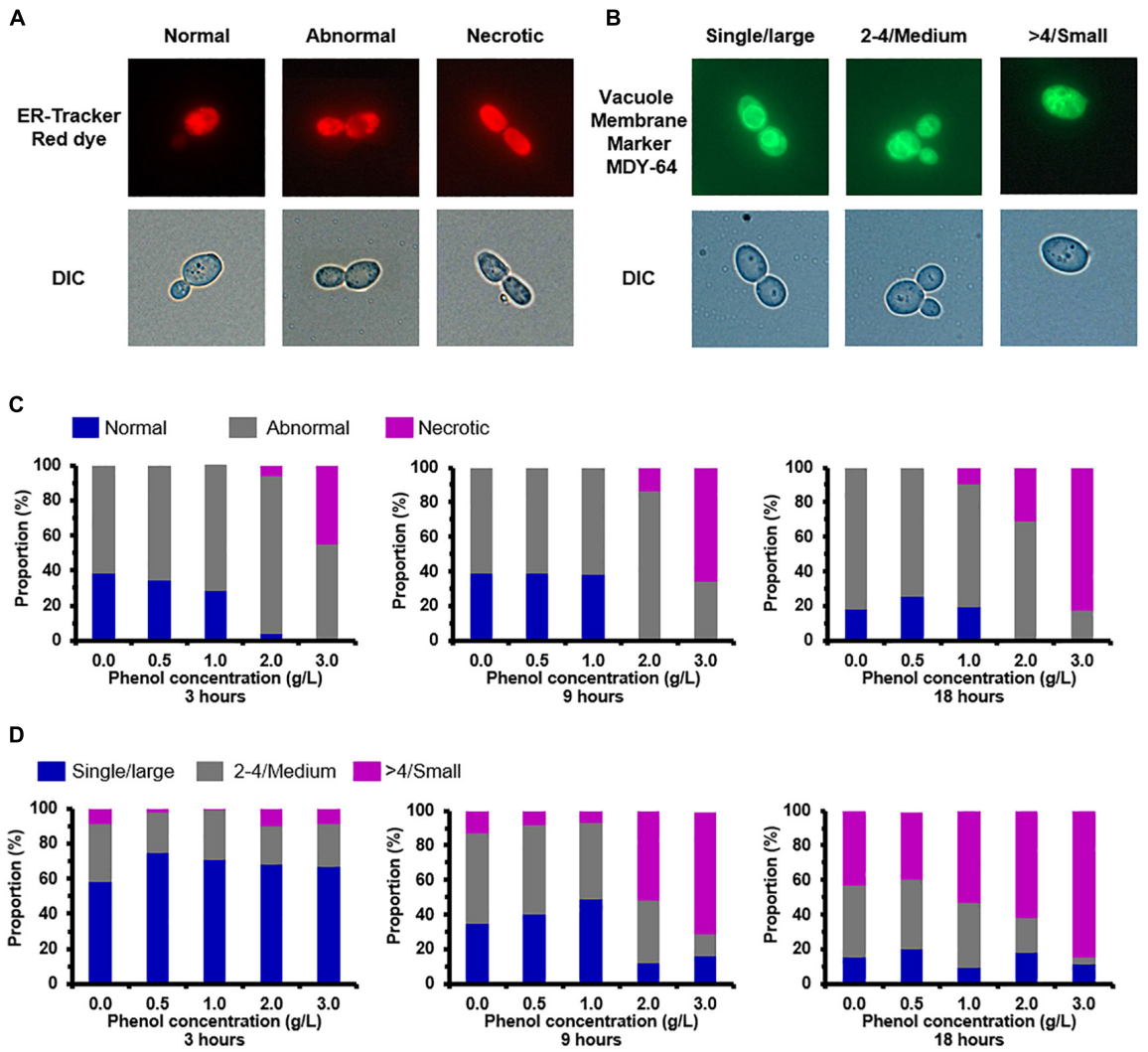

FIGURE 6 | Endoplasmic reticulum (ER) and vacuole damage caused by phenol. Representative images of cells stained with the ER-specific dye ER-Tracker™ Red and vacuole-targeted dye Yeast Vacuole Membrane Marker MDY-64 are shown in the top column, and images taken using a differential interference contrast (DIC) lens are shown in the bottom column. **(A)** Morphological structure analysis of the ER. **(B)** Morphological structure analysis of the vacuole. **(C)** Percentage of cells at each concentration of phenol that displayed normal, abnormal, and necrotic ER at 3, 9, and 18 h. **(D)** Percentage of cells at each concentration of phenol that contained large, medium, and small vacuoles at 3, 9, and 18 h. Data represent averages of three experiments. At least 100 cells were examined on each bright-field image.

(EC: 1.3.8.7), showed 147-, 12.1-, 2.8-, and 5.7-fold decreases in cells treated with 2.0 g/L phenol, respectively (**Figure 7**). The genes CTRG_01068 and CTRG_02168, which encode acetyl-CoA acyltransferase1 (2.3.1.16), were 7- and 3.7-fold down-regulated in cells treated with 2.0 g/L phenol (**Figure 7**). In addition, the differential expression analysis implicated genes encoding aldehyde dehydrogenase (1.2.1.3) and alcohol dehydrogenase (1.1.1.1) in the conversion of fatty acid to alcohol (**Figure 7**). Specifically, CTRG_05836, CTRG_00882, CTRG_05482, CTRG_01329, and CTRG_05010 were significantly down-regulated in response to 2.0 g/L phenol exposure (**Figure 7**). These results suggested that decreased fatty acid degradation efficiency, caused by the down-regulation of expression of related genes, could elevate the intracellular fatty acid content or change the fatty acid component in cells (Kurosawa et al., 2015; Zhou et al., 2017).

Cell-Wall Remodeling

Previous studies have found that cell-wall remodeling can lead to increased ethanol resistance in yeast (Teixeira et al., 2014). Our comparative transcriptome analysis revealed >2-fold up-regulation of six genes related to cell-wall biogenesis and integrity in response to 1.0 and 2.0 g/L phenol, including CTRG_05721, CTRG_05949, CTRG_00608, CTRG_00036, CTRG_01855, and CTRG_03473 (**Supplementary Table S6**). Genes involved in cell-wall biogenesis may contribute to the increased resistance of *C. tropicalis* SHC-03 to phenol. A series of differential expression analyses of genes up-regulated in response to 2.0 g/L

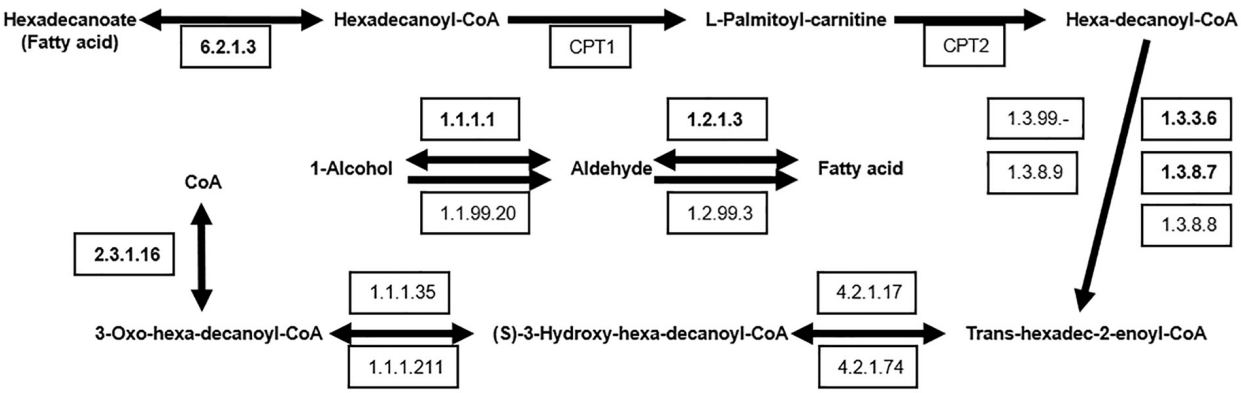

EC number	Enzyme name	Gene IDs
6.2.1.3	**Long-chain acyl-CoA synthetase**	**CTRG_02563(-3.5), CTRG_05500(-2.8)**
CPT1	Carnitine O-palmitoyltransferase 1	NA
CPT2	Carnitine O-palmitoyltransferase 2	NA
1.3.3.6	**Acyl-CoA oxidase**	**CTRG_02374(-7.2), CTRG_02377(-3.6), CTRG_02721(-1.5)**
1.3.8.7	**Acyl-CoA dehydrogenase**	**CTRG_05958(-2.5)**
1.3.8.8	Long-chain-acyl-CoA dehydrogenase	NA
1.3.8.9	Very long chain acyl-CoA dehydrogenase	NA
1.3.99.-	Acyl-CoA dehydrogenase	NA
4.2.1.17	Enoyl-CoA hydratase	NA
4.2.1.74	Long-chain-enoyl-CoA hydratase	NA
1.1.1.35	3-Hydroxyacyl-CoA dehydrogenase	NA
1.1.1.211	Enoyl-CoA hydratase	NA
2.3.1.16	**Acetyl-CoA acyltransferase 1**	**CTRG_01068(-2.8), CTRG_02168(-1.9)**
1.1.1.1	**Alcohol dehydrogenase**	**CTRG_05836(-1.2), CTRG_00882(-1.2), CTRG_05482(-4.7)**
1.2.1.3	**Aldehyde dehydrogenase**	**CTRG_01329(-3.9), CTRG_05010(-3.0)**
1.1.99.20	Alkan-1-ol dehydrogenase	NA
1.2.99.3	Aldehyde dehydrogenase	NA

FIGURE 7 | Fatty acid degradation pathway in *C. tropicalis* SHC-03. Known enzymatic reactions in *C. tropicalis* are shown in bold font. Expression levels of genes with values of $\log_2$(fold change) in response to 2.0 g/L phenol, compared with the control group, are shown. NA, none annotated.

phenol revealed enrichment in the chitin synthesis pathway (**Figure 8A** and **Supplementary Table S6**). As illustrated in **Figure 8A**, during the conversion of glucose to chitin, the expression levels of CTRG_00414, CTRG_00601, CTRG_01436, CTRG_03651, CTRG_03585, CTRG_05721, and CTRG_05949 were markedly increased. In addition, most of the genes in the chitin degradation pathway (chitin to chitobiose or N-Acetyl-D-glucosamine), including CTRG_05456 and CTRG_05827 (encoding chitinase) and CTRG_01063 (encoding beta-N-acetylhexosaminidase), were significantly down-regulated in expression (**Figure 8A** and **Supplementary Table S6**). In the process of converting chitin to chitosan, CTRG_01049, which encodes chitin deacetylase, was dramatically up-regulated; by 26.5-fold (**Figure 8A** and **Supplementary Table S6**). The up- and down-regulated expression of these genes probably served to increase the accumulation of chitin and chitosan in the cell wall. To confirm the increased phenol tolerance of cells that had undergone cell wall remodeling, we conducted cell-wall susceptibility analyses of the phenol-treated and non-phenol-treated cells using lytic enzyme, a β-1,3-glucanase from *Arthrobacter luteus* (Teixeira et al., 2014). After 3 h, the cell density (OD_{600}) of samples treated with 0.0 and 0.5 g/L phenol decreased significantly upon addition of lyticase to the medium. This decrease was even more pronounced in cells treated with 1.0 and 3.0 g/L phenol, decreasing to less than 10% of the initial cell density at 4 h (**Figure 8B**). The cell density of samples treated with 2.0 g/L phenol dropped slowly after lyticase was added into the medium for 4 h, decreasing to about 65% at 4 h (**Figure 8B**). After treatment with phenol for 9 h, the samples in 0.0 and 0.5 g/L phenol still displayed the most rapid cell-density decline in the lyticase-supplemented medium; the decrease in cell density in these samples was greater than the cell-density decrease seen in the samples in 1.0–3.0 g/L phenol (**Figure 8C**). However, the cell density of the sample in 3.0 g/L phenol dropped more quickly than all of the others, at 3 h (**Figure 8C**). The resistance of cells to lyticase after treatment with 1.0 and 2.0 g/L phenol for 9 h was similar to that of cells treated with the corresponding concentration of phenol for 3 h (**Figure 8C**). In cells exposed to phenol for 18 h, the cell density of the sample treated with 3.0 g/L phenol descended sharply, decreasing to about 12% after addition of lyticase to the medium and incubation for 4 h (**Figure 8D**). The cell density of samples treated with 1.0 and 2.0 g/L phenol for 18 h dropped slowly after the 4 h lyticase treatment. In contrast, the cell density in the samples with 0.0 and 0.5 g/L phenol showed no significant decline (**Figure 8D**). The results demonstrated that treatment for 3 and 9 h with 1.0–3.0 g/L phenol caused

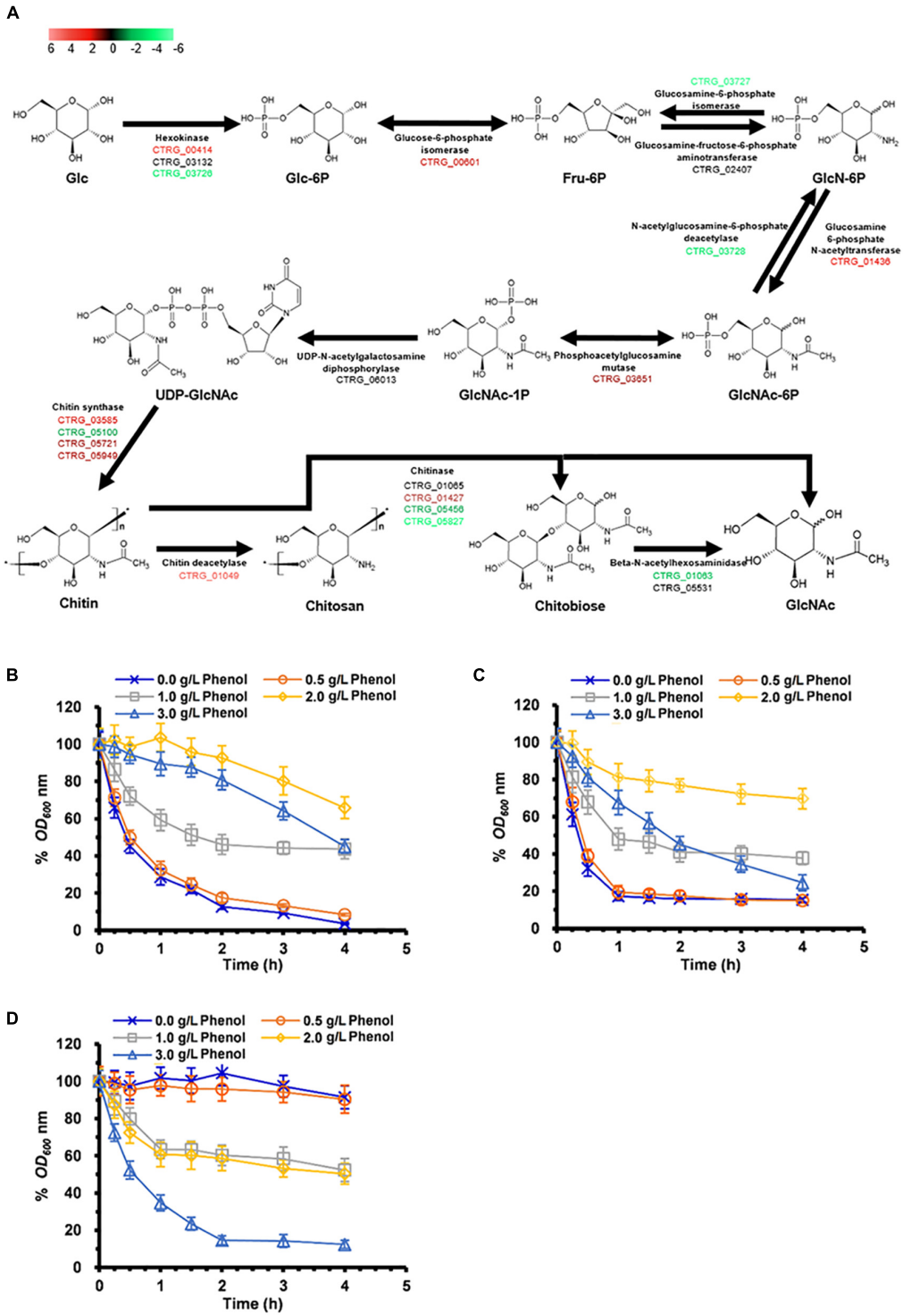

FIGURE 8 | Synthesis and degradation of chitin in cells exposed to 2.0 g/L phenol and susceptibility to lyticase of cells treated with 0.0–3.0 g/L phenol for 3, 9, and 18 h. **(A)** Pathway showing genes involved in chitin synthesis and degradation. The color codes *red, black,* and *green* represent up-regulated, normal, and down-regulated expression, respectively, in the presence of 2.0 g/L phenol. Glc, D-Glucose; Glc-6P, D-Glucose-6-phosphate; Fru-6P, D-Fructose-6-phosphate; GlcN-6P, D-Glucosamine-6-phosphate; GlcNAc-6P, N-Acetyl-D-glucosamine 6-phosphate; GlcNAc-1P, N-Acetyl-alpha-D-glucosamine 1-phosphate; UDP-GlcNAc, UDP-N-acetyl-alpha-D-glucosamine; GlcNAc, N-Acetyl-D-glucosamine. The expression levels of the genes (log_2 transformed) are listed in **Supplementary Table S6**. The mean values of relative optical density are presented with vertical error bars, each representing a single standard deviation (n = 3). **(B–D)** Change in cell density after treatment in PBS containing lyticase from 0 to 4 h after incubation. Cells treated for **(B)** 3 h, **(C)** 9 h, and **(D)** 18 h under phenol stress or no phenol stress. The mean values of relative optical density are presented with vertical error bars, each representing a single standard deviation (n = 3).

increased resistance of cells to lyticase, with a maximal effect seen at 2.0 g/L phenol. While 2.0 g/L phenol appeared to be the optimal concentration for lyticase resistance, cells treated with 0.0 and 0.5 g/L phenol also exhibited significantly increased resistance to lyticase after 18 h and cells treated with 3.0 g/L phenol for 18 h showed decreased resistance to lyticase compared with this treatment after 3 and 9 h.

MDR/MXR Transport

One effective detoxification mechanism is the active efflux mechanism, which has been shown to reduce the level of intracellular toxic compounds, resulting in retention of the physiological activities of the cells (Dos Santos et al., 2014). The major facilitator superfamily (MFS) and ATP-binding cassette (ABC) subfamily are the two most important groups of multidrug/multixenobiotic resistance (MDR/MXR) transporters responsible for the efflux of toxic compounds (Sa-Correia et al., 2009). In response to at least two concentrations of phenol, the MFS genes CTRG_03938, CTRG_00385, and CTRG_03729 showed a >2-fold increase in expression (**Supplementary Table S7**). Specifically, CTRG_00385 was up-regulated by 7-, 18-, and 169-fold in response to 0.5, 1.0, and 2.0 g/L phenol. Additionally, a statistical analysis of differential gene expression showed that 14 genes belonging to the MFS and ATP-binding cassette (ABC) subfamily exhibited greatly up-regulated expression in the presence of phenol (**Supplementary Table S7**). As illustrated in **Supplementary Table S7**, 2, 6, and 10 transporter genes were significantly up-regulated in response to 0.5, 1.0, and 2.0 g/L phenol, which indicated that the number of up-regulated transporter genes increased with the rise in phenol concentration.

Transcriptional Responses for Phenol Degradation

Previous studies have illustrated that phenol degradation is the vital detoxification mechanism of *C. tropicalis* in response to phenol (Jiang et al., 2005; Varma and Gaikwad, 2009). Considering the molecular mechanism, the biodegradation of phenol mainly relies on subsequent enzymatic steps via the β-ketoadipate pathway in *C. tropicalis* (Krug et al., 1985). The crucial enzyme in this pathway, phenol 2-monooxygenase (EC 1.14.13.7), is responsible for the hydroxylation of phenol to catechol, which is a rate-limiting step (Krug et al., 1985; **Figure 9**). To date, two genes encoding phenol 2-monooxygenase, CTRG_00423 and CTRG_03102, have been discovered in *C. tropicalis* strains JH8 and MYA-3404, respectively (Butler et al., 2009; Long et al., 2014). In the present study, the comparative transcriptomics data did not indicate that CTRG_00423 and CTRG_03102 were significantly up-regulated under phenol stress after treatment for 3 h (**Figure 9**). In the second step of the β-ketoadipate pathway, catechol 1,2-dioxygenase (EC 1.13.11.1) is responsible for the conversion of catechol to *cis*,*cis*-muconate (**Figure 9**). CTRG_01732 and CTRG_00171, encoding catechol 1,2-dioxygenase, were not significantly up-regulated in response to different concentrations of phenol (**Figure 9**). The above results suggest that the phenol degradation mechanism of *C. tropicalis* SHC-03 was probably not activated.

DISCUSSION

In this study, the cells recovered and returned to normal growth 20 h after the treatment (**Figure 1A**), which indicated that detoxification and/or tolerance mechanisms should be activated to protect the cells from the toxicity of phenol and retain the viability of cells throughout the stress period. The determination of phenol concentration in each sample showed that the degradation of phenol in *C. tropicalis* was not activated (**Figure 1B**). Meanwhile, the transcriptome analysis of key genes (CTRG_00423, CTRG_03102, CTRG_01732, and CTRG_00171) related to phenol degradation demonstrated that phenol did not stimulate the phenol degradation mechanism of *C. tropicalis* in YPD medium (**Figure 9**). Therefore, we considered that the tolerance mechanism of *C. tropicalis* to phenol plays a critical role in maintaining the viability of phenol-treated cells.

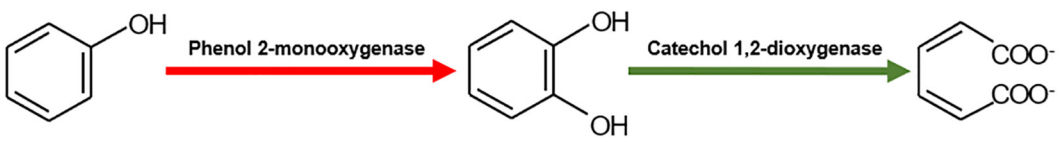

Gene IDs	Product	EC number	Expression		
			0.5	1.0	2.0
CTRG_00423	Phenol 2-monooxygenase	1.14.13.7	NS	NS	-2.6
CTRG_03102	Phenol 2-monooxygenase	1.14.13.7	NS	NS	NS
CTRG_01732	Catechol 1,2-dioxygenase	1.13.11.1	NS	NS	NS
CTRG_00171	Catechol 1,2-dioxygenase	1.13.11.1	NS	NS	NS

FIGURE 9 | The first and second step of the β-ketoadipate pathway in the biodegradation of phenol. Expression levels of genes involved in the first and second step of the β-ketoadipate pathway are represented by the values of $\log_2$(fold change) in response to different concentrations of phenol, compared with the control group. NA, not significant.

In the present study, the treated cells exhibited serious damage to the mitochondrial membrane and high-level accumulation of ROS after the treatment for 3 h, which can cause damage to DNA, proteins, lipids, and the cytoskeleton (**Figure 3**; Gourlay and Ayscough, 2005; Perrone et al., 2008; Rowe et al., 2008), and then seriously affect the physiological and biochemical functions of cells. Interestingly, the percentages of the cells accumulating ROS declined to a lower level at 9 h (**Figure 3D**). Since efficient enzymatic and non-enzymatic antioxidant defense systems were found to be responsible for the scavenging of excessive ROS and protection of cells from oxidative damage (Hossain et al., 2006), we speculated that the associated genes, such as SOD, GPX, CTT, GLR, might be activated. The results from RNA-seq showed that these genes were not up-regulated in response to 3 h exposure to several concentrations of phenol (**Supplementary Table S3**), which implied that these antioxidant defense systems were not activated at the transcriptional level in response to phenol. To clarify the mechanism related to the scavenging of the intracellular ROS between 3 and 9 h, the activity assays of SOD, GPX, CTT, and GLR, as well as determination of GSH content, were conducted (**Figure 4**). As illustrated in **Figure 4**, the activities of SOD, GPX, and GLR showed obvious changes correlating with different conditions (phenol concentration and processing time). These changes were distinct from those at the transcriptional level. We hypothesized that differing regulation at the translational level might lead to the above inconsistent findings.

The results from the SOD activity assays showed that the SOD activities in different treatments remained high at 3 and 6 h, but were very low at 9 h, which implies that most of the O_2^- probably had been converted to H_2O_2, and the SOD activity was sufficient to retain homeostasis of intracellular ROS at a low level after the treatment for 9 h (**Figure 4A**). During the conversion of H_2O_2 to H_2O, GPX activities in the treatments with 1.0 and 2.0 g/L phenol exhibited a dramatic increase, but CTT activity was not detected in any of the treatments, implying that GPX played an important role in the reduction of H_2O_2 after the treatment for 6 and 9 h. Additionally, the high activity of GLR guarantees sufficient supplementation of GSH activity to contribute to the reduction of H_2O_2 catalyzed by GPX at 6 and 9 h (**Figure 4D**). In summary, the up-regulation of intracellular SOD activity (involved in the dismutation of O_2^-) at 3 and 6 h, and the up-regulation of intracellular GPX activity (involved in the reduction of H_2O_2) at 6 and 9 h, promoted the detoxification of endogenous ROS induced by phenol and low-level intracellular ROS.

The morphological structure analysis of nuclei demonstrated that phenol did not induce significant chromatin damage when the concentration of phenol was climbing (**Figures 5A,B** and **Supplementary Table S4**). Since chromatin protection mechanisms are associated with the DNA damage response (Masutomi et al., 2005), we speculated that ROS did not cause serious DNA damage. The transcriptome data showed that up-regulated expression of these genes, responsible for DNA repair, DNA synthesis, dNTP production, and chromatin protection, probably played a key role in protecting DNA, dNTPs, and chromatin from damage by ROS, and contributed to the maintenance of the viability of cells and the increased tolerance of *C. tropicalis* SHC-03 to phenol. Additionally, phenolic compounds (luteolin and quercetin) as antioxidants have been found to significantly decrease DNA damage (Lima et al., 2006). Perhaps phenol can function in a similar manner to luteolin or quercetin, helping cells to retain DNA and chromatin homeostasis.

Phenol-induced redox imbalance and ROS-induced protein damage can also cause unfolded or misfolded proteins to accumulate in the ER lumen and thereby induce ER stress (ERS) (Perrone et al., 2008; Senft and Ronai, 2015). The high concentration of phenol (2.0 g/L) caused serious damage to the ER at 3–18 h after treatment (**Figure 6C**), but the cell growth recovered in the presence of 2.0 g/L phenol. These results suggested that several pathways were triggered by ERS to guarantee the refolding of unfolded protein, the degradation of misfolded proteins, the restoration of normal ER function, and the maintenance of cell survival (Senft and Ronai, 2015). Two key fundamental pathways have been associated with response to ERS: one based on chaperone proteins and the other based on autophagy (Senft and Ronai, 2015). Previous studies have shown that HSPs can act as molecular chaperones associated with the folding, trafficking, protection, and renaturation of cellular proteins that have undergone the heat shock response (Walter and Buchner, 2002). Additionally, the up-regulation of the genes in the Hsp70/Hsp90 family is implicated in the adaptation and resistance of *C. albicans* to stress (Demand et al., 2001; Doong et al., 2003). In the present study, the genes, annotated as Hsp21and the co-chaperone of the Hsp70/Hsp90 family, were up-regulated by more than 2-fold in the presence of phenol (**Supplementary Table S5**). Hence, the accumulation of these HSPs might serves to protect the cellular proteins and facilitate the degradation of misfolded proteins via the ubiquitin proteasome system and relieve ERS, thereby improving phenol resistance in *C. tropicalis* SHC-03. Additionally, UPR can activate 27 autophagy-related genes (ATGs) which control autophagy in *S. cerevisiae* (Suzuki and Ohsumi, 2007). In the present study, the transcriptome data showed that the ATGs, except for *ATG11*, *ATG23,* and *ATG25,* were no marked changes in the expression level. In addition, expression of the hydrolase genes *APE1* and *AMS1*, the encoded proteins of which are specifically transported by autophagy and the CVT pathway (a type of selective autophagy) to the vacuole for hydrolyzation of proteins (Wang and Klionsky, 2003), was down-regulated at 3 h after the phenol treatment. We also surveyed the expression of genes belonging to the PERK-eIF2α pathway, *ATF6*, *IRE1*, *ATF4,* and *CHOP*, which have been associated with the induction and regulation of autophagy and chaperones (Senft and Ronai, 2015). Only *IRE1* (CTRG_04146) showed a change in expression, and its expression was up-regulated by more than 2-fold in the presence of 2.0 g/L phenol at 3 h. In summary, compared with autophagy, HSP-mediated proteasomal degradation played the more dominant role in the relief of ERS triggered by phenol at the early stage of treatment.

As a compartmentalized organelle, the vacuole contains a series of hydrolases which can degrade damaged or unfolded

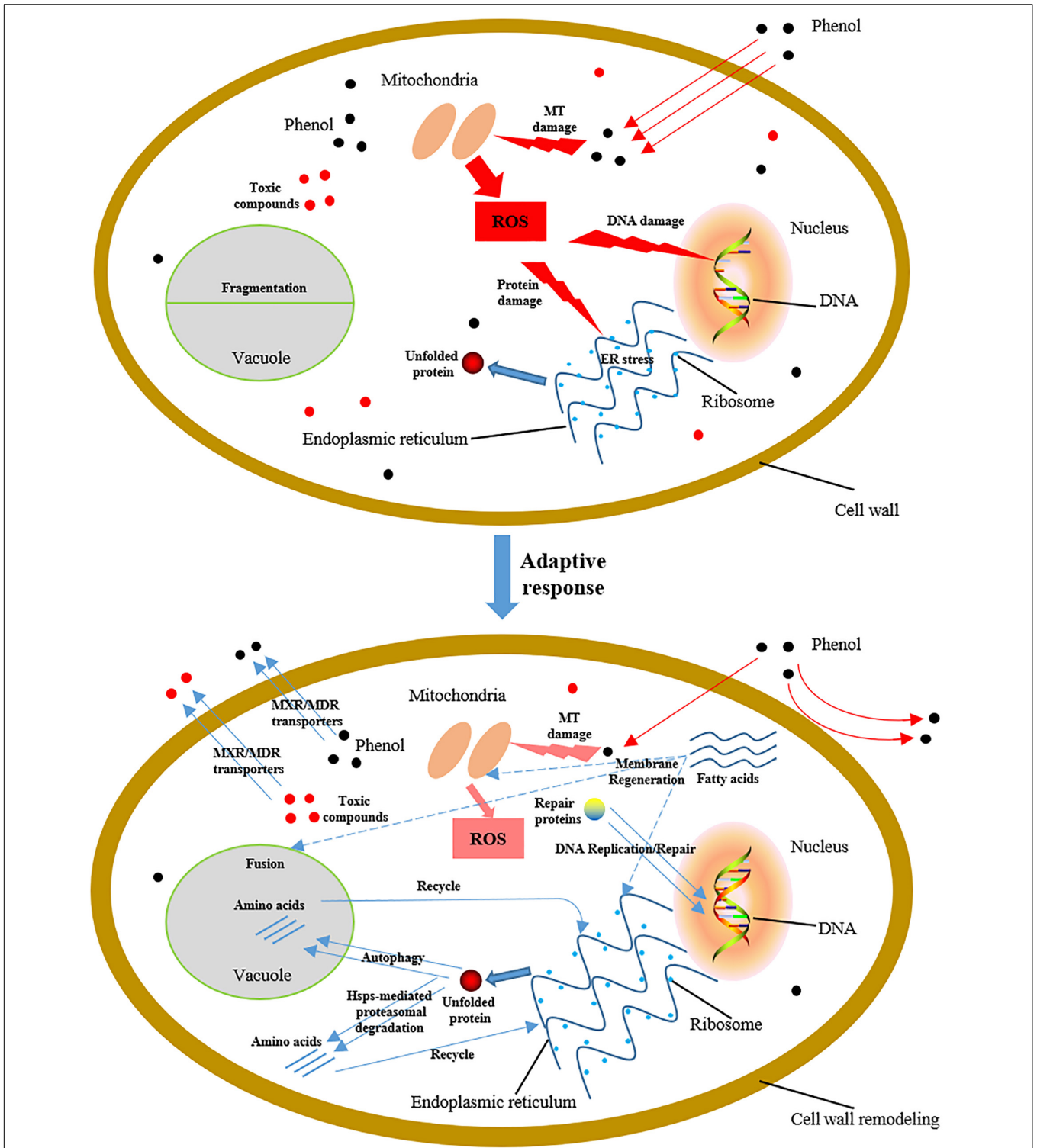

FIGURE 10 | Schematic diagram showing cellular damage to *C. tropicalis* SHC-03 caused by phenol, and tolerance mechanisms to phenol at the early stage of treatment. MT, mitochondria.

proteins from the cytoplasm in *S. cerevisiae* during autophagy (Wang and Klionsky, 2003). It has been found that increased vacuolar volume (or the fusion of a fragmented vacuole) can sufficiently improve the hydrolytic capacity for autophagy (Baba et al., 1994). Our morphological observation demonstrated that low concentrations of phenol might block the fragmentation of

the cellular vacuole in order to allow the cell to retain efficient autophagy (**Figure 6D**). Unfortunately, the results from RNA-seq demonstrated that the expression of the genes *TORC1*, *SIT4*, and *VPS1*, which regulate the fragmentation or fusion of the vacuole, did not significantly change under phenol stress at 3 h (data not shown). Perhaps several unknown genes involved in vacuole fusion were responsible for the higher proportion of cells containing large vacuoles. Therefore, a follow-up study will be conducted to characterize these genes. However, we did find that the proportion of cells containing large vacuoles was lower in the cells treated with 2.0 g/L phenol than in the untreated cells, at 9 and 18 h (**Figure 5D**). As the knockout of *VAC8* (CTRG_04061) has been shown to cause fragmentation of vacuoles (Oku et al., 2006), our results can probably be attributed to significant down-regulation of *VAC8* (**Supplementary Table S5**). Since the increased synthesis of fatty acid could promote the formation of lipid membranes and increase the tolerance of *S. cerevisiae* and *Chlorella* strains to phenol (Schneiter et al., 2000; Yang et al., 2012; Zhou et al., 2017), the accumulation of fatty acid in this study was likely related to the increased tolerance of *C. tropicalis* to high concentrations of phenol. Interestingly, the accumulation of fatty acids was found to be associated with the fragmentation of the vacuole (Schneiter et al., 2000). This might explain how the proportion of cells containing fragmented vacuoles when exposed to under 2.0 g/L phenol stress was higher than that in the untreated samples at 9 and 18 h (**Figure 6**).

Since chitin is a structural microfibrillar component and is associated with cell wall rigidity (Bulik et al., 2003; Ruiz-Herrera et al., 2002), accumulation of chitin in cell walls in this study might lead to cell wall remodeling and then promotes the adaptation of cells to hypo-osmotic conditions, increases the resistance of cells to stress, reduces the production of intracellular ROS, and prevents the entrance of phenol into the cells (Aguilar-Uscanga and Francois, 2003; Deshpande et al., 1997). Additionally, the cell wall susceptibility analysis demonstrated that phenol certainly induced the increased resistance of cells to stress. However, it remains to be studied whether it was the accumulation of chitin induced by phenol, and related to cell wall remodeling, that improved the phenol resistance of *C. tropicalis*.

The active efflux mechanism can enable the cell to retain the intracellular drug/xenobiotic concentration at low levels and maintain the viability of cells under stress from these toxic compounds (Sa-Correia et al., 2009; Ma and Liu, 2010). In our study, at different concentrations of phenol, 14 genes encoding MDR/MXR transporters, especially CTRG_00385, showed significantly up-regulated expression (**Supplementary Table S7**). Additionally, as the phenol concentration increased, the up-regulated transporter genes became more numerous. Based on these results, we reasoned that there were definite connections between an active efflux mechanism and the tolerance and response of *C. tropicalis* to phenol. In *S. cerevisiae*, QDR1 (YIL120W), a multidrug transporter from the MFS, modulates the assembly of the outer spore wall and is responsible for resistance to quinidine, ketoconazole, and fluconazole (Nunes et al., 2001; Lin et al., 2013). Additionally, as illustrated in **Figure 8A**, CTRG_01049, which encodes chitin deacetylase, an enzyme that catalyzes the conversion of chitin to chitosan, was up-regulated by 26.5-fold. Since the spore wall is primarily composed of chitosan (Baker et al., 2007; Neiman, 2011), up-regulated expression of CTRG_01049 should lead to excess accumulation of chitosan in the spore wall. Since mature spores, as quiescent cells, exhibit resistance to organic solvents, heat, and digestive enzymes, and since chitosan and dityrosine layers of the spore wall prominently contribute to stress resistance, a hypothesis has been proposed that sporulation of *C. tropicalis* is activated in order to reduce the assault of phenol to cells (Pammer et al., 1992; Kupiec et al., 1997). However, according to eosin Y staining method (Lin et al., 2013), we observed no spores in the samples at 3, 9, and 18 h after cells were exposed to different concentrations of phenol (data not shown). This suggests the possible need for further exploration of the mechanisms underlying sporulation in *C. tropicalis*.

CONCLUSION

C. tropicalis SHC-03 cells are treated with different concentrations of phenol as a representative of pollutants in environment for investigating the tolerance mechanisms of *C. tropicalis* to phenol. The experimental results indicated that phenol can result in massive accumulation of ROS. Although these intracellular ROS were found to be scavenged by SOD and GPX, the accumulation of ROS in the early stage after phenol treatment could cause damage to DNA, proteins, and lipids (**Figure 10**), and this stress could lead to morphological changes in the structure of the endoplasmic reticulum and vacuole. To reduce this damage, a series of protection mechanisms were activated. The DNA repair and synthesis system serve to ensure the stability of heredity, and key enzymes retain the fidelity of chromosome transmission and the stability of chromosomal structure. HSP-mediated proteasomal degradation and autophagy served to maintain intracellular protein homeostasis and accelerated recycling of proteins. Additionally, the accumulation of fatty acids contributed to the regeneration and repair of organelles with membrane systems. Cell wall remodeling minimized both import of phenol into the cells and production of intracellular ROS. The MXR/MDR transporters facilitated export of phenol and cytotoxic compounds from the cells, and maintained the intracellular drug concentration at low levels in order to maintain cell viability. This is the first study to shed light on the influence of phenol, a ubiquitous pollutant in wastewater, on the physiological characteristics of *C. tropicalis* SHC-03 and explore its tolerance mechanism to phenol stress.

DATA AVAILABILITY STATEMENT

The datasets generated for this study can be found in the Sequence files for all the treatment samples used in this study have been deposited at NCBI SRA with accession: PRJNA591802.

AUTHOR CONTRIBUTIONS

MM, HW, QL, QC, and XZ conceived and designed the project. QL, HW, YP, ZZ, XK, XHu, and XHa performed the experiments. QL, HW, QX, XY, KZ, LZ, YG, XiLi, and XiaLi performed the data analysis. HW, QL, YP, and ZZ wrote the manuscript. MM, BL, EA, and GA revised the manuscript. All authors read and approved the final manuscript.

FUNDING

We gratefully acknowledge financial support from China Scholarship Council. This work was financially supported by the National Natural Science Foundation of China (No. 31570086), the 2011 Collaborative Innovation Center for Farmland Protection and Agricultural Product Safety in Sichuan Province, the Talent Introduction Fund of Sichuan Agricultural University (No. 01426100), and the Research Interest Training Program for Undergraduate Students of Sichuan Agricultural University (No. 2019337).

ACKNOWLEDGMENTS

We are particularly grateful to Z. Lewis Liu, Bioenergy Research Unit, NCAUR-ARS, U.S. Department of Agriculture (Peoria, IL, United States) for providing the mRNA control mix as reference mRNA in the qRT-PCR reactions.

SUPPLEMENTARY MATERIAL

The Supplementary Material for this article can be found online at: https://www.frontiersin.org/articles/10.3389/fmicb.2020.00544/full#supplementary-material

REFERENCES

Adav, S. S., Chen, M. Y., Lee, D. J., and Ren, N. Q. (2007). Degradation of phenol by aerobic granules and isolated yeast *Candida tropicalis*. *Biotechnol. Bioeng.* 96, 844–852. doi: 10.1002/bit.21148

Aguilar-Uscanga, B., and Francois, J. M. (2003). A study of the yeast cell wall composition and structure in response to growth conditions and mode of cultivation. *Lett. Appl. Microbiol.* 37, 268–274. doi: 10.1046/j.1472-765x.2003.01394.x

Anders, S., and Huber, W. (2010). Differential expression analysis for sequence count data. *Genome Biol.* 11:R106. doi: 10.1186/gb-2010-11-10-r106

Ashburner, M., Ball, C., Blake, J., Botstein, D., Butler, H., Cherry, J., et al. (2000). Gene ontology tool for the unification of biology. *Nat. Genet.* 25, 25–29. doi: 10.1038/75556

Baba, M., Takeshige, K., Baba, N., and Ohsumi, Y. (1994). Ultrastructural analysis of the autophagic process in yeast: detection of autophagosomes and their characterization. *J. Cell Biol.* 124, 903–913. doi: 10.1083/jcb.124.6.903

Baker, L. G., Specht, C. A., Donlin, M. J., and Lodge, J. K. (2007). Chitosan, the deacetylated form of chitin, is necessary for cell wall integrity in *Cryptococcus neoformans*. *Eukaryot. Cell* 6, 855–867. doi: 10.1128/EC.00399-06

Banerjee, A., and Ghoshal, A. K. (2011). Phenol degradation performance by isolated *Bacillus cereus* immobilized in alginate. *Int. Biodet. Biodeg.* 65, 1052–1060. doi: 10.1016/j.ibiod.2011.04.011

Bulik, D. A., Olczak, M., Lucero, H. A., Osmond, B. C., Robbins, P. W., and Specht, C. A. (2003). Chitin synthesis in *Saccharomyces cerevisiae* in response to supplementation of growth medium with glucosamine and cell wall stress. *Eukaryot. Cell* 2, 886–900. doi: 10.1128/ec.2.5.886-900.2003

Busca, G., Berardinelli, S., Resini, C., and Arrighi, L. (2008). Technologies for the removal of phenol from fluid streams: a short review of recent developments. *J. Hazard. Mater.* 160, 265–288. doi: 10.1016/j.jhazmat.2008.03.045

Butler, G., Rasmussen, M. D., Lin, M. F., Santos, M. A., Sakthikumar, S., Munro, C. A., et al. (2009). Evolution of pathogenicity and sexual reproduction in eight *Candida* genomes. *Nature* 459, 657–662. doi: 10.1038/nature08064

Demand, J., Alberti, S., Patterson, C., and Hohfeld, J. (2001). Cooperation of a ubiquitin domain protein and an E3 ubiquitin ligase during chaperone/proteasome coupling. *Curr. Biol.* 11, 1569–1577. doi: 10.1016/s0960-9822(01)00487-0

Deshpande, M. V., O'Donnell, R., and Gooday, G. W. (1997). Regulation of chitin synthase activity in the dimorphic fungus *Benjaminiella poitrasii* by external osmotic pressure. *FEMS Microbiol. Lett.* 152, 327–332. doi: 10.1111/j.1574-6968.1997.tb10447.x

Doong, H., Rizzo, K., Fang, S., Kulpa, V., Weissman, A. M., and Kohn, E. C. (2003). CAIR-1/BAG-3 abrogates heat shock protein-70 chaperone complex-mediated protein degradation: accumulation of poly-ubiquitinated Hsp90 client proteins. *J. Biol. Chem.* 278, 28490–28500. doi: 10.1074/jbc.M209682200

Dos Santos, S. C., Teixeira, M. C., Dias, P. J., and Sa-Correia, I. (2014). MFS transporters required for multidrug/multixenobiotic (MD/MX) resistance in the model yeast: understanding their physiological function through post-genomic approaches. *Front. Physiol.* 5:180. doi: 10.3389/fphys.2014.00180

Florea, L., Song, L., and Salzberg, S. L. (2013). Thousands of exon skipping events differentiate among splicing patterns in sixteen human tissues. *F1000Res.* 2:188. doi: 10.12688/f1000research.2-188.v2

Gill, S. S., Anjum, N. A., Hasanuzzaman, M., Gill, R., Trivedi, D. K., Ahmad, I., et al. (2013). Glutathione and glutathione reductase: a boon in disguise for plant abiotic stress defense operations. *Plant Physiol. Biochem.* 70, 204–212. doi: 10.1016/j.plaphy.2013.05.032

Gourlay, C. W., and Ayscough, K. R. (2005). Identification of an upstream regulatory pathway controlling actin-mediated apoptosis in yeast. *J. Cell Sci.* 118, 2119–2132. doi: 10.1242/jcs.02337

Gu, H., Zhang, J., and Bao, J. (2015). High tolerance and physiological mechanism of *Zymomonas mobilis* to phenolic inhibitors in ethanol fermentation of corncob residue. *Biotechnol. Bioeng.* 112, 1770–1782. doi: 10.1002/bit.25603

Heipieper, H. J., Keweloh, H., and Rehm, H. J. (1991). Influence of phenols on growth and membrane permeability of free and immobilized *Escherichia coli*. *Appl. Environ. Microbiol.* 57, 1213–1217.

Horitsu, H., Yahashi, Y., Takamizawa, K., Kawai, K., Suzuki, T., and Watanabe, N. (1992). Production of xylitol from D-xylose by *Candida tropicalis*: optimization of production rate. *Biotechnol. Bioeng.* 40, 1085–1091. doi: 10.1002/bit.260400912

Hossain, M. Z., Teixeira da Silva, J. A., and Fujita, M. (2006). "Differential roles of glutathione S-transferase in oxidative stress modulation," in *Floriculture, Ornamental and Plant Biotechnology*, ed. J. A. Teixeira da Silva, (London: Global Science Books Ltd), 108–116.

Ibraheem, O., and Ndimba, B. K. (2013). Molecular adaptation mechanisms employed by ethanologenic bacteria in response to lignocellulose-derived inhibitory compounds. *Int. J. Biol. Sci.* 9, 598–612. doi: 10.7150/ijbs.6091

Jiang, Y., Wen, J., Li, H., Yang, S., and Hu, Z. (2005). The biodegradation of phenol at high initial concentration by the yeast *Candida tropicalis*. *Biochem. Eng. J.* 24, 243–247. doi: 10.1016/j.bej.2005.02.016

Kanehisa, M., Goto, S., Kawashima, S., Okuno, Y., and Hattori, M. (2004). The KEGG resource for deciphering the genome. *Nucleic Acids Res.* 32, D277–280. doi: 10.1093/nar/gkh063

Klaunig, J. E., Wang, Z., Pu, X., and Zhou, S. (2011). Oxidative stress and oxidative damage in chemical carcinogenesis. *Toxicol. Appl. Pharmacol.* 254, 86–99. doi: 10.1016/j.taap.2009.11.028

Krug, M., Ziegler, H., and Straube, G. (1985). Degradation of phenolic compounds by the yeast *Candida tropicalis* HP 15. I. Physiology of growth and substrate utilization. *J. Basic Microbiol.* 25, 103–110. doi: 10.1002/jobm.3620250206

Kupiec, M., Byers, B., and Esposito, R. (1997). "Meiosis and sporulation in *Saccharomyces cerevisiae*," in *The Molecular and Cellular Biology of the Yeast Saccharomyces cerevisiae*, eds J. Pringle, J. Broach, and E. Jones, (New York, NY: Cold Spring Harbor), 889–1036.

Kurihara, T., Ueda, M., Okada, H., Kamasawa, N., Naito, N., Osumi, M., et al. (1992). Beta-oxidation of butyrate, the short-chain-length fatty acid, occurs in peroxisomes in the yeast *Candida tropicalis*. *J. Biochem.* 111, 783–787. doi: 10.1093/oxfordjournals.jbchem.a123836

Kurosawa, K., Laser, J., and Sinskey, A. J. (2015). Tolerance and adaptive evolution of triacylglycerol-producing *Rhodococcus opacus* to lignocellulose-derived inhibitors. *Biotechnol. Biofuels* 8:76. doi: 10.1186/s13068-015-0258-3

Lanneau, D., Wettstein, G., Bonniaud, P., and Garrido, C. (2010). Heat shock proteins: cell protection through protein triage. *ScientificWorldJournal* 10, 1543–1552. doi: 10.1100/tsw.2010.152

Lima, C. F., Fernandes-Ferreira, M., and Pereira-Wilson, C. (2006). Phenolic compounds protect HepG2 cells from oxidative damage: relevance of glutathione levels. *Life Sci.* 79, 2056–2068. doi: 10.1016/j.lfs.2006.06.042

Lin, C. P., Kim, C., Smith, S. O., and Neiman, A. M. (2013). A highly redundant gene network controls assembly of the outer spore wall in *S. cerevisiae*. *PLoS Genet.* 9:e1003700. doi: 10.1371/journal.pgen.1003700

Liu, Z. L., and Slininger, P. J. (2007). Universal external RNA controls for microbial gene expression analysis using microarray and qRT-PCR. *J. Microbiol. Methods* 68, 486–496. doi: 10.1016/j.mimet.2006.10.014

Long, Y., Yang, S., Xie, Z., and Cheng, L. (2014). Identification and characterization of phenol hydroxylase from phenol-degrading *Candida tropicalis* strain JH8. *Can. J. Microbiol.* 60, 585–591. doi: 10.1139/cjm-2014-0417

Ma, M., and Liu, Z. L. (2010). Comparative transcriptome profiling analyses during the lag phase uncover YAP1, PDR1, PDR3, RPN4, and HSF1 as key regulatory genes in genomic adaptation to the lignocellulose derived inhibitor HMF for *Saccharomyces cerevisiae*. *BMC Genomics* 11:660. doi: 10.1186/1471-2164-11-660

Mahgoub, S., Abdelbasit, H., and Abdelfattah, H. (2014). Removal of phenol and zinc by *Candida* isolated from wastewater for integrated biological treatment. *Desalin. Water Treat.* 53, 3381–3387. doi: 10.1080/19443994.2014.934113

Mao, X., Cai, T., Olyarchuk, J. G., and Wei, L. (2005). Automated genome annotation and pathway identification using the KEGG Orthology (KO) as a controlled vocabulary. *Bioinformatics* 21, 3787–3793. doi: 10.1093/bioinformatics/bti430

Masutomi, K., Possemato, R., Wong, J. M., Currier, J. L., Tothova, Z., Manola, J. B., et al. (2005). The telomerase reverse transcriptase regulates chromatin state and DNA damage responses. *Proc. Natl. Acad. Sci. U.S.A.* 102, 8222–8227. doi: 10.1073/pnas.0503095102

Matjie, R. H., and Engelbrecht, R. (2007). Selective removal of dissolved silicon and aluminium ions from gas liquor by hydrometallurgical methods. *Hydrometallurgy* 85, 172–182. doi: 10.1016/j.hydromet.2006.08.012

Mayer, M. L., Gygi, S. P., Aebersold, R., and Hieter, P. (2001). Identification of RFC(Ctf18p, Ctf8p, Dcc1p) an alternative RFC complex required for sister chromatid cohesion in *S. cerevisiae*. *Mol. Cell* 7, 959–970. doi: 10.1016/s1097-2765(01)00254-4

Mishra, V. K., and Kumar, N. (2017). Microbial degradation of phenol: a review. *J. Water Pollut. Purif. Res.* 4, 17–22. doi: 10.1504/IJEP.2008.016895

Neiman, A. M. (2011). Sporulation in the budding yeast *Saccharomyces cerevisiae*. *Genetics* 189, 737–765. doi: 10.1534/genetics.111.127126

Nunes, P. A., Tenreiro, S., and Sa-Correia, I. (2001). Resistance and adaptation to quinidine in Saccharomyces cerevisiae: role of QDR1 (YIL120w), encoding a plasma membrane transporter of the major facilitator superfamily required for multidrug resistance. *Antimicrob. Agents Chemother.* 45, 1528–1534. doi: 10.1128/AAC.45.5.1528-1534.2001

Obeng, E. A., Carlson, L. M., Gutman, D. M., Harrington, W. J. Jr., and Lee, K. P. (2006). Proteasome inhibitors induce a terminal unfolded protein response in multiple myeloma cells. *Blood* 107, 4907–4916. doi: 10.1182/blood-2005-08-3531

Oku, M., Nishimura, T., Hattori, T., Ano, Y., Yamashita, S., and Sakai, Y. (2006). Role of Vac8 in formation of the vacuolar sequestering membrane during micropexophagy. *Autophagy* 2, 272–279. doi: 10.4161/auto.3135

Pammer, M., Briza, P., Ellinger, A., Schuster, T., Stucka, R., Feldmanns, H., et al. (1992). *DIT101* (*CSD2*, *CAL1*), a cell cycle-regulated yeast gene required for synthesis of chitin in cell walls and chitosan in spore walls. *Yeast* 8, 1089–1099. doi: 10.1002/yea.320081211

Perrone, G. G., Tan, S. X., and Dawes, I. W. (2008). Reactive oxygen species and yeast apoptosis. *Biochim. Biophys. Acta* 1783, 1354–1368. doi: 10.1016/j.bbamcr.2008.01.023

Pinto, R. T. P., Lintomen, L., Luz, L. F. L., and Wolf-Maciel, M. R. (2005). Strategies for recovering phenol from wastewater: thermodynamic evaluation and environmental concerns. *Fluid Phase Equilib.* 228-229, 447–457. doi: 10.1016/j.fluid.2004.09.005

Rowe, L. A., Degtyareva, N., and Doetsch, P. W. (2008). DNA damage-induced reactive oxygen species (ROS) stress response in *Saccharomyces cerevisiae*. *Free Radic. Biol. Med.* 45, 1167–1177. doi: 10.1016/j.freeradbiomed.2008.07.018

Ruiz-Herrera, J., Martı̀nez, A. I., and Sentandreu, R. (2002). Determination of the stability of protein pools from the cell wall of fungi. *Res. Microbiol.* 153, 373–378. doi: 10.1016/s0923-2508(02)01335-9

Sa-Correia, I., dos Santos, S. C., Teixeira, M. C., Cabrito, T. R., and Mira, N. P. (2009). Drug:H+ antiporters in chemical stress response in yeast. *Trends Microbiol.* 17, 22–31. doi: 10.1016/j.tim.2008.09.007

Sampaio, J. P. (1999). Utilization of low molecular weight aromatic compounds by heterobasidiomycetous yeasts: taxonomic implications. *Can. J. Microbiol.* 45, 491–512. doi: 10.1139/w99-020

Schneiter, R., Guerra, C., Lampl, M., Tatzer, V., Zellnig, G., Klein, H., et al. (2000). A novel cold-sensitive allele of the rate-limiting enzyme of fatty acid synthesis, acetyl coenzyme A carboxylase, affects the morphology of the yeast vacuole through acylation of Vac8p. *Mol. Cell. Biol.* 20, 2984–2995. doi: 10.1128/mcb.20.9.2984-2995.2000

Senft, D., and Ronai, Z. A. (2015). UPR, autophagy, and mitochondria crosstalk underlies the ER stress response. *Trends Biochem. Sci.* 40, 141–148. doi: 10.1016/j.tibs.2015.01.002

Suzuki, K., and Ohsumi, Y. (2007). Molecular machinery of autophagosome formation in yeast, *Saccharomyces cerevisiae*. *FEBS Lett.* 581, 2156–2161. doi: 10.1016/j.febslet.2007.01.096

Teixeira, M. C., Monteiro, P. T., Guerreiro, J. F., Goncalves, J. P., Mira, N. P., dos Santos, S. C., et al. (2014). The YEASTRACT database: an upgraded information system for the analysis of gene and genomic transcription regulation in *Saccharomyces cerevisiae*. *Nucleic Acids Res.* 42, D161–166. doi: 10.1093/nar/gkt1015

Teixeira, M. C., Raposo, L. R., Mira, N. P., Lourenco, A. B., and Sa-Correia, I. (2009). Genome-wide identification of *Saccharomyces cerevisiae* genes required for maximal tolerance to ethanol. *Appl. Environ. Microbiol.* 75, 5761–5772. doi: 10.1128/AEM.00845-09

Varma, R. J., and Gaikwad, B. G. (2009). Biodegradation and phenol tolerance by recycled cells of *Candida tropicalis* NCIM 3556. *Int. Biodeter. Biodegr.* 63, 539–542. doi: 10.1016/j.ibiod.2009.01.001

Walter, S., and Buchner, J. (2002). Molecular chaperones—cellular machines for protein folding. *Angew. Chem. Int. Ed. Engl.* 41, 1098–1113.

Wang, C. W., and Klionsky, D. J. (2003). The molecular mechanism of autophagy. *Mol. Med.* 9, 65–76. doi: 10.1007/BF03402040

Wang, S., Li, H., Fan, X., Zhang, J., Tang, P., and Yuan, Q. (2015). Metabolic responses in *Candida tropicalis* to complex inhibitors during xylitol bioconversion. *Fungal Genet. Biol.* 82, 1–8. doi: 10.1016/j.fgb.2015.04.022

Yang, J., Ding, M. Z., Li, B. Z., Liu, Z. L., Wang, X., and Yuan, Y. J. (2012). Integrated phospholipidomics and transcriptomics analysis of *Saccharomyces cerevisiae* with enhanced tolerance to a mixture of acetic acid, furfural, and phenol. *OMICS* 16, 374–386. doi: 10.1089/omi.2011.0127

Yao, R., Zhang, Z., An, X., Bucci, B., Perlstein, D. L., Stubbe, J., et al. (2003). Subcellular localization of yeast ribonucleotide reductase regulated by the DNA replication and damage checkpoint pathways. *Proc. Natl. Acad. Sci. U.S.A.* 100, 6628–6633. doi: 10.1073/pnas.1131932100

Yi, X., Gu, H., Gao, Q., Liu, Z. L., and Bao, J. (2015). Transcriptome analysis of *Zymomonas mobilis* ZM4 reveals mechanisms of tolerance and detoxification

of phenolic aldehyde inhibitors from lignocellulose pretreatment. *Biotechnol. Biofuels* 8:153. doi: 10.1186/s13068-015-0333-9

Yoneda, A., Henson, W. R., Goldner, N. K., Park, K. J., Forsberg, K. J., Kim, S. J., et al. (2016). Comparative transcriptomics elucidates adaptive phenol tolerance and utilization in lipid-accumulating *Rhodococcus opacus* PD630. *Nucleic Acids Res.* 44, 2240–2254. doi: 10.1093/nar/gkw055

Zhou, L., Cheng, D., Wang, L., Gao, J., Zhao, Q., Wei, W., et al. (2017). Comparative transcriptomic analysis reveals phenol tolerance mechanism of evolved *Chlorella* strain. *Bioresour. Technol.* 227, 266–272. doi: 10.1016/j.biortech.2016.12.059

Conflict of Interest: The authors declare that the research was conducted in the absence of any commercial or financial relationships that could be construed as a potential conflict of interest.

frontiers in Microbiology

ORIGINAL RESEARCH
published: 13 May 2020
doi: 10.3389/fmicb.2020.00675

Decolorization of Palm Oil Mill Effluent by *Klebsiella Pneumonia* ABZ11: Remediation Efficacy and Statistical Optimization of Treatment Conditions

Mohammed Abdulsalam[1,2], Hasfalina Che Man[1]*, Zurina Zainal Abidin[3], Khairul Faezah Yunos[4] and Aida Isma Idris[5]*

[1] Department of Biological and Agricultural Engineering, Faculty of Engineering, Universiti Putra Malaysia, Serdang, Malaysia, [2] Department of Agricultural and Bio-Resources Engineering, Faculty of Engineering, Ahmadu Bello University, Zaria, Nigeria, [3] Department of Chemical and Environmental Engineering, Faculty of Engineering, Universiti Putra Malaysia, Serdang, Malaysia, [4] Department of Food and Process Engineering, Faculty of Engineering, Universiti Putra Malaysia, Serdang, Malaysia, [5] Department of Chemical Engineering, Segi University, Kota Damansara, Malaysia

OPEN ACCESS

Edited by:
Mayur B. Kurade, Hanyang University, South Korea

Reviewed by:
Gaurav Saxena, Jawaharlal Nehru University, India
Tatoba Waghmode, Institute of Genetics and Developmental Biology (CAS), China

***Correspondence:**
Mohammed Abdulsalam
gs50431@student.upm.edu.my
Hasfalina Che Man
hasfalina@upm.edu.my

Specialty section:
This article was submitted to Microbiotechnology, a section of the journal Frontiers in Microbiology

Received: *29 November 2019*
Accepted: *24 March 2020*
Published: *13 May 2020*

Citation:
Abdulsalam M, Man HC, Abidin ZZ, Yunos KF and Idris AI (2020) Decolorization of Palm Oil Mill Effluent by Klebsiella Pneumonia ABZ11: Remediation Efficacy and Statistical Optimization of Treatment Conditions. Front. Microbiol. 11:675. doi: 10.3389/fmicb.2020.00675

Colorants contained in palm oil mill effluent (POME) are recalcitrant and carcinogenic in nature. The commonly applied ponding treatment methods have been reported inefficient for remediating the concentration of the colorants before discharge. The need for sustainable and efficient treatment technique is crucial in order to preserve the environment. In this view, this study reported the first attempt to decolorize POME using a proliferate *Klebsiella Pneumonia* ABZ11 at varied inoculum sizes of 5–25% (v/v), initial color concentration (650–2,600 ADMI) and treatment time of 5-40 h. The treatment conditions were optimized using Response Surface Methodology. At optimal conditions of 20% (v/v) inoculum size, initial-color concentration of 2,600 ADMI, initial pH of 7 and 35 h treatment retention time, over 80.40% color removal was achieved with insignificant disparity compared with the model predicted value of 81.538%. Also, the Monod model excellently described the decolorization kinetic process with 0.9214 coefficient of correlation (R^2), and the calculated maximum growth μ_{max}) and half-saturation constant (K_s) were 7.023 d^{-1} and 340.569 ADMI d^{-1}, respectively. This study revealed that the *Klebsiella Pneumonia* ABZ11 was highly prolific and such feature may favor a synergistic biodegradation process.

Keywords: POME, decolorization, colorants, *Klebsiella pneumonia* ABZ11, kinetic-model, optimization

INTRODUCTION

Industrial processing and extraction of oil palm are usually associated with the colossal generation of colored wastewater commonly known as palm oil mill effluent (POME). Reports have shown that about 2.5 t of raw colored POME are generated from every ton of crude oil-palm extracted (Choong et al., 2018). The dark brownish color of the effluent was due to excessive concentration of tannins, melanoidin and lignin compounds (Tamrin and Zahrim, 2017; Tan et al., 2017). However, reductase activities of microbes on the complex colorants could result in the formation of aromatic

ring amines compound which is more toxic than the precursor compounds (Neoh et al., 2013). Although, the initial form of the colorants compounds may not be considered as cytotoxic or carcinogenic substances. Conversely, decomposition of these compounds after discharged into the environment could lead to the formation of aromatic amines which are capable of inducing cancer or tumors (Ganapathy et al., 2019). More so, continues accumulation of POME in waterways is responsible for diminishing photosynthetic processes of the planktons, thereby distorting the stable ecosystem in the aquatic environment (Abdulsalam et al., 2018b). Therefore, the need for effectual treatments technique to reduce the concentration of the colorant before discharge into the environment is critical.

However, ponding system has being the most common method used for treating POME before discharge into the waterways but it has been proven ineffectual, particularly for color removal (Rana et al., 2017; Iskandar et al., 2018). Though physical and/or chemical treatment methods such as adsorption, chemical oxidation and reduction, precipitation, chemical-photolysis, and electrochemical processes decolorizes POME (Abdulsalam et al., 2018a), but they are economically unsustainable and often resulted in the generation of acidic secondary effluent which requires further treatment before discharge. Nonetheless, remediation of organic contaminants in POME using microorganisms such as fungus and bacteria, had demonstrated a promising performance. A consortium of fungi which constitutes *Yarrowia lipolytica, Trichoderma viride* spores, *Saccharomyces cerevisiae,* and *Trichoderma viride* mycelium reduces the initial color concentration by 60–70% under anaerobic condition (Bala et al., 2018). Also, the Brown-rot and White-rot fungus are widely applied for degradation of lignocellulose compounds in POME (Hermosilla et al., 2018). On the other hand, fungus mostly exhibits poor adaptability due to fluctuation in environmental factors such as pH, temperature and oxygen compositions, alongside with difficulty in genetic modification (Sharma et al., 2018).

As a result of the malleability and potency properties of bacteria, its application for wastewater treatment has gained significant attention (Yang et al., 2018; Fu et al., 2019). For example, it performed excellently in reducing the activity of xylanase in POME (Prasertsan et al., 2017), and production of cellulose, lipase, protease and exoglucanase (de Souza et al., 2015; Baraniya et al., 2016; Louhasakul et al., 2016). In another study, Ohimain and Izah (2017) applied an indigenous *Penicillium* consortium on different sources of POME sludge to produce lignin peroxidase. At pH of 7.3, it was observed that the *Penicillium* sequestered from fruit bunches demonstrated outstanding performance in terms of biodegradation of the contaminants present in the POME. Bala et al. (2018) isolated bacteria consortium from POME and applied for contaminants remediation. From the results, they concluded that the community microorganisms have a synergistic removal efficiency of 90.23, 91.06 and 92.23% for BOD, COD and TSS, respectively. Also, Cheah et al. (2018) used POME as a culture media for the cultivation of biomass using the combined *Pseudomonas* sp. and microalgae. The combined bacteria-algae give higher biomass yield (185.7 mg/L/day) and better pollutants degradation. Despite all these efforts, bio-decolorization of POME remains a serious challenge, as the existing techniques were unable to certify the discharge standard limits for color (Lee et al., 2019).

However, the applications of *Klebsiella Pneumonia* ABZ11 for POME decolorization under anaerobic conditions have received little or no attention despite its unique prolificacy and rapid adaptability to change in environmental factors. More interestingly, *Klebsiella Pneumonia* ABZ11 has been characterized to exhibit xenobiotic metabolism on polyphenol and lignocellulose substances using secreted hepatic extracellular polymeric substances and enzymes to facilitate oxidation, reduction, hydrolysis and/or hydration (Xu Z. et al., 2018). This implies that at favorable conditions, the bacteria could swiftly decompose the bio-polymeric colorants (such as the phenol, lignin, tannin and melanoidin) contained in POME (Xu R. et al., 2018). These are the main reasons that motivated this study in order to bridge the existing dearth information on the application of *Klebsiella Pneumonia* ABZ11 for POME decolorization. In this view, the inoculum was cultured to activate the stock, and then the viability was analyzed using optical density technique. Afterward, decolorization performance was examined at varied inoculum sizes (5–25% v/v), initial color concentrations (650–2,600 ADMI), and treatment retention time (5–40 h), while the initial pH of 7 and 120 rpm agitation speed remained fixed throughout the experiment. The treatment conditions were optimized using response surface methodology and the regression model was validated. The accuracy of the prediction using the model was examined based on the coefficient of correlation (R^2) and normality analysis. In addition, the results obtained were statistically analyzed using Design-Expert 10.0.7 and the significance of the treatment factors were examined based on the magnitude of the *F*-values, while the *P* value less than 0.05 is considered to be statistically significant with 95% confidence level.

MATERIALS AND METHODS

Experimental Materials

Nutrient broth (MERCK 1.05443.0500); Nutrient agar (MERCK 1.05450.0500); Micropipette tips (1,000 and 100 μL); microcentrifuge tube (1 mL); wire loops; disposable petri dish and Erlenmeyer flasks (250 mL) were all procured from SIGMA ADRICH (Merck). Also, about 25 L of final discharged POME was collected from an Oil Palm Milling industry, located at Carey Island, Malaysia The visible debris in the sample was separated using a cotton-filter and the initial physicochemical properties were determined using a standard procedure (APHA, 2005). Then, the remaining bulk of the filtrate sample was stored in a chiller at 4°C prior to the further use. In addition, both solid and liquid culturing media were applied in this study. The solid media was prepared using nutrients agar and petri dish following the standard procedure as stipulated by the manufacturer (SIGMA ADRICH). The nutrient agar is composed of partially digested protein (5 g/L); sodium chloride (8 g/L); beef extract (3 g/L) and agar (15 g/L). Approximately 20 g of the nutrient

agar was dissolved in 1,000 mL of distilled water under continues stirring condition at 90 rpm and 60°C and then autoclaved at 121°C temperature for a duration of 15 min. Afterward, 100 μL of the homogenous nutrient solution was pipetted into the agar plates (petri dish) and allowed to dehydrate under the laminar flow cabinet. Similar procedures were employed during the preparation of liquid media. However, only 8 g of the medium (compositions: yeast extract-2 g/L, beef extract-1 g/L, NaCl-5 g/L and peptone-5 g/L) was dissolved in 1,000 mL of distilled water, stirred thoroughly at steady agitation of 120 rpm. The mixture was autoclaved at 121°C for 15 min and then stored at 4°C.

Microorganism

The isolated *Klebsiella Pneumonia* ABZ11 from Antarctica seawater applied in this study was obtained from Universiti Teknologi Malaysia. The bacterium was analyzed using 16S rDNA array and the sequence shows a 99% correlation to *Klebsiella pneumoniae* with Accession Number of KX266892 (Mohammed and Zaharah, 2019)[1]. The 16S rRNA gene PCR amplifications were conducted using universal primers, such that the Forward primer and Reverse primer reads 14-F: 5′-AGAGTTTGATCCTGGCTCAG-3′ and 1492-R: 5′-CGGTTACCTTGTTACGACTT-3′, respectively. The detail reports on the screening, identification including the phylogenetic tree constructed have been reported and published previously (Mohammed and Zaharah, 2019). More so, additional information on the genomic DNA, PCR amplification, partial gene sequence and the phylogenetic relationship of Klebsiella sp. of the ABZ11 were available as **Supplementary Figures S1–S4**, respectively.

Preparation of Inoculum and Growth Analysis Using POME as a Media

A single colony was picked into 15 ml of nutrient broth (liquid media) contained in a tube. Initially, the media was adjusted to a pH of ≈7 using 0.1 M of HCl solution. Afterward, the inoculated media was incubated at 35°C and 120 rpm agitation for only 16 h (Singh et al., 2013). The activated inoculum was transferred into a conical flask (500 ml capacity) containing 85 mL of POME solution (25% color concentration i.e., DF = 4), then incubated for 72 h at 35°C and steady agitation of 120 rpm. At an interval of 4 h, about 2 mL of the sample was taken and used for the growth analyzed until the end of the incubation period (72 h). The analysis includes optical density reading (OD), coliform count (CC) and maximum growth analysis (μ_{max}) (based on Monod Kinetic model).

Optical Density

The OD was monitored by analyzing the changes in the turbidity of the incubated sample using UV-spectrophotometer (HACH 4000U) at a preset absorbance wavelength of 600 nm. Initially, 1 mL of the incubated samples were centrifuged at 10,000 × *g*, for 15 min. Supernatant of the centrifuged samples was discarded, while the accumulated cell pellets were suspended in brine solution of 1% concentration. Then, the suspended cell pellets were placed in a sterilized vial tube for the OD reading at 600 nm.

[1]http://blast.ncbi.nlm.nih.gov/Blast.cgi

Coliform Count

The colonies counts were determined in separate experiments using serial dilutions technique in a brine solution of 1% concentration with an initial stock of 1.0 ml. Each diluted stock was agitated to ensure a homogenous mixture. Afterward, the content was plated by pipetting 1 mL into the sets of nutrient agar media and then cultured at a temperature of 35°C for 24 h. The grown culture was used to determine the number of colonies formed (CFU/mL) with respect to the corresponding dilution factor, (DF: 10^1 to 10^{10}) using Eq. 1.

$$\text{CFU/ml} = \text{DF} \times N_t \tag{1}$$

where; DF is the dilution factor; N is the number of colonies formed.

Growth Kinetics

The maximum growth (μ_{max}) were determined using the Monod Kinetic Model. For the purpose of this study, only the lag and exponential phase of the bacteria growth were considered in the model equations, since the maximum growth of the microbes was defined based on retention time (Park et al., 2015). Thus, only the substrate utilization data obtained in the first 20 h of treatment time were fitted into the kinetic model. This procedure will reflect the more accurate result of the maximum growth during the bio-decolorization process with minimal bias (Park et al., 2015). The general form of the Monod Kinetic Model is expressed in Eq. 3, which rearranged to obtain Eq. 4;

$$\frac{1}{RT} = \frac{\mu_{max} \times C_e}{K_s + C_e} \tag{2}$$

$$RT = \left(\frac{K_s}{\mu_{max}}\right)\frac{1}{C_e} + \frac{1}{\mu_{max}} \tag{3}$$

where; RT is the treatment time (h) and C_e is the colorant concentration of the treated sample (ADMI). The maximum growth (μ_{max}) and the half-saturation constant (K_s) were obtained from the gradient and interception of the regression curve of $1/S_e$ with respect to RT.

Decolorization Efficacy Using Batch Experimental Approach

The batch decolorization experimental layout was developed using randomized multilevel categoric design (Design Expert Version-10.0.7) with a total of 120 runs and a fixed initial pH of ≈7 was maintained throughout the experiment. The schematic representation of the batch experimental set-up is shown in **Figure 1**. The cultured *Klebsiella Pneumonia* ABZ11 in the liquid media was used as inoculum at varied sizes (5–25% v/v) to examine its decolorization performance in a prepared POME sample of varying color concentrations (25–100%) and retention time (5–40 h). it should be noted that the color concentrations were varied by adding distilled water at dilutions factors of 4, 3, 2, and 1, and these give a corresponding color concentration of 650, 1,300, 1950, and 2,600 ADMI, respectively. At the end of each treatment, aliquots of the decolorized samples were taken and centrifuged at 10,000 × *g* for 15 min. The final

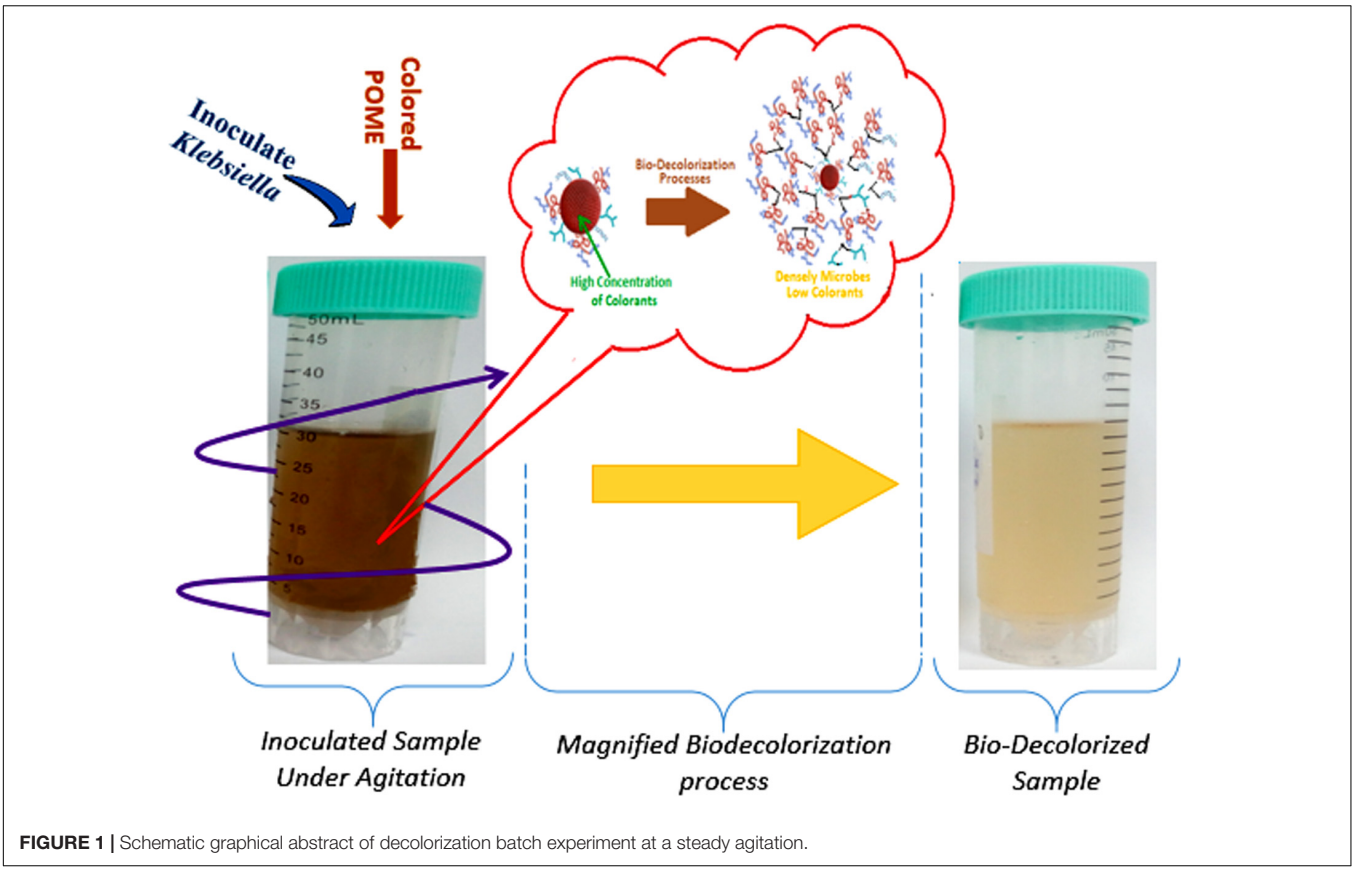

FIGURE 1 | Schematic graphical abstract of decolorization batch experiment at a steady agitation.

color concentration of the centrifuged supernatants of the treated samples was analyzed using a spectrophotometer (HACH 4000U) at 400 nm absorbance wavelength. All the experimental readings were triplicated in order to minimize bias. Finally, the percentage of color removal was calculated using Eq. 4;

$$\% \text{ Color removal} = \left(1 - \frac{C_e}{C_i}\right) \times 100 \tag{4}$$

where; C_i and C_e were color concentrations before and after treatment, respectively. The C_e and C_i were measured in ADMI scale. This scale is defined as American Dye Manufacturer's Institutes (ADMI). Normally it uses a spectral method to calculate a single color value that is independent of hue. It is used for tinted effluents with colors that are different from the widely used Pt-Co units. ADMI scaling is program into the spectrophotometer (HACH 4000U) and it analysis the level of color concentration at absorbance wavelength of 400 nm, as mentioned earlier. The analysis of the color was done before and after each of the treatment.

Performance Optimization

The Composite-Central-Design (Response Surface Methodology-Design Expert Version 10.0.7) was applied to develop the matrix for the optimization experiment with a total of 20 runs and the initial pH was fixed at ≈7 throughout. The multiple independent variables considered includes the *A*-inoculum size (5–25% v/v), *B*-initial color concentration (650–2,600, ADMI), and *C*-retention time (5–40 h). Basically, the interaction of the multiple's variables with respect to the predicted-response (Y_i-percentage of color removal) is usually expressed mathematically in the second-order polynomial model, as presented in Eq. 5;

$$Y_i = \alpha_0 + \sum_{i=1}^{k} \alpha_i x_i + \sum_{i=1}^{k} \alpha_{ii} x_i^2 + \sum_{i=1}^{k} \sum_{j=1}^{k} \propto_{ij} x_i x_j \tag{5}$$

where, Y_i denotes predicted response, α_o represents an offset term, while x_i and x_j are the input variables. Also, α_i is *i*th linear-coefficient, α_{ii} is *i*th quadratic-coefficient and α_{ij} is represent *ij*th interaction-coefficient.

The experimental matrix based on the stated independent variables is summarized in **Table 1**. The optimization experiments were performed in a series of 250 mL Erlenmeyer flasks. Each flask contains a proportionate amount of POME concentration (650–2,600 ADMI) with inoculum (5–25% v/v) based on the developed experimental matrix to give 50 mL mixture of sample sizes. The inoculated mixtures were placed in an incubator shaker and treated at variable retention time (5–40 h) under steady agitation of 120 rpm. The treated samples were centrifuged and the color concentration of the supernatants was analyzed using a spectrophotometer. Each of the analysis was triplicated and then took the average.

TABLE 1 | Optimization experimental layout summary for color removal.

Treatment factors	Unit	Symbol	Coded level		
			−1 (Lower level)	0	+1 (High level)
Inoculum size	%(v/v)	*A*	5	15	25
Initial color concentration	ADMI	*B*	650	1,625	2,600
Retention time	h	*C*	5	22.5	40

Statistical Analysis

Analysis of variance was accomplished with the Design-Expert 10.0.7 software package. In order to minimize error, all the experimental readings and procedures were triplicated, and the average reading was obtained. The significance of the treatment factors was examined based on the magnitude of the *F*-values, while the *P* value less than 0.05 is considered to be statistically significant with 95% confidence level.

Model Validation

The optimized treatment conditions were used to validate the regression model. The first three (3) predicted treatment conditions with the highest desirability index were selected and applied to examine the actual experimental percentage of color removal in the laboratory. The experimental data obtained were compared with the model predicted values based on the correlation coefficient (R^2). In addition, a normal residual analysis was conducted to further verify the accuracy of the model.

Analytical Methods

The analysis of the considered parameters (color, COD, turbidity, TSS, VSS, pH) were conducted in accordance with standard procedure (APHA, 2005). A calorimetric method was employed to determine the color, COD (vials of high concentration) and turbidity level using UV-spectrophotometer (HACH DR/4000U) at an absorbance wavelength of 400, 620, and 600 nm, respectively. Then, the percentage of color removal was determined using equation (4). The biomass suspended solids (TSS) were determined by filtering 100 mL of the sample through a 0.48 μm filter paper (Whatman, China); the retained residues were oven-dried at 105°C for 5 h. Whereas the VSS was determined by igniting the dried sample residue at 550°C using muffle furnace for a period of 15 min. The TSS and VSS were determined using Eqs 6 and 7, respectively. The pH was measured using a digital pH-meter (Ionix pH5S).

$$\text{TSS, } \left(\frac{\text{mg}}{\text{L}}\right) = \frac{M_{\text{solutes}}}{V_s} \times 1000 \tag{6}$$

$$\text{VSS, } \left(\frac{\text{mg}}{\text{L}}\right) = \frac{M_{\text{solutes}} - M_{550°\text{C}}}{V_s} \times 1000 \tag{7}$$

where; M_{solute} is mass of solute (mg); $M_{550\ \text{C}}$ is solute mass after ashed (mg); TSS is total suspended solid (mg/L) and VSS is volatile suspended solid (mg/L).

RESULTS AND DISCUSSION

Physicochemical Characterizations

Table 2 shows POME's initial physicochemical parameters. The concentrations of the analyzed parameters exceeded the DOE discharge limits. This shows that the color concentration and COD of the discharge is 2,600 ADMI and 1,264 mg/L, respectively. The contaminants concentration are far beyond the limits. Also, 320 mg/L of NH_3-N alongside with the excessive concentration of suspended solids (TSS and VSS) were observed. However, only the pH (8.5) was within the acceptable DOE limit (**Table 2**). Therefore, discharging such partially treated wastewater is hazardous due to the high concentration of the carcinogenic colorants (Kamal et al., 2019). Nonetheless, the carbonaceous complex colorants present in POME could be utilized as a sole carbon source for the indigenous and/or inoculated bacteria under favorable conditions, thereby metabolizing it into simpler and less harmful compounds (Azman et al., 2019). This is the main focus of the current study.

Viability Analysis of Inoculum

Figure 2A shows the coliform counts (log CFU/mL) with the corresponding OD readings at every growth phase in respect to retention time. As indicated in the figure, microbial growth between ① and ② presents the lag phase which lasted for ≈3.3 h and the corresponding OD readings were about ∼0.9. At this stage, the inoculum prepared for reproduction via binary fission and also synthesizes various inducible enzymes suitable for the subsequent degradation and metabolic processes (Cortes-Tolalpa et al., 2017). Therefore, a noticeable increase in the coliform is not expected at this phase (Oladipo et al., 2018). Conversely, a significant coliform reproduction takes place between ② and ③ such that an exponential increase in the population density from 8.8 to 9.9 log CFU/mL was achieved in this phase. This shows that a maximal rate of cells multiplication at minimal reproduction-time was attained. The maximum coliform (9.9 logs CFU/mL) was attained after 20 h retention with a corresponding OD reading of 3.5 (**Figure 2A**). At this exponential growth phase, the cellular constituents are produced at constant amounts relative to each other, thus showing the steadiest rate in the kinetic degradation process as well as the biochemical activities (Vello et al., 2018). On

TABLE 2 | Comparison of initial physicochemical properties of the POME sample and discharge standard limit.

Parameter	Unit	Initial concentration	Doe limit*
Color	ADMI	2,600	100A
COD	mg/L	1,264	100
pH	–	8.5	5–9
TSS	mg/L	1,540	200
VSS	mg/L	470	200
Turbidity	FAU	1,870	50
NH_3-N	mg/L	320	20

**Source: Din (2017).*

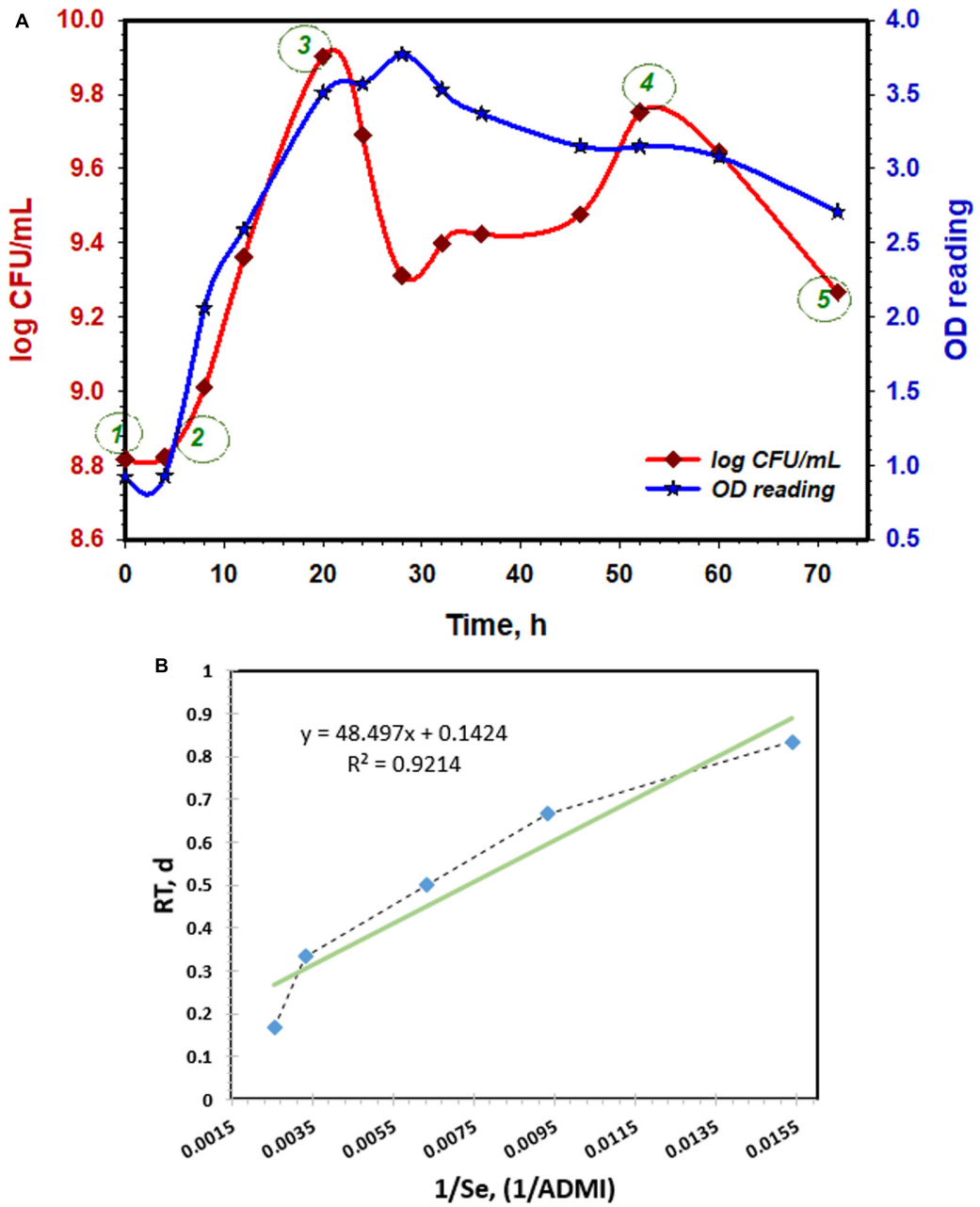

FIGURE 2 | (A) Growth trend of *Klebsiella Pneumonia* ABZ11 in terms of log CFU/mL with respective OD reading at 600 nm for a total period of 72 h. **(B)** Monod Kinetic Model linearized plot fitted with experimental data of growth rate during the lag-exponential phase.

this note, the maximum growth yield, active metabolism and the highest colorant degradation efficiency are expected in this phase. Further extension in the retention-period between ③ and ④, a malignant and unsteady state in the viability of the cells were observed (**Figure 2A**). This might be due to the depletion in the available nutrient which is not adequate to sustain the densely populated microbes (Langemann et al., 2010). As a result, an endogenous process took place such that actives cells feed on one another. Thus, a dramatic reduction in the coliform count from 9.90 to 9.25 log CFU/mL. However, at retention period of 52 h, the coliform count appreciated to ∼9.7 log CFU/mL. This suggests that after the initial coliform depletion, the available limited biodegradable nutrients were adequate to sustain the biochemical activities. Afterward, a steady diminishing in the coliform count with respect to retention-time set-in between ④ and ⑤. This observation prevailed because the number of dying cells exceeds that of the new-born cells at this stage, thereby amounting to a dramatic diminution in the viable bacterial cells (**Figure 2A**). This stage indicates the death phase of the growth analysis.

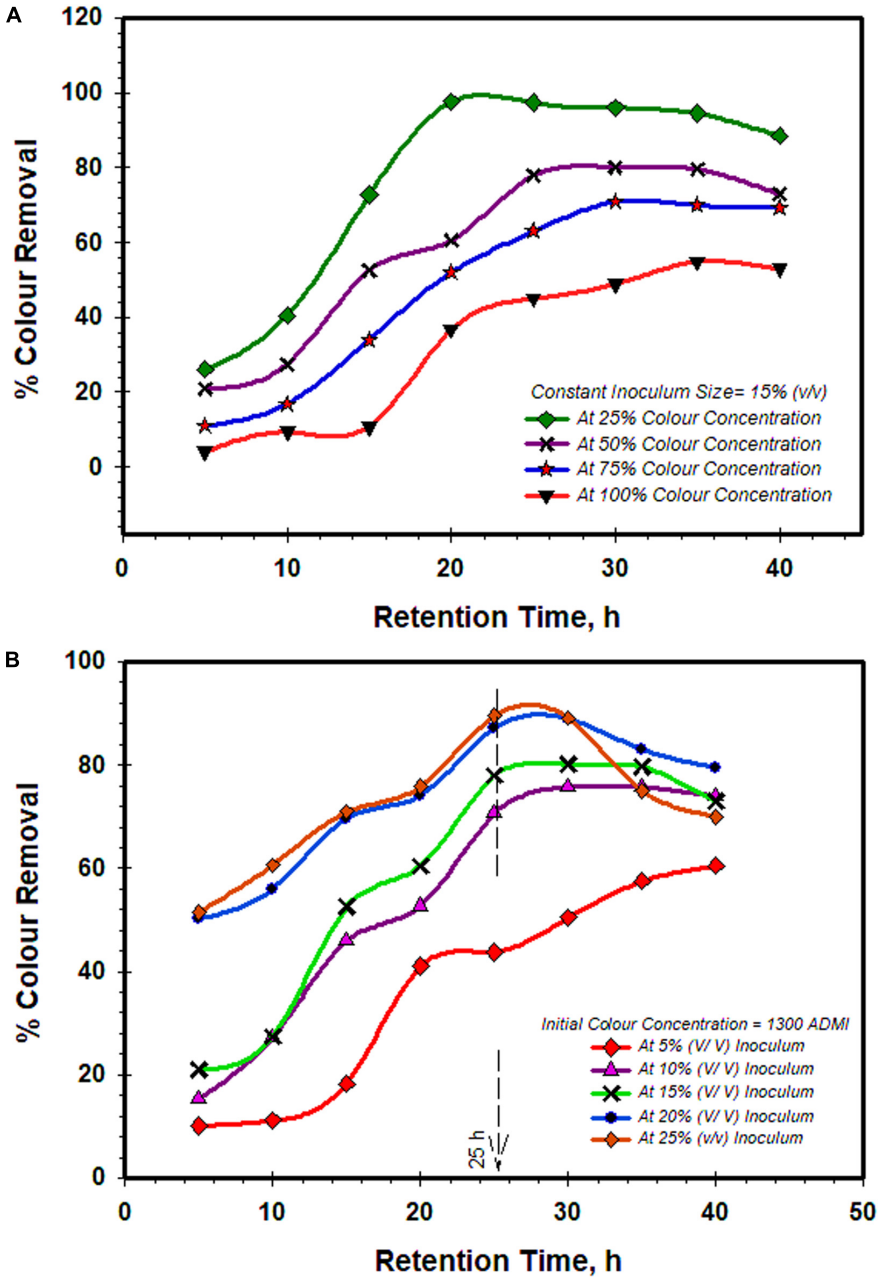

FIGURE 3 | The combined effect of treatment retention time with **(A)** initial color concentrations, and **(B)** inoculum sizes on bio-decolorization performance by *Klebsiella Pneumonia* ABZ11.

The kinetic coefficients (μ_{max} and K_s) of the bacteria growth were determined based on color depletion during the lag-exponential growth phase (Park et al., 2015). Throughout, the magnitude of color depletion was measured in ADMI. **Figure 2B** shows the linearized plot of the model such that the gradient (K_s/μ_{max}) and intercepts ($1/\mu_{max}$) were used to determine the coefficients. Initially, the best line of fits was obtained using the least square of the linear regression method and the corresponding values for each coefficient were calculated. The value of μ_{max} and K_s within the considered growth phase was 7.022 d^{-1} and 340.63 ADMI d^{-1}, respectively. Thus, the modified kinetic model based on the determined coefficients is expressed in Eq. 8;

$$\frac{1}{RT} = \frac{7.022 \times C_e}{340.63 + C_e} \quad (8)$$

where; C_e is the remnants concentration of the treated POME (ADMI); while RT is the treatment retention time, (d).

Despite the recalcitrant nature of the colorants present in POME, the μ_{max} and K_s obtained in this study were comparably

superior to that reported by Zhang et al. (2017), Ebrahimi et al. (2016) and Gonçalves et al. (2016). Collectively, the μ_{max} values stated in these works of literature ranges between 0.33 and 0.954 d^{-1}, while K_s varies within 120–243.564 mg/L, which are considerably lower compared to values achieved in the present study (7.022 d^{-1} and 340.63 ADMI d^{-1}). The higher value of μ_{max} (7.022 d^{-1}) obtained is an indication of proliferating performance of the *Klebsiella Pneumonia* ABZ11, as well as its good adaption to the treatment conditions applied. Consequently, efficient microbial extracellular activities alongside with high biodegradation capacity are expected (Chan et al., 2010). In addition, K_s value is an index measuring the capacity of substrate (colorants) degradation (Fonseca et al., 2018). In this study, the K_s value was 340.63 ADMI d^{-1} as against the reported data in the literature (Ebrahimi et al., 2016; Gonçalves et al., 2016; Zhang et al., 2017). However, the excellent degradation capacity might be due to the intrinsic metabolic characteristic of the inoculum, which enables it to adapt easily to any change in the environment or treatment conditions, and thereby generating suitable metabolic enzymes to sustain swift degradation of the colorants (Hameed and Ismail, 2018).

Batch Decolorization Performance

Effect of Initial Concentration at Varied Treatment Time With a Fixed Inoculum Size of 15% (v/v)

The initial color concentration demonstrated considerable influences on the rate of biodegradation of the colorants (**Figure 3A**). At a lower initial color concentration of 650 ADMI, the biodegradation process was considerably faster with 15% (v/v) inoculum, and over 97.73% color removal efficiency was attained after 20 h retention time. The percentage of the color removal remains relatively steady but diminished to 86% at a longer retention time of 40 h. The reduction in the removal efficiency might be due to endogenous process resulted due to the depleted organic contaminants (colorants) and available dissolved oxygen (Park et al., 2015). At a higher color concentration of 2,600 ADMI, the decolorization was rather lagging and no any significant color removal noticed in the first 15 h of retention (**Figure 3A**). However, over 57% of color removal was achieved after a retention period of 35 h. The impeded decolorization process observed earlier at this initial concentration (2,600 ADMI) could be due to the predominant complex aromatic ring structure of the recalcitrant contaminants (such as colorants) which are not easily broken by the microbes' metabolic and enzymatic activities (Hameed and Ismail, 2018). In addition, the presence of other toxic compounds (such as sulphonic groups) exerts an inhibitory effect on the extracellular activities of the microbes (Luo et al., 2014; Pernin et al., 2018). Thus, these compounds antagonize the overall bio-decolorization processes (Pernin et al., 2018). Nevertheless, the appreciable decolorization performance (57%) recorded afterward is an indication that the microbes were able to adapt and then secret suitable enzymes to degrade the high initial concentration (2,600 ADMI). In overview, it can be deduced that the efficiency of color removal decreases with increase in initial color concentrations, while the treatment retention time became much longer (**Figure 3A**). Researchers have attributed this effect to the excessive presence of toxics-recalcitrant contaminants (such as colorants) which rather inhibits the metabolic and physiological activities as well as the population density of the microbes (Luo et al., 2014; Hameed and Ismail, 2018; Pernin et al., 2018). Thus, the resulted relegation in the overall bio-degradation performance of the inoculum. This remark is also in accordance with other similar studies (Luo et al., 2014; Hameed and Ismail, 2018; Pernin et al., 2018).

Effect of Inoculum Sizes at Varied Treatment Times With a Fixed Initial Color Concentration of 1,300 ADMI

Figure 3B shows the effect of inoculum sizes with respect to treatment time on the color removal performance. A fixed initial color concentration of 1,300 ADMI was applied while the inoculum size was varied from 5 to 25% (v/v) with respect to treatment retention time (5–40 h). At inoculum size of 5% (v/v), a protracting lagging in the decolorization process (∼10.15%) was observed during the first 10 h of treatment time (**Figure 3B**). After 25 h of retention, an appreciable increase in the decolorization efficiency of 44% was attained and then improved to 60% after 40 h. However, it was generally noticed that higher inoculum size gives better decolorization performance. For example, at the 25 h of retention time, the treatment with inoculum sizes of 10, 15, 20, and 25% (v/v) recorded 70, 78, 87.5, and 89.25% of color removal. This advocate that with higher inoculum size, adequate active sites in conjunction with the intensive synergy of the metabolic process of the dense microbes are available to effectively degrade the colorants (Kumaran et al., 2016). Though, it can be perceived from this figure that the 25% (v/v) inoculum size makes no conspicuous distinction in decolorization performance compared with that of 20% (v/v). Therefore, it is reasonable to deduce that beyond inoculum size of 20% (v/v), there is no proportionate increase in the bio-decolorization proficiency with the upsurge in the inoculum size. More so, at a longer retention time of 40 h, a dramatic reduction in the percentage of color removal (68%) was observed in the treatment with 25% (v/v) inoculum size. This might be due to the copious population density of the microbes with limited nutrients (biodegradable contaminants) and dissolved oxygen (Park et al., 2015). Thus, an endogenous process prevails and this consequentially undermines the overall bio-decolorization performance. This observation was in good agreement with previous works (Moosvi et al., 2005; Mohana et al., 2007; Hameed and Ismail, 2018). Moosvi et al. (2005) reported that low count of available active microbes can result from a protracted endogenous process which later relegates the normal secretion of enzymatic substances required for the biodegradation. Also, Hameed and Ismail (2018) validated that better decolorization performances were achieved with higher inoculum size but diminished after an optimal size ranges. In another similar study reported by Mohana et al. (2007), the results confirmed that the highest decolorization and COD removal were obtained at 15% (v/v), but further increase resulted in no noticeable improvement in the remediation performance.

TABLE 3 | ANOVA for response surface quadratic model.

Source	Sum of Squares	*df*	Mean square	*F* value	*P*-value Prob > *F*	
Model	1,6907.93	9	1,878.66	13.46	0.0002	significant
A-Inoculum size	4,573.67	1	4,573.67	32.77	0.0002	–
B-Initial color concentration	3,234.80	1	3,234.80	23.17	0.0007	–
C-Retention time	6,780.16	1	6,780.16	48.57	<0.0001	–
AB	15.82	1	15.82	0.11	0.7433	–
AC	255.95	1	255.95	1.83	0.2055	–
BC	239.26	1	239.26	1.71	0.2197	–
A^2	1,256.55	1	1,256.55	9.00	0.0133	–
B^2	342.28	1	342.28	4.45	0.0384	–
C^2	1,688.73	1	1,688.73	12.10	0.0059	–
Residual	1,395.86	10	139.59	–	–	–
Lack of fit	1,392.57	5	278.51	–	–	–
Pure error	3.28	5	0.66	–	–	–
Cor total	18,303.78	19	–	–	–	–
R^2	0.9237	–	–	–	–	–
Adjusted-R^2	0.8551	–	–	–	–	–

Optimization Results

Analysis of Variance and Regression Model

Three significant experimental factors (A-inoculum size, B-initial color concentration and C-retention time) influencing decolorization of POME were optimized using center composite design (a component of RSM). The level of influences of the factors was analyzed using ANOVA, as summarized in **Table 3**. It was noticed that the regression model was statistically significant with an *F*-value of 13.46 and 0.0002 prob > *F* value. The *P*-value of 0.0002 implies that the model has less than 0.2% chance of bias due to noise. From the results, the level of significant modal terms was in the following order C, A and B with *F*-values of 48.57, 32.77, and 23.17, respectively. In addition, the terms of the polynomial such as C^2 and A^2 demonstrated considerable influences with modal *F*-value of 12.10 and 9.00, while B^2 recorded the least (4.45). Based on the level of *F*-value, C exhibited the most significant influence on the bio-decolorization process and then A was observed next to it. Thus, only the significant factors (C, A, B, A^2, C^2 and B^2) were used for developing the regression model Eq. 9. This is procedure is in accordance with Ghani et al. (2017).

$$\%\ \text{Color removal} = 5.4439 + 4.57547A - 4.10414 \times 10^{-3} B + 2.27197C - 0.10516A^2 - 5.16608 \times 10^{-6}B^2 - 0.04228C^2 \quad (9)$$

Figure 4A exemplifies the model predicted and actual values for the decolorization percentage. A good agreement was noticed between the predicted and actual values with 0.9237correlation (R^2), and also the deviation from diagonal points was insignificant. Fundamentally, the 0.9237 R^2 indicates that the notable factors (C, A, B, A^2, C^2 and B^2) have over 92% impacts on the bio-decolorization process (**Figure 4A**). Furthermore, the high R^2 (0.9237) value obtained demonstrate the reliability and confidence of the regression model, and thus it may be employed to navigate the design-space (Ghani et al., 2017). The accuracy of the model was further analyzed using normal plots of residual for the percentage of color removal, as presented in **Figure 4B**. Basically, the normal residuals point-out the amount at which the developed model satisfies ANOVA assumptions, while the studentized residuals is an index showing the level of deviation between the predicted and actual values (Mishra et al., 2019). From **Figure 4B**, it can be observed that virtually all the data points were on a straight diagonal line with insignificant deviations and this is an indication that application of response transformation is not required (Mishra et al., 2019). Therefore, it can be reasonably deduced that no apparent bias with the normality.

Perturbation Analysis

The combined effect of the three treatment factors (A, B and C) at a common point of retort was examined by the statistical design based on perturbation plot (Taherdanak et al., 2015). From **Figure 5**, the thinness of the curve reflects how subtle the response was whenever there are vicissitudes in any of the treatment factors (Mishra et al., 2019). It is obvious that the inoculum size (A), initial color concentration (B) and the retention time (C) have a considerable influence on the percentage of color removal. The optimal percentage of color removal of 81.5% was attained at the inoculum size of 20% (v/v) and the retention period of 35 h with an initial color concentration of 2,600 ADMI (without dilution). Both A and C demonstrated a positive correlation with the percentage of color removal, while B exhibited a negative correlation, (**Figure 5**). Essentially, the perturbation figure shows the common point for the combined factors where the highest synergistic influences were attained to sustain optimal decolorization process by the *Klebsiella Pneumonia* ABZ11. This implies that at this common perturbation point, the effect of the antagonist factors (AB, BC, and AC) are minimal (Eltarahony

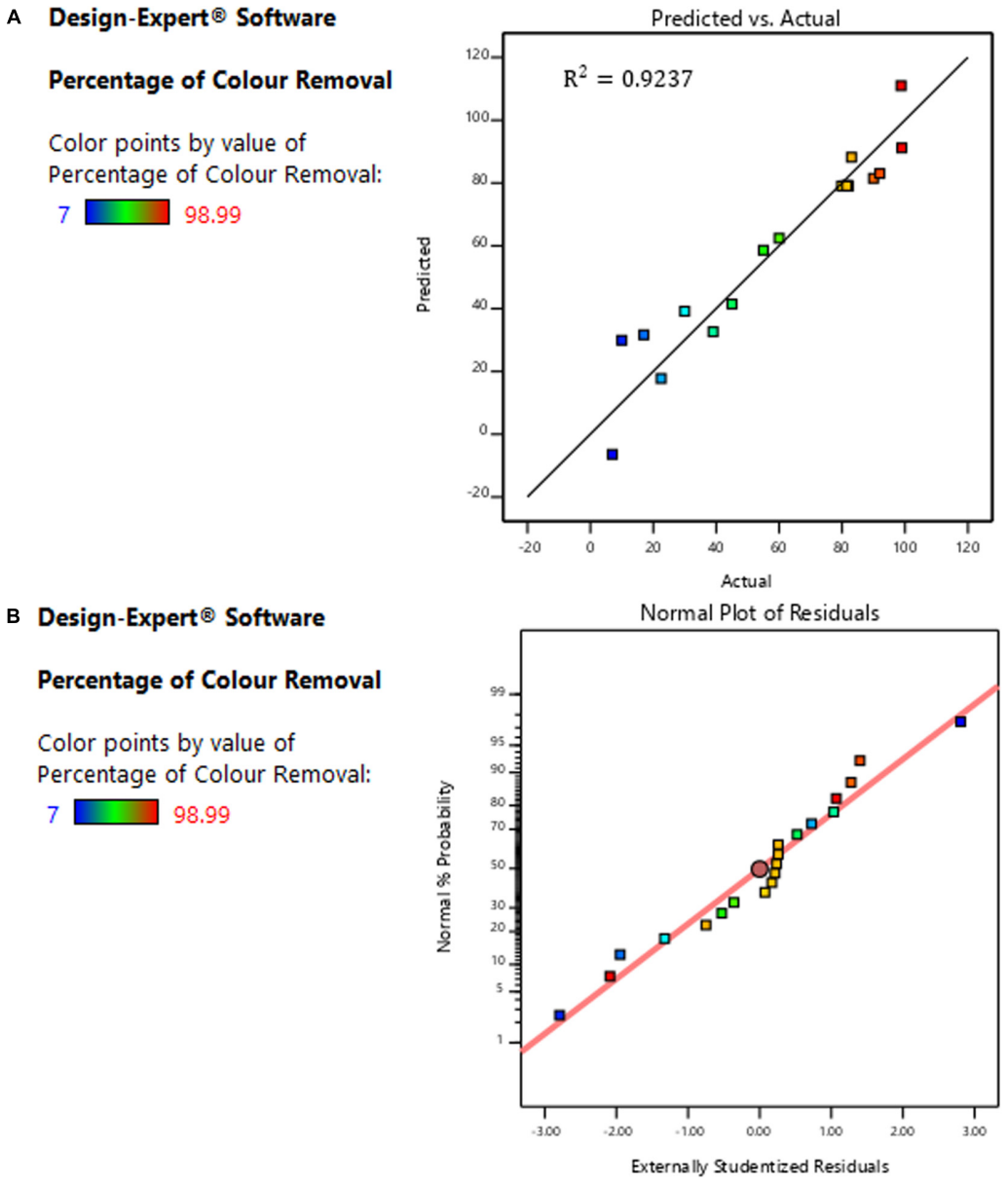

FIGURE 4 | (A) Comparison between model-predicted and actual experimental value. **(B)** Normal residuals plots showing level deviation from diagonal points.

et al., 2019; Mishra et al., 2019). Hence, the optimal treatment conditions at this point sustain the *Klebsiella Pneumonia* ABZ11 for effectual proliferation, metabolic activities alongside with protonic-balance which resulted in better degradation of the contaminants, and also neutralization of the toxic colorants (Mishra et al., 2019).

Optimized Synergy Effect of Inoculum Size and Initial Color Concentration

The optimized response surface and contour plot for the combined effect of factors A-inoculum sizes and B-initial color concentration on the percentage of color removal are presented in **Figure 6A** and (B), respectively. From **Figure 6A**, it can be noticed that the percentage of color removal increases with A but decreases with B. At the highest initial color concentration (B) of 2,600 ADMI (without dilution) and 20% (v/v) inoculum size, the optimal bio-decolorization of 81.4773% was attained after 35 h retention, (**Figure 6A**). It can be detected from **Figure 6B** that lower color concentrations (650 ADMI) give better performance (65–98.90%) irrespective of the inoculum sizes (A) and retention times (C). The negative correlation of initial color concentration with the remediation performance has been attributed to the predomination of toxic-recalcitrant contaminants characterized by complex structure (Neoh et al., 2017). Thus, the complexity of recalcitrant contaminants rather inhibits the extracellular activities of

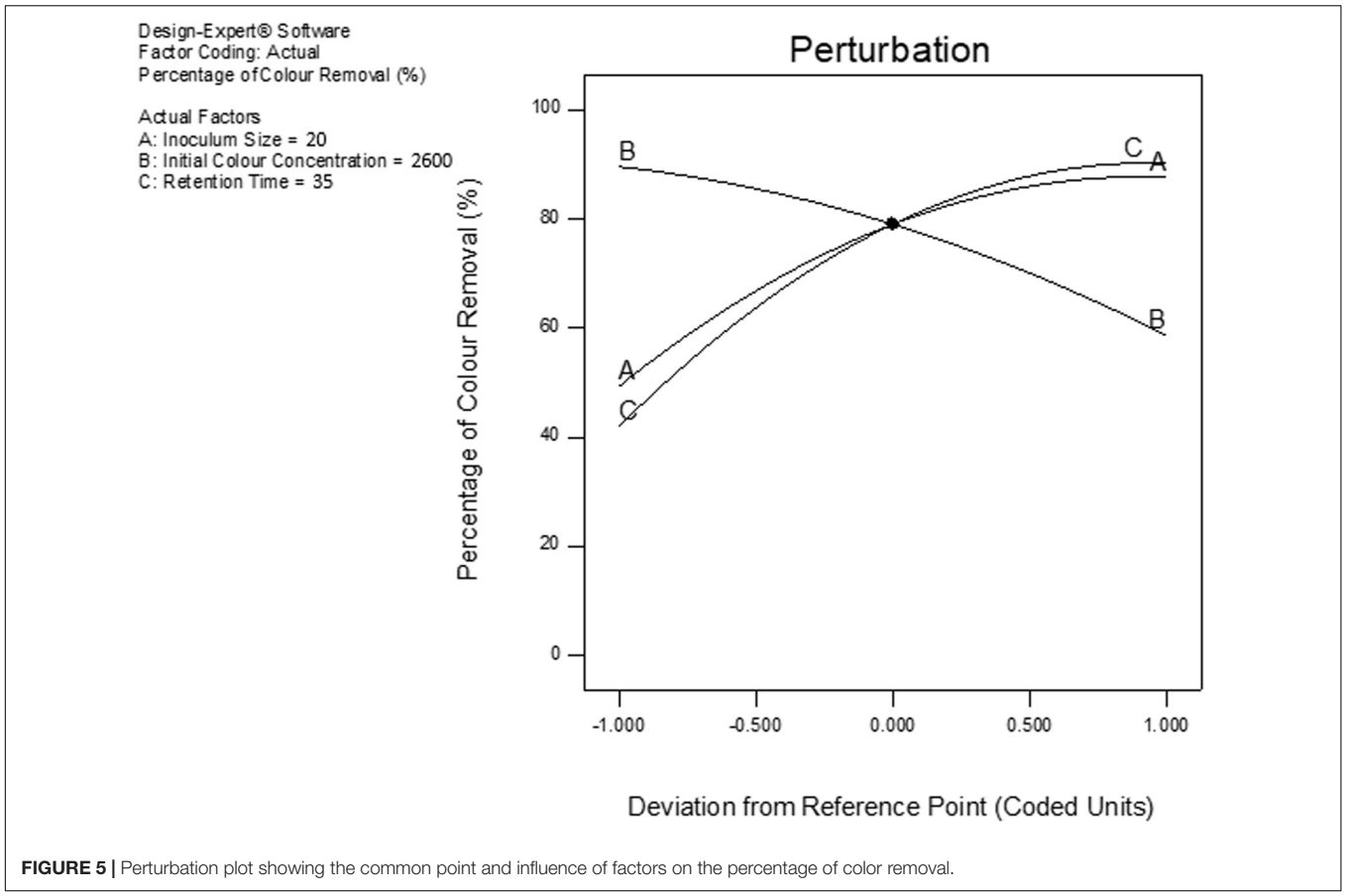

FIGURE 5 | Perturbation plot showing the common point and influence of factors on the percentage of color removal.

the bacteria thereby retarding the rate of decolorization (Hameed and Ismail, 2018).

Optimized Synergy Effect of A-Inoculum Size and C-Treatment Retention Time

Figure 6C shows the surface response 3-D plot of synergistic influences of the A-inoculum sizes with respect to C-treatment retention time. It is obvious that both the retention time (C) and the size of inoculum (A) have a positive correlation with the percentage of color removal. From **Figure 6A**, the lowest percentage of color removal was obtained with 5% (v/v) inoculum and 5 h retention time. However, a dramatic increase in the color removal was noticed with higher inoculum sizes (C). For example, at an optimal inoculum size of 20% (v/v) with a retention time of 35 h, over 81.47% of decolorization was attained even with the highest color concentration of 2,600 ADMI (without dilution). This implies that at the optimal condition, the effect of the antagonist factors (AB, AC and BC) were minimal while the metabolic activities of the microbes were maximized (**Figure 5**; (Mishra et al., 2019).

Optimized Synergy Effect of B-Initial Color Concentration and C-Treatment Retention Time

Figure 6D shows the surface response of the synergy effect of the A-initial color concentrations with respect to C-treatment retention times. The surface response curbed in the red region of the plot indicates excellent color removal efficiency (70–98%) and this was noticed at a lower initial concentration (650 ADMI). Conversely, at a higher initial color concentration (2,600 ADMI), a sudden decrease in the overall bio-decolorization efficiency was observed (**Figure 6D**). This might be due to the presence of excessive recalcitrant colorants which in turn inhibits the degradation process. Although, an appreciable increase in the decolorization efficiency of 81.4775% was attained at optimal retention time (35 h) and inoculum size of 20% (v/v). At this optimal treatment conditions, the common perturbation point with minimal effect of antagonist factors was established (**Figure 5**). Based on this observation, it can be deduced that at longer C, the microbes gradually adapt to the changes in the B and thereby developing suitable enzymes to facilitate degradation of the complex colorants (Chan et al., 2010). This observation is strongly in agreement with the previous studies (Sani and Banerjee, 1999; Islam et al., 2018). Sani and Banerjee (Sani and Banerjee, 1999) reported that lower initial concentration gives better remediation performance, especially when the inoculum size and the retention period are in optimal ranges. Similarly, Islam et al. (2018) reported that biodegradation performance of bacterial communities is often influenced by the concentration of medium because of the alteration in the pH, which could consequentially inhibit the bacterial growth as well as the metabolic and physiological activities of the

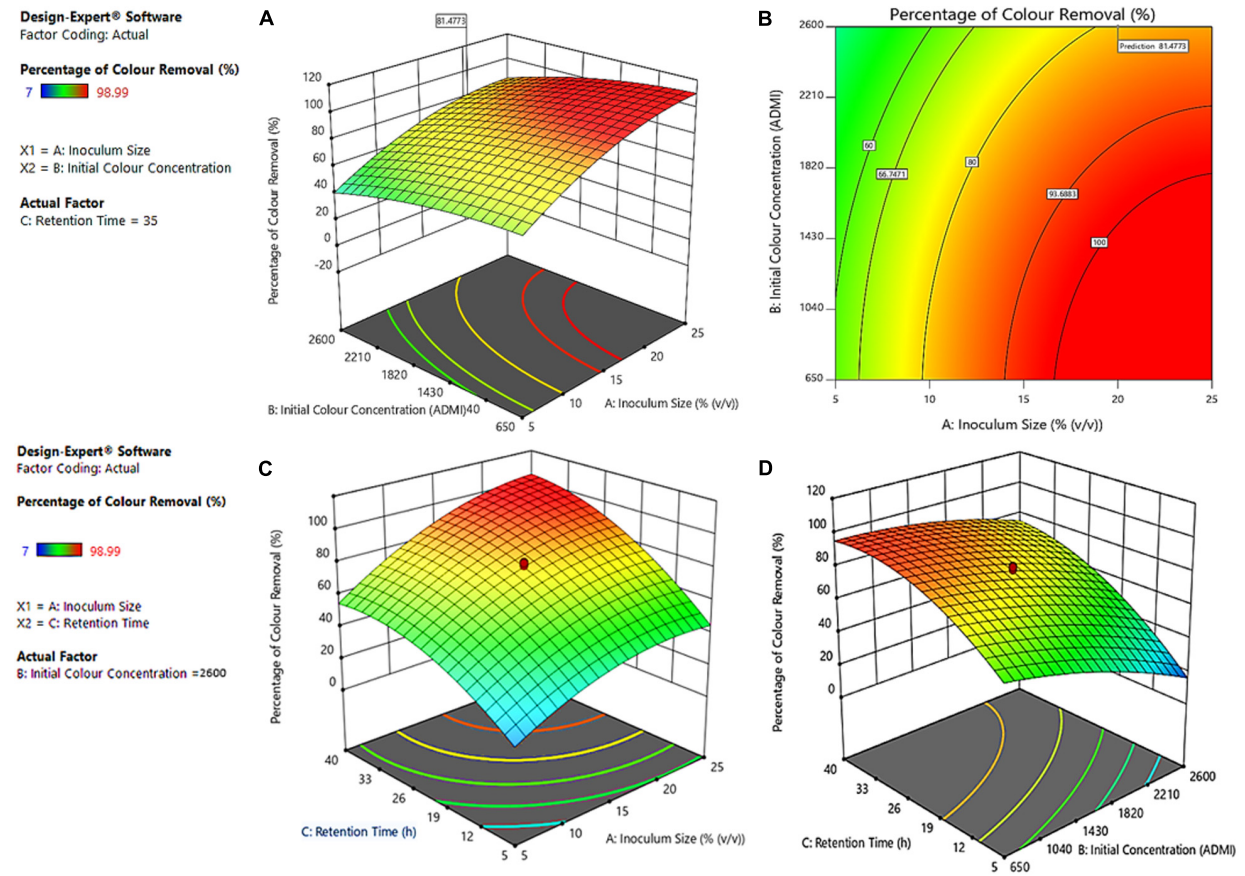

FIGURE 6 | (A) Surface response, and **(B)** contour plot of the optimized synergistic effect of inoculum size and initial color concentration. The surface response of the combined effect of **(C)** Inoculum sizes-A and Treatment retention Time-C, and **(D)** Initial color Concentrations-B and Treatment retention Time-C on percentage of color removal.

TABLE 4 | Experimental validation results of the regression model.

Inoculum size [%(v/v)]	Initial color concentration (ADMI)	Retention time (h)	Predicted value (%)	Desirability	Experimental value (%)
20.000	2,599.993∼2,600	35.000	81.477	0.949	79.89
20.000	2,586.721∼2,600	35.000	81.777	0.948	80.91
20.000	2,599.973∼2,600	34.852∼35.000	81.359	0.947	80.59
Average value			81.538		80.46

TABLE 5 | Summary of the *t*-Test and Normality analysis of the predicted and actual experimental values.

***t*-Test**

Data source	*N*	Missing	Mean	SD	SEM	*P*-value	*t*
Predicted value	3	0	81.538	0.216	0.124	0.030	3.297
Experimental Value	3	0	80.463	0.522	0.301		
Normality	0.945						
Power of performed test with alpha (α) = 0.050: 0.660							

Normality analysis (Shapiro–Wilk)

Source	*W*-statistic	*P*-value	Remark
Predicted data	0.941	0.530	Passed
Experimental data	0.956	0.595	Passed

inoculum. Thus, impeding the overall remediation performance (Islam et al., 2018).

Model Evaluation and Validation

The developed empirical regression model was validated by comparing the predicted with actual experimental values. The optimized treatment factors based on the set-criteria was employed to validate the accuracy of the model (equation 9). The criteria employed in this research targeted to minimize the inoculum size (A), and then maximize both initial color concentration (A) and percentage of color removal at the shortest retention time (C). Based on this, the first three experimental solutions recommended by the model were picked and verified in the laboratory by comparing with actual experimental values. The results were as presented in **Table 4**. The average percentages of the predicted and experimental color removal were 81.5 and 80.5%, respectively. The two values were in good conformity with the minimal and insignificant disproportion of 1.078%.

In addition, the deviation between the predicted and experimental values was statistically analyzed using *t*-test and normality test (Shapiro–Wilk), and the summary of the analysis is presented in **Table 5**. Basically, the *t*-test measures the significance of the deviation in the means (Kim, 2015) while the normality test analyzed the correlation of the data (Bhering, 2017). The *P*-value of the *t*-test was 0.030, which is less than 0.050. This shows that the deviations in the predicted and experimental values are statistically insignificant at 95% confidence level. Also, the passed remarks obtained from the normality test shows that the two sets of data match the design probable pattern with a normal distribution (Bhering, 2017). Based on this validation, it can be rationally deduced that the regression model predicted the actual experimental values with insignificant deviations.

CONCLUSION

Klebsiella Pneumonia ABZ11 was successfully applied to decolorize POME by utilizing the contained colorants as the sole carbon source to sustain its metabolic and physiological activities. The decolorization performance was examined at variable inoculum sizes, initial color concentrations and treatment retention times with fixed agitation of 120 rpm and initial pH of 7. Percentage of color removal at 650 ADMI initial concentration, 15% (v/v) inoculum and 25 h retention time was 97.73%, but at a higher initial color concentration of 2,600 ADMI, the color removal efficiency reduces considerably to 57% even with longer retention of 35 h. This might be due to the inhibitory effect of the colorants. In addition, at optimal conditions of 20% (v/v) inoculum, 2,600 ADMI initial color concentration and 35 h retention time, the color concentration reduces drastically by 80.43% and this result was in good correlation with the regression-model predicted value of 81.5%. The accuracy analysis based on normality test shows good matches with the probable normal distribution pattern (R^2 = 0.9237). In addition, the Monod model excellently described the bio-decolorization kinetic process and the calculated maximum growth (μ_{max}) and half-saturation constant (K_s) were 7.023 d^{-1} and 340.569 ADMI d^{-1}, respectively.

DATA AVAILABILITY STATEMENT

The datasets analyzed in this study are publicly available. The partial 16S rRNA gene sequence of the isolate has been deposited to GenBank: http://blast.ncbi.nlm.nih.gov/Blast.cgi, with the accession number KX266892.

AUTHOR CONTRIBUTIONS

MA and HM developed the research conceptualization and methodology. MA secured the software, did the investigation, data collation, formal analysis and original draft preparation. MA, HM, ZA, and KY validated the results. HM, ZA, KY, and AI provided the required resources, review-editing, visualization and supervision. HM was responsible for the project administration. Funding acquisition was achieved by HM and MA.

FUNDING

This research was funded by Universiti Putra Malaysia, grant number UPM/700-2/1/GPB/2017/9530900 and Tertiary Education Trust Fund (TETF/UNIV/ZARIA/ASTD/2017).

ACKNOWLEDGMENTS

The authors sincerely wish to acknowledge the immense support received from Prof. Zaharah Ibrahim, Universiti of Teknologi Malaysia for providing the *Klebsiella Pneumonia* ABZ11. Also, the resourceful information given by Hayatun Nasran of the Department of Biotechnology and Bio-molecular Science Universiti Putra Malaysia, cannot be over sighted.

SUPPLEMENTARY MATERIAL

The Supplementary Material for this article can be found online at: https://www.frontiersin.org/articles/10.3389/fmicb.2020.00675/full#supplementary-material

REFERENCES

Abdulsalam, M., Man, H. C., Idris, A. I., Abidin, Z. Z., and Yunos, K. F. (2018a). The pertinence of microwave irradiated coconut shell bio-sorbent for wastewater decolourization: structural morphology and adsorption optimization using the response surface method (RSM). *Int. J. Environ. Res. Public Health* 15:2200. doi: 10.3390/ijerph15102200

Abdulsalam, M., Man, H. C., Idris, A. I., Yunos, K. F., and Abidin, Z. Z. (2018b). Treatment of palm oil mill effluent using membrane bioreactor: novel processes and their major drawbacks. *Water* 10:1165. doi: 10.3390/w10091165

APHA (2005). *Standard Methods for the Examination of Water and Wastewater*, 21st Edn. Washington, DC: American Public Health Association/American Water Works Association/Water Environment Federation. (accessed April 17, 2020).

Azman, N. F., Megat Mohd Noor, M. J., Akhir, F. N., Ang, M. Y., Hashim, H., Othman, N., et al. (2019). Depolymerization of lignocellulose of oil palm empty fruit bunch by thermophilic microorganisms from tropical climate. *Bioresour. Technol.* 279, 174–180. doi: 10.1016/j.biortech.2019.01.122

Bala, J. D., Lalung, J., Al-Gheethi, A. A. S., Kaizar, H., and Ismail, N. (2018). Reduction of Organic Load And Biodegradation Of Palm Oil Mill Effluent By Aerobic Indigenous Mixed Microbial Consortium Isolated From Palm Oil Mill Effluent (POME). *Water Conserv. Sci. Eng.* 3, 139–156. doi: 10.1007/s41101-018-0043-9

Baraniya, D., Puglisi, E., Ceccherini, M. T., Pietramellara, G., Giagnoni, L., Arenella, M., et al. (2016). Protease encoding microbial communities and protease activity of the rhizosphere and bulk soils of two maize lines with different N uptake efficiency. *Soil Biol. Biochem.* 96, 176–179. doi: 10.1016/j.soilbio.2016.02.001

Bhering, L. L. (2017). Rbio: a tool for biometric and statistical analysis using the R platform. *Crop Breed. Appl. Biotechnol.* 17, 187–190. doi: 10.1590/1984-70332017v17n2s29

Chan, Y. J., Chong, M. F., and Law, C. L. (2010). Biological treatment of anaerobically digested palm oil mill effluent (POME) using a lab-scale sequencing batch reactor (SBR). *J. Environ. Manage.* 91, 1738–1746. doi: 10.1016/j.jenvman.2010.03.021

Cheah, W. Y., Show, P. L., Juan, J. C., Chang, J. S., and Ling, T. C. (2018). Enhancing biomass and lipid productions of microalgae in palm oil mill effluent using carbon and nutrient supplementation. *Energy Convers. Manag.* 164, 188–197. doi: 10.1016/j.enconman.2018.02.094

Choong, Y. Y., Chou, K. W., and Norli, I. (2018). Strategies for improving biogas production of palm oil mill effluent (POME) anaerobic digestion: a critical review. *Renew. Sustain. Energy Rev.* 82, 2993–3006. doi: 10.1016/j.rser.2017.10.036

Cortes-Tolalpa, L., Salles, J. F., and van Elsas, J. D. (2017). Bacterial synergism in lignocellulose biomass degradation - complementary roles of degraders as influenced by complexity of the carbon source. *Front. Microbiol.* 8:1628. doi: 10.3389/fmicb.2017.01628

de Souza, P. M., de Assis Bittencourt, M. L., Caprara, C. C., de Freitas, M., de Almeida, R. P. C., Silveira, D., et al. (2015). A biotechnology perspective of fungal proteases. *Braz. J. Microbiol.* 46, 337–346. doi: 10.1590/S1517-838246220140359

Din, A. K. (2017). *Malaysian Oil Palm Industry Performance 2016 and Prospects for 2017*. Bandar Baru Bangi: Malaysian Palm Oil Board.

Ebrahimi, M., Kazemi, H., Mirbagheri, S. A., and Rockaway, T. D. (2016). An optimized biological approach for treatment of petroleum refinery wastewater. *J. Environ. Chem. Eng.* 4, 3401–3408. doi: 10.1016/j.jece.2016.06.030

Eltarahony, M., Zaki, S., Kheiralla, Z., and Abd-El-Haleem, D. (2019). Study on the Antagonistic Potential of Biosynthesized Hematite Nanoparticles During Water and Wastewater Treatment. *Clean Soil Air Water* 47, 1–10. doi: 10.1002/clen.201800418

Fonseca, R. F., de Oliveira, G. H. D., and Zaiat, M. (2018). Development of a mathematical model for the anaerobic digestion of antibiotic-contaminated wastewater. *Chem. Eng. Res. Des.* 134, 319–335. doi: 10.1016/j.cherd.2018.04.014

Fu, G., Zhao, L., Huangshen, L., and Wu, J. (2019). Isolation and identification of a salt-tolerant aerobic denitrifying bacterial strain and its application to saline wastewater treatment in constructed wetlands. *Bioresour. Technol.* 290:121725. doi: 10.1016/j.biortech.2019.121725

Ganapathy, B., Yahya, A., and Ibrahim, N. (2019). Bioremediation of palm oil mill effluent (POME) using indigenous Meyerozyma guilliermondii. *Environ. Sci. Pollut. Res.* 26, 11113–11125. doi: 10.1007/s11356-019-04334-8

Ghani, Z. A., Yusoff, M. S., Zaman, N. Q., Zamri, M. F. M. A., and Andas, J. (2017). Optimization of preparation conditions for activated carbon from banana pseudo-stem using response surface methodology on removal of color and COD from landfill leachate. *Waste Manag.* 62, 177–187. doi: 10.1016/j.wasman.2017.02.026

Gonçalves, A. L., Pires, J. C. M., and Simões, M. (2016). Wastewater polishing by consortia of Chlorella vulgaris and activated sludge native bacteria. *J. Clean. Prod.* 133, 348–357. doi: 10.1016/j.jclepro.2016.05.109

Hameed, B. B., and Ismail, Z. Z. (2018). Decolorization, biodegradation and detoxification of reactive red azo dye using non-adapted immobilized mixed cells. *Biochem. Eng. J.* 137, 71–77. doi: 10.1016/j.bej.2018.05.018

Hermosilla, E., Rubilar, O., Schalchli, H., da Silva, A. S. A., Ferreira-Leitao, V., and Diez, M. C. (2018). Sequential white-rot and brown-rot fungal pretreatment of wheat straw as a promising alternative for complementary mild treatments. *Waste Manag.* 79, 240–250. doi: 10.1016/j.wasman.2018.07.044

Iskandar, M. J., Baharum, A., Anuar, F. H., and Othaman, R. (2018). Palm oil industry in South East Asia and the effluent treatment technology—A review. *Environ. Technol. Innov.* 9, 169–185. doi: 10.1016/j.eti.2017.11.003

Islam, M. A., Yousuf, A., Karim, A., Pirozzi, D., Khan, M. R., and Wahid, Z. A. (2018). Bioremediation of palm oil mill effluent and lipid production by Lipomyces starkeyi: a combined approach. *J. Clean. Prod.* 172, 1779–1787. doi: 10.1016/j.jclepro.2017.12.012

Kamal, M., Aziz, A., Okayama, T., Kose, R., Morad, N. A., Baini, N., et al. (2019). *Green Technologies for the Oil Palm Industry*. Singapore: Springer.

Kim, T. K. (2015). T test as a parametric statisticNo Title. *Korean J. Anesthesiol.* 68, 540–546. doi: 10.4097/kjae.2015.68.6.540

Kumaran, P., Hephzibah, D., Sivasankari, R., Saifuddin, N., and Shamsuddin, A. H. (2016). A review on industrial scale anaerobic digestion systems deployment in Malaysia: opportunities and challenges. *Renew. Sustain. Energy Rev.* 56, 929–940. doi: 10.1016/j.rser.2015.11.069

Langemann, T., Koller, V. J., Muhammad, A., Kudela, P., Mayr, U. B., and Lubitz, W. (2010). The bacterial ghost platform system: production and applications. *Bioeng. Bugs* 1, 326–336. doi: 10.4161/bbug.1.5.12540

Lee, Z. S., Chin, S. Y., Lim, J. W., Witoon, T., and Cheng, C. K. (2019). Treatment technologies of palm oil mill effluent (POME)and olive mill wastewater (OMW): a brief review. *Environ. Technol. Innov.* 15:100377. doi: 10.1016/j.eti.2019.100377

Louhasakul, Y., Cheirsilp, B., and Prasertsan, P. (2016). Valorization of Palm Oil Mill Effluent into Lipid and Cell-Bound Lipase by Marine Yeast Yarrowia lipolytica and Their Application in Biodiesel Production. *Waste Biomass Valoriz.* 7, 417–426. doi: 10.1007/s12649-015-9451-7

Luo, W., Zhu, X., Chen, W., Duan, Z., Wang, L., and Zhou, Y. (2014). Mechanisms and strategies of microbial cometabolism in the degradation of organic compounds - Chlorinated ethylenes as the model. *Water Sci. Technol.* 69, 1971–1983. doi: 10.2166/wst.2014.108

Mishra, P., Ameen, F., Zaid, R. M., Singh, L., Wahid, Z. A., Islam, M. A., et al. (2019). Relative effectiveness of substrate-inoculum ratio and initial pH on hydrogen production from palm oil mill effluent: kinetics and statistical optimization. *J. Clean. Prod.* 228, 276–283. doi: 10.1016/j.jclepro.2019.04.317

Mohammed, A., and Zaharah, I. (2019). *Batch Fermentation System for Biohydrogen Production by Klebsiella sp*. Available online at: http://dms.library.utm.my:8080/vital/access/manager/Repository/vital:124960 (accessed December 02, 2019).

Mohana, S., Desai, C., and Madamwar, D. (2007). Biodegradation and decolourization of anaerobically treated distillery spent wash by a novel bacterial consortium. *Bioresour. Technol.* 98, 333–339. doi: 10.1016/j.biortech.2005.12.024

Moosvi, S., Keharia, H., and Madamwar, D. (2005). Decolourization of textile dye Reactive Violet 5 by a newly isolated bacterial consortium RVM 11.1. *World J. Microbiol. Biotechnol.* 21, 667–672. doi: 10.1007/s11274-004-3612-3

Neoh, C. H., Yahya, A., Adnan, R., Abdul Majid, Z., and Ibrahim, Z. (2013). Optimization of decolorization of palm oil mill effluent (POME) by growing cultures of Aspergillus fumigatus using response surface methodology. *Environ. Sci. Pollut. Res.* 20, 2912–2923. doi: 10.1007/s11356-012-1193-5

Neoh, C. H., Yung, P. Y., Noor, Z. Z., Razak, M. H., Aris, A., Md Din, M. F., et al. (2017). Correlation between microbial community structure and performances of membrane bioreactor for treatment of palm oil mill effluent. *Chem. Eng. J.* 308, 656–663. doi: 10.1016/j.cej.2016.09.063

Ohimain, E. I., and Izah, S. C. (2017). A review of biogas production from palm oil mill effluents using different configurations of bioreactors. *Renew. Sustain. Energy Rev.* 70, 242–253. doi: 10.1016/j.rser.2016.11.221

Oladipo, O. G., Ezeokoli, O. T., Maboeta, M. S., Bezuidenhout, J. J., Tiedt, L. R., Jordaan, A., et al. (2018). Tolerance and growth kinetics of bacteria isolated from gold and gemstone mining sites in response to heavy metal concentrations. *J. Environ. Manage.* 212, 357–366. doi: 10.1016/j.jenvman.2018.01.038

Park, H., Chang, I., and Lee, K. (2015). *Principles of Membrane Bioreactors for Wastewater Treatment Waste Activated Sludge*. Boca Raton, Florida: CRC Press.

Pernin, A., Dubois-Brissonnet, F., Roux, S., Masson, M., Bosc, V., and Maillard, M. N. (2018). Phenolic compounds can delay the oxidation of polyunsaturated fatty acids and the growth of Listeria monocytogenes: structure-activity relationships. *J. Sci. Food Agric.* 98, 5401–5408. doi: 10.1002/jsfa.9082

Prasertsan, P., Khangkhachit, W., Duangsuwan, W., Mamimin, C., and O-Thong, S. (2017). Direct hydrolysis of palm oil mill effluent by xylanase enzyme to enhance biogas production using two-steps thermophilic fermentation under non-sterile condition. *Int. J. Hydrogen Energy* 42, 27759–27766. doi: 10.1016/j.ijhydene.2017.05.140

Rana, S., Singh, L., Wahid, Z., and Liu, H. (2017). A recent overview of palm oil mill effluent management via bioreactor configurations. *Curr. Pollut. Rep.* 3, 254–267. doi: 10.1007/s40726-017-0068-2

Sani, R. K., and Banerjee, U. C. (1999). Decolorization of triphenylmethane dyes and textile and dye-stuff effluent by Kurthia sp. *Enzyme Microb. Technol.* 24, 433–437. doi: 10.1016/S0141-0229(98)00159-8

Sharma, P., Singh, T. A., Bharat, B., Bhasin, S., and Modi, H. A. (2018). Approach towards different fermentative techniques for the production of bioactive actinobacterial melanin. *Beni Suef Univ. J. Basic Appl. Sci.* 7, 695–700. doi: 10.1016/j.bjbas.2018.08.002

Singh, P., Shera, S. S., Banik, J., and Banik, R. M. (2013). Optimization of cultural conditions using response surface methodology versus artificial neural network and modeling of l-glutaminase production by Bacillus cereus MTCC 1305. *Bioresour. Technol.* 137, 261–269. doi: 10.1016/j.biortech.2013.03.086

Taherdanak, M., Zilouei, H., and Karimi, K. (2015). Investigating the effects of iron and nickel nanoparticles on dark hydrogen fermentation from starch using central composite design. *Int. J. Hydrogen Energy* 40, 12956–12963. doi: 10.1016/j.ijhydene.2015.08.004

Tamrin, K. F., and Zahrim, A. Y. (2017). Determination of optimum polymeric coagulant in palm oil mill effluent coagulation using multiple-objective optimisation on the basis of ratio analysis (MOORA). *Environ. Sci. Pollut. Res.* 24, 15863–15869. doi: 10.1007/s11356-016-8235-3

Tan, Y. H., Goh, P. S., Ismail, A. F., Ng, B. C., and Lai, G. S. (2017). Decolourization of aerobically treated palm oil mill effluent (AT-POME) using polyvinylidene fluoride (PVDF) ultrafiltration membrane incorporated with coupled zinc-iron oxide nanoparticles. *Chem. Eng. J.* 308, 359–369. doi: 10.1016/j.cej.2016.09.092

Vello, V., Umashankar, S., Phang, S. M., Chu, W. L., Lim, P. E., Nazia, A. M., et al. (2018). Metabolomic profiles of tropical *Chlorella* and *Parachlorella* species in response to physiological changes during exponential and stationary growth phase. *Algal Res.* 35, 61–75. doi: 10.1016/j.algal.2018.08.014

Xu, R., Zhang, K., Liu, P., Han, H., Zhao, S., Kakade, A., et al. (2018). Lignin depolymerization and utilization by bacteria. *Bioresour. Technol.* 269, 557–566. doi: 10.1016/j.biortech.2018.08.118

Xu, Z., Qin, L., Cai, M., Hua, W., and Jin, M. (2018). Biodegradation of kraft lignin by newly isolated *Klebsiella pneumoniae*, *Pseudomonas putida*, and *Ochrobactrum tritici* strains. *Environ. Sci. Pollut. Res.* 25, 14171–14181. doi: 10.1007/s11356-018-1633-y

Yang, J., Gou, Y., Fang, F., Guo, J., Lu, L., Zhou, Y., et al. (2018). Potential of wastewater treatment using a concentrated and suspended algal-bacterial consortium in a photo membrane bioreactor. *Chem. Eng. J.* 335, 154–160. doi: 10.1016/j.cej.2017.10.149

Zhang, L., Narita, Y., Gao, L., Ali, M., Oshiki, M., and Okabe, S. (2017). Maximum specific growth rate of anammox bacteria revisited. *Water Res.* 116, 296–303. doi: 10.1016/j.watres.2017.03.027

Conflict of Interest: The authors declare that the research was conducted in the absence of any commercial or financial relationships that could be construed as a potential conflict of interest.

frontiers in Microbiology

ORIGINAL RESEARCH
published: 15 September 2020
doi: 10.3389/fmicb.2020.575361

Paraquat Degradation by Biological Manganese Oxide ($BioMnO_x$) Catalyst Generated From Living Microalga *Pediastrum duplex* AARL G060

*Jakkapong Thongpitak[1], Pamon Pumas[2] and Chayakorn Pumas[3]**

[1] PhD Degree Program in Environmental Science, Environmental Science Research Center, Faculty of Science, Chiang Mai University, Chiang Mai, Thailand, [2] Department of Environmental Science, Faculty of Science and Technology, Chiang Mai Rajabhat University, Chiang Mai, Thailand, [3] Department of Biology, Faculty of Science, Research Center in Bioresources for Agriculture, Industry and Medicine, Chiang Mai University, Chiang Mai, Thailand

OPEN ACCESS

Edited by:
Dayanand Kalyani, Royal Institute of Technology, Sweden

Reviewed by:
Sujit Jagtap, University of Illinois at Urbana-Champaign, United States
Umesh Uttamrao Jadhav, Savitribai Phule Pune University, India
Gajanan Ghodake, Dongguk University Seoul, South Korea

***Correspondence:**
Chayakorn Pumas
chayakorn.pumas@gmail.com

Specialty section:
This article was submitted to Microbiotechnology, a section of the journal Frontiers in Microbiology

Received: *23 June 2020*
Accepted: *24 August 2020*
Published: *15 September 2020*

Citation:
Thongpitak J, Pumas P and Pumas C (2020) Paraquat Degradation by Biological Manganese Oxide ($BioMnO_x$) Catalyst Generated From Living Microalga Pediastrum duplex AARL G060. Front. Microbiol. 11:575361. doi: 10.3389/fmicb.2020.575361

Paraquat is a non-selective fast-acting herbicide used to control weeds in agricultural crops. Many years of extensive use has caused environmental pollution and food toxicity. This agrochemical degrades slowly in nature, adsorbs onto clay lattices, and may require environmental remediation. Studies have shown that biosynthesized manganese oxide ($BioMnO_x$) successfully degraded toxic synthetic compounds such as bis-phenol A and diclofenac, thus it has potential for paraquat degradation. In this experiment, *P. duplex* AARL G060 generated low (9.03 mg/L) and high (42.41 mg/L) concentrations of $BioMnO_x$. The precipitated $BioMnO_x$ was observed by scanning electron microscopy (SEM), and the elemental composition was identified as Mn and O by energy-dispersive x-ray spectroscopy (EDS). The potential for $BioMnO_x$ to act as a catalyst in the degradation of paraquat was evaluated under three treatments: (1) a negative control (deionized water), (2) living alga with low $BioMnO_x$ plus hydrogen peroxide, and (3) living alga with high $BioMnO_x$ plus hydrogen peroxide. The results indicate that $BioMnO_x$ served as a catalyst in the Fenton-like reaction that could degrade more than 50% of the paraquat within 72 h. A kinetic study indicated that paraquat degradation by Fenton-like reactions using $BioMnO_x$ as a catalyst can be described by pseudo-first and pseudo-second order models. The pH level of the $BioMnO_x$ catalyst was neutral at the end of the experiment. In conclusion, $BioMnO_x$ is a viable and environmentally friendly catalyst to accelerate degradation of paraquat and other toxic chemicals.

Keywords: microalgae, photosynthesis, bio-oxidation, herbicide, catalyst

INTRODUCTION

Non-selective herbicides, such as glyphosate and paraquat, were developed based upon their antagonistic effects on non-specific species of weeds and crops. Paraquat (1,1'-dimethyl-4,4'-bipyridinium dichloride) transforms electron flow from the photosystem and inhibits reduction of oxidized nicotinamide adenine dinucleotide phosphate (NADPC) during photosynthesis

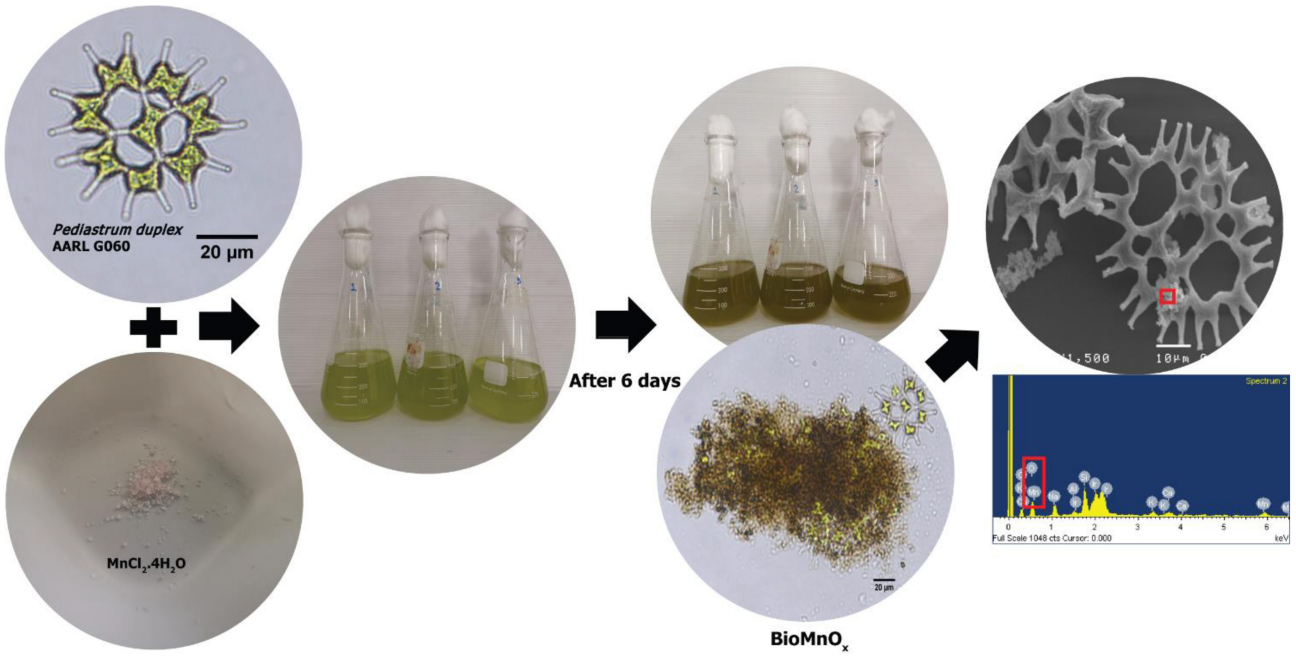

GRAPHICAL ABSTRACT | BiOMnOx catalyst generated from living *Pediastrum duplex* AARL G060.

(Huang et al., 2019). Intensive paraquat usage over decades has led to widespread contamination of soil and water, and the World Health Organization (WHO) set an advisory limit for paraquat in drinking water at 10 µg/L.

Previous studies reported paraquat contamination in many countries worldwide (Huang et al., 2019). A paraquat concentration of 3.95 µg/L was reported in water samples from irrigation channels and rivers in Spain (Fernández et al., 1998). Paraquat residue in surface water in Brazil was found to be 0.279 µg/L (Veríssimo et al., 2018). Paraquat concentrations of 30.69–134.08 µg/L were detected in a stream in Mai Chau province, Vietnam (Thi Hue et al., 2018). Paraquat concentrations of 9.3–87.0 µg/L were reported in surface water in Thailand (Insuwan and Rangsriwatananon, 2017). In Malaysia, 0.6–6.9 µg/L of paraquat residue was detected in water samples (Ismail et al., 2011). These contaminants accumulate in the food chain creating public health hazards for humans, animals, and the environment (Frimpong et al., 2018).

To protect human health from the toxic effects of paraquat, removal is required. Biological methods may provide limited paraquat degradation (e.g., microorganisms utilize and degrade <1% of paraquat in soil particles (Roberts et al., 2002; Huang et al., 2019); therefore, abiological processes may be required to facilitate natural paraquat degradation. Previous studies included various methods for paraquat removal, such as adsorption on modified zeolites, activated carbon, and organoclay (Guégan et al., 2015; Sieliechi and Thue, 2015; Keawkumay et al., 2016; Pukcothanung et al., 2018). On the other hand, physicochemical processes using titanium dioxide, ozone, and various advanced oxidation processes showed potential for paraquat removal and reduction of the physical and chemical effects of this pesticide on the environment and health (Florêncio et al., 2004; Mandal et al., 2010; Wang and Xu, 2012; Deng and Zhao, 2015; Hamad et al., 2016).

The advanced oxidation process (AOP) is a conventional method for paraquat degradation based on the generation of highly reactive and non-selective hydroxyl radicals (•OH) (Poyatos et al., 2009; Deng and Zhao, 2015; de Guimarães et al., 2016; Vagi and Petsas, 2017; Garrido-Cardenas et al., 2020). The high oxidative power of this radical can oxidize organic compounds to CO_2 and H_2O in aqueous solution. Fenton's reaction is an AOP invented in 1894 when Fenton used ferrous ion and hydrogen peroxide as a reagent to improve tartaric acid oxidation (Nidheesh, 2015). Since then, this method has been widely used in wastewater treatment. The chemical process of this reaction is shown in Eqs. (1–3):

$$H_2O_2 + Fe^{2+} \rightarrow Fe^{3+} + OH^- + \bullet OH, \quad (1)$$

$$\text{Organic matter} + \bullet OH \rightarrow \text{Oxidation intermediates, and} \quad (2)$$

$$\text{Oxidation intermediates} + \bullet OH \rightarrow CO_2 + H_2O. \quad (3)$$

The reaction between iron and hydrogen peroxide produces hydroxyl radicals (eq. 1) with high oxidative potential. These radicals attack organic matter in wastewater (eq. 2) and generate oxidation intermediates which are further attacked by hydroxyl radicals to produce CO_2 and H_2O (eq. 3). However, Fenton's reaction requires acidic conditions (i.e., a pH value in the range of 3–5 for high performance degradation of paraquat (Bishop et al., 1968; Kiwi et al., 1993; Barbusiński and Filipek, 2001), and the acidic by-products are not environmentally

acceptable. Thus, reactions to proceed at pH levels higher than that Fenton reaction.

Another non-acidic AOP is a "Fenton-like" reaction, a process that operates at nearly neutral pH. The pH value of the run-off effluent from this Fenton-like reaction is environmentally friendly and depends on other metals, such as copper, cobalt, manganese, and chromium, instead of iron (II), as catalysts for H_2O_2 decomposition (Nidheesh, 2015; Kim et al., 2017). The reaction of transition metals and hydrogen peroxide to generate hydroxyl radicals is shown in Eq. (4).

$$\text{Metal} + H_2O_2 \rightarrow \text{Metal} + \bullet OH + OH^- . \quad (4)$$

Various microorganisms can oxidize manganese, including bacteria, fungi, and algae (Greene and Madgwick, 1991; Li et al., 2019; Zhou and Fu, 2020). Previous studies revealed that some microalgae, such as *Desmodesmus* sp. WR1 and *P. duplex* AARL G060 increase dissolved oxygen content due to microalgal photosynthesis (Wang et al., 2017; Thongpitak et al., 2019). In addition, microalgae take up CO_2 and HCO_3^- from the culture medium on a cellular level. A decrease in H^+ in the culture medium indirectly increased pH levels and generated microenvironments with pH values greater than 9 (Richardson et al., 1988; Richardson and Stolzenbach, 1995; Knauer et al., 1999; Chi et al., 2011). These mechanisms create conditions suitable for Mn oxidation as shown in Eq. (5):

$$Mn^{2+} + 0.5O_{2\text{from microalgal photosynthesis}} + H_2O \rightarrow \text{BioMnO}_x . \quad (5)$$

Use of microalgae to generate BioMnO$_x$ has several advantages: it is environmentally friendly, and has higher efficiency and lower operation and maintenance costs than those of chemically (Li et al., 2019); however, some microalgae are sensitive to high manganese concentrations (Knauer et al., 1999).

Manganese oxide is a transition metal oxide used as a catalyst in various reactions (Corma et al., 2005; Asgari et al., 2020). It was found to be capable of oxidizing a wide range of recalcitrant compounds, including compounds with phenolic and fluoroquinolonic moieties and some antibacterial compounds (Wu et al., 2017). Manganese oxide has gained attention as a technologically important compound for degradation of toxins in the laboratory and in the field (Kim et al., 2012; Birkner et al., 2013; Robinson et al., 2013; Furgal et al., 2015; Kim et al., 2017). However, Mn oxides are prepared via chemical methods which require high energy and chemical reagents to convert the metal ions into precipitates (Fu et al., 2010; Shaker and Abdalsalm, 2018; Tian et al., 2018).

Recent research demonstrated the application of BioMnO$_x$ produced by microorganisms for wastewater treatment (Sabirova et al., 2008; Hennebel et al., 2009; Forrez et al., 2010). Another paper reported that BioMnO$_x$ can oxidize As(III) to As(V), which is a preliminary step for As removal (Tani et al., 2004). The removal of 17α-Ethinylestradiol (EE2) by oxidation in flow through bioreactors was achieved up to 57% using a BioMnO$_x$ catalyst (Hennebel et al., 2009). In addition, BioMnO$_x$ produced by green microalgae was used to degrade phenols and small organic molecules (Wang et al., 2017). For example, diclofenac, a non-steroidal anti-inflammatory drug, was removed by BioMnO$_x$ at neutral pH. This was 10-fold faster than removal with chemically synthesized MnO$_x$ (Forrez et al., 2010). However, the application of BioMnO$_x$ as a catalyst in paraquat degradation was not investigated, so the objective of this experiment was to evaluate the feasibility of using BioMnO$_x$ as a catalyst for paraquat (as model pollutant compound) degradation. The BioMnO$_x$ was prepared using living microalga *P. duplex* AARL G060 via a biological reaction process. The results of this study demonstrate the feasibility of applying BioMnO$_x$ for removal of harmful agents in the environment.

MATERIALS AND METHODS

Living Microalga Culture of *Pediastrum duplex* AARL G060

Living green microalga *P. duplex* AARL G060 was obtained from the Applied Algal Research Laboratory (AARL), Department of Biology, Faculty of Science, Chiang Mai University, Thailand. Thongpitak et al. (2019) demonstrated that *P. duplex* can generate BioMnO$_x$ at high concentrations of Mn, and so this algal strain was selected for use in this study. An axenic culture of microalgal stock was maintained in Jaworski's Medium under the following condition: 72.51 $\mu E \cdot m^{-2} \cdot s^{-1}$ light intensity from a light emitting diode, 25°C ambient temperature, and continuous shaking at 130 rpm.

Chemicals and Reagents

Chromatographic separation of paraquat was performed by application of high-performance liquid chromatography (HPLC). Paraquat (98% pure) was purchased from MilliporeSigma. Acetonitrile of HPLC grade was purchased from Merck KGaA. All other reagents were analytical grade.

Paraquat Stock Solution

Paraquat stock solution, at a concentration of 1,000 mg/L, was prepared by dissolving 0.6910 g of paraquat in 1,000 mL of DW. The paraquat stock solution was then diluted to the desired concentration using simple dilution methods (Knepil, 1977).

Natural Contaminated Wastewater

Water samples obtained from the surface of a rehabilitated lignite coal-mine reservoir in the northern part of Thailand (500292m E, 1966086m N). Water samples were collected in November and December 2017. Some physico-chemical parameters of the water sample were published elsewhere (Thongpitak et al., 2019). High-density polyethylene bottles of 20 L capacity were filled with natural wastewater and stored at 4°C prior to use; water samples were used to generate BioMnO$_x$ using microalgae.

Batch Experiment

Effect of Paraquat on Growth in *Pediastrum duplex* AARL G060

Living green microalga *P. duplex* AARL G060 were cultivated in water samples obtained from the rehabilitated reservoir. The microalga was cultivated with nutrients containing $NaNO_3$ (0.09438 g/L), KH_2PO_4 (0.02606 g/L), $CaHCO_3$ (0.0159 g/L), and $MgSO_4.7H_2O$ (0.0500 g/L, Thongpitak et al., 2018). The initial concentration of paraquat was 10 mg/L. The initial microalgal optical density was set at 0.2 for each treatment. The batch culture of *P. duplex* AARL G060 was inoculated into 150 mL of modified medium in DW (LA-Pq, i.e., living microalga with paraquat) to compare to the control (modified medium in DW without paraquat). All treatments were performed in triplicate at ambient temperature and 111.81 mE m^{-2} s^{-1} light intensity using LED illumination. The microalga density was determined daily by measuring the OD_{665} using a Thermo Fisher Scientific^{TM} GENESYS^{TM} 20 Visible Spectrophotometer, and the pH value of the cultures was measured using a Starter 3100 pH Bench (Ohaus, United States). Living microalga cultures in flasks were shaken three times per day by hand to confirm that all algal cells were suspended and to prevent the dissolution of oxygen due to agitation which interferes with Mn oxidation during photosynthesis.

Production of BioMnO$_x$ by *Pediastrum duplex* AARL G060

Manganese concentrations in this experiment were assigned the highest Mn concentrations found in the rehabilitated reservoir (20 mg/L, Thongpitak et al., 2019). The BioMnO$_x$ nanoparticles were prepared via photosynthesis of *P. duplex* AARL G060 and designated as low or high concentration. At low BioMnO$_x$ concentration (LA-Low-BioMnO$_x$), the microalga was inoculated in 300 mL of natural wastewater containing a Mn concentration of 20 mg/L. For high BioMnO$_x$ concentration (LA-High-BioMnO$_x$), living microalga was inoculated in 900 mL of natural wastewater containing a Mn concentration of 60 mg/L, triple the concentration of low BioMnO$_x$. After six days of cultivation, cell pellets containing BioMnO$_x$ were collected by centrifugation at 3,500 rpm for 20 min. Next, samples were washed twice with a phosphate buffer at a pH of 8.00. Then washed with DW to remove residual Mn ions from the microalgal cells. The amount of precipitated BioMnO$_x$ that remained on the cell pellets was dissolved with 10 mL of 1 mM EDTA at a pH of 3.40 and analyzed using the same method applied to Mn concentrations in the supernatant (Kenduzler and Turker, 2002; Webster et al., 2011; Thongpitak et al., 2019). The BioMnO$_x$ concentration of the microalga was determined by atomic absorption spectroscopy (AAS).

Analysis of BioMnO$_x$ Formation Using Scanning Electron Microscope With Energy Dispersive Spectroscopy (SEM-EDS)

The BioMnO$_x$ catalyst produced by *P. duplex* AARL G060 was collected by centrifugation at 4,000 rpm. Cell pellets were fixed with 2.5% glutaraldehyde in 0.1 M of phosphate buffer at a pH of 8.00 overnight at 4°C. The samples were then washed with a phosphate buffer at a pH of 8.00. After that, the samples were dehydrated with an ethanol concentration series. Next step, the sample was mounted on stubs and thereafter gold-sputtered (Michalak et al., 2014). Characterization of BioMnO$_x$ was observed using a JEOL-5410LV SEM equipped with an Oxford INCA EDS system to capture the distribution of the elemental composition of MnO$_x$ displayed on the microalgal cell walls. The X-ray spectrum of each sample revealed the microelement composition.

Paraquat Degradation by Fenton-Like Reactions Using BioMnO$_x$ as a Catalyst

BioMnO$_x$ generated by *P. duplex* AARL G060 for a duration of 6 days, was evaluated for its potential as a catalyst in paraquat degradation. The initial concentration of paraquat was 10 mg/L, which was mixed with the modified medium in DW in preparation for the following three treatments: 1) the control (i.e., the modified medium in DW), 2) the culture containing the living *P. duplex* AARL G060 with low BioMnO$_x$ (LA-Low-BioMnO$_x$), and 3) a culture containing living *P. duplex* AARL G060 with high BioMnO$_x$ (LA-High-BioMnO$_x$). Paraquat degradation was performed in 150 mL of culture in a 250 mL Erlenmeyer flask. Then, 13.5 mL of H_2O_2 was added to LA-Low-BioMnO$_x$ and LA-High-BioMnO$_x$ treatments following the method of Fang et al. (2017). During the experiment, samples from each treatment were collected at 0, 3, 6, 12, 24, 48, and 72 h by centrifuging at 3,500 rpm for 15 min to determine the amount of paraquat remaining. The pH was measured, and the paraquat degradation efficiency was calculated using eq. 6:

$$\text{Degradation efficiency } (\%) = [1 - \frac{C_t}{C_0}] \times 100, \qquad (6)$$

where C_0 is the initial paraquat concentration and C_t is the concentration at time t.

Paraquat Determination by High Performance Liquid Chromatography

The HPLC was operated under the following conditions: the HPLC column was a VertiSep UPS-C18 analytical column (4.6 mm × 250 mm i.d., 5 μm) maintained at a temperature of 30°C. The mobile phase consisted of 0.14 mol sodium chloride and acetonitrile (60:40, v:v). All samples were eluted at a flow rate of 1 mL/min. The column eluent was monitored by HPLC at ambient temperature (25°C) using a Diode-Array Detection (DAD) detector (HP Series 1260, Agilent Technology). The wavelength was fixed at 257 nm. Calibration curves for the analysis were established with a standard solution of paraquat.

Data Analysis

All of the graphs and statistical analyses were completed using Microsoft^{TM} Excel 2016.

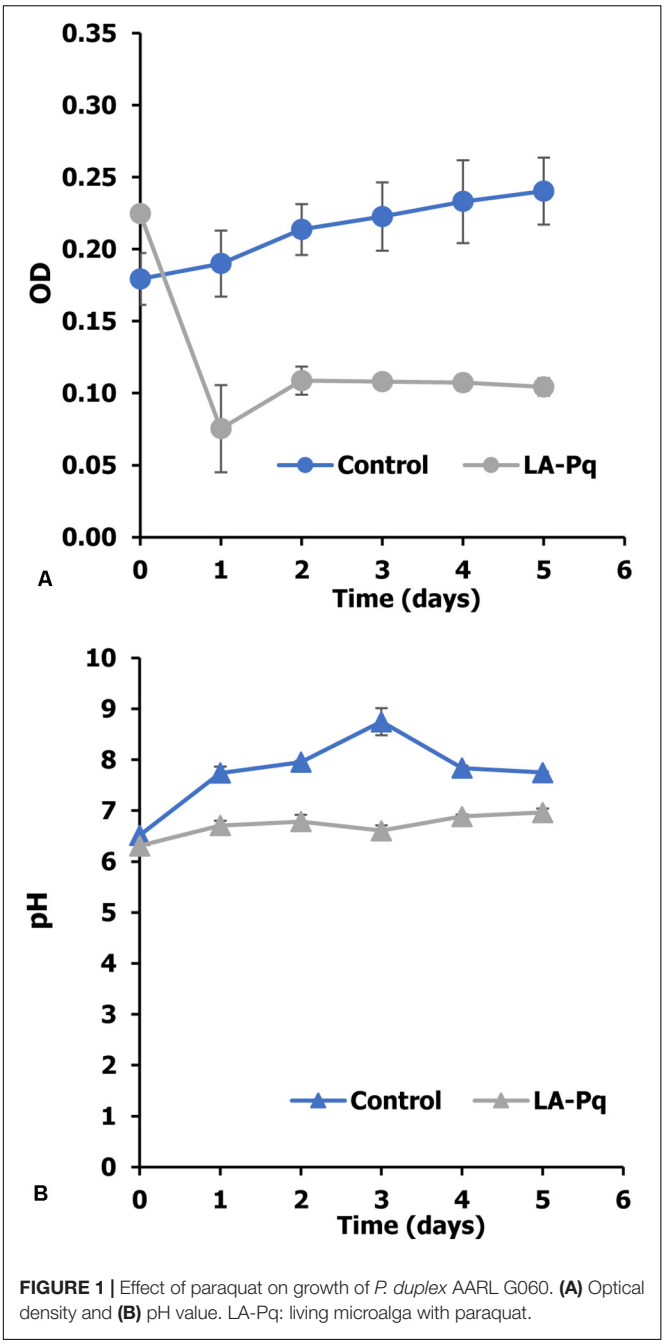

FIGURE 1 | Effect of paraquat on growth of *P. duplex* AARL G060. **(A)** Optical density and **(B)** pH value. LA-Pq: living microalga with paraquat.

RESULTS

Effect of Paraquat on Growth of *P. duplex* AARL G060

In this experiment, *P. duplex* AARL G060 was cultivated in a medium containing of N, P, C, and Mg to measure its growth (Thongpitak et al., 2019) using OD_{665}. The results show that *P. duplex* AARL G060 grow well in the control medium (**Figure 1A**). The OD_{665} increased from 0.17 to 0.24. The growth of microalga also increased the pH level in the cultures; the highest pH level of a control treatment increased from 6.51 to 8.74 by the third day (**Figure 1B**). Meanwhile, the OD_{665} of the LA-Pq treatment decreased rapidly after the first day of cultivation (**Figure 1A**), and the pH level remained stable at approximately 6.80 until the end of the experiment.

Biological Mn Oxide (BioMnO$_x$) Generated by *P. duplex* AARL G060

The BioMnO$_x$ catalyst was generated by *P. duplex* AARL G060 under the modified medium supplemented with Mn. Living microalgal growth was indicated by OD_{665}). The oxide form of the Mn (MnO_x) was achieved when the pH level in culture was raised. The results indicate that *P. duplex* AARL G060 grow well in both LA-Low-BioMnO$_x$ and LA-High-BioMnO$_x$ treatments (**Figure 2A**). The OD_{665} value increased from 0.20 to 0.26 on the last day, with the OD value of the LA-High-BioMnO$_x$ treatment increased from 0.59 to 0.88 on the last day (**Figure 2B**), and the pH increased in both LA-Low-BioMnO$_x$ and LA-High-BioMnO$_x$ treatments to a level that supports Mn oxidation. The maximum pH level of LA-Low-BioMnO$_x$ treatment was 8.35 on day 3. Similarly, the pH of the LA-High-BioMnO$_x$ treatment was 8.01 on day 3. The BioMnO$_x$ concentration in LA-Low-BioMnO$_x$ treatment was 2.82 mg by day 6 (**Figure 2C**), and the BioMnO$_x$ concentration for the LA-High-BioMnO$_x$ treatment was 12.73 mg.

Characterization of BioMnO$_x$ Catalyst

During the BioMnO$_x$ process, the living microalgal culture presented dark brown particles of MnO_x on the cell surfaces which were investigated using the SEM. The microphotographs of *P. duplex* AARL G060 showed that Mn precipitation was not observed on the surface of the cells in the control group (**Figure 3A**). The cells of *P. duplex* AARL G060 were smooth and lacked Mn precipitation on cell surfaces. The SEM images of *P. duplex* AARL G060 with BioMnO$_x$ are presented in **Figure 3A**. The results reveal that after 6 days of Mn generation, dark brown particles appeared in the microalgal culture. The brown deposits were only found as aggregates of algal cells with high levels of Mn. Aggregates of MnO_x were observed on cell surfaces in the SEM images shown in **Figure 3B**. Various sizes and irregular forms of BioMnO$_x$ were presented on the microalgal cell surfaces. The relative elemental content of BioMnO$_x$ was investigated using EDS. The EDS spectrum of the control treatment indicated the absence of Mn ions on microalgal cell surfaces. Mn was later detected in the EDS spectrum after 6 days of cultivation, and the BioMnO$_x$ consisted of Mn and O in the complex (**Figure 3C**).

Paraquat Degradation by Fenton-Like Reactions Using BioMnO$_x$ as a Catalyst

The efficiency of paraquat degradation was studied starting with an initial paraquat concentration of 10 mg/L. The effect of BioMnO$_x$ loading on paraquat degradation efficiency shows that the LA-High-BioMnO$_x$-H_2O_2 treatment has higher paraquat removal efficiency than that of LA-Low-BioMnO$_x$-H_2O_2 treatment (**Figure 4A**). This treatment degraded paraquat from 100 to 35.24% within 12 h of contact time and degraded up to 54.64% within 72 h. The results show that catalyst

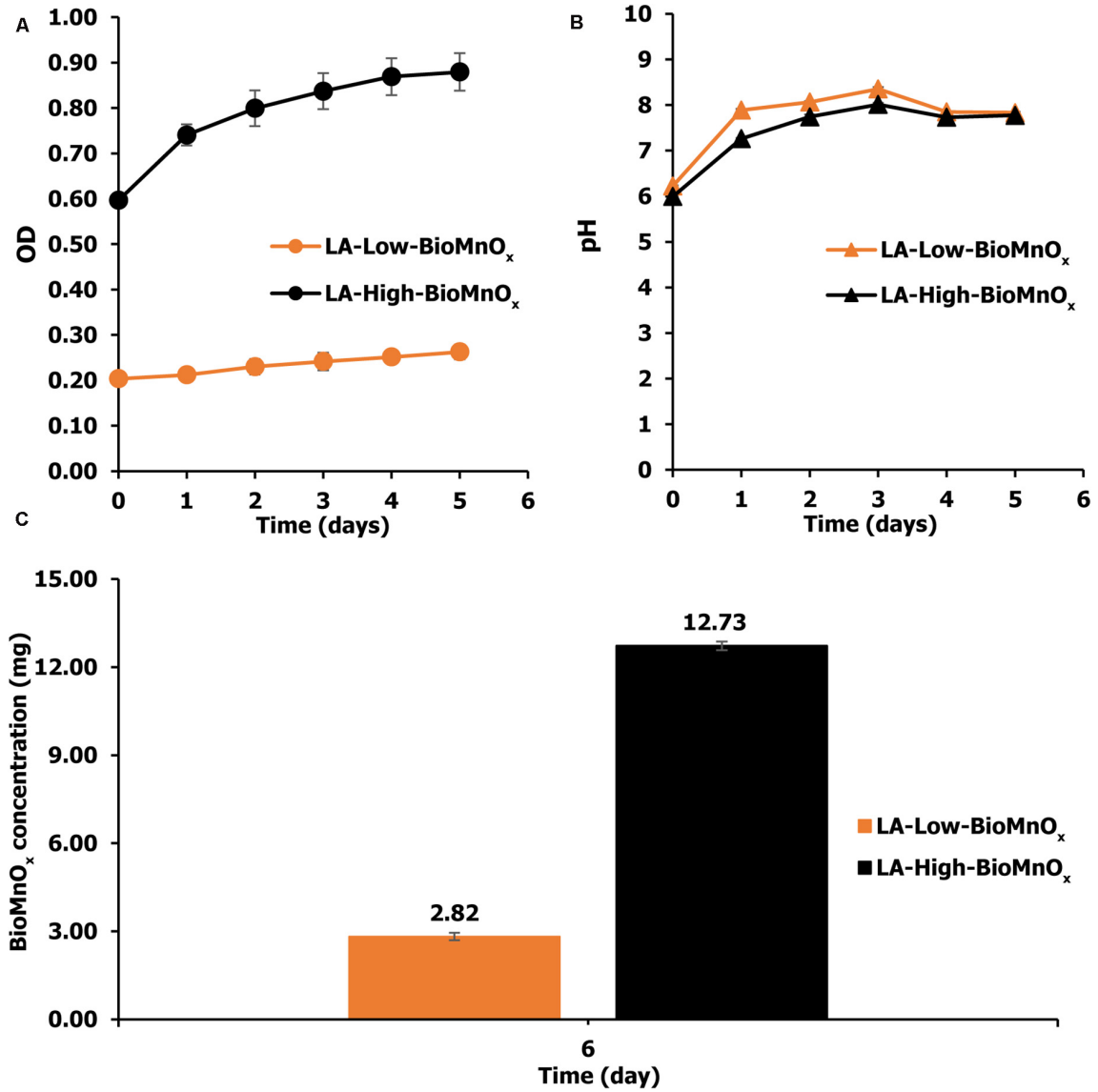

FIGURE 2 | (A) Optical density, **(B)** pH value, and **(C)** concentration of BioMnO$_x$ generated by *P. duplex* AARL G060. LA-Low-BioMnO$_x$: living microalga with low BioMnO$_x$ and LA-High-BioMnO$_x$: living microalga with high BioMnO$_x$.

loading had a considerable effect on paraquat degradation efficiency, and that paraquat degrading efficiency improved as the loading increased. The LA-Low-BioMnO$_x$-H_2O_2 treatment degraded paraquat from 100 to 83.84% within 12 h of contact time. Meanwhile, the control (DW) treatment maintained fairly stable paraquat concentrations. The pH level was above 5 from the initial time to the last hour of contact time (**Figure 4B**), and the HPLC chromatogram shows that the paraquat was degraded (**Figure 5**).

Kinetic Study of Paraquat Degradation

A kinetic study of paraquat degradation in a Fenton-like reaction using BioMnOx as a catalyst was performed, and the pseudo-first order and pseudo-second-order kinetic models were applied to model the kinetics of paraquat degradation under different BioMnO$_x$ concentrations. Each reaction proceeded at different rates. The pseudo first-order model is represented by Eq. (7):

$$C_t = C_0 exp\,(-k1.t), \tag{7}$$

where C_0 and C_t represents are initial paraquat concentration and concentration at time t, k_1 is the rate of degradation (constant) and the time t. Events for the pseudo-second-order model were described by Eq. (8):

$$C_t = \frac{C_0}{1 + k_2.t.C_0}, \tag{8}$$

in which, k_2 is the constant rate of degradation.

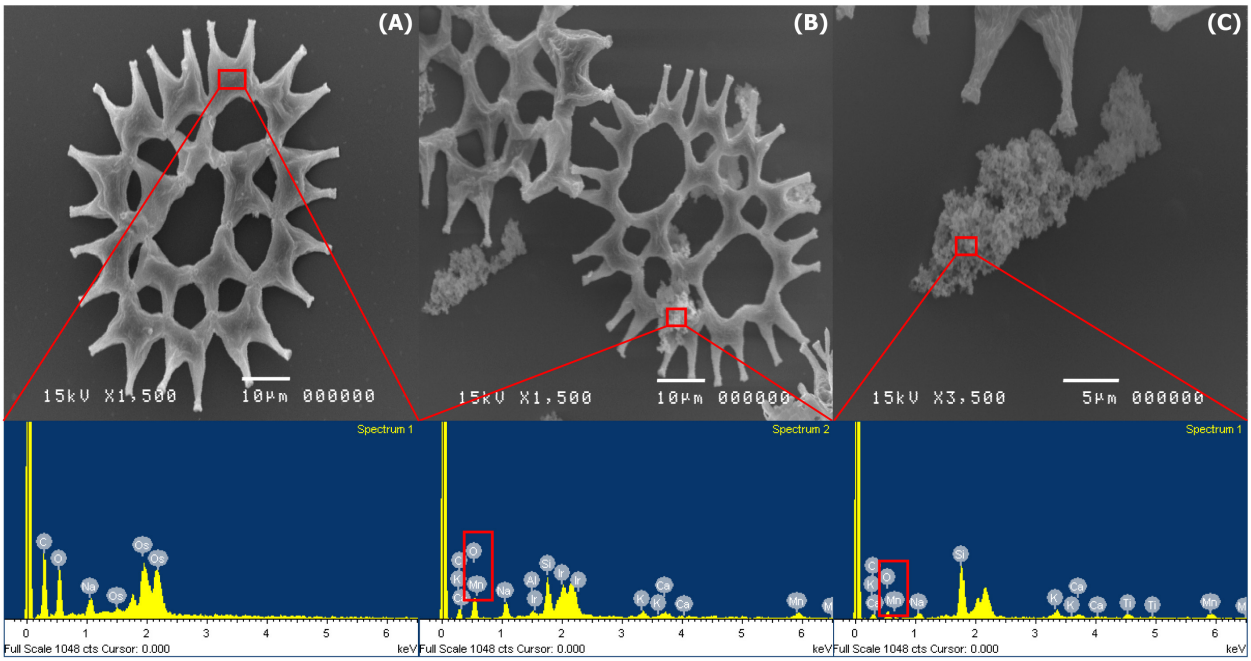

FIGURE 3 | SEM microphotographs and EDS spectrums of BioMnO$_x$ on the cell surface of *P. duplex* AARL G060. **(A)** Control and EDS spectra of selected area on cell surface. **(B,C)** Microalga cell and aggregate of BioMnO$_x$ in culture and EDS spectra of selected area on day 6.

The results of the kinetic study indicate that paraquat degradation in LA-Low-BioMnO$_x$-H_2O_2 treatment was fast during the initial period of 0–6 h, and the highest R^2 value for this treatment was described as pseudo-first order and pseudo-second order kinetic model (**Table 1**). This first phase showed that the kinetic rate constants k_1 and k_2 were 0.0441 h^{-1} and 0.006 L.mg.h^{-1}, respectively. The degradation rates in first period were faster than paraquat degradation in the Fenton-like reactions. For the LA-High-BioMnO$_x$-H_2O_2 treatment, paraquat degradation was highest during the first period (0–6 h). This treatment could be described as pseudo-first order model because the k_1 value was 0.2012 h^{-1}. Higher constant rates revealed in this treatment demonstrated paraquat degradation efficiency higher than that of the LA-Low-BioMnO$_x$-H_2O_2 treatment. Meanwhile, in a later period (6–72 h), the reaction of both treatments showed low degradation rates, which indicates a slower reaction.

DISCUSSION

The results from this study indicate that paraquat affects the growth of *P. duplex* AARL G060. The growth of microalga in LA-Pq treatment decreased with time. A previous study reported that paraquat accepted electrons from photosystem I, thus preventing electron transport to NADPH, and this action may block photosynthesis (Sétif, 2015; Reczek et al., 2017; Huang et al., 2019). Free radicals also react with oxygen, yielding superoxide anions, which led to the formation of hydrogen peroxide and hydroxyl radicals. The hydroxyl radicals caused changes in the ultrastructure of the cells and damaged the DNA in the microalgae (Qian et al., 2009; Zhang et al., 2014).

Living *P. duplex* AARL G060 converted Mn ions into solid Mn via photosynthesis and the oxidation process. After 6 days of cultivation, BioMnO$_x$ was recorded on cell walls of the microalga. Photosynthesis of the living microalga increased the pH level of the water and produced oxygen. The oxygen was released to the environment to oxidize Mn ions and turn them into MnO$_x$ on the microalgal cell surfaces, appearing as a dark brown solid aggregates (Taguchi, 1976; Richardson et al., 1988; Renger and Wydrzynski, 1991; Richardson and Stolzenbach, 1995; Bohutskyi et al., 2016). The results are consistent with previous studies which found that *Scenedesmus subspicatus* oxidized Mn, and MnO was observed both intracellularly and extracellularly (Knauer et al., 1999). In addition, the green microalga *Desmodesmus* sp. WR1 generated 13 mg/L of BioMnO$_x$ after 3 days from an initial Mn concentration of 30 mg/L (Wang et al., 2017). The different quantities of Mn oxide depend on the level of oxygen production, the pH value, the number and size of microalgal cells, and the growth rate of each microalga species. For bacteria, previous studies revealed that the Mn-oxidizing bacterium *Aeromonas hydrophila* strain DS02 had a high tolerance for Mn(II) stress and generated up to 240 mg/L of Mn oxide in 6 days. The BioMnO$_x$ coupled with peroxymonosulfate (PMS) activation degraded 99.5% of 2,4-dimethylaniline within 80 min (Zhang et al., 2019). Stuetz et al. (1996) reported that algal-bacterial oxidation by *Haemaetococcus* sp., *Chlamydomonas* sp., and *Chorella* sp. generated 210 ± 0.04, 170 ± 0.05, and 180 ± 0.05 mg/L of BiOMnO$_x$ in 30 days, respectively (**Table 2**).

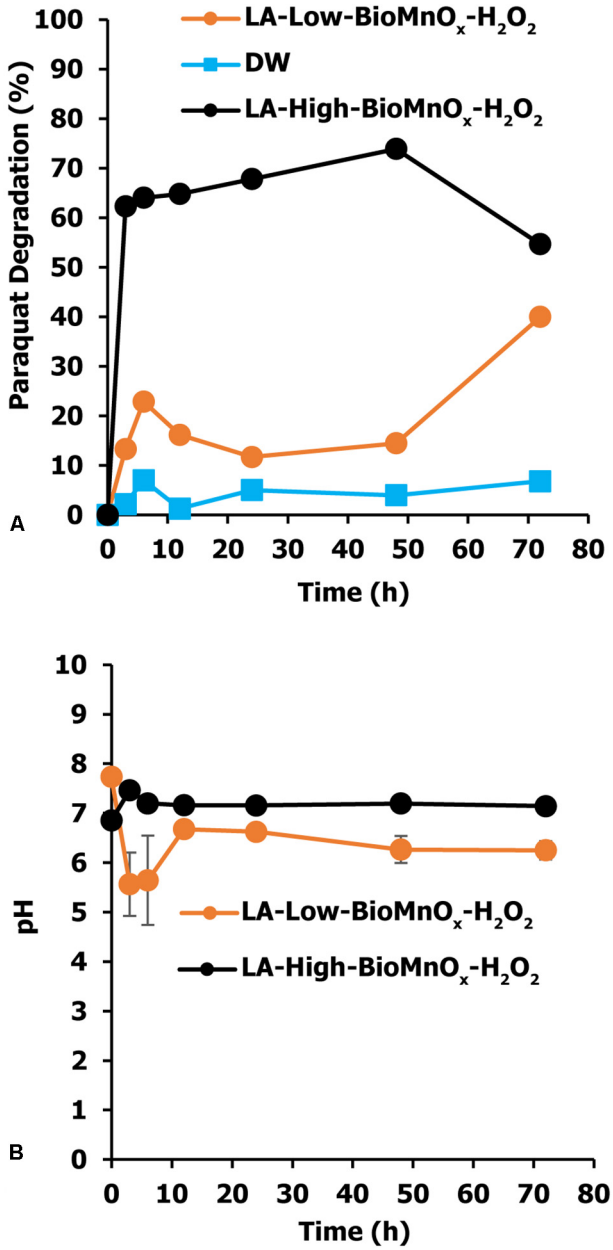

FIGURE 4 | Paraquat degradation by Fenton-like reaction using BioMnO$_x$ as catalyst. **(A)** Percent paraquat degradation and **(B)** pH level in paraquat degradation. LA-Low-BioMnO$_x$-H$_2$O$_2$, living microalga with low BioMnO$_x$ plus H$_2$O$_2$; DW, deionized water (control); LA, living microalga; CSMnO$_x$-H$_2$O$_2$, chemical synthesis of MnOx plus H$_2$O$_2$; LA-High-BioMnO$_x$, living microalga with high BioMnO$_x$ plus H$_2$O$_2$.

The application of chemical paraquat degradation methods discovered that the chemical process is a Fenton-like reaction that relies on metals, such as cerium, chromium, manganese, cobalt, and copper, to directly decompose H_2O_2 into •OH (Bokare and Choi, 2014; Nidheesh, 2015). A biological process characteristic of a Fenton-like reaction was also involved in the generation of the biocatalyst BioMnO$_x$ by living microalga. The MnO_2 generated showed potential as a strong oxidant that can transform aqueous pollutants according to (eq. 9):

$$MnO_2 + \text{org/inorganic substrate} \rightarrow Mn^{2+} + \text{oxidized organic/inorganic substrate.} \quad (9)$$

Then, a Fenton-like reaction, involving Mn ions proceeded as shown in Eqs. (10–13):

$$Mn^{3+} + H_2O_2 \rightarrow Mn^{4+} + \bullet OH + OH^-, \quad (10)$$

$$Mn^{4+} + H_2O_2 \rightarrow Mn^{3+} + HO_2^{\bullet} + H^+, \quad (11)$$

$$HO_2^{\bullet} \longleftrightarrow H^+ + O_2^{\bullet -}, \text{ and} \quad (12)$$

$$Pq + \bullet OH + O_2^{\bullet -} \rightarrow \text{degradationproducts.} \quad (13)$$

Interconversion between Mn^{2+} and Mn^{4+} through intermediate Mn^{3+} species should allow the Mn-catalyzed Fenton-like activation of H_2O_2. The advantages of MnO$_x$ oxidation have received intensive attention due to the large application area and environmental friendliness (Zhang et al., 2014).

The biological catalyst in the LA-Low-BioMnO$_x$ treatment easily degraded paraquat in first period (0–6 h). The kinetics of the Fenton-like reaction during this initial period was described as pseudo-first and pseudo-second order kinetic models. During this period, the Fenton-like reaction used Mn ions which could increase reaction rates. During the last period (6–72 h), this treatment showed slower reaction rates and a decrease in paraquat degradation. The reason for this phenomenon is unclear but may be explained as follows. First, when *P. duplex* AARL G060 synthesized BioMnO$_x$, Mn particles were generated both intracellularly and extracellularly (Thongpitak et al., 2019). Next, in two degradation steps, Mn^{3+} and Mn^{4+} from Mn oxide on cell surfaces reacted with H_2O_2 and generated OH which degrades paraquat. After that, when the microalga died, intercellular metal ions were released into solution. The Mn ions most abundant in solution were water-soluble Mn^{2+} and Mn^{3+} compounds. In aerobic neutral pH conditions, the oxidation of Mn^{2+} to Mn^{4+} and interconversion between Mn^{2+} and Mn^{4+} via intermediate Mn^{3+} species enabled the Mn-catalyzed Fenton-like activation of H_2O_2 (Bokare and Choi, 2014).

The results of the LA-High-BioMnO$_x$ treatment also demonstrated the ability to degrade paraquat in solution by degrading more than 50% of the paraquat within 72 h. In addition, the amount of BioMnO$_x$ catalyst produced had a positive effect on process efficiency. The initial period (0–6 h) of this treatment showed a high kinetic rate constant (0.2012 h^{-1}). This degradation percentage of paraquat in LA-High-BioMnO$_x$ was higher than that of LA-Low-BioMnO$_x$ treatment during this period. During the last period (6–72 h), the kinetic rate constant was lower than the first period and also indicated that degradation rates stabilized in this phase. Even for the amount of BioMnO$_x$ catalyst loading observed, the results are consistent with previous studies that attributed catalyst loading to an increase in the active substances; which, in turn, form more active radicals to contact the target pollutant (Fang

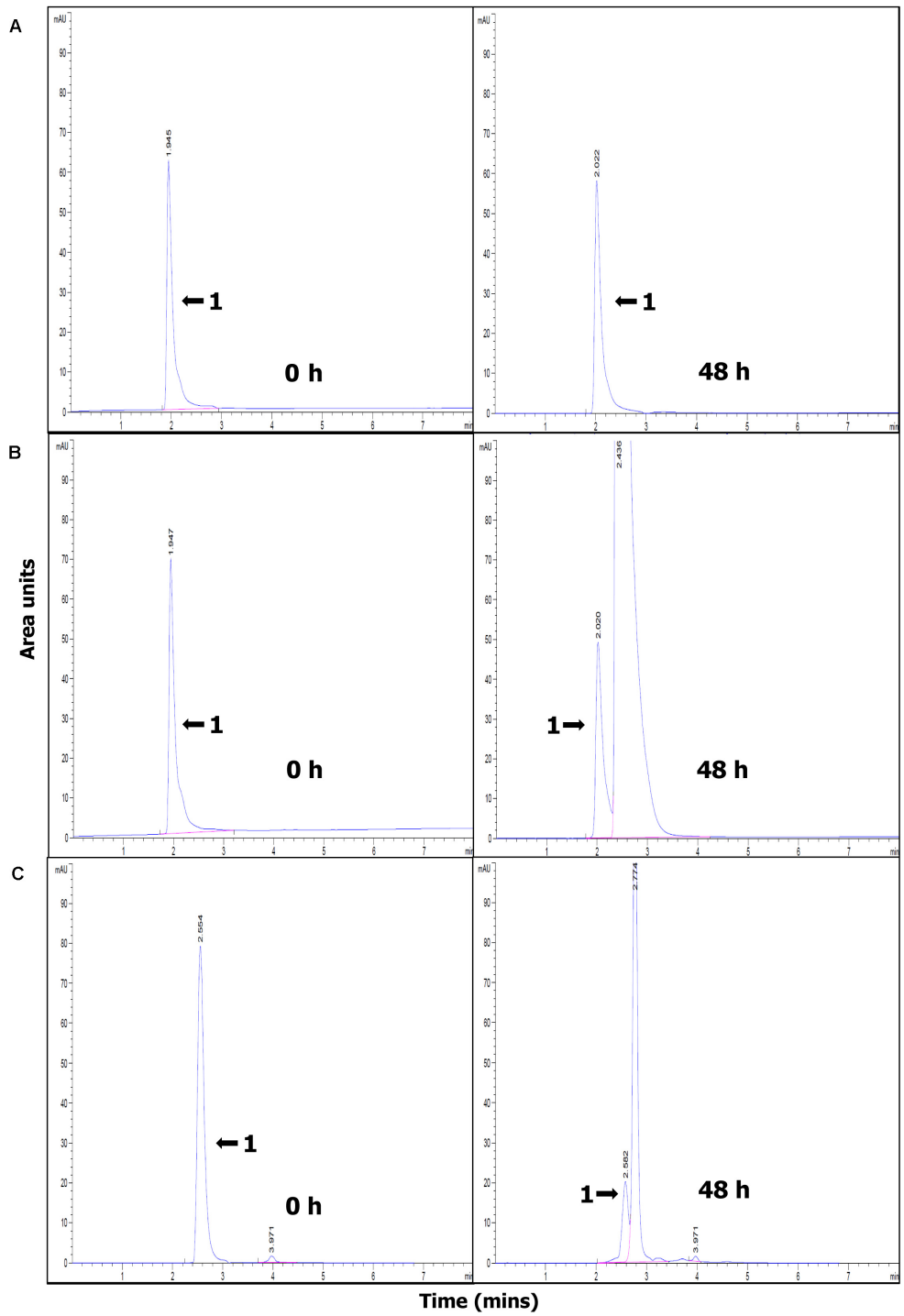

FIGURE 5 | HPLC chromatogram showing paraquat degradation at 0 and 48 h. **(A)** DW (control), **(B)** LA-Low-BioMnO$_x$-H_2O_2, and **(C)** LA-High-BioMnO$_x$-H_2O_2 (the arrow with the number 1 indicates the peak representing paraquat). DW, deionized water; LA-Low-BioMnO$_x$-H_2O_2, living microalga with low BioMnO$_x$ plus H_2O_2; LA-High-BioMnO$_x$, living microalga with high BioMnO$_x$ plus H_2O_2.

et al., 2017; Abdellah et al., 2018; Sabouni and Gomaa, 2019), consistent with previous studies. Application of manganese oxide removed approximately 78% of bisphenol A within 168 h (Wang et al., 2017). Moreover, manganese oxide was used as act a catalyst in a Fenton-like reaction to completely degrade methylene blue in a short duration of 20 min (Kim et al., 2017). In addition, the co-synthesized Fe_3O_4-MnO_2 nano-complex removed up to 96.8% of acid orange 7. The MnO catalyst

TABLE 1 | Kinetic parameters for Fenton-like oxidation of paraquat.

	Time (h)	Pseudo-first order k_1 (h^{-1})	R^2	Pseudo-second order k_2 ($L.mg.h^{-1}$)	R^2
LA-Low-BioMnO$_x$-H_2O_2	0–6	0.0441	0.9986	0.0060	0.9997
	6–72	0.0062	0.7876	0.0007	0.4560
LA-High-BioMnO$_x$-H_2O_2	0–6	0.2012	0.9137	0.0284	0.8035
	6–72	0.0203	0.5803	0.0003	0.0254

TABLE 2 | BioMnO$_x$ productivity of *Pediastrum duplex* AARL G060 compared with previous studies.

Microorganisms	Initial Mn concentration	BioMnO$_x$ (mg/L)	No. of days	BioMnO$_x$ productivity (mg/L/day)	References
Desmodesmus sp. WR1	30 mg/L (Mn^{2+} stock solution)	13.00	3	4.32	Wang et al., 2017
Aeromonas hydrophila strain DS02	1,258 mg/L (10 mM) ($MnCl_2$)	240.00	6	40.00	Zhang et al., 2019
Algal-bacterial oxidation					Stuetz et al., 1996
Haemaetococcus sp.	5 g/L ($MnSO_4.H_2O$)	210.00 ± 0.04	30	7.00	
Chlamydomonas sp.	5 g/L ($MnSO_4.H_2O$)	170.00 ± 0.05	30	5.00	
Chorella sp.	5 g/L ($MnSO_4.H_2O$)	180.00 ± 0.05	30	6.00	
P. duplex AARL G060	20 mg/L ($MnCl_2.4H_2O$)	9.03	6	1.50	This study
P. duplex AARL G060	60 mg/L ($MnCl_2.4H_2O$)	42.41	6	7.06	This study

performed better and degraded more toxin than either Fe_3O_4 or MnO_2 alone.

Paraquat degradation efficiency depended on the dispersions of the catalyst. The highly aggregated BiOMnO$_x$ on microalgal cell surfaces are shown in **Figure 3**. The nanoparticle catalyst may be well-dispersed that could support paraquat degradation. The size of BioMnO$_x$ nanoparticles varied according to different Mn ion concentrations, microalgae concentrations, and cultivation time. Other than using viable microalgal cells, cell free extracts were also possible to biosynthesize for nano MnO (Kumar et al., 2017). In Kumar's study, the size of nanoparticles was varied by alteration of metal ion concentrations, cell free extract concentrations, metal ion volume, cell free extract volume, and incubation temperature.

The observed paraquat degradation by the Fenton-like LA-High-BiOMnO$_x$-H_2O_2 treatment after 72 h decreased. Regeneration of the catalyst could help degradation efficiency remain nearly constant. Cao et al. (2009) revealed a highly effective method for recovering the iron catalyst from Fenton and Fenton-like reactions in which samples were dewatered, dried, and baked at 350–400°C for 20–30 min. For the Mn catalyst, Poyraz et al. (2016) studied the recycling of manganese oxide cathodes for lithium-based batteries and found that thermal regeneration was a suitable method for recycling catalysts.

The HPLC profiles showed rapid disappearance of the peak corresponding to paraquat, accompanied by the appearance of new peaks. Although degradation products of paraquat were not evaluated in this study, degradation products from AOPs were suggested elsewhere. The degradation products may correspond to demethylation products such as 4,40-bipyridine and monopyridone and hydroxylation or oxidative ring cleavage products such as 4-carboxy-1-methyl-pyridinium ion, 4-picolinic acid, and hydroxyl-4-picolinic acid, in accordance with paraquat degradation by UV-ozonation (Kearney et al., 1988), or degradation products such as 4-carboxy-1-methylpyridinium ion, paraquat pyridine, and paraquat dipyridone as suggested by Florêncio et al. (2004) who studied paraquat degradation by titanium dioxide photodegradation. And Burrows et al. (2002) showed that irradiation of paraquat in the presence of oxygen led to formation of 4,4-bipyridyl and 4-picolinic acid. The degradation products of paraquat via Mn catalyzed Fenton-like reaction were not investigated in this study, but this issue should be considered in future studies.

The Fenton-like reactions using BiOMnO$_x$ as a catalyst to remove contaminants from real-life full-scale wastewater provides a viable environmentally friendly alternative technology for the treatment of industrial wastewater.

CONCLUSION

Based on the results of this study, *P. duplex* AARL G060 was found to be a potent strain of living green microalgae for BioMnO$_x$ production. The BioMnO$_x$ served as a biocatalyst that degraded 54.64% of the paraquat in aqueous solution, and the pH level of this operation was above 5. This result demonstrates that BioMnO$_x$ is an environmentally friendly alternative catalyst to remove toxins in wastewater. The insights gained from this experiment will be used to develop better treatments for degradation of toxins and remediation of wastewater.

DATA AVAILABILITY STATEMENT

All datasets generated for this study are included in the article/**Supplementary Material**.

AUTHOR CONTRIBUTIONS

All authors listed have made a substantial, direct and intellectual contribution to the work, and approved it for publication.

FUNDING

This research was partially supported by the Chiang Mai University and The Graduate School and the Research Center in Bioresources for Agriculture, Industry, and Medicine, Chiang Mai University.

SUPPLEMENTARY MATERIAL

The Supplementary Material for this article can be found online at: https://www.frontiersin.org/articles/10.3389/fmicb.2020.575361/full#supplementary-material

REFERENCES

Abdellah, M. H., Nosier, S. A., El-Shazly, A. H., and Mubarak, A. A. (2018). Photocatalytic decolorization of methylene blue using TiO2/UV system enhanced by air sparging. *Alexandria Eng. J.* 57, 3727–3735. doi: 10.1016/j.aej.2018.07.018

Asgari, G., Seidmohammadi, A., Esrafili, A., Faradmal, J., Noori Sepehr, M., and Jafarinia, M. (2020). The catalytic ozonation of diazinon using nano-MgO@CNT@Gr as a new heterogenous catalyst: the optimization of effective factors by response surface methodology. *RSC Adv.* 10, 7718–7731. doi: 10.1039/c9ra10095d

Barbusiñski, K., and Filipek, K. (2001). Use of Fenton's reagent for removal of pesticides from industrial wastewater. *Polish J. Environ. Stud.* 10, 207–212.

Birkner, N., Nayeri, S., Pashaei, B., Najafpour, M. M., Casey, W. H., and Navrotsky, A. (2013). Energetic basis of catalytic activity of layered nanophase calcium manganese oxides for water oxidation. *Proc. Natl. Acad. Sci. U.S.A.* 110, 8801–8806. doi: 10.1073/pnas.1306623110

Bishop, D. F., Stern, G., Fleischman, M., and Marshall, L. S. (1968). Hydrogen peroxide catalytic oxidation of refractory organics in municipal waste waters. *Ind. Eng. Chem. Process Des. Dev.* 7, 110–117. doi: 10.1021/i260025a022

Bohutskyi, P., Kligerman, D., Byers, N., Nasr, L. K., Cua, C., Chow, S., et al. (2016). Effects of inoculum size, light intensity, and dose of anaerobic digestion centrate on growth and productivity of Chlorella and *Scenedesmus microalgae* and their poly-culture in primary and secondary wastewater. *Chemosphere* 19, 278–290. doi: 10.1016/j.algal.2016.09.010

Bokare, A. D., and Choi, W. (2014). Review of iron-free Fenton-like systems for activating H2O2 in advanced oxidation processes. *J. Hazard Mater.* 275, 121–135. doi: 10.1016/j.jhazmat.2014.04.054

Burrows, H. D., Canle, L. M., Santaballa, J. A., and Steenken, S. (2002). Reaction pathways and mechanisms of photodegradation of pesticides. *J. Photochem. Photobiol. B Biol.* 67, 71–108. doi: 10.1016/s1011-1344(02)00277-4

Cao, G., Sheng, M., Niu, M., Feng, W., Fei, Y. L., and Li, D. (2009). Regeneration and reuse of iron catalyst for Fenton-like reactions. *J. Hazard Mater.* 172, 1446–1449. doi: 10.1016/j.jhazmat.2009.08.010

Chi, Z., O'Fallon, J. V., and Chen, S. (2011). Bicarbonate produced from carbon capture for algae culture. *Trends Biotechnol.* 29, 537–541. doi: 10.1016/j.tibtech.2011.06.006

Corma, A., Garcia, H., and Leyva, A. (2005). Catalytic activity of palladium supported on single wall carbon nanotubes compared to palladium supported on activated carbon: study of the Heck and Suzuki couplings, aerobic alcohol oxidation and selective hydrogenation. *J. Mol. Catal. A Chem.* 230, 97–105. doi: 10.1016/j.molcata.2004.11.030

de Guimarães, B. S., Bernardes, A. A., Salcedo, G. M., Caldas, S. S., Jorge, M. B., Bianchini, A., et al. (2016). Photocatalytic degradation for treating multipesticide residues using [Ru(bipy)3]Cl2-Doped TiO2/SiO2 based on surface response methodology. *J. Braz. Chem. Soc.* 27, 2256–2263.

Deng, Y., and Zhao, R. (2015). Advanced oxidation processes (AOPs) in wastewater treatment. *Curr. Pollut. Rep.* 1, 167–176. doi: 10.1007/s40726-015-0015-z

Fang, Z., Zhang, D., Liu, K., Fan, J., and Zhao, J. Y. Z. W. (2017). Fenton-like oxidation of azo dye in aqueous solution using magnetic Fe3O4 -MnO2 nanocomposites as catalysts. *Water Sci. Eng.* 10, 326–333. doi: 10.1016/j.wse.2017.10.005

Fernández, M., Ibáñez, M., Picó, Y., and Mañes, J. (1998). Spatial and temporal trends of paraquat, diquat, and difenzoquat contamination in water from marsh areas of the Valencian community (Spain). *Arch. Environ. Contam. Toxicol.* 35, 377–384. doi: 10.1007/s002449900391

Florêncio, M. H., Pires, E., Castro, A. L., Nunes, M. R., Borges, C., and Costa, F. M. (2004). Photodegradation of diquat and paraquat in aqueous solutions by titanium dioxide: evolution of degradation reactions and characterisation of intermediates. *Chemosphere* 55, 345–355. doi: 10.1016/j.chemosphere.2003.11.013

Forrez, I., Carballa, M., Verbeken, K., Vanhaecke, L., Ternes, T., Boon, N., et al. (2010). Diclofenac oxidation by biogenic manganese oxides. *Environ. Sci. Technol.* 44, 3449–3454. doi: 10.1021/es9027327

Frimpong, J. O., Ofori, E. S. K., Yeboah, S., Marri, D., Offei, B. K., Apaatah, F., et al. (2018). Evaluating the impact of synthetic herbicides on soil dwelling macrobes and the physical state of soil in an agro-ecosystem. *Ecotoxicol. Environ. Saf.* 156, 205–215. doi: 10.1016/j.ecoenv.2018.03.034

Fu, J., He, Z., Wang, H., Liang, W., and Guo, C. (2010). Preparation of chemical manganese dioxide from manganese sulfate. *Min. Sci. Technol.* 20, 877–881. doi: 10.1016/s1674-5264(09)60299-4

Furgal, K. M., Meyer, R. L., and Bester, K. (2015). Removing selected steroid hormones, biocides and pharmaceuticals from water by means of biogenic manganese oxide nanoparticles in situ at ppb levels. *Chemosphere* 136, 321–326. doi: 10.1016/j.chemosphere.2014.11.059

Garrido-Cardenas, J. A., Esteban-García, B., Agüera, A., Sánchez-Pérez, J. A., and Manzano-Agugliaro, F. (2020). Wastewater treatment by advanced oxidation process and their worldwide research trends. *Int. J. Environ. Res. Public Health* 17:170. doi: 10.3390/ijerph17010170

Greene, A. C., and Madgwick, J. C. (1991). Microbial formation of manganese oxides. *Appl. Environ. Microbiol.* 57, 1114–1120. doi: 10.1128/aem.57.4.1114-1120.1991

Guégan, R., Giovanela, M., Warmont, F., and Motelica-Heino, M. (2015). Nonionic organoclay: a 'Swiss Army knife' for the adsorption of organic micro-pollutants? *J. Colloid Interface Sci.* 437, 71–79. doi: 10.1016/j.jcis.2014.09.043

Hamad, D., Dhib, R., and Mehrvar, M. (2016). Photochemical degradation of aqueous polyvinyl alcohol in a continuous UV/H2O2 process: experimental and statistical analysis. *J. Polym. Environ.* 24, 72–83. doi: 10.1007/s10924-016-0750-2

Hennebel, T., De Gusseme, B., Boon, N., and Verstraete, W. (2009). Biogenic metals in advanced water treatment. *Trends Biotechnol.* 27, 90–98. doi: 10.1016/j.tibtech.2008.11.002

Huang, Y., Zhan, H., Bhatt, P., and Chen, S. (2019). Paraquat degradation from contaminated environments: current achievements and perspectives. *Front. Microbiol.* 10:1754. doi: 10.3389/fmicb.2019.01754

Insuwan, W., and Rangsriwatananon, K. (2017). Removal of paraquat from aqueous solutions onto zeolite LTL. *Eng. J.* 21, 15–23. doi: 10.4186/ej.2017.21.2.15

Ismail, B. S., Sameni, M., and Halimah, M. (2011). Evaluation of herbicide pollution in the Kerian ricefields of Perak, Malaysia. *World Appl. Sci. J.* 15, 05–13.

Kearney, P. C., Muldoon, M. T., Somich, C. J., Ruth, J. M., and Voaden, D. J. (1988). Biodegradation of ozonated atrazine as a wastewater disposal system. *J. Agric. Food Chem.* 36, 1301–1306. doi: 10.1021/jf00084a044

Keawkumay, C., Rakmae, S., Rongchapo, W., Suppakarn, N., Prayoonpokarach, S., and Wittayakun, J. (2016). Adsorption of paraquat and pirimiphos-methyl by montmorillonite modified with tetradecylammonium chloride and intragallery templating method. *Adsorpt. Sci. Technol.* 35, 357–371. doi: 10.1177/0263617416677351

Kenduzler, E., and Turker, A. R. (2002). Determination of iron, manganese and zinc in water samples by flame atomic absorption spectrophotometry after preconcentration with solid-phase extraction onto Ambersorb 572. *Anal. Sci.* 18, 917–921. doi: 10.2116/analsci.18.917

Kim, D. G., Jiang, S., Jeong, K., and Ko, S. O. (2012). Removal of 17α-Ethinylestradiol by biogenic manganese oxides produced by the *Pseudomonas* putida strain MnB1. *Water Air Soil Pollut.* 223, 837–846. doi: 10.1007/s11270-011-0906-6

Kim, E. J., Oh, D., Lee, C. S., Gong, J., Kim, J., and Chang, Y. S. (2017). Manganese oxide nanorods as a robust Fenton-like catalyst at neutral pH: crystal phase-dependent behavior. *Catal. Today* 282, 71–76. doi: 10.1016/j.cattod.2016.03.034

Kiwi, J., Pulgarin, C., Peringer, P., and Grätzel, M. (1993). Beneficial effects of homogeneous photo-Fenton pretreatment upon the biodegradation of anthraquinone sulfonate in waste water treatment. *Appl. Catal. B Environ.* 3, 85–99. doi: 10.1016/0926-3373(93)80070-t

Knauer, K., Jabusch, T., and Sigg, L. (1999). Manganese uptake and Mn(II) oxidation by the alga *Scenedesmus subspicatus*. *Aquat. Sci.* 61, 44–58. doi: 10.1007/pl00001321

Knepil, J. (1977). A short, simple method for the determination of paraquat in plasma. *Clin. Chim. Acta* 79, 387–390. doi: 10.1016/0009-8981(77)90433-8

Kumar, V., Singh, K., Panwar, S., and Mehta, S. K. (2017). Green synthesis of manganese oxide nanoparticles for the electrochemical sensing of p-nitrophenol. *Int. Nano Lett.* 7, 123–131. doi: 10.1007/s40089-017-0205-3

Li, Y., Xu, Z., Ma, H., and Hursthouse, A. S. (2019). Removal of manganese (II) from acid mine wastewater: a review of the challenges and opportunities with special emphasis on. *Water* 11:2493. doi: 10.3390/w11122493

Mandal, T., Maity, S., Dasgupta, D., and Datta, S. (2010). Advanced oxidation process and biotreatment: their roles in combined industrial wastewater treatment. *Desalination* 250, 87–94. doi: 10.1016/j.desal.2009.04.012

Michalak, I., Marycz, K., Basiñska, K., and Chojnacka, K. (2014). Using SEM-EDX and ICP-OES to investigate the elemental composition of green macroalga *Vaucheria sessilis*. *Sci. World J.* 2014:891928. doi: 10.1155/2014/891928

Nidheesh, P. V. (2015). Heterogeneous fenton catalysts for the abatement of organic pollutants from aqueous solution: a review. *RSC Adv.* 5, 40552–40577. doi: 10.1039/c5ra02023a

Poyatos, J. M., Muñio, M. M., Almecija, M. C., Torres, J. C., Hontoria, E., and Osorio, F. (2009). Advanced oxidation processes for wastewater treatment: state of the art. *Water Air Soil Pollut.* 205:187.

Poyraz, A. S., Huang, J., Cheng, S., Bock, D. C., Wu, L., Zhu, Y., et al. (2016). Effective recycling of manganese oxide cathodes for lithium based batteries. *Green Chem.* 18, 3414–3421. doi: 10.1039/c6gc00438e

Pukcothanung, Y., Siritanon, T., and Rangsriwatananon, K. (2018). The efficiency of zeolite Y and surfactant-modified zeolite Y for removal of 2,4-dichlorophenoxyacetic acid and 1,1'-dimethyl-4,4'-bipyridinium ion. *Micropor. Mesopor. Mater.* 258, 131–140. doi: 10.1016/j.micromeso.2017.08.035

Qian, H., Chen, W., Sun, L., Liu, W., and Fu, Z. (2009). Inhibitory effects of paraquat on photosynthesis and the response to oxidative stress in *Chlorella vulgaris*. *Ecotoxicology* 18, 537–543. doi: 10.1007/s10646-009-0311-8

Reczek, C. R., Birsoy, K., Kong, H., Martínez-Reyes, I., Wang, T., Gao, P., et al. (2017). A CRISPR screen identifies a pathway required for paraquat-induced cell death. *Nat. Chem. Biol.* 13, 1274–1279. doi: 10.1038/nchembio.2499

Renger, G., and Wydrzynski, T. (1991). The role of manganese in photosynthetic water oxidation. *Biol. Met.* 4, 73–80. doi: 10.1007/bf01135382

Richardson, L. L., Aguilar, C., and Nealson, K. H. (1988). Manganese oxidation in pH and O2 microenvironments produced by phytoplankton. *Limnol. Oceanogr.* 33, 352–363. doi: 10.4319/lo.1988.33.3.0352

Richardson, L. L., and Stolzenbach, K. D. (1995). Phytoplankton cell size and the development of microenvironments. *FEMS Microbiol. Ecol.* 16, 185–191. doi: 10.1111/j.1574-6941.1995.tb00282.x

Roberts, T. R., Dyson, J. S., and Lane, M. C. G. (2002). Deactivation of the biological activity of paraquat in the soil environment: a review of long-term environmental fate. *J. Agric. Food Chem.* 50, 3623–3631. doi: 10.1021/jf011323x

Robinson, D. M., Go, Y. B., Mui, M., Gardner, G., Zhang, Z., Mastrogiovanni, D., et al. (2013). Photochemical water oxidation by crystalline polymorphs of manganese oxides: structural requirements for catalysis. *J. Am. Chem. Soc.* 135, 3494–3501. doi: 10.1021/ja310286h

Sabirova, J. S., Cloetens, L. F. F., Vanhaecke, L., Forrez, I., Verstraete, W., and Boon, N. (2008). Manganese-oxidizing bacteria mediate the degradation of 17α-ethinylestradiol. *Microb. Biotechnol.* 1, 507–512. doi: 10.1111/j.1751-7915.2008.00051.x

Sabouni, R., and Gomaa, H. (2019). Photocatalytic degradation of pharmaceutical micro-pollutants using ZnO. *Environ. Sci. Pollut. Res.* 26, 5372–5380. doi: 10.1007/s11356-018-4051-2

Sétif, P. (2015). Electron-transfer kinetics in cyanobacterial cells: methyl viologen is a poor inhibitor of linear electron flow. *Biochim. Biophys. Acta Bioenerg.* 1847, 212–222. doi: 10.1016/j.bbabio.2014.10.008

Shaker, K. S., and Abdalsalm, A. H. (2018). Synthesis and characterization nano structure of MnO2 via chemical method. *Engr. Tech. J.* 36, 946–950. doi: 10.30684/etj.36.9a.1

Sieliechi, J. M., and Thue, P. S. (2015). Removal of paraquat from drinking water by activated carbon prepared from waste wood. *Desalin. Water Treat.* 55, 986–998. doi: 10.1080/19443994.2014.922504

Stuetz, R. M., Greene, A. C., and Madgwick, J. C. (1996). Microalgal-facilitated bacterial oxidation of manganese. *J. Ind. Microbiol.* 16, 267–273. doi: 10.1007/bf01570033

Taguchi, S. (1976). Relationship between photosynthesis and cell size of marine diatom. *J. Phycol.* 12, 185–189. doi: 10.1111/j.1529-8817.1976.tb00499.x

Tani, Y., Miyata, N., Ohashi, M., Ohnuki, T., Seyama, H., Iwahori, K., et al. (2004). Interaction of inorganic arsenic with biogenic manganese oxide produced by a Mn-oxidizing fungus, strain KR21-2. *Environ. Sci. Technol.* 38, 6618–6624. doi: 10.1021/es049226i

Thi Hue, N., Nguyen, T. P. M., Nam, H., and Hoang Tung, N. (2018). Paraquat in surface water of some streams in Mai Chau province, the northern Vietnam: concentrations, profiles, and human risk assessments. *J. Chem.* 2018:8521012.

Thongpitak, J., Pekkoh, J., and Pumas, C. (2018). Simple medium formulation for manganese remediation by green microalga *Pediastrum* duplex AARLG060. *Chiang Mai J. Sci.* 45, 1247–1256.

Thongpitak, J., Pekkoh, J., and Pumas, C. (2019). Remediation of manganese-contaminated coal-mine water using bio-sorption and bio-oxidation by the microalga *Pediastrum* duplex (AARLG060): a laboratory-scale feasibility study. *Front. Microbiol.* 10:2605. doi: 10.3389/fmicb.2019.02605

Tian, N., Tian, X., Nie, Y., Yang, C., Zhou, Z., and Li, Y. (2018). Biogenic manganese oxide: an efficient peroxymonosulfate activation catalyst for tetracycline and phenol degradation in water. *Chem. Eng. J.* 352, 469–476. doi: 10.1016/j.cej.2018.07.061

Vagi, M. C., and Petsas, A. S. (2017). "Advanced oxidation processes for the removal of pesticides from wastewater: recent review and trends," in *Proceedings of the 15th International Conference on Environmental Science and Technology*, Rhodes.

Veríssimo, G., Moreira, J., and Meyer, A. (2018). Paraquat contamination in surface waters of a rural stream in the mountain region in the state of Rio De Janeiro southeastern Brazil. *J. Environ. Toxicol. Stud.* 2:111.

Wang, J. L., and Xu, L. J. (2012). Advanced oxidation processes for wastewater treatment: formation of hydroxyl radical and application. *Crit. Rev. Environ. Sci. Technol.* 42, 251–325. doi: 10.1080/10643389.2010.507698

Wang, R., Wang, S., Tai, Y., Tao, R., Dai, Y., Guo, J., et al. (2017). Biogenic manganese oxides generated by green algae *Desmodesmus* sp. *WR1* to improve bisphenol A removal. *J. Hazard. Mater.* 339, 310–319. doi: 10.1016/j.jhazmat.2017.06.026

Webster, R. E., Dean, A. P., and Pittman, J. K. (2011). Cadmium exposure and phosphorus limitation increases metal content in the freshwater alga *Chlamydomonas reinhardtii*. *Environ. Sci. Technol.* 45, 7489–7496. doi: 10.1021/es200814c

Wu, R., Wu, H., Jiang, X., Shen, J., Faheem, M., Sun, X., et al. (2017). The key role of biogenic manganese oxides in enhanced removal of highly recalcitrant 1,2,4-triazole from bio-treated chemical industrial wastewater. *Environ. Sci. Pollut. Res.* 24, 10570–10583. doi: 10.1007/s11356-017-8641-1

Zhang, W., Liu, M., Zhang, P., Yu, F., Lu, S., Li, P., et al. (2014). Effects of paraquat on photosynthetic pigments, antioxidant enzymes, and gene expression in Chlorella pyrenoidosa under mixotrophic compared with

autotrophic conditions. *Arch. Environ. Contam. Toxicol.* 67, 593–600. doi: 10.1007/s00244-014-0067-x

Zhang, Y., Tang, Y., Qin, Z., Luo, P., Ma, Z., Tan, M., et al. (2019). A novel manganese oxidizing bacterium-*Aeromonas hydrophila* strain DS02: Mn(II) oxidization and biogenic Mn oxides generation. *J. Hazard Mater.* 367, 539–545. doi: 10.1016/j.jhazmat.2019.01.012

Zhou, H., and Fu, C. (2020). Manganese-oxidizing microbes and biogenic manganese oxides: characterization, Mn(II) oxidation mechanism and environmental relevance. *Rev. Environ. Sci. Biotechnol.* 19, 489–507. doi: 10.1007/s11157-020-09541-1

Conflict of Interest: The authors declare that the research was conducted in the absence of any commercial or financial relationships that could be construed as a potential conflict of interest.

frontiers in Microbiology

ORIGINAL RESEARCH
published: 18 September 2020
doi: 10.3389/fmicb.2020.574966

Development of Digital Image Processing as an Innovative Method for Activated Sludge Biomass Quantification

*Hashem Asgharnejad and Mohammad-Hossein Sarrafzadeh**

School of Chemical Engineering, College of Engineering, University of Tehran, Tehran, Iran

Activated sludge process is the most common method for biological treatment of industrial and municipal wastewater. One of the most important parameters in performance of activated sludge systems is quantitative monitoring of biomass to keep the cell concentration in an optimum range. In this study, a novel method for activated sludge quantification based on image processing and RGB analysis is proposed. According to the results, the intensity of blue color in the macroscopic image of activated sludge culture can be a very accurate index for cell concentration measurement and R^2 coefficient, Root Mean Square Error (RMSE), Mean Absolute Error (MAE), and Mean Absolute Percentage Error (MAPE) which are 0.990, 2.000, 0.323, and 13.848, respectively, prove this claim. Besides, in order to avoid the difficulties of working in the three-parameter space of RGB, converting to grayscale space has been applied which can estimate cell concentration with R^2 = 0.99. Ultimately, an exponential correlation between RGB values and cell concentrations in lower amounts of biomass has been proposed based on Beer-Lambert law which can estimate activated sludge biomass concentration with R^2 = 0.97 based on B index.

Keywords: activated sludge, biomass quantification, cell concentration, image processing, RGB analysis

OPEN ACCESS

Edited by:
Mayur B. Kurade,
Hanyang University, South Korea

Reviewed by:
Humaira Nisar,
Tunku Abdul Rahman University, Malaysia
Huseyin Guven,
Istanbul Technical University, Turkey
Shekhar B. Jadhav,
The Institute of Science, India

***Correspondence:**
Mohammad-Hossein Sarrafzadeh
sarrafzdh@ut.ac.ir

Specialty section:
This article was submitted to Microbiotechnology, a section of the journal Frontiers in Microbiology

Received: *22 June 2020*
Accepted: *31 August 2020*
Published: *18 September 2020*

Citation:
Asgharnejad H and Sarrafzadeh M-H (2020) Development of Digital Image Processing as an Innovative Method for Activated Sludge Biomass Quantification. Front. Microbiol. 11:574966. doi: 10.3389/fmicb.2020.574966

INTRODUCTION

Use of activated sludge (AS) is the most common biological method for wastewater treatment (Gernaey et al., 2004). AS is a complex of viable microorganisms which is generally composed of mainly heterotrophic bacteria which can utilize organic matters, measured as biological oxygen demand (BOD) or chemical oxygen demand (COD), in the wastewater to survive and remove them from wastewater, consequently (Garakani et al., 2011; Ratkovich et al., 2013; Ju and Zhang, 2015). Quantitative and qualitative monitoring of different features of AS sometimes plays a key role in good operation of a wastewater treatment plant. Among all, controlling AS biomass concentration in the optimum range is most vital, because any deviation from the optimum range may result either in poor BOD removal or release of suspended solids into the effluent stream of the wastewater treatment plant which may cause microbial pollutions (Gernaey et al., 2001). Therefore, numerous attempts have been carried out for monitoring of biomass concentration in the AS systems described here.

Methods of biomass concentration measurement are categorized into two groups of direct and indirect techniques (Frasier et al., 2016). In direct techniques, the weight or cell numbers of the biomass will be measured directly, while in indirect techniques, a physical, chemical, or biological property which is depended on the biomass concentration will be used as a proxy for determination of biomass concentration (Ratkovich et al., 2013). Mixed liquor suspended solids (MLSS) is the most popular index which is used for biomass concentration in AS systems and is defined as the concentration of total suspended solids including biomass in a specific volume of sample taken from bioreactors (Martín-Pascual et al., 2015). Incapability of online measurement, noticeable errors of sampling, procedure of the measurement and having time-lag in reporting the results are the main drawbacks of direct methods such as MLSS measurement. Therefore, the attentions of the researchers of this field have been focused on development of appropriate indirect methods during last few years. Laser reflectance measurement (Expósito et al., 2017), measurement of ultrasound attenuation and backscattering (Rodriguez-Molares et al., 2014; Elvira et al., 2016), determination of cellular compounds and metabolites content such as adenosine triphosphate (ATP) (Abushaban et al., 2019), respirometry and measurement of oxygen uptake rate (OUR) in aerobic sludge (Garcia-Ochoa et al., 2010), flow cytometry (Brown et al., 2019), density measurement (Cano et al., 2014), and measurement of biomass electrical properties such as permittivity, capacitance, and impedance (Sarrafzadeh et al., 2005; Bobowski and Johnson, 2012; Zhang et al., 2012; Shariati et al., 2013; Pajoum-Shariati et al., 2014) are the most applied techniques which have been developed for biomass concentration measurement in different biological systems, especially bacterial ones such as activated sludge. A part of these methods successfully find their commercial place in several biotechnology processes but not in the biological wastewater treatment plants (Sarrafzadeh et al., 2005, 2015b). Because they are often considered as high-tech and complicated methods that need trained operators in addition to high capital consuming to be applied in wastewater plant.

Image processing has largely been used in recent years for quantitative analysis of biological systems such as yeast, bacteria and microalgae (Selinummi et al., 2005; Acevedo et al., 2009; Sarrafzadeh et al., 2015a). This method is generally based on analyzing the visual characteristics of the biological cultures such as color, light intensity, etc. through their images (Murphy et al., 2014). RGB analysis is one of the simplest and most common methods of image processing in which the intensities of three colors of red (R), green (G), and blue (B) of the image of culture will be extracted (Uyar, 2013). Different methods of image processing for monitoring of AS systems has found their positions among other methods of biomass quantification during recent years and analysis of sludge microscopic images has been used to estimate total suspended solids (TSS), sludge volume index (SVI), settling ability, sludge abnormalities, and disturbances (Amaral and Ferreira, 2005; Mesquita et al., 2009, 2011a,b, 2013; Amaral et al., 2013). However, using image processing for monitoring of AS cultures has been limited to the microscopic images of the cells and not macroscopic digital images. Microscope imaging not only makes online monitoring infeasible, but also the errors related to the operator and limited view scope of the microscope are normally significant. Besides, needing complex devices of microscopy will increase the costs of analysis in this technique. Therefore, using macroscopic digital imaging taken by simple camera or smart cell phone, not only facilitates the procedure of analysis, but also is a very good tool for online quantification of the biomass (Sarrafzadeh et al., 2015b).

Most of current methods of activated sludge monitoring needs sampling which increases inaccuracy due to human interference. On the other hand, image processing, is a non-destructive method with the potential of online application which can measure the activated sludge concentration accurately with minimum time lag. Moreover, the cheap methods of activated sludge monitoring (including drying and weighting, cytometry, etc.) are incapable of distinguishing between living and dead cells, however, combination of image processing with staining techniques or microscopic images can give valuable information about qualitative conditions of the cells in activated sludge culture (Saladra and Kopernik, 2016). Methods like permittivity or OUR measurement which are capable of provide a qualitative study of the activated sludge cells are either high-tech and need expensive devices and trained operators or are not generalizable and have limited area of application like OUR measurement which is only applicable in aerobic sludge.

In this study, it is tried to develop image processing as a non-invasive method for quantification of the activated sludge using macroscopic digital images and the advantages and limitations of this technique are discussed completely. The main purpose of this research is to study the feasibility of RGB analysis in order to measure the biomass concentration in AS systems.

MATERIALS AND METHODS

Activated Sludge Samples and MLSS Measurement

AS was pre-cultivated in a 500 mL bottle with glucose as the carbon source for biomass growth. The inoculum size for precultivation was 172,000 cells per mL which was measured by plastic Neubauer (Improved DHC-N01, C-Chip, NanoEnTek, Korea) hemocytometer. The culture was continuously aerated with flowrate of 100 $mL.min^{-1}$ to provide adequate mixing. After increasing the MLSS and reaching a desirable amount, the AS was injected to a 2 L Plexiglas fed-batch bioreactor with glucose as the carbon source and feeding rate of 3 g glucose (COD = 3200 $mg.L^{-1}$) per 12 h (Rezaee et al., 2015; Leong et al., 2018). Then, sampling was carried out from the bioreactor at different times. A 100 mL plastic syringe was utilized for sampling AS from the reactor. In order to have a homogenous sample, representing the whole biomass in the bioreactor, sampling was carried out from three different heights of the bioreactor (surface, center, and bottom) with equal size and mixed together.

MLSS is the main index for AS biomass concentration which shows the weight of suspended particles of sludge in a specific volume. In order to measure the MLSS, a specific volume of the AS mixture is filtered in order to separate the liquid and solid

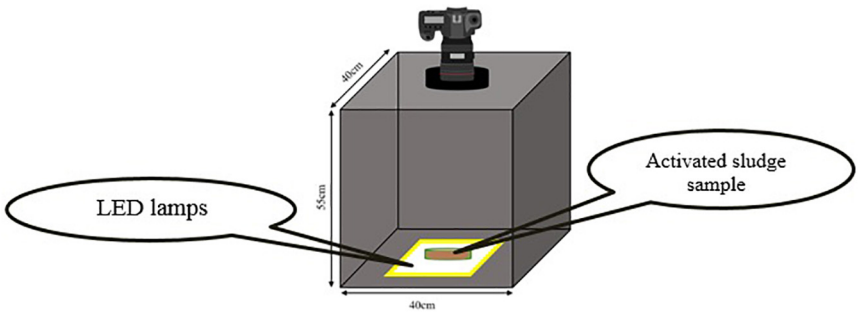

FIGURE 1 | Schematic illustration of photography setup for taking images.

phases. For filtration, pre-weighted filter papers (chm, 125 mm, Spain), Büchner funnel and vacuum pump (Value, single stage, VE 115N, China) are used. After filtration, the residue and filter are dried in an oven at 103–105°C for more than 1 h. Then, the dried filter and sludge are weighted and after subtraction from the weight of the filter paper, the dry weight of AS in the initial specific volume are determined. Calculation of the dry weight in 1 L of the mixture results in activated sludge MLSS in $g.L^{-1}$ (Baird et al., 2017).

Photography Conditions and Taking Images

It is essential that all images be taken in the constant conditions. In order to preserve the consistency of photography conditions, all environmental parameters such as light intensity, distance between light camera and the samples and light source location which can interfere with the quality of images must remain the same. Therefore, a box with no entrance of light from the outside and with specific dimensions for obtaining best images was designed (**Figure 1**). In order to provide the necessary light for photography, cool white LED lamps were utilized. The box height is designed in a way that the best distance for the camera to be able to focus, be provided.

The camera used in this research was (Nikon D5300, Japan) equipped with (Nikon, 18–140 mm f/3.5-5.6 VR, Japan) lens. Since using camera zoom significantly affects the focal length of the lens and the image resolution consequently, all the images are acquired with the constant zoom of 140/18. The focal length of the lens under this circumstance will be 140 mm.

The samples must be poured into appropriate dishes with minimum light absorption and refraction coefficients. Besides, the height of dishes must be negligible in comparison to the distance between camera and the sample in order to avoid the influences of liquid height on the quality of images. For this purpose, glass petri dishes (diameter = 54 mm, PIREX, United Kingdom) were used in which the light refraction is negligible due to high transparency and very low thickness. Five milliliter of the sample is poured into the petri dishes in each test using sampler. Five milliliter was the minimum amount that could completely cover the surface of petri-dish with negligible height. Minimizing the height of the sample is the key point, since increasing the height, increases the light absorption logarithmically during diffusion through the sample and makes images darker than their real value and decreases measurement accuracy (Durduran et al., 2010). It is also important that the sample which is being poured into the dished be well mixed to be considered as a homogenous sample of the whole culture.

Diaphragm diameter, shutter speed and ISO number are three main parameters which can noticeably influence the resolution, light and colors intensities in the images (Radulescu and Vladareanu, 2017).

In order to keep the photography conditions constant during the tests, parameters of photography are set as **Table 1**. The criteria for choosing the photography conditions are totally qualitative and are based on the resolution and color intensities of the images. The logic of choosing these conditions depends on the range of MLSS changing and they will be chosen in a way that image resolution can cover the highest range of MLSS changes. It is more critical in very low and very high MLSS in which images are too bright and too dark, respectively. Therefore, the best solution is to make an estimation of the highest MLSS that may achieve during the process (about 15 $g.L^{-1}$ in this research) and set the imaging conditions in this MLSS in a way that RGB analysis is possible and the image is not completely black. Then, the settings will be adjusted for MLSS $\leq$ 1 $g.L^{-1}$ as well in order to avoid capturing too bright images which make RGB analysis infeasible and the image is completely white. Since, the criterion for evaluating the quality of images is qualitative (not quantitative) statistical analysis and design of experiments is infeasible for reducing the number of images and this innovative method based on evaluation in boundaries must be followed. However, defining a quantitative criterion for quality of images in the process of RGB analysis can be a suggestion for further studies.

TABLE 1 | Photography conditions and camera settings for taking images.

Parameter	Value
f number	5.6
Shutter time (s)	1/160
ISO	100
Zoom	140/18
Focal length (mm)	140

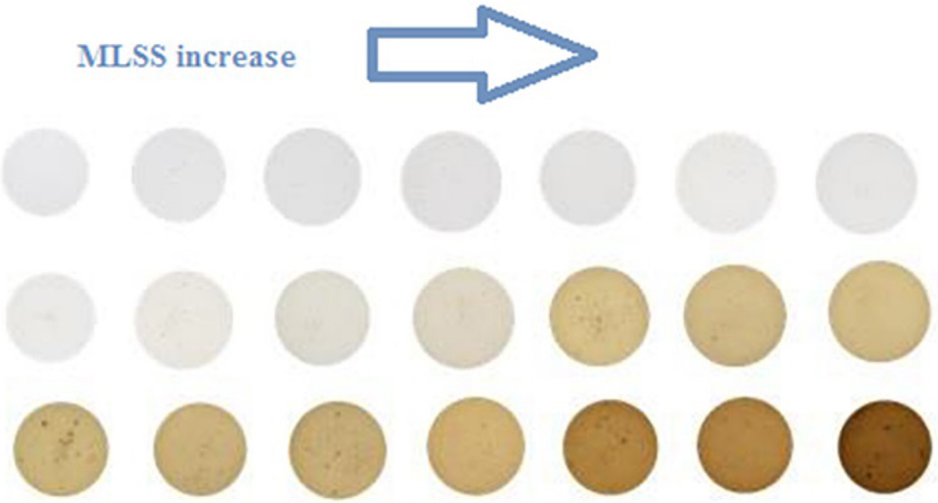

FIGURE 2 | Color changing with MLSS increase in activated sludge.

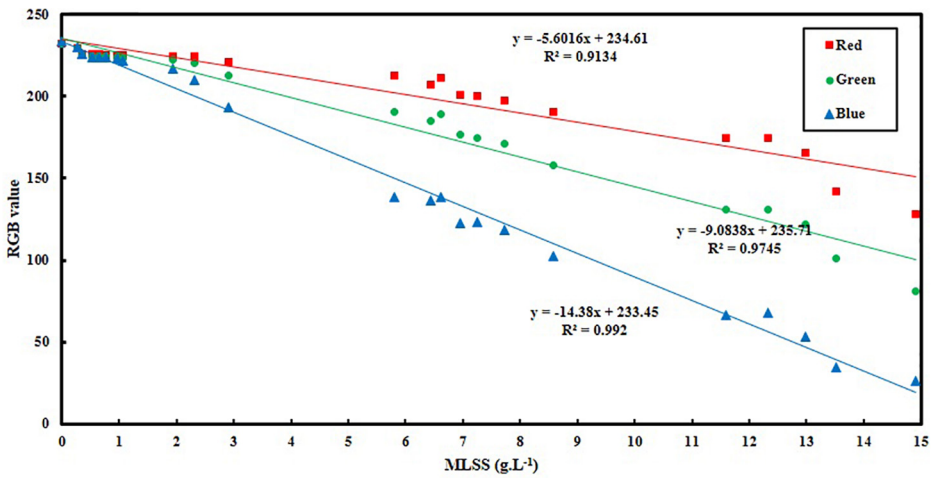

FIGURE 3 | Variation of RGB values vs. activated sludge MLSS.

In this research, the optimum conditions for acquiring the most appropriate images are obtained (**Table 1**) with 9 different images. In activated sludge applications, since 15 $g.L^{-1}$ is usually the darkest concentration that can be reached, these settings can be applied to the most of other cases in which image processing is being used for MLSS measurement in activated sludge systems.

For each sample, imaging are conducted three times and the final value of RGB is considered as the average value of the RGB of all three images.

Image Processing Procedure

RGB analysis of AS means extraction of red, green and blue intensities in the images of sludge and correlate them to a quantitative parameter of the studied system such as MLSS. RGB extraction will be carried out using ImageJ® which is an open-source software for image management, editing and processing (Schneider et al., 2012). In RGB model, a three-vector coordination for each pixel of the image will be defined based on R, G and B which shows the color intensity of the pixel. Each color is defined as an 8-bit data package and considering three vectors of R, G and B for each color, $8^3 = 256$ different numbers for all of the colors existing in an image are designated. Therefore, RGB numbers are in the range between 0 and 255 where (0,0,0) and (255,255,255) are black and white respectively (Kelda and Kaur, 2014). However, dealing with three-parameter space of RGB is not always simple and it is usually more desirable to work in a single-parameter space. Grayscale is a conversion which is commonly used for changing RGB space to a single-parameter space (Bala and Braun, 2003).

There are various equations and procedures for converting RGB space to grayscale which has been used based on the application in which image processing is used.

TABLE 2 | MLSS and RGB data in this study.

MLSS (g.L^{-1})	R	G	B
0	232.08	232.09	233.6
0.263	229.51	229.35	229.71
0.34	225.81	225.51	225.66
0.527	225.85	224.62	223.85
0.644	225.58	224.5	223.7
0.772	225.4	224.41	223.49
0.966	225.03	224.11	223.001
1.053	224.97	223.36	221.49
1.931	224.46	222.18	216.78
2.318	224.26	220.21	210.13
2.897	221.07	212.37	193.21
5.795	212.44	190.33	138.33
6.623	211.21	188.84	138.42
6.439	207.118	184.67	136.23
6.954	200.72	176.9	122.58
7.243	200.35	174.85	123.05
7.726	197.4	170.91	118.35
8.585	190.2	157.97	102.74
11.59	174.36	130.76	66.12
12.33	174.56	131.07	67.7
12.98	165.33	121.65	53.14
13.52	142.19	101.2	34.193
14.901	128.15	81.26	26.2

TABLE 3 | Grayscale conversion coefficients for activated sludge MLSS.

Coefficient	Value
M_R	−5.3117
M_G	−8.9099
M_B	−14.404
K_R	0.185
K_G	0.311
K_B	0.503

Córdoba-Matson et al. (2010) have proposed a new approach for grayscale conversion in order to determine the cell numbers in microalgae cultures by image processing. In this approach, Eqs 1–4 are used to convert the color image to grayscale:

$$\text{Grayscale} = K_R R + K_G G + K_B B \quad (1)$$

K_R, K_G, and K_B are gray coefficients for red, green and blue respectively which are calculated as following:

$$K_R = M_R/(M_R + M_G + M_B) \quad (2)$$

$$K_G = M_G/(M_R + M_G + M_B) \quad (3)$$

$$K_B = M_B/(M_R + M_G + M_B) \quad (4)$$

where M_R, M_G, and M_B are the slopes of linear fitting of R, G, and B values vs. desired parameter (MLSS in this case).

RESULTS AND DISCUSSION

Figure 2 shows the color variation with increase in MLSS in activated sludge. It helps the reader to have a better understanding about the results of RGB analysis and trends in **Figure 3**. In other words, **Figure 2** is the realization of **Figure 3** for generating a visual image about what is going on in reality with changing RGB. Moreover, it is obvious from **Figure 2** that the color of the culture noticeably changes with MLSS and it proves that RGB analysis can be an appropriate technique for studying activated sludge MLSS variation. It can be seen in **Figure 2** that the samples get darker with increase in MLSS. Therefore, it is expected that with MLSS growth, RGB values decrease consequently.

Figure 3 and **Table 2** show the variation of RGB values with MLSS in AS. RGB acquisition has been carried out in 21 different samples with different MLSS. Each sample was photographed three times and RGB data of each sample is the average of the RGB data of these three images. Totally, 63 images were taken and processed whose results are provided in **Figure 3**.

It can be concluded from **Figure 3** that B is the best vector for MLSS estimation in AS systems which shows R^2 = 0.99. Since, blue color is located at the end of electromagnetic spectra and very close to UV region, its absorption coefficient is higher in comparison to green and red and its variation is more intensive consequently. Therefore, when the range of variation of MLSS in AS mixture gets wider (0–15 g.L^{-1}), B will be fitted more accurately for studying the system. This range of MLSS is the most applicable is AS systems. Conventional activated sludge systems cannot operate efficiently in concentrations higher than 5 g.L^{-1} and their operational MLSS lies between 1 and 5 g.L^{-1} with optimal value of 3–4 g.L^{-1}. On the other hand, membrane bioreactors (MBRs) are usually operated at higher concentrations (5–15 g.L^{-1}) (Sari Erkan et al., 2018). Therefore, the method is accurate enough for being applied in both conventional and MBR systems of AS.

As it is mentioned before, in order to avoid dealing with three-parameter space of RGB, grayscale conversion is usually used. According to the results of **Figure 3**, **Table 3** is obtained which shows the grayscale conversion coefficients for activated sludge MLSS based on Eqs 1–4. Linear fitting has been applied using RGB data and MLSS and the slopes are reported as M_R, M_G and M_B. Then K_R, K_G and K_B are defined using M data and according to Eqs 2–4. Replacing K data in Eq. 1 results in Eq. 5.

Using the data provided in **Table 3**, equation 1 is rewritten as equations 5 and the graph of gray tone variation with MLSS is obtained as **Figure 4**.

$$\text{Grayscale} = 0.185R + 0.311G + 0.503B \quad (5)$$

Equation 5 is the grayscale conversion equation for AS which converts the RGB image into the grayscale image.

The slope and intercept of the achieved correlation for MLSS estimation using gray tone is so similar to B and the R^2 coefficients are almost the same. Therefore, it can be concluded that choosing B as the best vector for MLSS estimation in AS systems is rational and accurate.

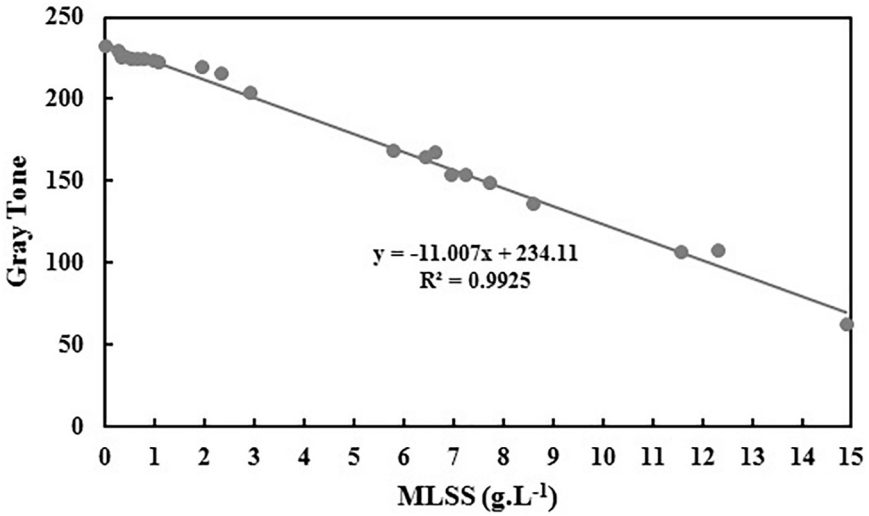

FIGURE 4 | Variation of gray tone vs. activated sludge MLSS.

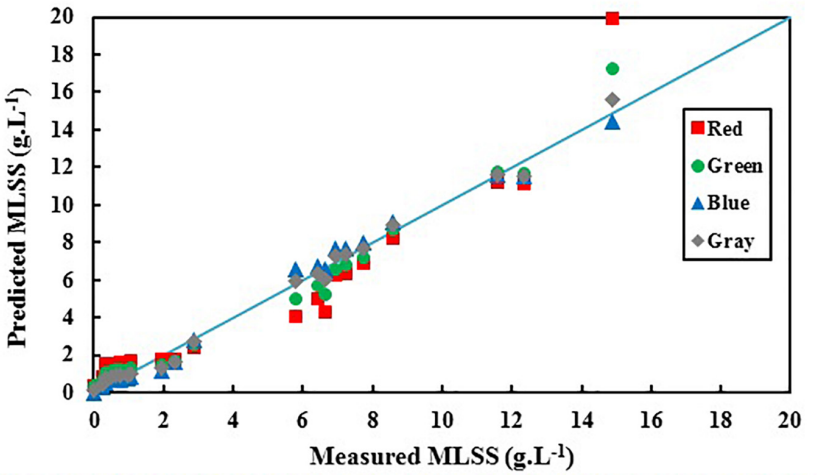

FIGURE 5 | Predicted activated sludge MLSS based on red, green, blue, and gray colors vs. actual biomass MLSS.

Figure 5 shows the deviation between predicted values of activated sludge MLSS by RGB analysis and the actual measured values.

It is obvious in **Figure 5** that predicted MLSS based on B shows the least deviation from the actual results comparing R, G and gray. **Table 4** shows the summary of the results of statistical analysis for R, G, and B in order to choose the most accurate index for activated sludge MLSS estimation.

According to the data of **Table 3**, blue index (B) shows the least errors and highest R^2 and least errors which makes it the most accurate index for activated sludge MLSS estimation which has been proposed earlier. Also, gray shows sufficient accuracy in activated sludge MLSS measurement which may come helpful considering its cumulative nature.

In the lower ranges of MLSS which are common in conventional activated sludge systems ($< 6\ g.L^{-1}$), the changes in darkness of images are not so intensive, so that G also shows the proficient accuracy in MLSS measurement, while the deviation in R accuracy increases, because G is in the middle zone of the light spectrum and is less sensitive to harsh changes. Still, B shows the higher R^2 value and confirms the claim that B is most accurate vector in all ranges of MLSS, since it shows the least deviation from the actual data (**Figure 5**) in all ranges. **Figure 6** shows variation of RGB data with MLSS in low ranges.

As it is mentioned, the image which is recorded by the camera is the result of the light which has been diffused through the AS sample and reached to the camera. In other words, the intensity of the light which is reached to the camera controls the image qualities including colors intensity. Therefore, it is predicted that within the range of biomass concentration where light absorption is negligible in comparison to light diffusion, variation of RGB values vs. MLSS be similar to variation of light intensity.

According to the theory of optical diffuse, light intensity changes exponentially with the differences in cell concentration (Ripoll et al., 2003). Hence, RGB must change exponentially with MLSS in lower amounts of cell concentration, since with increase in MLSS the culture gets more turbid and light absorption increases consequently. As a result to light absorption increase, the light scattering in the AS culture increases and deviation from the theory of optical diffuse increases subsequently. In this section, it is try to test the results of this study to see if they are in accordance with the assumptions of optical diffuse. **Figure 7** shows the exponential trend of RGB values with MLSS.

TABLE 4 | Statistical deviations of MLSS estimation based on RGB indices individually.

Index	RMSE*	MAE**	MAPE*** (%)	R^2
R	6.714	1.058	67.136	0.900
G	3.547	0.605	42.584	0.970
B	2.000	0.323	13.848	0.990
Gray	0.045	0.291	20.649	0.992

*Root mean square error. **Mean absolute error. ***Mean absolute percentage error.*

As it is shown in **Figure 7**, for the MLSS < 8 g.L^{-1}, exponential relation can accurately analyze the AS system using all three vectors of R, G and B. However, B still shows the greatest accuracy in comparison to R and G. In lower MLSS ranges (MLSS < 8 g.L^{-1}), the diffuse approximation is valid for light transfer and the assumption of a logarithmic correlation between RGB data and MLSS is physically logical which is in accordance with optical diffuse assumption (Gibson and Dehghani, 2009). It also proves proficiency of B as the most appropriate vector in

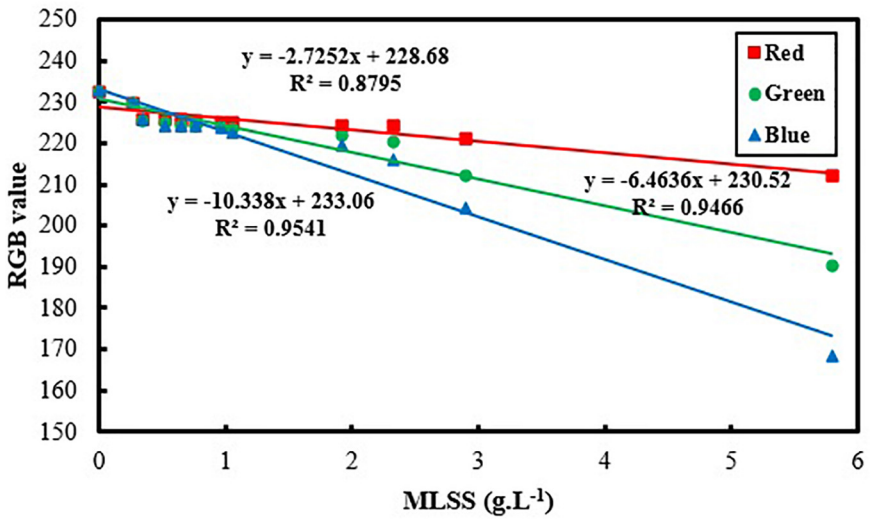

FIGURE 6 | Variation of RGB values vs. activated sludge MLSS in low ranges (MLSS < 6 g.L^{-1}).

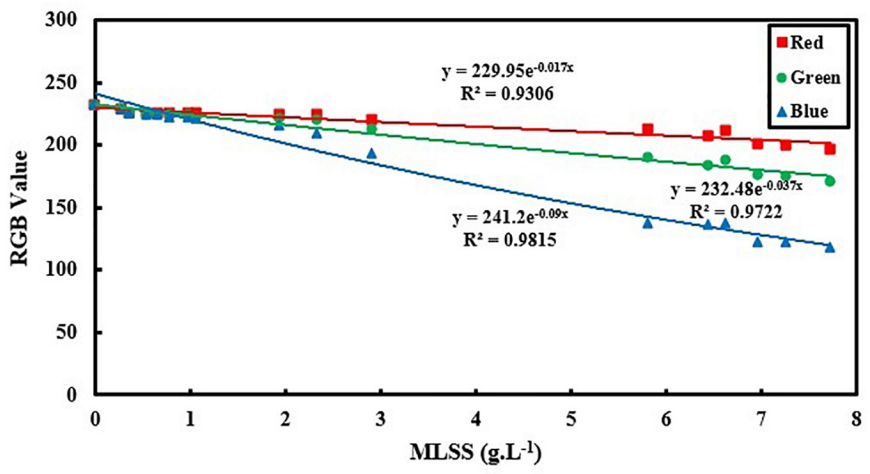

FIGURE 7 | Exponential relation between RGB values and activated sludge MLSS based on optical diffuse theory.

all ranges of MLSS. However, comparing the results of **Figure 6** with **Figure 3** reveals that the linear fitting developed in this manuscript for MLSS measurement using B is still more accurate that logarithmic fitting which is probably due to some simplifying assumptions in optical diffuse approximation which may not be applicable in activated sludge environment and reduce the accuracy of measurement.

CONCLUSION

Biomass concentration is the key parameter in activated sludge wastewater treatment systems which must be monitored during the process in order to reassure the optimum performance of treatment system. In this research, a new method is proposed for measurement of activated sludge concentration based on macroscopic imaging and RGB analysis. The method proposed in this study shows acceptable results in activated sludge quantification without needing expensive or complicated devices or skills. However, it is early stages of applying this method for online monitoring of activated sludge cultures and some considerations must be taken into account in order to not only make the method capable of online measurement but also to provide the situation of qualitative study of the system which will be the main focus of our future research. Applying this method in large industrial scales (e.g., a wastewater treatment plant) needs different pre-requisites most of which are addressed in this research such as criteria for image acquisition, choosing the most accurate vector for image analysis, fitting equation, and the statistical analysis of the method. Therefore, the results of this research are essential for applying this method. Consequently, considering the results of current study, measurement of other concentration-related parameters of activated sludge such as its settling properties by image processing and RGB analysis can be good subjects for further studies of the researchers of this field. In comparison to other methods of MLSS quantification in activated sludge systems, image processing has showed to be cheaper since there is no need to high-tech devices in this method. It has a great potential for applying online which makes it a very appropriate candidate for commercializing evaluations. Since, the process of sampling and sample preparations is almost eliminated in this method, human errors are minimized which brings acceptable accuracy for this method. Moreover, it has the capacity of combination with microscopic imaging which provides the capability of simultaneous qualitative and quantitative study of activated sludge systems and can be a subject to further studies in this field.

DATA AVAILABILITY STATEMENT

The authors confirm that all data supporting the findings of this study are available within the article.

AUTHOR CONTRIBUTIONS

HA: experiments, data analysis, data validation, software application, and writing – original draft. M-HS: conceptualization, supervision, project administration, and writing – reviewing and editing. Both authors contributed to the article and approved the submitted version.

REFERENCES

Abushaban, A., Salinas-Rodriguez, S. G., Mangal, M. N., Mondal, S., Goueli, S. A., Knezev, A., et al. (2019). ATP measurement in seawater reverse osmosis systems: eliminating seawater matrix effects using a filtration-based method. *Desalination* 453, 1–9. doi: 10.1016/j.desal.2018.11.020

Acevedo, C. A., Skurtys, O., Young, M. E., Enrione, J., Pedreschi, F., and Osorio, F. (2009). A non-destructive digital imaging method to predict immobilized yeast-biomass. *LWT Food Sci. Technol.* 42, 1444–1449. doi: 10.1016/j.lwt.2009.03.013

Amaral, A., and Ferreira, E. (2005). Activated sludge monitoring of a wastewater treatment plant using image analysis and partial least squares regression. *Analyt. Chim. Acta* 544, 246–253. doi: 10.1016/j.aca.2004.12.061

Amaral, A. L., Mesquita, D. P., and Ferreira, E. C. (2013). Automatic identification of activated sludge disturbances and assessment of operational parameters. *Chemosphere* 91, 705–710. doi: 10.1016/j.chemosphere.2012.12.066

Baird, R. B., Eaton, A. D., Rice, E. W., and Bridgewater, L. (2017). *Standard Methods for the Examination of Water and Wastewater*. Washington, DC: American Public Health Association.

Bala, R., and Braun, K. M. (2003). "Color-to-grayscale conversion to maintain(discriminability)," in *Proceedings of the Color Imaging IX: Processing, Hardcopy, and Applications*, San Jose, CA.

Bobowski, J. S., and Johnson, T. (2012). Permittivity measurements of biological samples by an open-ended coaxial line. *Prog. Electromagn. Res. B* 40, 159–183. doi: 10.2528/PIERB12022906

Brown, M., Hands, C., Coello-Garcia, T., Sani, B., Ott, A., Smith, S., et al. (2019). A flow cytometry method for bacterial quantification and biomass estimates in activated sludge. *J. Microbiol. Methods* 160, 73–83. doi: 10.1016/j.mimet.2019.03.022

Cano, G., Mouahid, A., Carretier, E., and Moulin, P. (2014). Biomass concentration by density measurement: activated sludge and membrane bioreactor. *J. Water Sustain.* 4:49.

Córdoba-Matson, M. V., Gutiérrez, J., and Porta-Gándara, M. Á (2010). Evaluation of Isochrysis galbana (clone T-ISO) cell numbers by digital image analysis of color intensity. *J. Appl. Phycol.* 22, 427–434. doi: 10.1007/s10811-009-9475-0

Durduran, T., Choe, R., Baker, W. B., and Yodh, A. G. (2010). Diffuse optics for tissue monitoring and tomography. *Rep. Prog. Phys.* 73:076701. doi: 10.1088/0034-4885/73/7/076701

Elvira, L., Vera, P., Cañadas, F. J., Shukla, S. K., and Montero, F. (2016). Concentration measurement of yeast suspensions using high frequency ultrasound backscattering. *Ultrasonics* 64, 151–161. doi: 10.1016/j.ultras.2015.08.009

Expósito, P. L., Suárez, A. B., and Álvarez, C. N. (2017). Laser reflectance measurement for the online monitoring of *Chlorella sorokiniana* biomass concentration. *J. biotechnol.* 243, 10–15. doi: 10.1016/j.jbiotec.2016.12.020

Frasier, I., Noellemeyer, E., Fernández, R., and Quiroga, A. (2016). Direct field method for root biomass quantification in agroecosystems. *MethodsX* 3, 513–519. doi: 10.1016/j.mex.2016.08.002

Garakani, A. K., Mostoufi, N., Sadeghi, F., Hosseinzadeh, M., Fatourechi, H., Sarrafzadeh, M., et al. (2011). Comparison between different models for rheological characterization of activated sludge. *Iran. J. Environ. Health Sci. Eng.* 8:255.

Garcia-Ochoa, F., Gomez, E., Santos, V. E., and Merchuk, J. C. (2010). Oxygen uptake rate in microbial processes: an overview. *Biochem. Eng. J.* 49, 289–307. doi: 10.1016/j.bej.2010.01.011

Gernaey, A. K., Petersen, B., Ottoy, J.-P., and Vanrolleghem, P. (2001). Activated sludge monitoring with combined respirometric-titrimetric measurements. *Water Res.* 35, 1280–1294. doi: 10.1016/s0043-1354(00)00366-3

Gernaey, K. V., Van Loosdrecht, M. C., Henze, M., Lind, M., and Jørgensen, S. B. (2004). Activated sludge wastewater treatment plant modelling and simulation: state of the art. *Environ. Model. Softw.* 19, 763–783. doi: 10.1016/j.envsoft.2003.03.005

Gibson, A., and Dehghani, H. (2009). Diffuse optical imaging. *Philos. Trans. R. Soc. A* 367, 3055–3072.

Ju, F., and Zhang, T. (2015). Bacterial assembly and temporal dynamics in activated sludge of a full-scale municipal wastewater treatment plant. *ISME J.* 9:683. doi: 10.1038/ismej.2014.162

Kelda, H. K., and Kaur, P. (2014). A review: color models in image processing. *Intern. J. Comput. Technol. Appl.* 5, 319–322.

Leong, W.-H., Lim, J.-W., Lam, M.-K., Uemura, Y., Ho, C.-D., and Ho, Y.-C. (2018). Co-cultivation of activated sludge and microalgae for the simultaneous enhancements of nitrogen-rich wastewater bioremediation and lipid production. *J. Taiwa. Instit. Chem. Eng.* 87, 216–224. doi: 10.1016/j.jtice.2018.03.038

Martín-Pascual, J., Reboleiro-Rivas, P., López-López, C., Leyva-Díaz, J., Jover, M., Muñío, M., et al. (2015). Effect of the filling ratio, MLSS, hydraulic retention time, and temperature on the behavior of the hybrid biomass in a hybrid moving bed membrane bioreactor plant to treat urban wastewater. *J. Environ. Eng.* 141:04015007. doi: 10.1061/(asce)ee.1943-7870.0000939

Mesquita, D., Amaral, A., and Ferreira, E. (2011a). Characterization of activated sludge abnormalities by image analysis and chemometric techniques. *Analyt. Chim. Acta* 705, 235–242. doi: 10.1016/j.aca.2011.05.050

Mesquita, D., Amaral, A., and Ferreira, E. (2011b). Identifying different types of bulking in an activated sludge system through quantitative image analysis. *Chemosphere* 85, 643–652. doi: 10.1016/j.chemosphere.2011.07.012

Mesquita, D., Dias, O., Dias, A., Amaral, A., and Ferreira, E. (2009). Correlation between sludge settling ability and image analysis information using partial least squares. *Analyt. Chim. Acta* 642, 94–101. doi: 10.1016/j.aca.2009.03.023

Mesquita, D. P., Amaral, A. L., and Ferreira, E. C. (2013). Activated sludge characterization through microscopy: a review on quantitative image analysis and chemometric techniques. *Analyt. Chim. Acta* 802, 14–28. doi: 10.1016/j.aca.2013.09.016

Murphy, T. E., Macon, K., and Berberoglu, H. (2014). Rapid algal culture diagnostics for open ponds using multispectral image analysis. *Biotechnol. Prog.* 30, 233–240. doi: 10.1002/btpr.1843

Pajoum-Shariati, F., Sarrafzadeh, M.-H., Mehrnia, M.-R., Sarzana, G., Ghommidh, C., Grasmick, A., et al. (2014). Dielectric monitoring and respirometric activity of a high cell density activated sludge. *Environ. Technol.* 35, 425–431. doi: 10.1080/09593330.2013.831459

Radulescu, M., and Vladareanu, V. (2017). Aerial photography and the use of photo cameras attached to drones. *Sci. Res. Educ. Air Force* 1, 201–206.

Ratkovich, N., Horn, W., Helmus, F., Rosenberger, S., Naessens, W., Nopens, I., et al. (2013). Activated sludge rheology: a critical review on data collection and modelling. *Water Res.* 47, 463–482. doi: 10.1016/j.watres.2012.11.021

Rezaee, S., Sarrafzadeh, M.-H., Mehrnia, M.-R., Mohammadi, A.-R., and Pajoum-Shariati, F. (2015). Determination of ozone adsorption in activated sludge system and its effect on sludge properties. *Desalin. Water Treat.* 54, 3575–3581. doi: 10.1080/19443994.2014.923203

Ripoll, J., Schulz, R. B., and Ntziachristos, V. (2003). Free-space propagation of diffuse light: theory and experiments. *Phys. Rev. Lett.* 91:103901.

Rodriguez-Molares, A., Howard, C., and Zander, A. (2014). Determination of biomass concentration by measurement of ultrasonic attenuation. *Appl. Acoust.* 81, 26–30. doi: 10.1016/j.apacoust.2014.02.008

Saladra, D., and Kopernik, M. (2016). Qualitative and quantitative interpretation of SEM image using digital image processing. *J. Microsc.* 264, 102–124. doi: 10.1111/jmi.12431

Sari Erkan, H., Bakaraki Turan, N., and Önkal Engin, G. (2018). "Membrane bioreactors for wastewater treatment," in *Fundamentals of Quorum Sensing, Analytical Methods and Applications in Membrane Bioreactors*, eds D. Chormey, S. Bakirdere, N. Turan, and G. Engin (Amsterdam: Elsevier Publishing Company), 151–200.

Sarrafzadeh, M., Belloy, L., Esteban, G., Navarro, J., and Ghommidh, C. (2005). Dielectric monitoring of growth and sporulation of Bacillus thuringiensis. *Biotechnol. Lett.* 27, 511–517. doi: 10.1007/s10529-005-2543-x

Sarrafzadeh, M. H., La, H.-J., Lee, J.-Y., Cho, D.-H., Shin, S.-Y., Kim, W.-J., et al. (2015a). Microalgae biomass quantification by digital image processing and RGB color analysis. *J. Appl. Phycol.* 27, 205–209. doi: 10.1007/s10811-014-0285-7

Sarrafzadeh, M. H., La, H.-J., Seo, S.-H., Asgharnejad, H., and Oh, H.-M. (2015b). Evaluation of various techniques for microalgal biomass quantification. *J. Biotechnol.* 216, 90–97. doi: 10.1016/j.jbiotec.2015.10.010

Schneider, C. A., Rasband, W. S., and Eliceiri, K. W. (2012). NIH Image to ImageJ: 25 years of image analysis. *Nat. Methods* 9:671. doi: 10.1038/nmeth.2089

Selinummi, J., Seppälä, J., Yli-Harja, O., and Puhakka, J. A. (2005). Software for quantification of labeled bacteria from digital microscope images by automated image analysis. *Biotechniques* 39, 859–863. doi: 10.2144/000112018

Shariati, F. P., Heran, M., Sarrafzadeh, M. H., Mehrnia, M. R., Sarzana, G., Ghommidh, C., et al. (2013). Biomass characterization by dielectric monitoring of viability and oxygen uptake rate measurements in a novel membrane bioreactor. *Bioresour. Technol.* 140, 357–362. doi: 10.1016/j.biortech.2013.04.099

Uyar, B. (2013). A novel non-invasive digital imaging method for continuous biomass monitoring and cell distribution mapping in photobioreactors. *J. Chem. Technol. Biotechnol.* 88, 1144–1149. doi: 10.1002/jctb.3954

Zhang, J., Hu, H., Dong, J., and Yan, Y. (2012). Concentration measurement of biomass/coal/air three-phase flow by integrating electrostatic and capacitive sensors. *Flow Measur. Instrument.* 24, 43–49. doi: 10.1016/j.flowmeasinst.2012.03.003

Conflict of Interest: The authors declare that the research was conducted in the absence of any commercial or financial relationships that could be construed as a potential conflict of interest.

NOMENCLATURE

Terminology	Abbreviation	Terminology	Abbreviation
Activated Sludge	AS	Green	G
Biological Oxygen Demand	BOD	Blue	B
Chemical Oxygen Demand	COD	Total Suspended Solids	TSS
Mixed Liquor Suspended Solids	MLSS	Sludge Volume Index	SVI
Oxygen Uptake Rate	OUR	Ultra Violet	UV
Red	R	Membrane Bioreactor	MBR

frontiers in Microbiology

ORIGINAL RESEARCH
published: 24 September 2020
doi: 10.3389/fmicb.2020.576680

Degradation and Toxicity Analysis of a Reactive Textile Diazo Dye-Direct Red 81 by Newly Isolated *Bacillus* sp. DMS2

Shivani Amin[1], Rajesh Prasad Rastogi[1†], Mukesh Ghanshyam Chaubey[2], Kunal Jain[1], Jyoti Divecha[3], Chirayu Desai[4] and Datta Madamwar[1,4*]*

[1] Post-Graduate Department of Biosciences, UGC-Centre of Advanced Study, Sardar Patel University, Satellite Campus, Bakrol, India, [2] Department of Biotechnology, Shree A. N. Patel PG Institute of Science and Research, Sardar Patel University, Anand, India, [3] Department of Statistics, Sardar Patel University, Vallabh Vidyanagar, India, [4] P.D. Patel Institute of Applied Sciences, Charotar University of Science and Technology (CHARUSAT), Changa, India

OPEN ACCESS

Edited by:
Sanjay Prabhu Govindwar, Shivaji University, India

Reviewed by:
Ganesh Dattatraya Saratale, Dongguk University, South Korea
Rahul Khandare, Amity Institute of Biotechnology, Amity University, India

***Correspondence:**
Datta Madamwar
datta_madamwar@yahoo.com
Rajesh Prasad Rastogi
raj_rastogi@rediffmail.com

†Present address:
Rajesh Prasad Rastogi, Ministry of Environment, Forests and Climate Change, New Delhi, India

Specialty section:
This article was submitted to Microbiotechnology, a section of the journal Frontiers in Microbiology

Received: *26 June 2020*
Accepted: *25 August 2020*
Published: *24 September 2020*

Citation:
Amin S, Rastogi RP, Chaubey MG, Jain K, Divecha J, Desai C and Madamwar D (2020) Degradation and Toxicity Analysis of a Reactive Textile Diazo Dye-Direct Red 81 by Newly Isolated Bacillus sp. DMS2. Front. Microbiol. 11:576680. doi: 10.3389/fmicb.2020.576680

An efficient diazo dye degrading bacterial strain, *Bacillus* sp. DMS2 was isolated from a long-term textile dye polluted environment. The strain was assessed for its innate ability to completely degrade and detoxify Direct Red 81 (DR81) textile dye under microaerophilic conditions. The degradation ability of strain showed significant results on optimizing the nutritional and environmental parameters. Based on statistical models, maximum efficiency of decolorization achieved within 24 h for 100 mg/l of dye supplemented with glucose (0.02%), $MgSO_4$ (0.002%) and urea (0.5%) at 30°C and pH (7.0). Moreover, a significant catabolic induction of a laccase and azoreductase suggested its vital role in degrading DR81 into three distinct metabolites (intermediates) as by-products. Further, toxicity analysis of intermediates were performed using seeds of common edible plants, aquatic plant (phytotoxicity) and the nematode model (animal toxicity), which confirmed the non-toxic nature of intermediates. Thus, the inclusive study of DMS2 showed promising efficiency in bioremediation approach for treating industrial effluents.

Keywords: Direct Red 81, toxicity, *Caenorhabditis elegans*, *Lemna minor*, biodegradation, response surface methodology

INTRODUCTION

Azo dyes (R_1-N=N-R_2) are well known industrially synthesized organic compounds. The chemical structure of these dyes are easy to incorporate or replace its functional group, which make them highly versatile and stable in the environment (Balapure et al., 2014). During processing, textile and dyeing industries uses huge amount of water and such type of effluent contains about 10–40% of unused dyestuff which upon released into the environment causes serious pollution problem (Sahasrabudhe et al., 2014). Continuous disposal of such toxic dyestuff into the water bodies increases the organic load of natural reservoirs, which in turn leads to the negative impact on aquatic or terrestrial environments and its ecological functions (Saratale et al., 2015). Thus, it becomes essential to eliminate these compounds before it gets released into the environment (Das and Mishra, 2017).

Several conventional methods for treatment of textile dye effluents and polluted sites have been applied to date with limited success, alternatively microbial treatment methods are cost-effective and environmental-friendly (Agrawal et al., 2014; Govindwar et al., 2014). Microorganisms from contaminated environment adapt and modify themselves for the degradation of xenobiotic compounds exhibiting the prodigious catabolic activity toward the polluted environment (Hsueh et al., 2017). Therefore, the indigenous microorganisms are more favorably used for the development of bioremediation strategies. Many algae, fungi, actinomycetes and bacteria have been reported for decolorization and degradation of the azo dyes, among which bacterial cultures are economically favorable and shows promising results for the elimination of textile azo dyes effluents (Tan et al., 2013; Balapure et al., 2014; Kurade et al., 2016).

Biodegradation or decolorization efficiency depends on establishing the type of community adaption and providing the proper environment for the growth and activity of the enriched culture. Generally, reduction of azo compound occurs into the two phases; in first phase azo bond breaks by liberating the aromatic amine, which is comparatively more toxic than the parent dye (Balapure et al., 2014). While in the second phase, the mineralization of such aromatic compounds has been observed (Jayapal et al., 2018). Hence, to understand the feasibility of the bioremediation strategy in real-field applications, it is necessary to measure the toxicity of the metabolites produced after dye decolorization (Govindwar et al., 2014).

Direct Red 81 (DR81) is a diazo compound, having hydrophilic properties. Upon reduction of azo bonds under anaerobic or reducing environment, the corresponding aromatic compound may exert cytotoxic or genotoxic effect on microbial and human cells (Sahasrabudhe et al., 2014). In the present study, DR81 degrading pure culture of *Bacillus* sp. DMS2 was isolated from long-term azo dye polluted sites. To enhance the efficiency and understand the effect of one factor on another, the Plackett-Burman and response surface method (RSM) was performed for the optimization of nutritional and environmental parameters. The degradation pattern of DR81 was observed by enzymatic estimation and metabolic profiling using various analytical methods such as FTIR, LC-MS, NMR and UV-visible spectroscopy. To understand the efficacy of DMS2 and its potential in detoxification of textile dyes, toxicity assays were implemented using nematode and seed germination models.

MATERIALS AND METHODS

Chemicals and Dye Stuff

Diazo sulfonated DR81 (CAS No.: 2610-11-9; Disodium 7-benzamido-4-hydroxy-3-[[4-[(4-sulphonatophenyl)azo] phenyl]azo] naphthalene-2-sulfonate) and other structurally different dyes were purchased from the local textile industry, Amardeep Dye industries, Vatva, Ahmedabad, Gujarat, India. All other chemicals used were of analytical grade purchased from Sigma (St. Louis, MO, United States), HiMedia, Merck and SRL (India).

Bacterial Enrichment and Culture Conditions

Soil sediment was collected from Vapi industrial disposal site (20°22′N 72°54′E), Gujarat, India. Different dilutions of 10% soil sediment were plated on Bushnell Hass minimal medium amended with Glucose (2 g/l) and Beef extract (2 g/l) (BGB medium) along with DR81 (100 mg/l) at 37°C. Bacterial isolates with clear zone around colonies were screened for their dye decolorization ability. The strain with high decolorization capacity was used for azo-reduction analysis. The isolate was continuously sub-cultured into the fresh BGB medium amended with DR81 dye (100 mg/l) under microaerophilic condition and further maintained in BGB medium at 4°C.

Identification and Phylogenetic Analysis of Bacterial Culture

The 16S rRNA gene sequence analysis was performed for the identification of strain DMS2. The bacterial culture was allowed to grow for 24 h. Genomic DNA of strain DMS2 was extracted using the previously described protocol (Ausubel et al., 1997). Universal primer 8F and 1492R were used for the 16S rRNA gene amplification. A 1.5 kb PCR amplicon product was purified and sequenced using automated DNA analyzer 3500 using BigDye^{TM} Terminator Cycle Sequencing v3.1 chemistry (Life Technologies, United States). Phylogenetic analysis was performed using MEGA 4.0 software (Shah et al., 2016).

Azo-Reduction Experiment

Bacterium was grown in BGB (100 ml) medium amended with DR81 (100 mg/l) at 35°C for 24 h. Three milliliter of grown *Bacillus* sp. DMS2 was harvested at 7000 × g for 10 min at 4°C. The cell mass obtained were resuspended in sterile 1 ml distilled water and used as inoculum for further experiments, such as nutrient optimization study (by statistical model, as described in following sections), effect of various environmental conditions (NaCl concentration (0–100 g/l); DR81 concentration (100–2000 mg/l), 30 structurally different dyes as described above (100 mg/l each) on dye decolourization and degradation process under microaerophilic conditions at 35°C. The azo-reduction (decolourization) of DR81 was spectrophotometrically measured at 514 nm (Double Beam Specord® 210 BU UV-Vis spectrophotometer, Analytical Jena AG, Germany). The abiotic control consists of uninoculated media containing 100 mg/l DR81. All the experiments were performed in triplicates.

The azo-reduction efficiency was calculated using an Equation 1 (Liu et al., 2017).

$$\% \text{ decolorization} = (I\text{-}F)/I \times 100 \quad (1)$$

where, I and F represent the absorbance at initial (I) and final (F) experiment, respectively.

Statistical Designs for the Dye Decolorization

Media optimization for dye decolorization by DMS2 was carried out using the statistical design of experiments in two steps. In the first step, manageable set of variables were screened out

by Plackett-Burman design and in the second step significant variables were optimized by employing central composite design (CCD). MINITAB v16 (Minitab Inc., State College, PA, United States) software was used for designing and analysis of the experiments.

Plackett-Burman Design

Total twenty medium components including carbon sources, organic-inorganic nitrogen sources, buffering agent and minerals were evaluated at higher concentration (+) and lower concentration (−) for dye decolorization (**Supplementary Table S1**). With respect to their main effects, Plackett-Burman design of 24 variables was selected for twenty media components with three dummy variables (**Supplementary Table S2**) and the dye decolorization response was measured (Plackett and Burman, 1946). The incorporation of dummy variables in an experiment is needed to estimate the experimental error. Highest positive influence showing variables from the Pareto chart analysis were considered to have a greatest impact on dye decolorization.

Central Composite Design (CCD) for Maximum Decolorization

Synchronizing the interaction between variables (statistical approach) may provide idea about the most favorable condition for the dye decolorization. Response surface methodology is a statistical approach used to design the experiments and evaluating the effect of variables by searching the optimum condition for specific responses. Here, CCD was performed for the maximum dye decolorization using MINITAB software. Significant and highly positive independent variables (five) from the Plackett–Burman experiment were selected for further optimization. Five individual variables i.e., $MgSO_4$ (X1), glucose (X2), urea (X3), pH (X4) and temperature (X5) were selected for optimization. Combined effect of variables was studied (**Supplementary Table S3**). As per five factor design, *Bacillus* sp. DMS2 was observed for dye decolorization after 24 h of incubation. The independent variables were coded using Equation 2.

$$xi = (Xi\text{-}Xo)/\Delta Xi \quad (2)$$

Here, Xi-variables: Xo-midpoint of Xi; ΔXi-change in Xi; and xi-code value of Xi; i = 1, 2, 3, 4 variables.

In this experiment, each constituent were considered with five levels, among which maximum values were coded as + 2 and the center point as zero. Forty-two combinations of five level and five center point replicate runs were performed. Here, central points were replicated to check the non-linear relationship between variables (**Table 1**).

The optimal point can be predicted by understanding the relationship between individual variables (X1–X5 and Y-dye decolorization) using an Equation 3.

$$Y = \beta o + \Sigma \beta iXi + \Sigma \beta ijXi2 + \Sigma \beta ijXiXj \quad (3)$$

Here, Y-predicted dye decolorization; βo, βi, βii, βij-fixed regression coefficients of the model; Xi and Xj (i = 1, 2, 3, 4 and 5, $i \neq j$, $i < j$ = 1, 2, 3, 4, 5, 6) represent independent variables.

TABLE 1 | Estimated regression coefficients for percent decolorization.

Term	Coef SE	Coef	*T*	*P*
Constant	0.8162	3.329	0.245	0.808
$MgSO_4$ (%)	1.1169	2.567	0.435	0.667
Glucose (%)	22.0557	2.567	8.591	0.000
Urea (%)	−1.7576	2.567	−0.685	0.500
pH	4.3434	2.541	1.709	0.099
Temperature	−49.5491	2.614	−18.956	0.000
$MgSO_4$ (%)*$MgSO_4$ (%)	54.1225	5.806	9.322	0.000
Glucose (%)*Glucose (%)	29.3170	5.806	5.049	0.000
Urea (%)*Urea (%)	13.2448	5.806	2.281	0.031
pH*pH	13.6402	5.264	2.591	0.015
Tem.*Tem.	56.5538	5.856	9.657	0.000
$MgSO_4$ (%)*Glucose (%)	4.1571	5.387	0.772	0.447
$MgSO_4$ (%)*Urea (%)	−4.8686	5.387	−0.904	0.374
$MgSO_4$ (%)*pH	6.3523	4.818	1.318	0.199
$MgSO_4$ (%)*Tem.	−3.2979	5.507	−0.599	0.554
Glucose (%)*Urea (%)	7.2733	5.387	1.350	0.189
Glucose (%)*pH	−0.1040	4.818	−0.022	0.983
Glucose (%)*Tem.	−30.2152	5.507	−5.487	0.000
Urea (%)*pH	−12.6753	4.818	−2.631	0.014
Urea (%)*Tem.	10.4294	5.507	1.894	0.069
pH*Tem.	3.8082	4.925	0.773	0.446

Azo-Reduction in the Presence of Other Stress Compounds

DMS2 was studied for the azo-reduction in the presence of different NaCl concentration (0–100 g/l), initial dye concentration (50–2000 mg/l) and thirty structurally different dyes under optimized conditions.

Enzymes Responsible for the Dye Decolorization

At regular time interval of azo-reduction, cell-mass was harvested by centrifuging at 8,000 × *g* for 15 min at 4°C. Cell free extract of DMS2 were prepared using previously published protocol (Balapure et al., 2014). Cell free lysate was further analyzed for the production of different enzymes like laccase, azo-reductase, NADH-DCIP reductase, tyrosinase and lignin peroxidase.

Laccase production was assessed as described in previous study (Hatvani and Mécs, 2001). Azo-reduction was performed by measuring the decrease in the absorbance of DR81 at 514 nm (Zimmermann et al., 1982). NADPH-DCIP, Tyrosinase and lignin peroxidase activity were estimated by using the previously reported protocols (Meng et al., 2012). The specific unit activity of the enzyme was defined as a change in absorbance/min/mg of enzyme protein under ambient conditions. Total protein was estimated by Folin-Lowry method (Lowry et al., 1951). All the experiments were performed in triplicates (n = 3).

Azo-Reduction Pathway Analysis

DMS2 was allowed to grow in presence of DR81 (100 mg/l) in the optimized medium (Urea, Glucose and $MgSO_4$) under

microaerophilic condition at 30°C. Cell free supernatant was harvested after 8, 12, 24, and 48 h and centrifuged at 8,000 × *g* for 30 min. Cell free supernatant were concentrated using Rota evaporator (Bruker, United States), operated at 40°C and 100 rpm speed with 30 Pa of pressure. These concentrated metabolites were used for HRLC-MS, FTIR, NMR and UV-visible analysis.

LC-MS analysis was performed using Ultra-HPLC equipped with a PDA Detector-Mass spectrometer (Agilent Technologies, United States) and a C18 reverse phase column (5 μm, 250 × 4.6 mm). Methanol:water (60:40) was used as a mobile phase with the flow rate of 1.0 ml/min. The fractions from the liquid chromatogram were further analyzed by electron spray ionization (ESI) mass spectrometry (MS) using a LCQ Fleet Ion Trap LC/MS (Thermo Scientific, United States) (Nouren et al., 2017). Concentrated metabolites were mixed with FTIR grade potassium bromide (KBr) in the ratio of 3:97 (Sample:KBr) and analyzed from 600 to 4000 cm^{-1} with 20 scan speeds using FTIR spectrophotometer (Bruker, United States). Metabolites were further analyzed using 400 MHz of ^{1}H and 100 MHz of ^{13}C Advance-II FT-NMR spectrophotometer (Bruker, United States). To understand the degradation pattern, UV-visible scan from 200 to 800 cm^{-1} was performed by using Double Beam Specord® 210 BU UV-Vis Spectrophotometer, Analytical Jena AG, Germany.

Toxicity Analysis

Phytotoxic Analysis

Phytotoxicity study was performed to understand the toxic effect of DR81 and its metabolites produced after degradation by DMS2. The seeds of *Raphanus sativus, Vigna radiata* and *Abelmoschus esculentus* were used in the phytotoxicity assays because they are the common agricultural crops (Shah et al., 2016). The seeds were allowed to germinate in the presence of dye and metabolites. Plumule length and radical length were measured after 10 days of development. Simultaneously, experiment was carried out with distilled water under ambient conditions (Balapure et al., 2014).

Furthermore, *Lemna minor* (Duck weed) a model aquatic plant was cultivated under controlled condition (22°C, humidity-50RH and provided with white light) in 24 well plates (well volume of 5 ml, well surface area of 9.62 cm^2; NUNC A/S, Denmark) with Steinberg medium (SM) (3 ml/well) provided with DR81 (100 mg/l) and metabolites (100 mg/l) (Zezulka et al., 2013). Plantlets were observed for germination, dry weight and content of photosynthetic pigments (chlorophyll-a and b). Reactive oxygen species (ROS) production was studied using a ROS sensing probe 2′,7′-Dichlorodihydrofluorescein diacetate (DCFH-DA) (Eugene, OR, United States) (Rastogi et al., 2010).

Effect of Dye and Metabolites on *Caenorhabditis elegans*

Caenorhabditis elegans N2 Bristol (Wild Type) obtained from the Caenorhabditis Genetics Center (CGC) at the University of Minnesota, Minneapolis MN, United States, which were grown at 20°C on Nematode growth medium (NGM). Experiment was carried out to study the worm synchronization and life assay of *C. elegans* seeded with *E. coli* OP50 under standard laboratory conditions and protocols (Sonani et al., 2014). The effect of dye and metabolites was confirmed on NGM plate supplemented with different concentrations ranging from 25 to 100 ppm. The number of dead worms was counted on every alternate day and the live worms were transferred to fresh NGM plates supplemented with or without metabolites and dyes of different concentrations. The mechanical stimulus and pharyngeal pumping rate were considered as substitute markers to record dead nematodes. The rhythmic convulsions of pharynx over 20 s were counted manually on 1st and 4th days to determine the rate of pharyngeal pumping (Sonani et al., 2014). To acquire the mean lifespan of treated and untreated worms, the plot of fraction survival against time (days) was constructed by taking treatment day as first day and subjected to log-rank test.

Locomotion assay was carried out under stereo-microscope by counting the number of body bends of 1st and 4th day adult worms during a 30 s interval. The altered reciprocating movement of mid-body bending in worms was defined as a body bend and experiment was performed with or without metabolites and dyes supplemented NGM with their respective concentration (Kumar et al., 2010).

Statistical Analysis

All the data other than optimization were statistically analyzed using one-way analysis of variance (ANOVA) and Tukey-Kramer multiple comparison test.

RESULTS AND DISCUSSION

Screening for Azo-Reduction

Isolation and screening of bacterial culture from polluted soil sample was carried out by culture enrichment technique using minimal medium (BGB) and DR81 (100 mg/l) as sole source of energy. Bacterial strain was selected on the basis of their ability to form larger clear zone indicating faster decolorization on DR81 containing BGB plate. Isolated bacteria was gram-positive, rod shaped, facultative anaerobic with flagella and produces white colored colonies. The 16S rRNA gene homology study revealed that bacterial strain DMS2 was closely related to the *Bacillus* sp. Hence, selected strain was identified as *Bacillus* sp. DMS2 (NCBI accession number MH201195) (**Supplementary Figure S1**).

Industrial effluents usually contain structurally diverse and different class of dyes of synthetic origin. We therefore, have examined *Bacillus* sp. DMS2 for its capability to decolorize 30 structurally different dyes. More than 90% of dye decolorization was observed with eleven different dyes among which DR81 showed highest decolorization, while 25% of other dyes showed >80% decolorization (**Figure 1**). There were only five dyes showing <30% decolorization. The dissimilar rate in dye decolourization by DMS2 can be attributed to the variation in chemical nature and structure of different dyes (Kurade et al., 2013; Pramanik and Chaudhuri, 2018). Based on the observed results, DR81 was selected as a model dye for further studies.

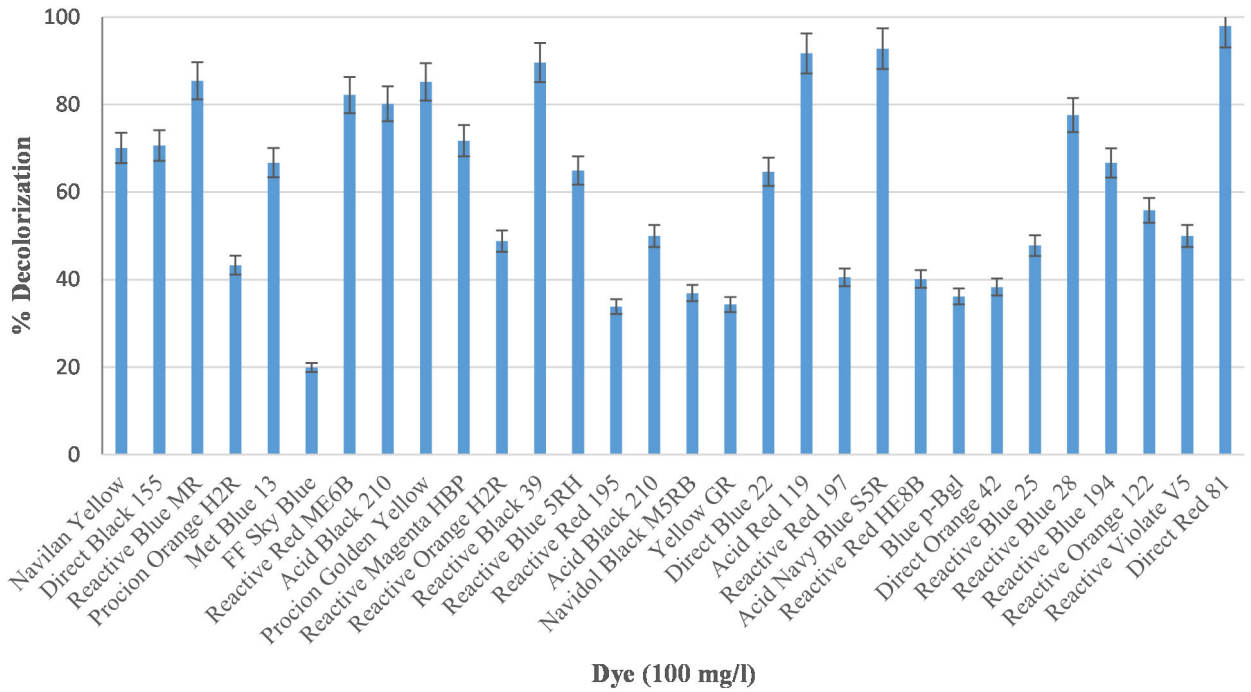

FIGURE 1 | Decolorization efficiency of *Bacillus* sp. DMS2 toward 30 different azo dyes under optimized conditions.

Optimization of Nutritional and Environmental Parameters Using Statistical Parameters

The nutrient requirement and effect of environmental parameters on dye degradation was optimized using statistical methods. Plackett-Burman Design (PBD) predicts the significantly positive variables and Response surface method (RSM) predicts the interaction and the range of the independent variables. In the present study, effect of 20 different sources like carbon, nitrogen and minerals were evaluated for the dye decolorization using PBD (**Supplementary Table S1**). Significantly positive variables were selected for further optimization (**Supplementary Figure S2**). For the Central Composite Design (CCD) approach based on Response Surface Methodology was applied to five variables i.e., $MgSO_4$, Glucose, Urea, pH and temperature. From the CCD, 47 runs with interaction of five independent variables were performed as shown in **Supplementary Table S4**. To determine the significance of the regression co-efficient with variables, student's *T*-test and *P*-values were determined, which indicates the level of significance of parameters. The *P*-value of <0.05 indicate the high significance of the parameters. ANOVA analysis of the model revealed that this second order RSM model (Equation 3) was significantly fitted ($p = 0.000$) for the dye decolorization (**Table 1**).

Using MINITAB, for each run's decolorization activity was predicted from the regression Equation 3 and accordingly experimental response was observed (**Supplementary Table S4**). ANOVA also showed that linear coefficients of glucose and urea were highly significant with the *P*-value of 0.000. The corresponding coefficient term is more significant when the magnitude of T is larger and *P*-value is smaller (Montgomery, 1991). Previous studies reported that lower the probability of Fisher value ($p = 0.000$) the higher significance for regression model (Kainthola et al., 2019). In the model, the determination coefficient $R^2 = 96.48\%$ and adjusted determination coefficient $R^2 = 93.77\%$ shows the significant performance of the model.

A graphical presentation of the model shows the interaction between the independent test variables. **Figure 2A** illustrates the relationship between glucose and $MgSO_4$ for the dye decolorization at 30°C under microaerophilic condition. Counter plot of the model shows that the decolorization activity was decreased at middle value of $MgSO_4$ with both nutritional sources (glucose and urea) and at low temperature range, decolorization increased, irrespective of pH range (**Figures 2B,C**). Hence, from the model, it has been revealed that $MgSO_4$ and temperature play a critical role in dye decolorization and organism is highly stable under alkaline or acidic conditions. Here, from this model, results suggested that interaction between glucose and pH, $MgSO_4$ and temperature, $MgSO_4$ and urea were not significant. Asserts that the decolorization efficiency of newly isolated bacterial culture *Bacillus* sp. DMS2 remain stable with wide range of pH. In a similar previous study, a dye decolorizing, pH stable *Acinetobacter* sp. and *Klebsiella* sp. was isolated from the dye contaminated wastewater (Meerbergen et al., 2018). Azo dyes contain electro-deficient functional groups like $-SO_3$, which make dye less susceptible to degradation. Hence, co-substrates along with dye (carbon and nitrogen source) are needed for the growth and decolorization (Balapure et al., 2014).

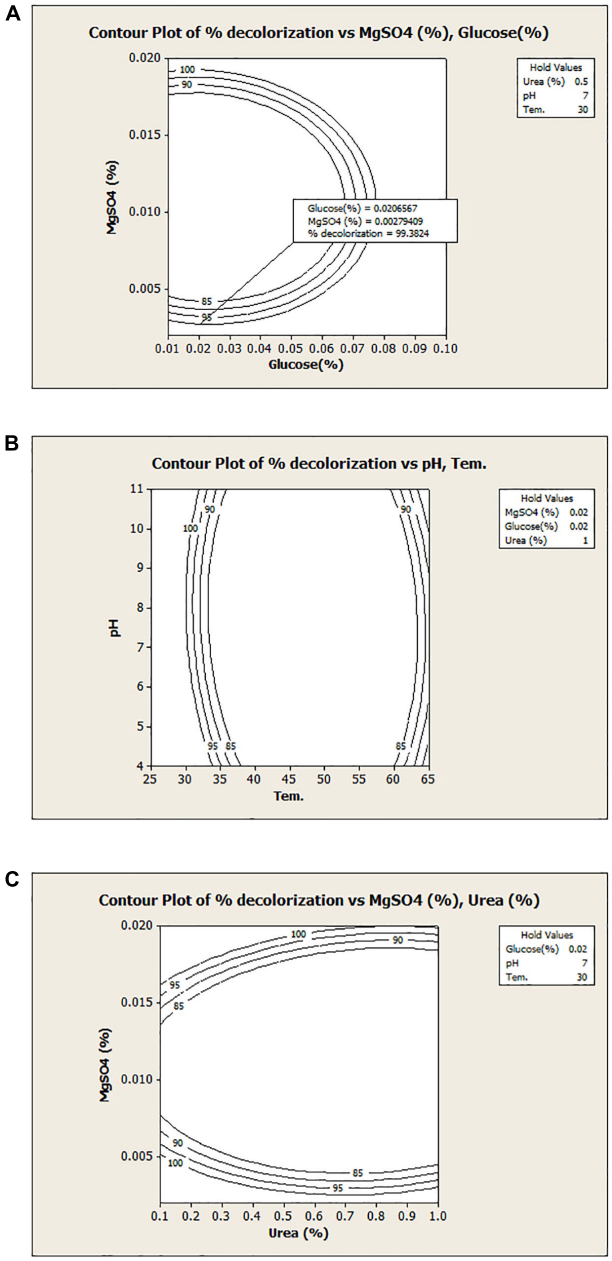

FIGURE 2 | Contour plots of the decolorization with different variables: **(A)** $MgSO_4$ *v/s* Glucose; **(B)** temperature *v/s* pH and **(C)** $MgSO_4$ *v/s* urea.

Validation of Model

To validate the model, experiment was carried out under optimized conditions i.e., Glucose (0.02%) $MgSO_4$ (0.002%), Urea (0.5%) at pH-7.0 and 30°C for 24 h under microaerophilic conditions. About 98.62% decolorization was observed under optimized conditions, while the predicted value from the model was 99.38%, which was in similar range that of experimental value. It was observed that optimization using the statistical approach has enhanced the dye decolorization capacity of *Bacillus* sp. DMS2 by nearly two-fold. After optimization, biodegradation time of DR81 decreased as compared to the initial experiment. Similarly, in another study app. 1.5 fold increase was noted in Amido black 10B decolorization after statistical optimization using *Kocuria kristinae* RC3 (Uppala et al., 2019).

Decolorization Assessment in the Presence of Other Environmental Parameters

Salts are essentially required in dye and textile industries and their effluent might contain high salt concentration (i.e., ∼2000 to 3000 ppm), which may go up-to 15–20% (Guo et al., 2020). High salt and initial dye concentration decrease the cell metabolic activity, which might reduce dye decolorization rate of the bacterium (Balapure et al., 2014). Hence, the bacterial system for dye remediation must tolerate high salt concentration (Saratale et al., 2011). **Supplementary Figure S3A** shows that *Bacillus* sp. DMS2 has a capacity to tolerate up to 50 g/l of NaCl concentration and simultaneously decolorize 97% of DR81. Previous study has shown the halophilic alkalithermophilic bacterial consortium having the capacity to tolerate up to 10% of the NaCl (Guo et al., 2020). While in this study, upon increasing NaCl concentration >50 g/l, the decolorization capacity of DMS2 significantly decreased. Similar type of results were observed previously, using *Scheffersomyces spartinae* TLHS-SF1 for decolorization of Acid Scarlet 3R (20 mg/l) with initial salt concentration 30 g/l (Tan et al., 2016).

Initial dye concentration is inversely proportional to the decolorization capacity of the organisms. The decolorization capacity of the DMS2 at different initial dye concentration was pictorially measured. DMS2 was allowed to decolorize different dye concentrations and results were captured at different time intervals as shown in **Figure 3**. The observed results showed that DMS2 has decolorized 1000 mg/l of DR81 within 24 h. While with 1500 mg/l of DR81, DMS2 required 32 h for 80%

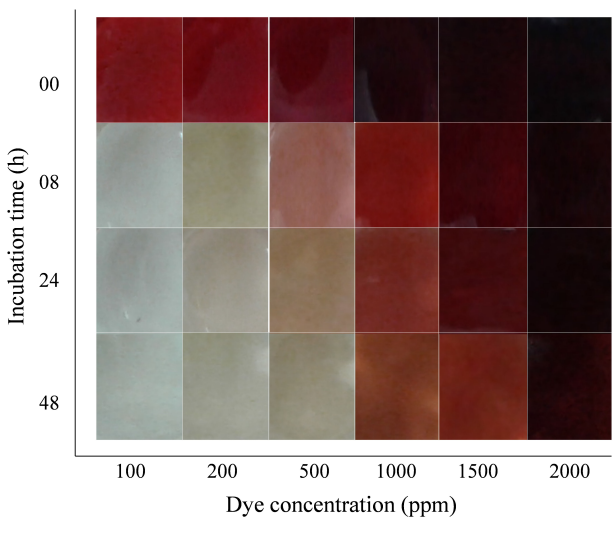

FIGURE 3 | Effect of initial dye concentration on DMS2 decolorization capacity.

decolorization (**Supplementary Figure S3B**). In our study, the decrease in efficiency was observed due to high toxicity of dye and the metabolites produced after degradation (Tan et al., 2016). Also, an earlier research described the linear increase in decolorization with initial dye concentration up to certain extent and which eventually reached the steady state due to toxicity (Guo et al., 2020).

Assessing the Catabolic Efficiency of DMS2

A number of microbial enzymes have been reported for dye decolorization and degradation processes. For the biotransformation of xenobiotic compounds, cascade of various oxido-reductive enzymes play an important role (Saratale et al., 2013). To understand the decolorization and degradation mechanism of DMS2, enzyme activity of azoreductase, laccase, NADH-DCIP, lignin peroxidase and tyrosinase were studied (Kurade et al., 2016; Liu, 2017). Azo-bonds of the dye were broken down via azoreductase enzymes and generate aromatic amines (Singh et al., 2015; Zahran et al., 2019). Consequently, these amines undergo further cleavage by the use of different oxidative enzymes, which finally enter into the central metabolic pathways. DMS2 shows the significant induction of laccase (2.32 ± 0.11) and azoreductase (0.67 ± 0.001) compared to lignin peroxidase (0.05 ± 0.001), NADH-DCIP (0.1241 ± 0.003) and tyrosinase (0.07 ± 0.000) for the complete decolorization of DR81 (**Table 2**). Profiling of the catalytic action revealed the synergistic action of oxido-reductive enzymes for the total mineralization of DR81. Similar results were reported previously in which the induction of laccase activities were observed in *Bacillus stratosphericus* SCA1007 for methyl orange mineralization (Akansha et al., 2019).

Metabolites Estimation

To unveil the decolorization and degradation profiles of DR81, UV-visible, FTIR, LC-MS, ^{13}C- and ^{1}H-NMR was performed. UV-vis spectra (300–800 nm) of the dye showed its absorption maximum at 514 nm. Decrease in absorption of the culture metabolites supernatant withdrawn at different time intervals indicated the decolorization and decrease in concentration of DR81. The complete decolorization of the dye was observed within 8 h (**Supplementary Figure S4**). Disappearance of peak obtained at 514 nm indicated a complete decolorization of the DR81 dye. The result obtained here is in agreement with previous reports (Sahasrabudhe et al., 2014; Singh et al., 2015).

The degradation pattern of DR81 was studied using FTIR at 400–4000 cm^{-1} (mid-IR region). The IR spectra of pure DR81 showed the characteristic peaks of the dye compounds, where –N=N– stretching azo group was exhibited between 1500 and 1600 cm^{-1}. The peak at 1656 cm^{-1} confirms the –C=N– stretching and –NH bending of secondary aromatic amines. The aromatic rings in the dye molecules showed characteristic peaks at 849, 714, 701, 638, and 610 cm^{-1}. The meta-substituted $–SO_3$ showed peak at 1387 cm^{-1}. The –C-H stretching of unsaturated $–CH_2$ exhibited peaks at 2959 and 2855 cm^{-1} (**Supplementary Figure S5**; Balapure et al., 2014). The ^{1}H-NMR spectrum showed the characteristic downfield signal between δ 6 and 8 and intense signal at δ 7.45 of naphthalene ring of intact dye molecule. The signal at δ 2.2 showed the presence of amide group of dye compound. The ^{13}C-NMR also showed the characteristic peaks of aromatic carbons and of other functional groups of dye molecules.

During decolorization and degradation of DR81 after 12 h, the IR spectra of the peaks of aromatic rings between 600 and 900 cm^{-1} were observed but with the lower intensity as that of intact dye compound. The specific peak at 619 cm^{-1} confirms the formation of corresponding aromatic amines. The peak at 1114 cm^{-1} indicates the overlapping of two functional group i.e., $–SO_3$ and primary $–NH_2$. While during further degradation, peaks for aromatic compounds disappeared. The peak at 1082 cm^{-1} confirmed the presence of bonded –OH group in the degraded intermediate and peak at 1656 cm^{-1} showed the –C=C– alkyl group. Asymmetrical vibration of free –S=O showed peak at 1082 cm^{-1}. Another overlapping peaks for presence of bonded –OH and primary amine showed peak at 1080 cm^{-1}. The absence of peak at 1191 cm^{-1} after 24 h indicates the complete disappearance of –S = O group. In ^{1}H-NMR and ^{13}C-NMR spectra, the intensity of peaks between δ 6–8 and δ 105–155 decreases with the progress in the degradation of DR81 (**Supplementary Figure S6**). In ^{13}C-NMR at different stages of dye degradation, peaks at δ 129 showed the presence of substituted alkenes, peaks between δ 68 and 71 showed the presence of alcohols/ethers including nitro-group in the compound $–CNO_2$. While the intermediate containing carboxylic acid group and ketone group were detected through ^{13}C-NMR. Further, LC-MS analysis also illustrates the presence of non-toxic degraded metabolite compounds of the dye.

TABLE 2 | Estimation of enzymes responsible for dye decolorization and degradation.

Enzymes	0 h	12 h	24 h	32 h	48 h
Laccase[a]	0.03 ± 0.09	0.84 ± 0.01	2.32 ± 0.11	1.79 ± 0.06	0.42 ± 0.01
Azoreductase[b]	0.01 ± 0.02	0.31 ± 0.01	0.67 ± 0.05	0.45 ± 0.02	0.19 ± 0.04
Lignin peroxidase[a]	0.04 ± 0.03	0.05 ± 0.05	0.05 ± 0.04	0.05 ± 0.06	0.05 ± 0.01
NADH-DCIP[c]	0.04 ± 0.06	0.07 ± 0.03	0.12 ± 0.03	0.08 ± 0.05	0.05 ± 0.04
Tyrosinase[a]	0.01 ± 0.06	0.06 ± 0.02	0.07 ± 0.05	0.06 ± 0.02	0.04 ± 0.03

Mean of three experiments ± SEM. Significantly difference form control cell at $p < 0.05$ and $p < 0.01$ by one way ANOVA with Turkey-Kramer comparison test. [a] Enzyme activity in unit/min/mg protein. [b] Enzyme activity in μM Methyl red reduced/min/mg protein. [c] Enzyme activity in μg DCIP reduced/min/mg protein.

Through all the spectral analysis of DR81 degraded products at different time intervals revealed that at the initial stage, catabolic activity of DMS2 showed the increased azoreductase activity which is responsible for initial cleavage of diazo bond. This toxic catalytic products where further neutralized by the increased activity of the laccase enzyme present in *Bacillus* sp. DMS2. Hence, the synergistic effect of azoreductase and laccase resulted the formation of three intermediate compounds namely, 4-Hydroxystyrene (m/z, 103), 2-Napthaleneacetic acid-6-hydroxy (m/z, 120) and N,N-Dimethylaniline N-oxide (m/z, 185). The results from above study suggested that DR81 was symmetrically cleaved by DMS2. Hence, from all spectral analysis method described above the possible degradation pathway of DR81 was deduced and is illustrated in **Supplementary Figure S7**. There are number of reports which show similar proposed pathways in bacterial system on the basis of spectral analysis (Balapure et al., 2014; Shah et al., 2016).

Toxicity Analysis

Several reports have shown that the toxicity of metabolites formed after dye degradation is comparatively higher than its parent dye compounds (Misal and Gawai, 2018; Saini et al., 2018). So, to verify the acceptance of degradation, it is important to measure the toxicity response of parent dye and its degraded products. The pollutants and degraded metabolites have highly toxic effects on aquatic and terrestrial environment; hence, we conducted phytotoxicity study on both environments. Furthermore, we also tested the toxicity of dye and metabolites on nematode model *C. elegans*.

Terrestrial Phytotoxicity

In the presence of dye DR81, the reduced germination of *V. radiata*, *R. sativus* and *A. esculentus* seeds was observed with only 30, 30, and 36% of seeds germination, respectively. After decolorization/degradation of dye, the germination extended further to more than 90% in presence of metabolites. We measured plant's photosynthesis apparatus, root length and shoot

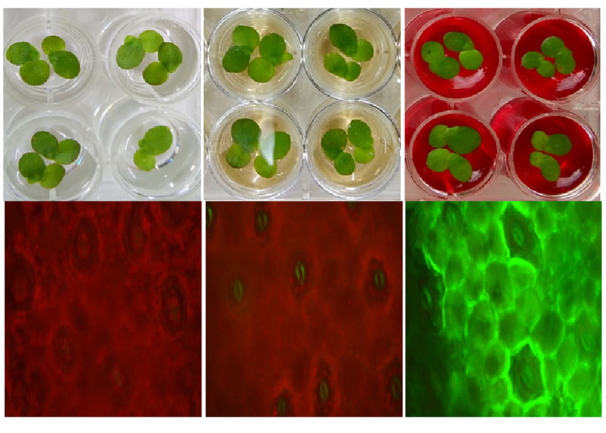

FIGURE 4 | *In vivo* ROS production in *L. minor* seed germination with **(A)** control sample; **(B)** dye degraded products and **(C)** dye.

TABLE 3 | Phytotoxicity analysis of DR81 (100 mg/l) and metabolites produced after decolorization.

	V. radiate			*R. sativus*			*A. esculentus*		
	Control	**Dye**	**Product**	**Control**	**Dye**	**Product**	**Control**	**Dye**	**Product**
Germination (%)	99.00 ± 1.00	30.00 ± 2.00	96.60 ± 1.52	99.66 ± 0.57	30.00 ± 2.64	940.0 ± 1.00	99.33 ± 1.15	36.33 ± 1.15	94.66 ± 1.52
Root length (cm)	9.18 ± 0.02	4.25 ± 0.32	8.56 ± 0.30	8.13 ± 0.20	4.13 ± 0.20	7.19 ± 0.13	12.76 ± 0.28	6.30 ± 0.26	10.33 ± 0.41
Shoot length (cm)	7.30 ± 0.26	2.16 ± 0.12	6.60 ± 0.30	8.31 ± 0.25	5.11 ± 0.08	6.15 ± 0.29	7.23 ± 0.09	2.06 ± 0.12	5.95 ± 0.10
Biomass (g)	0.30 ± 0.07	0.09 ± 0.01	0.27 ± 0.09	0.20 ± 0.03	0.07 ± 0.06	0.19 ± 0.03	0.41 ± 0.07	0.19 ± 0.02	0.39 ± 0.06
Chlorophyll-a (μ g/ml)	11.26 ± 0.37	8.14 ± 0.22	10.24 ± 0.62	12.13 ± 0.22	8.58 ± 0.52	11.41 ± 0.39	11.98 ± 0.07	8.29 ± 0.34	11.13 ± 0.13
Chlorophyll-b (μ g/ml)	4.54 ± 0.35	2.50 ± 0.39	4.12 ± 0.22	4.34 ± 0.21	2.77 ± 0.34	4.19 ± 0.22	5.10 ± 0.16	2.30 ± 0.13	4.67 ± 0.38
Carotenoids (μ g/ml)	8.49 ± 0.93	3.56 ± 0.17	8.26 ± 0.08	11.15 ± 1.78	3.72 ± 0.46	8.25 ± 0.46	10.22 ± 0.92	3.97 ± 0.31	7.09 ± 0.89

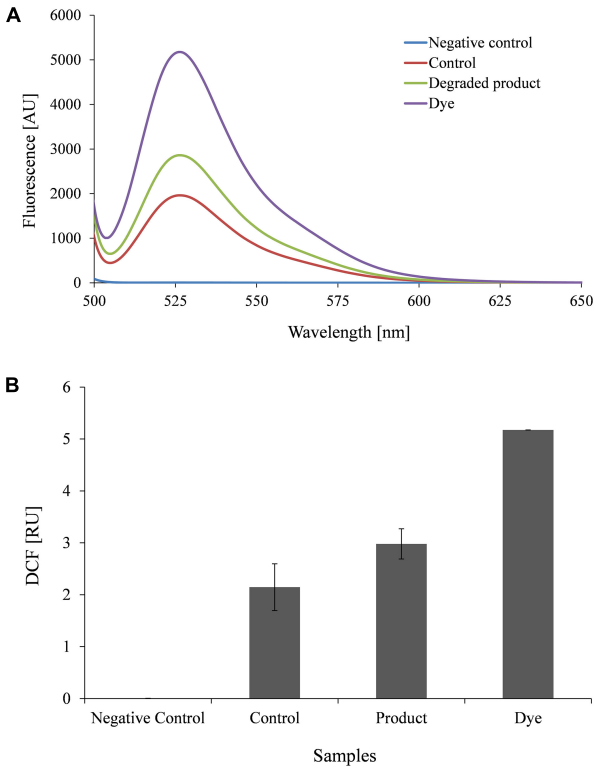

FIGURE 5 | Fluorophotometric analysis of *in vitro* ROS production in *L. minor* growing with dye and degraded dye products **(A)** Emission spectra of DCF fluorescence **(B)** DCF fluorescence intensity.

length to validate our results (**Table 3**). In comparison to dye, better growth of experimental plants was observed when grown under dye degraded products. The previous studies using *Phaseolus mungo* and *Vigna radiata* to understand the toxic effects of the dye also revealed the non-toxic nature of degraded products after decolorization (Bedekar et al., 2015; Shah et al., 2016).

Aquatic Phytotoxicity

To understand toxicity of dye and its degraded products, we conducted the aqua-phytotoxicity assay on a model aquatic plant *L. minor*. After 10 d of incubation in the presence of dye, 90% growth inhibition was measured, while only 10% of growth inhibition was observed in presence of metabolites (**Supplementary Table S5**). To validate the results, physiological parameters such as *in vivo* and *in vitro* production of ROS in was measured in *L. minor* (**Figures 4**, **5**). DCFH dye was non-fluorescent, but become highly fluorescent (green colored) when oxidized into DCF at the time of ROS production. **Figure 5** represents the *in vitro* production of ROS in *L. minor* in the presence of dye and degraded products. In comparison to control and degraded product, treated samples, maximum ROS production was observed in dye-treated samples (**Figures 4**, **5**). High production of ROS and reduction in chlorophyll level in the presence of dye was observed, indicating its toxic effects on plants of aquatic habitat (Souza et al., 2019; Sun et al., 2019).

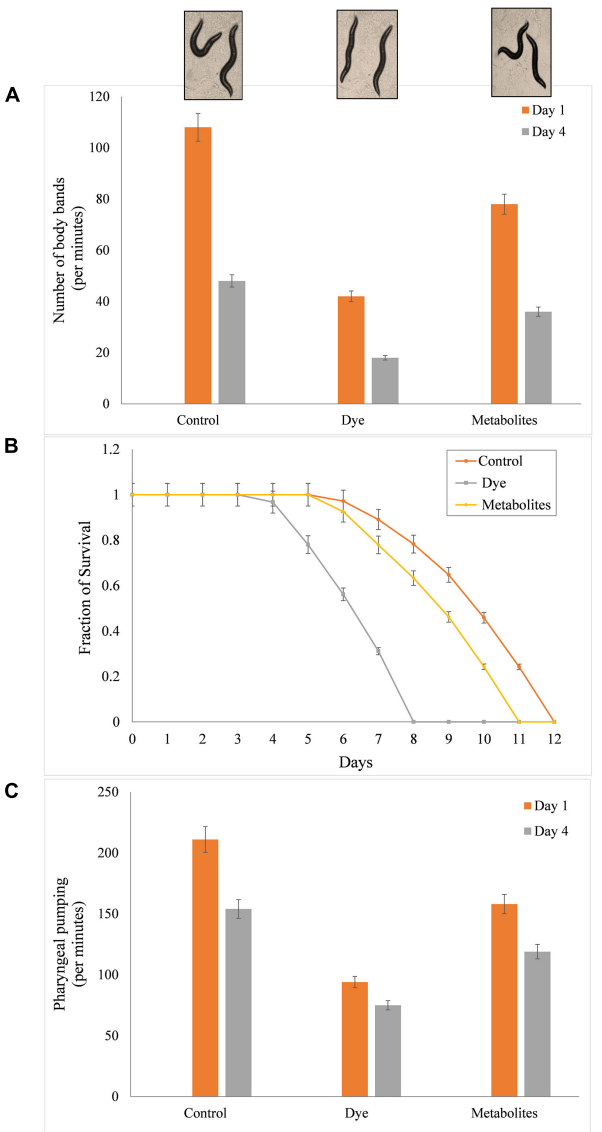

FIGURE 6 | (A) Mean survival time of *C. elegans* with dye (100 mg/l) and metabolites produced after incubation with DMS2, **(B)** Toxicity analysis on the life span of *C. elegans* and **(C)** Effect on pharyngeal pumping.

The levels of ROS and reduction of chlorophyll level was less in presence of degraded metabolites of DR81 (**Supplementary Table S5**; Karuppanapandian et al., 2011). A number of previous reports have confirmed the ROS production in plants in presence of some hazardous pollutants (Radić et al., 2018; Sun et al., 2019).

Effect of Dye on the Lifespan of *C. elegans*

The effect of dye and metabolites on lifespan of *C. elegans* was studied by growing L4 stage worms at 20°C under varying concentration (0, 25, 50, and 100 ppm) of metabolites and dye. **Figure 6** shows the culturing of worms under control (without dye), in presence of dye and product of treated sample. The mean lifespan of control nematodes was found to be 12 ± 0.1

(mean lifespan ± standard error mean) days. While, metabolites and dyes treated nematodes showed values of 11 ± 0.1 days and 8 ± 0.2 days for 50 ppm, respectively ($p > 0.05$, log-rank test) (**Figure 6B**). Metabolites treated worms showed significant increase in longevity in comparison to dye treated worms. To determine the potency of metabolite in reducing the toxic effect of dye and its effect on the longevity of worms, we counted substitute physiological indicators of aging like rate of worm locomotion and pharyngeal pumping rate in metabolites treated and dye treated worms in time course of aging (1st and 4th day of post adulthood) (**Figures 6A,C**). The rate of pharyngeal pumping for control worms were found to 199 ± 1.05/min and 145 ± 1.38/min on 1st and 4th day, whereas metabolites and dye treated worms showed the rate of pharyngeal pumping upto 158 ± 3.5 and 119 ± 2.94/min, 94 ± 3.18 and 75 ± 2.83/min, respectively (**Figure 6C**). The locomotory behavior of metabolites and dye treated worms were assayed by counting the number of body bends per minute. The number of body bends per minute were 108 ± 0.31 ($p < 0.0001$, *t*-test) and 48 ± 0.40 ($p < 0.0001$, *t*-test) for control worm on 1st and 4th days, respectively. In compared to control, metabolites treated and day treated worms showed the body bends (per minute) upto 35.4 ± 0.40 ($p < 0.0001$, *t*-test) and 25 ± 1.61 ($p < 0.0001$, *t*-test), whereas 42 ± 0.50 ($p < 0.0001$, *t*-test) and 18 ± 0.31 ($p < 0.0001$, *t*-test) on 1st day and 4th day, respectively (**Figure 6A**). Metabolites treated worms showed significant improvement in pharyngeal pumping rate and locomotory response compared to control worms. Results suggested that metabolites treated worms showed attenuation in the aging associated declining in physiological functions such as feeding and locomotion to a certain extent. Henceforth, the degraded products are less of non-toxic for the both animal and plant systems, which proves that the newly isolated organism *Bacillus* sp. DMS2 is feasible for the filed application. This study was restricted up-to the laboratory level, however, we are working on scale up and then we will go for the *in situ* application.

TECHNICAL CHALLENGES AND FUTURE RESEARCH PERSPECTIVES

The real technical challenge for this study is to apply such bioremediation strategy *in situ* field. Further, observations in this research must be studied and verified for large scale industrial applications.

CONCLUSION

There are very few reports which show a complete metabolism and toxicity reduction of the diazo dye compounds by a single bacterium. This study provides a complete understanding of the mechanism of textile diazo dye degradation by *Bacillus* sp. DMS2 along with the plausible interpretation of the dye degradation and metabolites formed after bacterial treatment. The experimental results revealed that *Bacillus* sp. DMS2 was not only effective in the decolourization of many textile dyes tested, but also simultaneously reduced the toxicity of degraded intermediates and parent dye compound under microaerophilic conditions. Results, obtained in this study indicate that the bacterium *Bacillus* sp. DMS2 can effectively decolourize and degrade the textile diazo dyes with low nutrient supplements and under ambient conditions.

Moreover, the treatment of DR81 dye by the bacterium showed significant reduction in its toxicity on plant and animal models. Therefore, *Bacillus* sp. DMS2 can be used as an efficient, cost-effective and eco-friendly bioremediation agent in bio-reactors treating textile wastewaters or for bioaugmentation of textile dye polluted soils to achieve biodegradation and reduction in toxicity of textile dyes.

DATA AVAILABILITY STATEMENT

The datasets generated for this study can be found in the *Bacillus* sp. strain DMS2 (Accession number MH201195).

AUTHOR CONTRIBUTIONS

SA performed the dye decolonization, degradation, as well as toxicity experimentation along with RR. MC performed experiments of *C. elegans*. JD helped in designing the experiments for RSM and interpreting its results. SA and KJ drafted the initial manuscript. RR and CD edited and refined the manuscript. KJ and DM provided the initial concept. SA developed the further objectives. All the authors read and approved the manuscript.

FUNDING AND ACKNOWLEDGMENTS

The authors wish to acknowledge Department of Biotechnology (DBT), Ministry of Science and Technology, New Delhi, India for financial support (BT/01/CEIB/09/V/05).

SUPPLEMENTARY MATERIAL

The Supplementary Material for this article can be found online at: https://www.frontiersin.org/articles/10.3389/fmicb.2020.576680/full#supplementary-material

FIGURE S1 | Phylogenetic analysis of *Bacillus* sp. DMS2.

FIGURE S2 | Pareto chart for the effects of variables.

FIGURE S3 | Effect of DMS2 on NaCl concentration **(A)** and initial dye concentration **(B)**.

FIGURE S4 | UV-vis overlay spectra at different interval during decolorization of DR81 by *Bacillus* sp. DMS2 under optimized conditions.

FIGURE S5 | FTIR spectrum analysis of DR81 and its products after degradation by *Bacillus* sp. DMS2 at different time interval.

FIGURE S6 | H^1-NMR spectrum of DR81 and their degraded products by DMS2 at various time interval.

FIGURE S7 | Proposed degradation pathway analysis of DR81 by consortium DMS2.

REFERENCES

Agrawal, S., Tipre, D., Patel, B., and Dave, S. (2014). Optimization of triazo Acid Black 210 dye degradation by *Providencia* sp. SRS82 and elucidation of degradation pathway. *Process Biochem.* 49, 110–119. doi: 10.1016/j.procbio.2013.10.006

Akansha, K., Chakraborty, D., and Sachan, S. G. (2019). Decolorization and degradation of methyl orange by *Bacillus stratosphericus* SCA1007. *Biocatalysis Agric. Biotechnol.* 18:101044. doi: 10.1016/j.bcab.2019.101044

Ausubel, F. M., Brent, R., Kingston, R. E., Moore, D. D., Seidman, J. A., Smith, J. G., et al. (1997). *Current Protocols in Molecular Biology*. New York, NY: John Wiley and Sons.

Balapure, K. H., Jain, K., Chattaraj, S., Bhatt, N. S., and Madamwar, D. (2014). Co-metabolic degradation of diazo dye—Reactive blue 160 by enriched mixed cultures BDN. *J. Hazard. Mater.* 279, 85–95. doi: 10.1016/j.jhazmat.2014.06.057

Bedekar, P. A., Kshirsagar, S. D., Gholave, A. R., and Govindwar, S. P. (2015). Degradation and detoxification of methylene blue dye adsorbed on water hyacinth in semi continuous anaerobic–aerobic bioreactors by novel microbial consortium-SB. *RSC Adv.* 5, 99228–99239. doi: 10.1039/C5RA17345K

Das, A., and Mishra, S. (2017). Removal of textile dye reactive green-19 using bacterial consortium: process optimization using response surface methodology and kinetics study. *J. Environ. Chem. Eng.* 5, 612–627. doi: 10.1016/j.jece.2016.10.005

Govindwar, S. P., Kurade, M. B., Tamboli, D. P., Kabra, A. N., Kim, P. J., and Waghmode, T. R. (2014). Decolorization and degradation of xenobiotic azo dye reactive yellow-84A and textile effluent by *Galactomyces geotrichum*. *Chemosphere* 109, 234–238. doi: 10.1016/j.chemosphere.2014.02.009

Guo, G., Hao, J., Tian, F., Liu, C., Ding, K., Zhang, C., et al. (2020). Decolorization of metanil yellow G by a halophilic alkalithermophilic bacterial consortium. *Bioresource Technol.* 316:123923. doi: 10.1016/j.biortech.2020.123923

Hatvani, N., and Mécs, I. (2001). Production of laccase and manganese peroxidase by *Lentinus edodes* on malt-containing by-product of the brewing process. *Process Biochem.* 37, 491–496. doi: 10.1016/s0032-9592(01)00236-9

Hsueh, C.-C., Chen, C.-T., Hsu, A.-W., Wu, C.-C., and Chen, B.-Y. (2017). Comparative assessment of azo dyes and nitroaromatic compounds reduction using indigenous dye-decolorizing bacteria. *J. Taiwan Inst. Chem. Eng.* 79, 134–140. doi: 10.1016/j.jtice.2017.04.017

Jayapal, M., Jagadeesan, H., Shanmugam, M., and Murugesan, S. (2018). Sequential anaerobic-aerobic treatment using plant microbe integrated system for degradation of azo dyes and their aromatic amines by-products. *J. Hazard. Mater.* 354, 231–243. doi: 10.1016/j.jhazmat.2018.04.050

Kainthola, J., Kalamdhad, A. S., and Goud, V. V. (2019). Optimization of methane production during anaerobic co-digestion of rice straw and hydrilla verticillata using response surface methodology. *Fuel* 235, 92–99. doi: 10.1016/j.fuel.2018.07.094

Karuppanapandian, T., Moon, J.-C., Kim, C., Manoharan, K., and Kim, W. (2011). Reactive oxygen species in plants: their generation, signal transduction, and scavenging mechanisms. *Aust. J. Crop Sci.* 5:709.

Kumar, J., Choudhary, B. C., Metpally, R., Zheng, Q., Nonet, M. L., Ramanathan, S., et al. (2010). The *Caenorhabditis elegans* Kinesin-3 motor UNC-104/KIF1A is degraded upon loss of specific binding to cargo. *PLoS Genet.* 6:e1001200. doi: 10.1371/journal.pgen.1001200

Kurade, M. B., Waghmode, T. R., Kabra, A. N., and Govindwar, S. P. (2013). Degradation of a xenobiotic textile dye, Disperse Brown 118, by *Brevibacillus laterosporus*. *Biotechnol. Lett.* 35, 1593–1598. doi: 10.1007/s10529-013-1253-z

Kurade, M. B., Waghmode, T. R., Khandare, R. V., Jeon, B.-H., and Govindwar, S. P. (2016). Biodegradation and detoxification of textile dye Disperse Red 54 by *Brevibacillus laterosporus* and determination of its metabolic fate. *J. Biosci. Bioeng.* 121, 442–449. doi: 10.1016/j.jbiosc.2015.08.014

Liu, W., Liu, C., Liu, L., You, Y., Jiang, J., Zhou, Z., et al. (2017). Simultaneous decolorization of sulfonated azo dyes and reduction of hexavalent chromium under high salt condition by a newly isolated salt-tolerant strain Bacillus circulans BWL1061. *Ecotoxicol. Environ. Safety* 141, 9–16. doi: 10.1016/j.ecoenv.2017.03.005

Liu, Y. (2017). Industrial pollution resulting in mass incidents: urban residents' behavior and conflict mitigation. *J. Clean. Prod.* 166, 1253–1264. doi: 10.1016/j.jclepro.2017.08.125

Lowry, O. H., Rosebrough, N., Farr, A., and Randall, R. (1951). Protein measurement with Folin-phenol reagent. *J. Biol. Chem.* 193, 265–275.

Meerbergen, K., Willems, K. A., Dewil, R., Van Impe, J., Appels, L., and Lievens, B. (2018). Isolation and screening of bacterial isolates from wastewater treatment plants to decolorize azo dyes. *J. Biosci. Bioeng.* 125, 448–456. doi: 10.1016/j.jbiosc.2017.11.008

Meng, X., Liu, G., Zhou, J., Fu, Q. S., and Wang, G. (2012). Azo dye decolorization by *Shewanella aquimarina* under saline conditions. *Bioresour. Technol.* 114, 95–101. doi: 10.1016/j.biortech.2012.03.003

Misal, S. A., and Gawai, K. R. (2018). Azoreductase: a key player of xenobiotic metabolism. *Bioresour. Bioprocess.* 5:17. doi: 10.1186/s40643-018-0206-8

Montgomery, D. C. (1991). Experiments with a single factor: the analysis of variance. *Des. Anal. Exp.* 7, 87–89.

Nouren, S., Bhatti, H. N., Iqbal, M., Bibi, I., Kamal, S., Sadaf, S., et al. (2017). By-product identification and phytotoxicity of biodegraded Direct Yellow 4 dye. *Chemosphere* 169, 474–484. doi: 10.1016/j.chemosphere.2016.11.080

Plackett, R. L., and Burman, J. P. (1946). The design of optimum multifactorial experiments. *Biometrika* 33:305. doi: 10.2307/2332195

Pramanik, S., and Chaudhuri, S. (2018). Laccase activity and azo dye decolorization potential of *Podoscypha elegans*. *Mycobiology* 46, 79–83. doi: 10.1080/12298093.2018.1454006

Radić, S., Medunić, G., Kuharić, Ž, Roje, V., Maldini, K., Vujčić, V., et al. (2018). The effect of hazardous pollutants from coal combustion activity: phytotoxicity assessment of aqueous soil extracts. *Chemosphere* 199, 191–200. doi: 10.1016/j.chemosphere.2018.02.008

Rastogi, R. P., Singh, S. P., Häder, D.-P., and Sinha, R. P. (2010). Detection of reactive oxygen species (ROS) by the oxidant-sensing probe 2', 7'-dichlorodihydrofluorescein diacetate in the cyanobacterium Anabaena variabilis PCC 7937. *Biochem. Biophys. Res. Commun.* 397, 603–607. doi: 10.1016/j.bbrc.2010.06.006

Sahasrabudhe, M. M., Saratale, R. G., Saratale, G. D., and Pathade, G. R. (2014). Decolorization and detoxification of sulfonated toxic diazo dye C.I. Direct Red 81 by *Enterococcus faecalis* YZ 66. *J. Environ. Health Sci. Eng.* 12:151. doi: 10.1186/s40201-014-0151-1

Saini, A., Doda, A., and Singh, B. (2018). "Recent advances in microbial remediation of textile Azo dyes," in *Phytobiont and Ecosystem Restitution*, eds V. Kumar, M. Kumar, and R. Prasad (Singapore: Springer Singapore), 45–62. doi: 10.1007/978-981-13-1187-1_3

Saratale, R. G., Gandhi, S. S., Purankar, M. V., Kurade, M. B., Govindwar, S. P., Oh, S. E., et al. (2013). Decolorization and detoxification of sulfonated azo dye C.I. Remazol Red and textile effluent by isolated *Lysinibacillus* sp. RGS. *J. Biosci. Bioeng.* 115, 658–667. doi: 10.1016/j.jbiosc.2012.12.009

Saratale, R. G., Saratale, G. D., Chang, J. S., and Govindwar, S. P. (2011). Bacterial decolorization and degradation of azo dyes: a review. *J. Taiwan Inst. Chem. Eng.* 42, 138–157. doi: 10.1016/j.jtice.2010.06.006

Saratale, R. G., Saratale, G. D., Govindwar, S. P., and Kim, D. S. (2015). Exploiting the efficacy of *Lysinibacillus* sp. RGS for decolorization and detoxification of industrial dyes, textile effluent and bioreactor studies. *J. Environ. Sci. Health Part A* 50, 176–192. doi: 10.1080/10934529.2014.975536

Shah, B., Jain, K., Jiyani, H., Mohan, V., and Madamwar, D. (2016). Microaerophilic symmetric reductive cleavage of reactive Azo Dye—remazole brilliant violet 5R by Consortium VIE6: community synergism. *Appl. Biochem. Biotechnol.* 180, 1029–1042. doi: 10.1007/s12010-016-2150-4

Singh, R. L., Singh, P. K., and Singh, R. P. (2015). Enzymatic decolorization and degradation of azo dyes – a review. *Int. Biodeterior. Biodegrad.* 104, 21–31. doi: 10.1016/j.ibiod.2015.04.027

Sonani, R. R., Singh, N. K., Awasthi, A., Prasad, B., Kumar, J., and Madamwar, D. (2014). Phycoerythrin extends life span and health span of *Caenorhabditis elegans*. *AGE* 36:9717. doi: 10.1007/s11357-014-9717-1

Souza, L. R. R., Bernardes, L. E., Barbetta, M. F. S., and da Veiga, M. A. M. S. (2019). Iron oxide nanoparticle phytotoxicity to the aquatic plant *Lemna minor*: effect on reactive oxygen species (ROS) production and chlorophyll a/chlorophyll b ratio. *Environ. Sci. Pollut. Res.* 26, 24121–24131. doi: 10.1007/s11356-019-05713-x

Sun, Y., Sun, P., Wang, C., Liao, J., Ni, J., Zhang, T., et al. (2019). Growth, physiological function, and antioxidant defense system responses of *Lemna minor* L. to decabromodiphenyl ether (BDE-209) induced phytotoxicity. *Plant Physiol. Biochem.* 139, 113–120. doi: 10.1016/j.plaphy.2019.03.018

Tan, L., He, M., Song, L., Fu, X., and Shi, S. (2016). Aerobic decolorization, degradation and detoxification of azo dyes by a newly isolated salt-tolerant yeast Scheffersomyces spartinae TLHS-SF1. *Bioresour. Technol.* 203, 287–294. doi: 10.1016/j.biortech.2015.12.058

Tan, L., Ning, S., Zhang, X., and Shi, S. (2013). Aerobic decolorization and degradation of azo dyes by growing cells of a newly isolated yeast *Candida tropicalis* TL-F1. *Bioresour. Technol.* 138, 307–313. doi: 10.1016/j.biortech.2013.03.183

Uppala, R., Sundar, K., and Muthukumaran, A. (2019). Response surface methodology mediated optimization of decolorization of azo dye amido black 10B by *Kocuria kristinae* RC3. *Int. J. Environ. Sci. Technol.* 16, 4203–4214. doi: 10.1007/s13762-018-1888-3

Zahran, S. A., Ali-Tammam, M., Hashem, A. M., Aziz, R. K., and Ali, A. E. (2019). Azoreductase activity of dye-decolorizing bacteria isolated from the human gut microbiota. *Sci. Rep.* 9:5508.

Zezulka, Š, Kummerová, M., Babula, P., and Váňová, L. (2013). *Lemna minor* exposed to fluoranthene: growth, biochemical, physiological and histochemical changes. *Aquat. Toxicol.* 140–141, 37–47. doi: 10.1016/j.aquatox.2013.05.011

Zimmermann, T., Kulla, H. G., and Leisinger, T. (1982). Properties of purified orange II azoreductase, the enzyme initiating Azo Dye degradation by *Pseudomonas* KF46. *Eur. J. Biochem.* 129, 197–203. doi: 10.1111/j.1432-1033.1982.tb07040.x

Conflict of Interest: The authors declare that the research was conducted in the absence of any commercial or financial relationships that could be construed as a potential conflict of interest.

frontiers in Microbiology

ORIGINAL RESEARCH
published: 16 October 2020
doi: 10.3389/fmicb.2020.576438

Removal of Nutrients From Anaerobically Digested Swine Wastewater Using an Intermittent Cycle Extended Aeration System

*Nguyen Hong Dan[1], Eldon R. Rene[2] and Tran Le Luu[3]**

[1]Department of Chemical Engineering, Nong Lam University, Ho Chi Minh City, Vietnam, [2]Department of Environmental Engineering and Water Technology, IHE Delft Institute for Water Education, Delft, Netherlands, [3]Master Program in Water Program Technology, Reuse and Management, Vietnamese German University, Thu Dau Mot, Vietnam

Swine wastewater contains high concentrations of organic compounds, nutrients (nitrogen and phosphorus), heavy metals, and residual antibiotics, amongst others, that have negative impacts on the water environment. The main aim of this work was to remove nutrients from anaerobically digested swine wastewater using an intermittent cycle extended aeration system (ICEAS). The effects of operational parameters such as cycle time, organic loading rate, C/N ratio, and aeration/mixing ratio on the pollutant removal efficiencies of ICEAS were studied and compared with the performance of a conventional sequencing batch reactor (SBR). The following optimal conditions were obtained: cycle time, 6 h; organic loading rate, 0.86 kg COD m^{-3} day^{-1}; C/N ratio, 2.49–2.82; and aeration/mixing ratio, 1.57. The pH was maintained in the range of 6.0–8.0. The total organic carbon (TOC), total nitrogen (TN), ammonium (NH_4^+), total phosphorus (TP), and color removal efficiencies of ICEAS were higher than those of the conventional SBR, with removal efficiencies of 95.22, 88.29, 97.69, 85.81, and 97.84%, respectively, compared to 94.34, 81.16, 94.15, 77.94, and 96.95%, respectively, observed in the SBR. TOC, TN, NH_4^+, TP, and the color removal efficiencies of ICEAS were higher by 0.88, 7.13, 3.54, 7.87, and 0.95%, respectively, than the conventional SBR. The good results from this study show that ICEAS is a promising technology for the removal of organic contaminants and nutrients from anaerobically digested swine wastewater and that the effluent water quality meets the Vietnamese discharge standard (QCVN 62-MT:2016/BTNMT) for swine wastewater effluents.

Keywords: swine wastewater, intermittent cycle extended aeration system, nutrient, biological, anaerobic

OPEN ACCESS

Edited by:
Byong-Hun Jeon,
Hanyang University, South Korea

Reviewed by:
Jiu-Qiang Xiong,
Ocean University of China, China
Shashi Kant Bhatia,
Konkuk University, South Korea
Gaurav Saxena,
Jawaharlal Nehru University, India
El-Sayed Salama,
Lanzhou University, China

****Correspondence:***
Tran Le Luu
luu.tl@vgu.edu.vn

Specialty section:
This article was submitted to Microbiotechnology, a section of the journal Frontiers in Microbiology

Received: *29 June 2020*
Accepted: *18 September 2020*
Published: *16 October 2020*

Citation:
Dan NH, Rene ER and Le Luu T (2020) Removal of Nutrients From Anaerobically Digested Swine Wastewater Using an Intermittent Cycle Extended Aeration System. Front. Microbiol. 11:576438. doi: 10.3389/fmicb.2020.576438

INTRODUCTION

The livestock sector, especially the swine industry, plays an important role in promoting agricultural development and the economy of a country (Shin et al., 2005). The swine wastewater generated from pig farms can cause a negative effect on the water environment when discharged without adequate treatment. Swine wastewater is a mixture of pig urine, floor washing water, sediment, and fecal matter (Sakar et al., 2009). It contains high concentrations of many toxic

compounds such as organic substances, nitrogen, phosphorous, and residual antibiotics (Zhou et al., 2007; Rajagopal et al., 2011; Richardson and Ternes, 2011; Li et al., 2012; Wegst-Uhrich et al., 2014; Bailey et al., 2016). Anaerobic digestion (AD) of swine wastewater can convert organic compounds to biogas and renewable energy (Sui et al., 2014). AD offers the following advantages: (i) treatment of high-strength wastewater, (ii) high conversion of chemical oxygen demand (COD) to biogas, (iii) ease of maintenance, (iv) good process control, (v) ability to tolerate fluctuating COD loads, i.e., feast and famine conditions, and (vi) good stability of the anaerobic biomass. Nevertheless, this technique produces large amounts of anaerobically digested effluent that contains nutrients, inorganic salts, organic compounds (amino acid and B vitamins), and trace/heavy metals (Fe, Cu, and Zn). This effluent, when left untreated, affects the water environment and causes problems such as the eutrophication of rivers and lakes and odor problems (Wen et al., 2016). Besides that, the emission of unpleasant smell during the anaerobic process of swine wastewater may induce air pollution that brings about adverse impacts on human health. Therefore, the development of a new technology to treat anaerobically digested swine wastewater is urgently required to satisfy the environmental discharge regulations (An et al., 2007; Daumer et al., 2007; Dosta et al., 2008).

Several physicochemical and biological technologies have been used to treat swine wastewater, namely, electrocoagulation (Mores et al., 2016), electrochemical (Huang et al., 2016, 2018) and biological methods such as anaerobic-aerobic (Aziza et al., 2019; Shoukat et al., 2019), moving bed biofilm reactor (MBBR; Yang et al., 2015), and membrane bioreactor (MBR; Guglielmi and Andreottola, 2011; Guadie et al., 2014). However, these technologies have limitations such as high initial investment cost, consumption of large quantities of chemicals, requiring large footprint, complex operation and control of parameters, and low nitrogen and phosphorous removal efficiencies. Typically, most of the large- (>1,000 pigs) and small-scale (<100 pigs) pig farms in Vietnam are using the AD process for swine wastewater treatment (Sakar et al., 2009). However, the anaerobically digested swine wastewater does not meet the Vietnamese discharge standard for swine wastewater effluent QCVN 62-MT:2016/BTNMT, especially for COD, biochemical oxygen demand (BOD_5), and NH_4^+. The treated water cannot be reused, causing waste of water and environmental pollution. Therefore, it is necessary to adopt a suitable treatment technology to treat this wastewater, minimize the environmental pollution, and build a water reuse cycle in pig farms. This is one of the main driving forces behind this practically relevant case study.

Recently, the intermittent cycle extended aeration system (ICEAS) technology has been widely applied for the treatment of many types of wastewaters because it offers the following advantages: (i) small footprint, (ii) low energy consumption, (iii) good process control and sequenced operational cycles, and (iv) high removal of nitrogen and organic pollutants (Li et al., 2008; Zhang et al., 2012). The ICEAS technology is an improved version of the sequencing batch reactor (SBR) technology, with continuously flowing influent, and it is fully automatic (Coelho et al., 2000; Fikar et al., 2005; Spagni and Marsili-Libelli, 2009). Due to its mode of operation and design, its advantages include: (i) reduced consumption of dissolved oxygen (DO), (ii) less energy requirement, i.e., 10–15% less energy for aeration compared to aeration-based biological processes (Liu and Wang, 2017; Sanchez et al., 2018), (iii) ability to tolerate shock loads of organics, (iv) reduced emission of greenhouse gas (~36%), and (v) high total nitrogen (TN) removal efficiency compared to the SBR technology (Spagni and Marsili-Libelli, 2009). Several previous research works have also reported on the removal of nutrients (nitrogen and phosphorus) from different wastewater sources using ICEAS. For example, Qiu et al. (2019) achieved TN removal of 81.5% during landfill leachate treatment, Zhang et al. (2011) reported TN removal of 76.5% for anaerobically digested swine wastewater, and Al-Rekabi et al. (2017) treated municipal wastewater and reported a total phosphorus (TP) removal efficiency >72%. Moreover, the biodegradability of nitrogen-rich wastewater is high in an ICEAS compared to other traditional technologies, especially for swine wastewater. However, for successful long-term operation, the optimization of the aeration/stirring ratio will reduce the operation time and increase the nitrogen removal efficiency (Mosquera-Corral et al., 2005; Gabarro et al., 2013; Pan et al., 2014a; Zheng et al., 2017). In an ICEAS, all the unit operations and biological reactions occur in the same tank, and the tank is controlled automatically with the help of sensors and actuators, which is suitable for installation and operation in small pig farms.

Besides, ICEAS can be used to treat many different types of wastewaters such as industrial, municipal, and tannery wastewater (Yoong et al., 2000; Maranón et al., 2008; Elmolla and Chaudhuri, 2011; Mojiri et al., 2014; Wang et al., 2015). Bao-Cang et al. (2018) used synthetic wastewater and showed total organic carbon (TOC) and ammonium (NH_4^+) removal efficiencies of 81.6 and 92.1%, respectively. The TN and TP removal efficiency of municipal wastewater using ICEAS was ~90% (Liu and Wang, 2017). Goncalves et al. (2005) used wool dyeing wastewater and indicated that the COD and BOD_5 removal efficiencies were >80%. Li et al. (2008) treated slaughterhouse wastewater using ICEAS and showed that the COD, TN, and TP removal efficiencies were 96 and 99%, respectively. ICEAS has also been applied to treat other specific sources of wastewaters, e.g., landfill leachate treatment (Qiu et al., 2019), municipal wastewater (Xu et al., 2020), and domestic wastewater (Khondabi et al., 2019). The main microbial communities of ICEAS include the following: ammonium-oxidizing bacteria (AOB), e.g., *Nitrosomonas*, *Nitrosococcus*, *Nitrobacter*, and *Nitrococcus* (Koops and Pommerening-Roser, 2001), which play important roles in ammonium oxidation, and nitrogen-oxidizing bacteria (NOB), e.g., *Nitrobacter*, *Nitrococcus*, *Nitrospina*, and *Nitrospira* (Ge et al., 2015), which play important roles in denitrification. It is noteworthy to mention that nitrogen removal in a ICEAS occurs according to the following main mechanisms involving nitrification/denitrification by AOB and NOB (Eq. 1).

$$NH_4^+ \rightarrow NO_2^- \rightarrow NO_3^- \rightarrow N_2 \quad (1)$$

Besides, ammonium is converted into N_2 gas *via* the partial nitrogen process, according to Eq. 2 (Yamamoto et al., 2008; Bournazou et al., 2013; Anjali and Sabumon, 2017; Zheng et al., 2017).

$$\begin{aligned} &NH_4^+ + 1.31NO_2^- + \\ &0.066HCO_3^- + 0.13H^+ \rightarrow 1.02N_2 + 026NO_3^- \\ &\qquad + 0.066CH_2O_{0.5}N_{0.5} + 2.03H_2O \end{aligned} \quad (2)$$

Phosphorus removal is an integral part of a wastewater treatment plant, and in biological treatment systems, phosphorus is normally treated by absorption into cell biomass by polyphosphate-accumulating organisms (PAOs). In a previous study, the phosphorus removal efficiency of ICEAS was reported to be >90%, which is higher than that of the conventional activated sludge technology (~10–20% P removal; Dutta and Sudipta Sarkar, 2015). Nitrogen removal from nitrite occurs under oxygen-limiting conditions (DO ≤ 0.5 mg/L; Guisasola et al., 2005); therefore, the DO concentration in the bioreactor has to be adjusted by optimizing the aeration/mixing rates. This unit operation requires prior operational knowledge of the reactor's operational modes and good process control instrumentation to control the different parameters of the reactor. Anew, other factors such as the carbon source, reaction time, and pollution load also have adverse impacts on the efficiency of this process. Hence, the main aim of this research was to study the effects of operating conditions such as cycle time, organic loading rate, C/N ratio, and aeration/mixing ratio on the removal of nutrients and organics present in anaerobically digested swine wastewater using the ICEAS technology.

MATERIALS AND METHODS

Swine Wastewater

Swine wastewater was collected at the swine farm of Ms. Nguyen Thi Tin, located in Village 1, Tan Dinh Commune, Ben Cat District, Binh Duong Province, Vietnam "11-0452551; 106-6447753." The farm has a capacity of 100 swines. Swine wastewater was collected from the anaerobic tank of the existing anaerobic wastewater treatment plant. The swine wastewater before and after anaerobic treatment still contains pollutants that exceed the Vietnamese allowable discharge standard for swine wastewater effluent, i.e., according to the rule QCVN62-MT:2016/BTNMT, as shown in **Table 1**. The influent swine wastewater was subjected to primary treatment where sand particles, residual solids, and large garbage were removed and the primary treated water was settled for 1 h. The seed activated sludge, i.e., the inoculum, was collected in an anaerobic SBR (ASBR) tank of the domestic wastewater treatment plant of Thu Dau Mot City, Binh Duong, Vietnam. The inoculum was acclimated using swine wastewater for a period of 2 weeks. The sludge volume index (SVI) was kept constant at 3,000 ml/g, and the BOD_5/COD ratio of the influent swine wastewater was 0.5.

Experimental System

A lab-scale ICEAS system was constructed using plastic acrylic material, with dimensions of 500 mm × 200 mm × 450 mm (L × W × H) and with a total working volume of 40 L, as shown in **Figure 1**. The ICEAS consists of two reaction zones (i.e., the pre-reaction zone and the main-reaction zone) which are connected to each other with the help of a 20-mm bottom space. The pre-reaction zone has dimensions of 100 mm × 200 mm × 450 mm (L × W × H), with a working volume of 8 L, while the main reaction zone has dimensions of 400 mm × 200 mm × 450 mm (L × W × H), with a working volume of 32 L. The pre-reaction zone was stabilized with a continuous flow of the influent in order to limit organic shock load to the microorganisms present in the main reaction zone. The oxygen was supplied using air blower systems and air pumps. The DO concentration was maintained at 2.5 mg/L during the operation of the ICEAS. Activated sludge was stirred using a 380-mm paddled motor. The input swine wastewater was filled into the pre-reaction zone (continuous inflow) by a peristaltic pump and then the wastewater flowed into the main reaction zone *via* the bottom space. Herein, the intermittent aeration process occurred and, finally, the treated water was decanted into the output tank using a pump. The cycle includes four phases of fill, reaction phase (aeration/mixing period), settling phase, and decanting phase. First, an aeration time of 45 min and a mixing time of 15 min, and then the cycle is repeated two times. After the completion of the reaction period, the aeration and mixing process was stopped and settling was

TABLE 1 | Properties of raw swine wastewater after anaerobic treatment and after the intermittent cycle extended aeration system (ICEAS).

No.	Parameter	Unit	Raw swine wastewater	After anaerobic treatment	After ICEAS treatment	Vietnamese discharge standard QCVN62-MT:2016/BTNMT (column B)
1	pH	–	6.9	8.4	8.8	5.5–9.0
2	Color	Pt–Co	4,576.52	4,104.21	88.33	–
3	COD	mg/L	3,459.43	2,267.62	157.78	300
4	BOD_5	mg/L	2,100.34	1,133.23	13.89	100
5	TN	mg/L	975.45	862.92	96.67	150
6	NH_4^+	mg/L	623.86	476.35	10.94	–
7	Nitrate	mg/L	377.43	462.67	50.98	–
9	TOC	mg/L	389.34	341.18	16.30	–
10	TP	mg/L	482.62	415.34	52.46	–

COD, chemical oxygen demand; BOD_5, biochemical oxygen demand; TN, total nitrogen; TOC, total organic carbon; TP, total phosphorus.

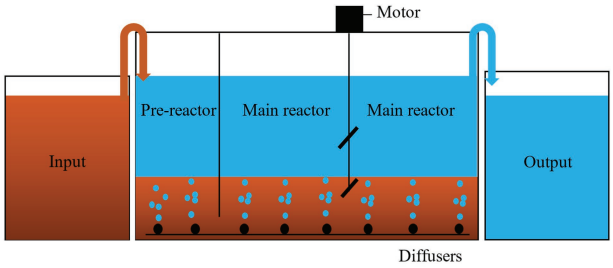

FIGURE 1 | Schematic of the ICEAS system.

done for 60 min. After that, the treated water was decanted for 30 min. The effects of cycle time, organic loading rate, and the aeration/mixing time on the nutrient and organic removal efficiencies were evaluated. The cycle times were varied from 4.5 to 8 h. The organic loading rate was increased from 0.34 to 2.58 kg COD m^{-3} day^{-1}, while the aeration/mixing times were varied from 75 to 195 min. Then, the pollutant removal efficiencies of ICEAS were compared with those of the conventional SBR process.

Wastewater Analysis

All the parameters monitored in this study were determined according to the protocols described in the Standard Methods for the Examination of Water and Wastewater (APHA et al., 2012). Wastewater was withdrawn and collected for the analysis of different pollutants' concentrations at regular time intervals. The experiments were replicated three times and the average values are shown in this study (Tien and Luu, 2020). The pH, color, and conductivity were measured using a Metrohm 900 multimeter (Switzerland). COD was measured using a Lovibond RD125 Thermoreactor (England), which uses the closed reflux titrimetric method for analysis. The TOC and TN contents were measured using a TOC Shimadzu 00936 (Japan). BOD_5 was measured using the Winkler method in a strong base environment at 20°C for 5 days using a BOD-System (Lovibond, Germany). The NO_3^-, NH_4^+, and TP concentrations were determined using ion chromatography [Metrohm IC 883, Switzerland; limit of detection (LOD) ≤ 0.05 mg/L]. The pollutant removal efficiencies were calculated based on the difference between the input and output wastewater concentrations, according to Eq. 3.

$$\text{Removal efficiency} = \frac{\text{ONt} - \text{ONs}}{\text{ONt}} \times 100 \quad (3)$$

where ONt and ONs (in milligrams per liter) are the concentrations of pollutants in swine wastewater before and after treatment, respectively.

RESULTS AND DISCUSSION

Effect of Cycle Time

The swine wastewater treatment using the ICEAS at different cycle times is shown in **Figure 2**. The cycle time was changed by changing the mixing time for the 4.5-h cycle (45 min mixing), 6-h cycle (135 min mixing), and 8-h cycle (255 min mixing). The experiment to determine the optimal cycle time was conducted during the first 18 days, wherein the organic loading rate was maintained at 1.71 kg COD m^{-3} day^{-1} in order to support adequate microbial growth without causing substrate-induced inhibition to the microorganisms. Previous reports have also used similar ranges of organic loading rates, e.g., Liang et al. (2019) used a range of 1.8–2.5 kg COD m^{-3} day^{-1}. The results show that, at a cycle time of 4.5 h (experiment was conducted from day 1 to 6), the TN, TP, and NH_4^+–N removal efficiencies were not high and were only 51.67, 72.46, and 69.12%, respectively. The next experiment was performed in order to increase the mixing time to 135 min (6-h cycle time). The TN, TP, and ammonium removal efficiencies increased to 79.57, 81.44, and 80.75%, respectively. This can be explained by the fact that increasing the mixing time will increase the denitrification by the partial nitrogen process, leading to an increase in the TN and NH_4^+–N removal efficiencies.

However, in this study, it was not possible to conclude that the 6-h cycle is optimal for high performance of the reactor. Therefore, the mixing time was increased to 255 min (8-h cycle), between days 13 and 18. The nitrogen and phosphorus removal efficiencies after a cycle time of 8 h significantly decreased compared to those with a cycle time of 6 h. The nitrogen and phosphorus removals mainly occurred in the non-aerated phase (Gao et al., 2013) by the conversion of nitrate (NO_3^-) into N_2 gas and phosphate (PO_4^{3-}) consumption by phosphorus-accumulating bacteria (i.e., for every 1 mg/L of phosphorus consumed, approximately 7.5–10.7 mg/L of COD; Song et al., 2017). Thus, the nitrogen and phosphorus removal efficiencies increased when increasing the non-aerated phase time (mixing time; Akin and Ugurlu, 2004; Melidis, 2014). However, when the mixing time was too long (i.e., the hydraulic retention time increases), the degradation of organic compounds was efficient, although nutrient depletion caused a reduction in the efficiency of microorganisms. A similar observation was previously reported by Melidis (2014) during landfill leachate treatment. The nitrogen and phosphorus removal efficiencies also decreased when the mixing time was 2 h. The TOC and BOD_5 removal efficiencies in all the three cycles were over 90%, which proves the ability of ICEAS to treat organic compounds. The TN and TP removal efficiencies in all the three cycles were low due to the effect of stirring time. Therefore, it can be concluded that the most optimal cycle time is 6 h. In a previous work, used an 8-h cycle time for treating slaughterhouse wastewater and obtained COD, TN, and TP removal efficiencies >90%. Pan et al. (2014a) showed that treating slaughterhouse wastewater at a cycle time of 12 h in an ICEAS tank reached TN removal efficiency of 42.8%. Kayranli and Ugurlu (2011) indicated that the cycle time of 6 h was best for municipal wastewater treatment. Sheng et al. (2017) treated swine wastewater using ICEAS at a cycle time of 8 h and reported TN and NH_4^+ removal efficiencies of 79 and 89%, respectively. Zhang et al. (2011) performed swine wastewater treatment using ICEAS and reported TN removal efficiency of 97% at a cycle time of 8 h. In another recent study,

Xu et al. (2020) reported a nitrogen removal efficiency of 89% when operating the ICEAS with a cycle time of 7 h. Furthermore, the authors also indicated that, when the cycle time was increased, an increased nitrate accumulation was noticed in the reactor. Khondabi et al. (2019) applied ICEAS for domestic wastewater treatment, with a cycle time of 8 h, and reported COD and BOD_5 removals of 93 and 95%, respectively.

Effect of Organic Loading Rates

The effect of organic loading rate was ascertained by performing experiments at different organic loading rates, i.e., 0.34, 0.86, and 2.58 kg COD m^{-3} day^{-1}. The organic loading rate was reduced from 1.71 to 0.86 kg COD m^{-3} day^{-1} between days 25 and 30. At an organic loading rate of 0.86 kg COD m^{-3} day^{-1}, the COD, BOD_5, TOC, and color removal efficiencies were 86.37, 97.60, 93.68, and 87.63%, respectively. At this organic loading rate, the TN, TP, and ammonium removal efficiencies were respectively 89.44, 85.94, and 97.39% higher than those observed at 1.71 kg COD m^{-3} day^{-1}. Thereafter, the organic loading rate was decreased to 0.34 kg COD m^{-3} day^{-1} from day 19 onwards, and the COD, TN, and TP removals were 89.45, 58.42, and 97.36%, respectively (**Figures 4D–F**). Reducing the inflow volume also affected the pollutant removal efficiencies, especially nitrogen and phosphorus. Due to a decrease in the nutrient content of the influent wastewater, nutritional imbalances might have occurred and reduced the activity of the microorganisms. The consumption of organic carbon during the aerobic phase caused a shortage of carbon source required for the denitrification process while enhancing nitrite accumulation (Kulikowska and Bernat, 2013). A C/N ratio of 6.0 was sufficient for nitrogen and phosphorus removal, while a C/N ratio <4.0 will lead to a deficiency of the carbon source for nitrogen and phosphorus removal (Renou et al., 2008). Thus, when decreasing the organic loading rate to 0.34 kg COD m^{-3} day^{-1}, there was a deficit of biodegradable organic substances, thereby contributing to a decline in the nitrogen and phosphorus removal efficiencies.

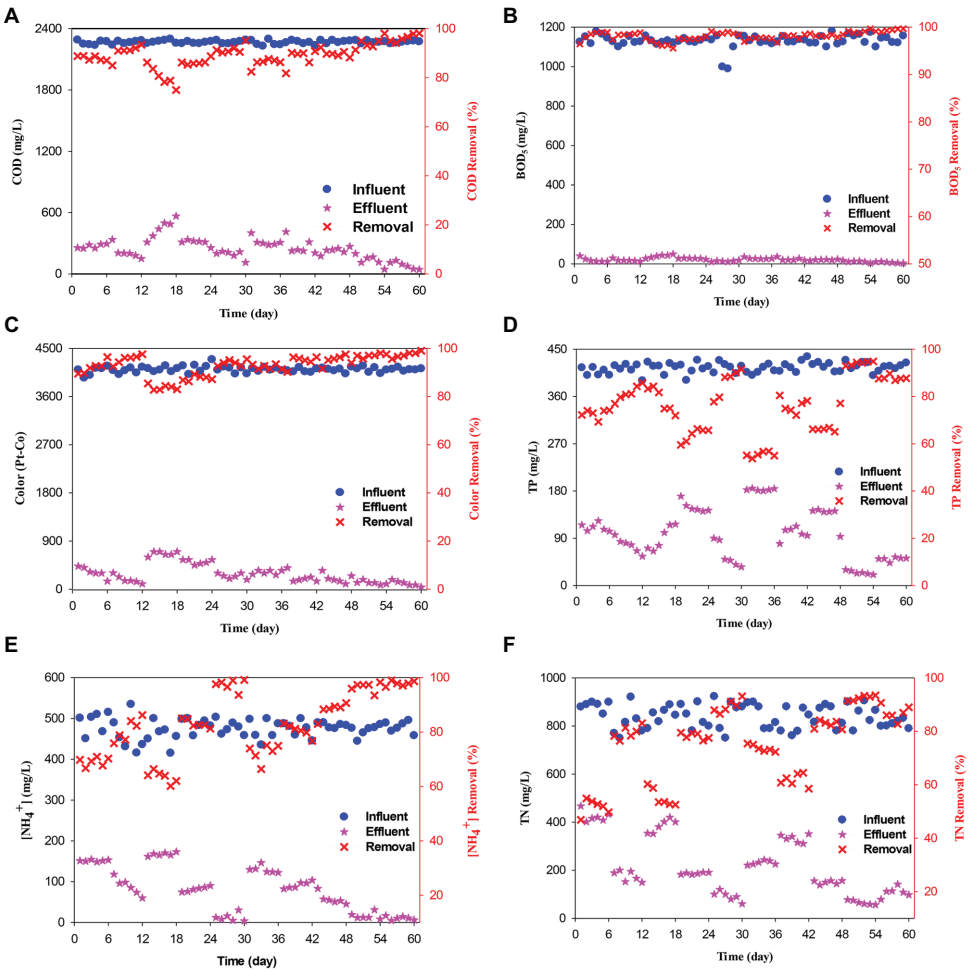

FIGURE 2 | Swine wastewater treatment using the ICEAS at different cycle times, organic loading rates, and aeration/mixing rates. **(A)** COD, **(B)** BOD_5, **(C)** color, **(D)** TP, **(E)** ammonium (NH_4^+–N), and **(F)** TN removal efficiencies.

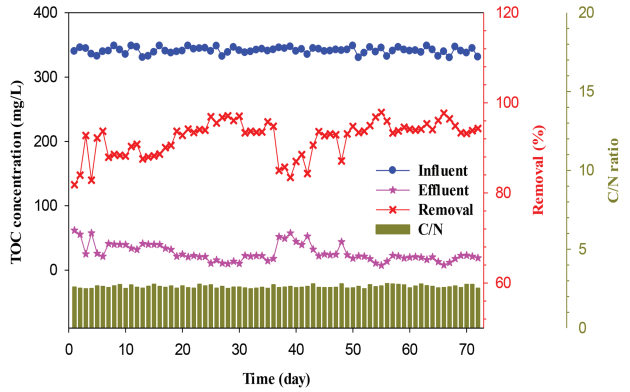

FIGURE 3 | Effect of the C/N ratio on the TOC removal efficiency of the ICEAS.

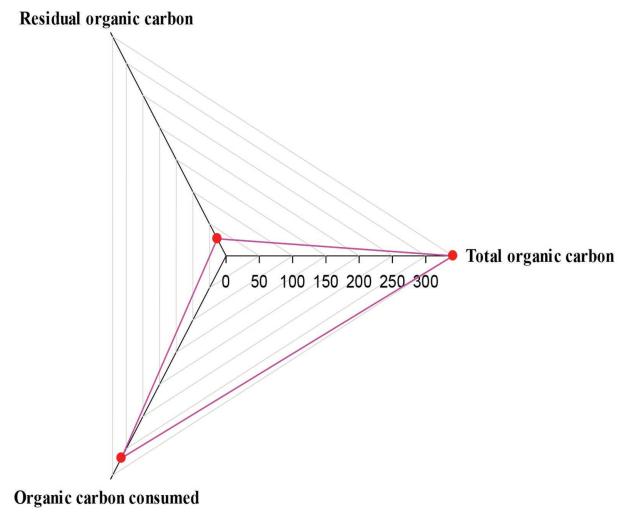

FIGURE 4 | Consumption of organic carbon in the ICEAS reactor.

Miao et al. (2015) reported that increasing the C/N ratio from 2.0 to 4.0 during landfill leachate treatment increased the nitrogen removal efficiency from 60 to 98%. Masłoń et al. (2019) ascertained that reducing the organic loading rate in synthetic wastewater from 0.68 down to 0.52 kg COD m^{-3} day^{-1} led to a decrease in the organic carbon removal efficiency from 96.7 to 93.9% and that the best organic carbon loading rate was 0.62 kg COD m^{-3} day^{-1}. However, in this study, in the experiment with an organic loading rate of 2.58 kg COD m^{-3} day^{-1} (days 31–36), the TN, TP, and ammonium removal efficiencies were decreased compared to those observed at rates of 0.34 and 0.86 kg COD m^{-3} day^{-1}. This behavior can be explained as due to a decline in the activity of the microorganisms caused by an organic shock load. The organic loading rate is an important parameter to be considered for bioreactor operation because an unexpected increase in the organic loading rate will cause a shock load stress and affect the structure and composition of the microbial communities, biomass-liquid separation, surface properties of the sludge, activity of the microbial community, and the pollutant removal efficiencies (Yang et al., 2018). Chelliapan et al. (2017) showed that the organic carbon rate affected the COD removal efficiency, wherein COD removal efficiencies of 99, 95, and 36.5% were obtained at organic loading rates of 0.258, 0.787, and 2.471, respectively. Singh et al. (2019) indicated that, at organic loading rates in the range of 2.55–3.15 kg COD m^{-3} day^{-1}, the COD removal efficiency was in the range of 92–96% and the ammonium removal efficiency was in the range of 81–85%.

Liang et al. (2019) reported that, when the organic loading rate was increased from 1.8 to 2.5 kg COD m^{-3} day^{-1}, the pollutant removal efficiency did not necessarily increase. Zhang et al. (2012) reported a COD removal efficiency of 89.8% at an organic loading rate of 1.5 kg COD m^{-3} day^{-1} of anaerobic pig manure. Zheng et al. (2017) showed that the removal of veterinary antibiotics was 85.1% at 0.17 kg COD m^{-3} day^{-1} and dropped to 75.9 and 49.3% when the COD volumetric load was increased to 0.65 and 1.07 kg COD m^{-3} day^{-1}, respectively. Based on the good results achieved, it can be concluded that the optimal organic loading rate for this study is 0.86 kg COD m^{-3} day^{-1}.

Effect of C/N Ratio

The denitrification process depends on the organic carbon/nitrogen ratio (C/N ratio), and a shortage of carbon sources for the denitrification process will strongly affect the nitrogen removal efficiency. **Figure 3** shows the effect of C/N ratio on the TOC removal efficiency and carbon balance. The TOC concentration in the influent wastewater and the C/N ratio did not fluctuate much, i.e., the TOC concentration was in the range of 330.12–348.56 mg/L, while the C/N ratio was in the range of 2.49–2.82. However, the TOC concentration in the effluent wastewater fluctuated from 7.33 to 61.78 mg/L. This observation clearly indicated that the low C/N ratio adversely affected the growth of microorganisms and the consumption rate of organic carbon present in the wastewater. Therefore, the optimal operation conditions are important factors in ICEAS, such as the aeration time and mixing time, to increase TOC removal efficiency.

The consumption of organic carbon in the ICEAS at an organic loading rate of 0.86 kg COD m^{-3} day^{-1} is shown in **Figure 4**. TOC influent = residual TOC + TOC consumed (used by the microorganisms + converted to different gas forms, e.g., CO_2). In this study, the average residual TOC concentration was low, i.e., 26.2 mg/L. TOC removal was 92.16% compared to the TOC residual value of 7.81%, while the COD removal efficiency was 89.85% and the residual COD was 10.15%. The COD removal/TOC consumption was 6.48, and this implies that, for every 1 kg of TOC consumed, the COD removed will correspond to 6.48 kg.

Effect of Aeration/Mixing Ratio

The effect of aeration/mixing ratio in the ICEAS was tested at aeration times of 75, 105, 165, and 195 min. The results

show that the TN and TP removal efficiencies after an aeration time of 105 min (from day 43 to 48) were lower than those observed at an aeration time of 135 min (6-h cycle time). From a practical perspective, it is necessary to balance the aeration time and the mixing time in order to limit the accumulation of nitrate and convert nitrite into N_2O and N_2 gas. Thereafter, the aeration time was reduced to 75 min, from day 37 to 42. The results show that the TN and TP removal efficiencies sharply decreased to 60.82 and 67.90%, respectively. The average TN and TP concentrations in the effluent were 332.11 and 133.85 mg/L, respectively, which are much higher than the values observed at an aeration time of 135 min (135 min was the total aeration time in the operation cycle in the experiment to determine the optimal cycle time). The reduction of aeration time will decrease the function of the microorganisms during the conversion of ammonium into nitrate and nitrate into N_2, resulting in the reduction of nitrogen and phosphorus removal efficiencies. Therefore, the aeration time and stirring time should be appropriately selected and maintained to achieve high performance of the ICEAS.

In the next step, the total aeration time was increased to 165 min between days 49 and 54. The removal efficiencies of TN, TOC, TP, ammonium, BOD_5, COD, and color increased to 92.51, 94.46, 94.07, 96.65, 98.99, 94.19, and 97.06%, respectively. The treatment efficiencies at an aeration time of 165 min were higher than the values observed at an aeration time of 75 min, especially for TN and TP removal, i.e., 60.82 and 67.90%, respectively. The concentrations of COD, BOD_5, and TN in the effluent were within the Vietnamese discharge standard values for swine wastewater effluent QCVN 62-MT:2016/BTNMT, with concentrations of 131.99, 11.62, and 65.46 mg/L, respectively. The concentrations of color, TP, TOC, and ammonium were 120.83 Pt–Co and 24.86, 18.85, and 15.83 mg/L, respectively.

The bioconversion processes were carried out with sufficient oxygen concentrations required for the growth of microorganisms (Denecke et al., 2011), leading to an increase in the conversion of ammonium to nitrate. However, the aeration time of 165 min was unlikely to be optimized. Therefore, in the next experiment, the aeration time was increased to 195 min during days 55–60. The results show that the treatment efficiency after an aeration time of 195 min was nearly similar to those achieved at an aeration time of 165 min, with TN, TOC, TP, ammonium, BOD_5, and COD removal efficiencies of 86.9, 94.9, 87.8, 97.8, 99.34, and 96.2%, respectively. From **Figure 5**, it is evident that an aeration/mixing ratio of 0.63 (105 min aeration/165 min mixing) resulted in ammonium, nitrate, and TN removal efficiencies of 88.16, 81.89, and 82.48%, respectively. Almost all the nitrogen present in swine wastewater was converted by the nitrification/denitrification ($NH_4^+ \rightarrow NO_2^- \rightarrow NO_3^- \rightarrow N_2$, N_2O, N_xO; Pan et al., 2014b) and partial nitrogen pathways, according to Eqs 3–6, respectively (Anjali and Sabumon, 2017).

$$NH_4^+ + 1.5O_2 \rightarrow 2H^+ + NO_2^- + H_2O \quad (4)$$

$$NH_4^+ + 1.31NO_2^- + 0.13H^+ + 0.066HCO_3^- \rightarrow 0.066CH_2O_{0.5}N_{0.15} + 2.03H_2O + 0.26NO_3^- + 1.02N_2 \quad (5)$$

$$2NO_3^- + 1.25CH_3COOH \rightarrow N_2 + 2.5CO_2 + 1.5H_2O + OH^- \quad (6)$$

When this ratio was reduced to 0.38 (75 min aeration/195 min mixing), the ammonium, nitrate, and TN removal efficiencies decreased to 80.62, 70.94, and 61.82%, respectively. It is noteworthy to mention that, when reducing the aeration/mixing ratio, there is a dissolved oxygen deficit, causing a lower microbial growth rate and activity and a reduction in the pollutant removal efficiencies. The results indicate that an aeration/mixing ratio of 1.57 (165 min aeration/105 min mixing) was determined as the optimal condition, as shown in **Figure 5**. This also implies that nitrite accumulation is almost negligible at an aeration/mixing ratio of 1.57, and the activity and the diversity of the microorganisms were high. The ammonium, nitrate, and TN concentrations in the effluent decreased on day 51, with concentrations of 12.42, 30.98, and 65.72 mg/L, respectively. When the aeration/mixing ratio was increased to 2.60 (195 min aeration/75 min mixing), the nitrate and ammonium removals were not different compared to the values observed at a ratio of 1.57.

However, the sharp drop in TN removal efficiency suggested that increasing the aeration time will increase the microbial activity and lead to an increase in the nitrate and ammonium removal capacity and enhance the nitrite accumulation. This can also be explained by the fact that the long aeration time will promote the growth of ammonium oxidation bacteria (AOB), and this will cause a reduction in the organic carbon content. According to Xu et al. (2020), nitrogen removal from municipal wastewater in an ICEAS depends on the mixing time, and the best performance of 89% was achieved at an aeration/mixing rate of 1.5. Wang et al. (2018) indicated that an aeration/mixing rate of 1 will promote the denitrification process and improve the nitrogen removal efficiency. Song et al. (2017) carried out swine wastewater treatment at an aeration/mixing ratio of 0.63 and achieved an ammonium removal efficiency of 96.5%.

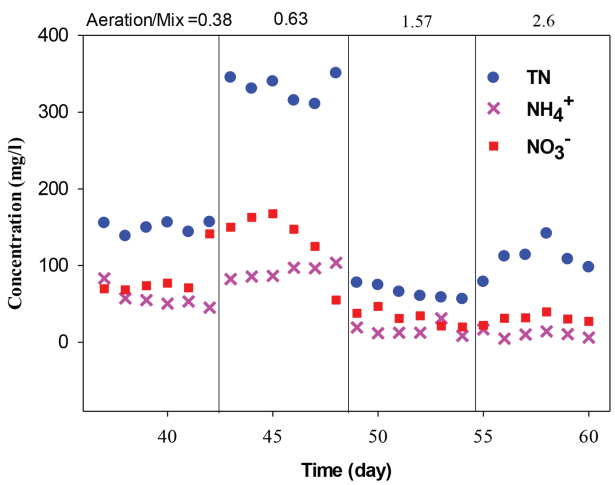

FIGURE 5 | Nitrogen removal efficiency at different aeration/mixing ratios.

Similarly, Qiu et al. (2019) performed experiments using landfill leachate wastewater in a bioreactor and reported an optimal aeration/mixing ratio of 0.5. According to Correa et al. (2018), the optimal aeration/mixing ratio was 2 when treating municipal wastewater achieved an ammonium removal efficiency of 86%. Zhang et al. (2011) treated swine wastewater using ICEAS at an aeration/mixing ratio of 2.08 and reported COD removal efficiencies >99%. The results of these previous literatures as well as the results of this study show that the optimal aeration/mixing ratio of ICEAS depends on the wastewater type and the amount of biodegradable organic compounds present in the influent wastewater. Thus, based on the results of these experiments, it can be deduced that a cycle time of 6 h, i.e., total aeration time of 165 min, mixing time of 105 min, settling time of 60 min, and a decant time of 30 min, can be considered as the optimal condition for a reliable ICEAS performance.

Comparison With Traditional SBR

After determining the optimal operation cycle, a comparison of the performance of ICEAS was made with a conventional SBR that was operated in parallel, under the same conditions as those of the ICEAS. According to **Figure 6**, the TOC (95.22%), TN (88.29%), ammonium (97.69%), TP (85.81%), and color (97.84%) removals were higher in the ICEAS than in the traditional SBR. However, the COD, BOD_5, and TOC removal efficiencies in both reactor configurations were >90%. Khondabi et al. (2019) reported COD and BOD_5 efficiencies of 93, and 95%, respectively, in a SBR and an ICEAS reactor. This can be explained as due to both tanks using the same activated sludge, microbial communities. Moreover, both reactors were operated at the same cycle time and hydraulic retention time, which led to having similar organic compound removal efficiencies. These results also agreed with the results reported previously by Zhang et al. (2011), wherein the nitrogen removal efficiency of ICEAS was higher than that of the conventional SBR, with values of 97 and 76.5%, respectively. Al-Rekabi et al. (2017) reported high ammonium, TP, and TN removal efficiencies of 83, 60, and 72%, respectively, in an ICEAS when compared to the conventional SBR (81, 58, and 69%, respectively) during municipal wastewater treatment. Optimizing the partial nitrification process will also help to increase the nitrogen removal efficiency of an ICEAS reactor (Ouyang et al., 1994; Zeinaddine et al., 2013). In an ICEAS, the aeration and mixing processes are time sequenced/controlled, therefore helping to maintain the desired microbial community structure and composition in the bioreactor.

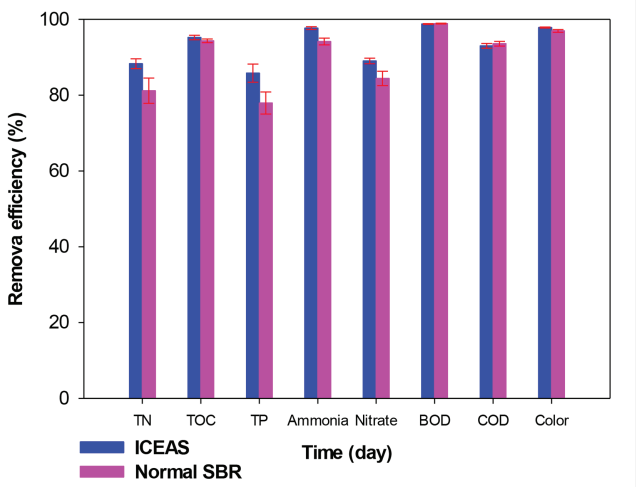

FIGURE 6 | Comparison of TN, TOC, TP, ammonium, nitrate, BOD_5, COD, and color removal efficiencies between the ICEAS and traditional sequencing batch reactor (SBR) technology.

Effluent Quality and Resource Recovery Possibility

The effluent water quality of ICEAS is within the permissible values recommended by the Vietnamese discharge regulation for swine effluent (QCVN 62-MT:2016/BTNMT) that can be used for agricultural irrigation. Besides, the treated water is rich in ammonium, nitrate, and phosphate ions which are beneficial for plant growth and development. Besides, the residual activated sludge rich in phosphorus and nitrogen can be mixed with agricultural residues (e.g., coconut fibers, rice straw, and water hyacinth) to produce biofertilizers. ICEAS is a promising technology that can be applied to treat the organics and nutrients present in anaerobically digested wastewater and recover useful value-added products.

CONCLUSION

The performance of an ICEAS to treat anaerobically digested wastewater was evaluated and high nitrogen and phosphorus removal efficiencies were achieved during long-term operation. The optimal cycle time was 6 h, with 165 min aeration, 105 min of mixing, 60 min settling, and 30 min of decanting time. The optimal aeration/mixing ratio was 1.57. The ICEAS was influenced by the organic loading rate (optimum value, 0.86 kg COD m^{-3} day^{-1}). The performance of the ICEAS was comparatively better than that of the traditional SBR technology in terms of nutrient removal. The treated water quality was within the Vietnamese discharge standard for swine effluent (QCVN 62-MT:2016/BTNMT) for pH, COD, BOD, and TN. The ICEAS can also be applied to treat wastewaters with different physicochemical and biological characteristics, e.g., landfill leachate and industrial and municipal wastewaters. Future research should be aimed at combining/integrating the ICEAS technology with ecological treatment systems such as wetlands and waste stabilization ponds. The long-term performance of the ICEAS should also be investigated by adopting a good process control system for controlling the state variables such as pH, dissolved oxygen concentration, oxygen and reduction potential, solids retention time, and the organic loading rate.

Efforts should also be made to scale up the process from a laboratory scale to a pilot and semi-industrial scale by performing suitable cost and environmental assessment studies.

DATA AVAILABILITY STATEMENT

The original contributions presented in the study are included in the article/**Supplementary Material**, further inquiries can be directed to the corresponding author.

AUTHOR CONTRIBUTIONS

ND working on experiment design. TL working on data collection and preparing the manuscript. ER support in manuscript revision. All authors contributed to the article and approved the submitted version.

FUNDING

This research is funded by Vietnam National Foundation for Science and Technology Development (NAFOSTED) under grant number 105.08-2019.22.

ACKNOWLEDGMENTS

ER thanks IHE Delft (Netherlands) for providing staff time (project: support to the society) and infrastructural support to collaborate with researchers from Vietnam.

SUPPLEMENTARY MATERIAL

The Supplementary Material for this article can be found online at: https://www.frontiersin.org/articles/10.3389/fmicb.2020.576438/full#supplementary-material

REFERENCES

Akin, B. S., and Ugurlu, A. (2004). The effect of an anoxic zone on biological phosphorus removal by a sequential batch reactor. *Bioresour. Technol.* 94, 1–7. doi: 10.1016/j.biortech.2003.11.022

Al-Rekabi, S. W., Abbas, K. A. H. A., and Abbas, A. S. (2017). Municipal wastewater treatment of Basrah city using intermittent cycle extended aeration system (ICEAS). *J. Eng. Sustaina. Develop.* 21, 1–14.

An, J. Y., Kwon, J. C., Ahn, D. W., Shin, D. H., Shin, H. S., and Kim, B. W. (2007). Efficient nitrogen removal in a pilot system based on up flow multi-layer bioreactor for treatment of strong nitrogenous swine wastewater. *Process Biochem.* 42, 764–772. doi: 10.1016/j.procbio.2007.01.020

Anjali, G., and Sabumon, P. C. (2017). Development of simultaneous partial nitrification, ANAMMOX and denitrification (SNAD) in a non-aerated SBR. *Int. Biodeterior. Biodegradation* 119, 43–55. doi: 10.1016/j.ibiod.2016.10.047

APHA, AWWA, WPCF (2012). *Standard methods for the examination of water and wastewater. 17th Edn.* Washington DC: American Water Works Association.

Aziza, A., Basheer, F., Sengar, A., Irfanullah, Khan, S. U., and Farooqi, I. H. (2019). Biological wastewater treatment (anaerobic-aerobic) technologies for safe discharge of treated slaughterhouse and meat processing wastewater. *Sci. Total Environ.* 686, 681–708. doi: 10.1016/j.scitotenv.2019.05.295

Bailey, C., Spielmeyer, A., Hamscher, G., Schüttrumpf, H., and Frings, R. M. (2016). The veterinary antibiotic journey: comparing the behaviour of sulfadiazine, sulfamethazine, sulfamethoxazole and tetracycline in cow excrement and two soils. *J. Soils Sediments* 16, 1690–1704. doi: 10.1007/s11368-016-1370-0

Bao-Cang, H., Wei-Li, J., Zhang, Y., Wei, W., and Chen, J. (2018). Profile of organic carbon and nitrogen removal by a continuous flowing conventional activated sludge reactor with pulse aeration. *Process Saf. Environ.* 117, 439–445. doi: 10.1016/j.psep.2018.05.022

Bournazou, C. N. M., Hooshiar, K., Arellano-Garcia, H., Wozny, G., and Lyberatos, G. (2013). Model based optimization of the intermittent aeration profile for SBRs under partial nitrification. *Am. J. Environ. Sci.* 47, 3399–3410. doi: 10.1016/j.watres.2013.03.044

Chelliapan, S., Din, M. F. M., Anuar, N. A., and Selvam, B. S. (2017). Effect of organic loading rate (OLR) on the performance of modified anaerobic baffled reactor (MABR) supported by slanted baffles. *Desalin. Water Treat.* 79, 56–63. doi: 10.5004/dwt.2017.20838

Coelho, M. A. Z., Russo, C., and Araujo, O. Q. F. (2000). Optimization of a sequencing batch reactor for biological nitrogen removal. *Water Res.* 33, 2809–2817. doi: 10.1016/S0043-1354(00)00010-5

Correa, C., Prates, C. M. V. K., Oliveir, F. E., Lopes, D. D., and Barana, C. A. (2018). Nitrification/denitrification of real municipal wastewater in an intermittently aerated structured bed reactor. *J. Water Proc. Eng.* 23, 134–141. doi: 10.1016/j.jwpe.2018.03.013

Daumer, M. L., Béline, F., Guiziou, F., and Sperandio, M. (2007). Influence of pH and biological metabolism on dissolved phosphorus during biological treatment of piggery wastewater. *Biosyst. Eng.* 96, 379–386. doi: 10.1016/j.biosystemseng.2006.11.011

Denecke, M., Eilmus, S., Roder, N., Roesh, C., and Bothe, H. (2011). Molecular identification of the microbial diversity in two sequencing batch reactors with activated sludge. *Environ. Biotechnol.* 93, 1725–1734. doi: 10.1007/s00253-011-3474-1

Dosta, J., Rovira, J., Galí, A., Macé, S., and Mata-Álvarez, J. (2008). Integration of a coagulation/flocculation step in a biological sequencing batch reactor for COD and nitrogen removal of supernatant of anaerobically digested piggery wastewater. *Bioresour. Technol.* 99, 5722–5730. doi: 10.1016/j.biortech.2007.10.021

Dutta, A., and Sudipta Sarkar, S. (2015). Sequencing batch reactor for wastewater treatment: recent advances. *Curr. Poll. Rep.* 1, 177–190. doi: 10.1007/s40726-015-0016-y

Elmolla, E. S., and Chaudhuri, M. (2011). The feasibility of using combined TiO_2 photocatalysis-SBR process for antibiotic wastewater treatment. *Desalination* 272, 24–218. doi: 10.1016/j.desal.2011.01.020

Fikar, M., Chachuat, B., and Latifi, M. A. (2005). Optimal operation of alternating activated sludge processes. *Control. Eng. Pract.* 13, 853–861. doi: 10.1016/j.conengprac.2004.10.003

Gabarro, J. A., Hernandez-del, E. A., Amo, F., Gich, M., Ruscalleda, M. D., Balaguer, J., et al. (2013). Nitrous oxide reduction genetic potential from the microbial community of an intermittently aerated partial nitritation SBR treating mature landfill leachate. *Water Res.* 47, 7066–7077. doi: 10.1016/j.watres.2013.07.057

Gao, D., Yin, H., Liu, L., Li, X., and Liang, H. (2013). Effects of idle time on biological phosphorus removal by sequencing batch reactors. *J. Environ. Sci.* 25, 2396–2402. doi: 10.1016/S1001-0742(12)60294-0

Ge, S., Wang, S., Yang, X., Qiu, S., Li, B., and Peng, Y. (2015). Detection of nitrifiers and evaluation of partial nitrification for wastewater treatment: a review. *Chemosphere* 140, 85–89. doi: 10.1016/j.chemosphere.2015.02.004

Goncalves, P. S., Matos, M. C. I., Santos, A. R., Franco, F., and Pinheiro, H. M. (2005). Evaluation of an integrated anaerobic/aerobic SBR system for the treatment of wool dyeing effluents. Purification of wool dyeing effluent in a SBR. *Biodegradation* 16, 81–89. doi: 10.1007/s10531-004-0431-7

Guadie, A., Xia, S., Zhang, Z., Zeleke, J., Guo, W., Ngo, H. H., et al. (2014). Effect of intermittent aeration cycle on nutrient removal and microbial community in a fluidized bed reactor-membrane bioreactor combo system. *Bioresour. Technol.* 156, 195–205. doi: 10.1016/j.biortech.2014.01.008

Guglielmi, G., and Andreottola, G. (2011). Alternate anoxic/aerobic operation for nitrogen removal in a membrane bioreactor for municipal wastewater treatment. *Water Sci. Technol.* 64, 1730–1735. doi: 10.2166/wst.2011.755

Guisasola, A., Jubany, I., Baeza, J. A., Carrera, J., and Lafuente, J. (2005). Respirometric estimation of the oxygen affinity constants for biological ammonium and nitrite oxidation. *J. Chem. Technol. Biotechnol.* 80, 388–396. doi: 10.1002/jctb.1202

Huang, H., Zhang, D., Guoa, G., Jianga, Y., Wang, M., Zhang, P., et al. (2018). Dolomite application for the removal of nutrients from synthetic swine wastewater by a novel combined electrochemical process. *Chem. Eng. J.* 335, 665–675. doi: 10.1016/j.cej.2017.11.013

Huang, H., Zhang, P., Zhang, Z., Liu, J., Xiao, J., and Gao, F. (2016). Simultaneous removal of ammonia nitrogen and recovery of phosphate from swine wastewater by struvite electrochemical precipitation and recycling technology. *J. Clean. Prod.* 127, 302–310. doi: 10.1016/j.jclepro.2016.04.002

Kayranli, B., and Ugurlu, A. (2011). Effects of temperature and biomass concentration on the performance of anaerobic sequencing batch reactor treating low strength wastewater. *Desalination* 278, 77–83. doi: 10.1016/j.desal.2011.05.011

Khondabi, G. V., Fazlali, A., and Zolfaghari, M. (2019). Evaluation of the performance of the intermittent cycle extended aeration system in detergent removal from bathroom greywater. *J. App. Res. Wat. Wast.* 11, 51–55. doi: 10.22126/ARWW.2019.1131

Koops, H. P., and Pommerening-Roser, A. (2001). Distribution and ecophysiology of the nitrifying bacteria emphasizing cultured species. *FEMS Microbiol. Ecol.* 37, 1–9. doi: 10.1016/S0168-6496(01)00137-4

Kulikowska, D., and Bernat, K. (2013). Nitritation–denitritation in landfill leachate with glycerine as a carbon source. *Bioresour. Technol.* 142, 297–303. doi: 10.1016/j.biortech.2013.04.119

Li, P. J., Healy, G. M., Zhan, M. X., and Rodgers, M. (2008). Nutrient removal from slaughterhouse wastewater in an intermittently aerated sequencing batch reactor. *Bioresour. Technol.* 99, 7644–7650. doi: 10.1016/j.biortech.2008.02.001

Li, W. H., Shi, Y. L., Gao, L. H., Liu, J. M., and Cai, Y. Q. (2012). Occurrence of antibiotics in water, sediments, aquatic plants, and animals from Baiyangdian Lake in North China. *Chemosphere* 89, 1307–1315. doi: 10.1016/j.chemosphere.2012.05.079

Liang, J., Maia, W., Tang, J., and Wei, Y. (2019). Highly effective treatment of petrochemical wastewater by a super-sized industrial scale plant with expanded granular sludge bed bioreactor and aerobic activated sludge. *Chem. Eng. J.* 360, 15–23. doi: 10.1016/j.cej.2018.11.167

Liu, G., and Wang, J. (2017). Enhanced removal of total nitrogen and total phosphorus by applying intermittent aeration to the Modified Ludzack-Ettinger (MLE) process. *J. Clean. Prod.* 166, 163–171. doi: 10.1016/j.jclepro.2017.08.017

Maranón, E., Vázquez, I., Rodríguez, J., Castrillón, L., Fernández, Y., and López, H. (2008). Treatment of coke wastewater in a sequential batch reactor (SBR) at pilot plant scale. *Bioresour. Technol.* 99, 4192–4198. doi: 10.1016/j.biortech.2007.08.081

Masłońa, A., Tomaszeka, J. A., Zamorska, J., Zdeb, M., Piech, A., Opalińskic, I., et al. (2019). The impact of powdered keramsite on activated sludge and wastewater treatment in a sequencing batch reactor. *J. Environ. Manag.* 237, 305–312. doi: 10.1016/j.jenvman.2019.02.035

Melidis, P. (2014). Landfill leachate nutrient removal using intermittent aeration. *Environ. Process* 1, 221–230. doi: 10.1007/s40710-014-0022-x

Miao, L., Wang, S., Li, B., Cao, T., Xue, T., and Peng, Y. (2015). Advanced nitrogen removal via nitrite using stored polymers in a modified sequencing batch reactor treating landfill leachate. *Bioresour. Technol.* 192, 354–360. doi: 10.1016/j.biortech.2015.05.013

Mojiri, A., Aziz, H. A., Zaman, N. Q., Aziz, S. Q., and Zahed, M. A. (2014). Powdered ZELIAC augmented sequencing batch reactors (SBR) process for co-treatment of landfill leachate and domestic wastewater. *J. Environ. Manag.* 139, 1–14. doi: 10.1016/j.jenvman.2014.02.017

Mores, R., Treichel, H., Zakrzevski, A. C., Kunz, A., Steffens, J., and Dallago, M. R. (2016). Remove of phosphorous and turbidity of swine wastewater using electrocoagulation under continuous flow. *Sep. Purif. Technol.* 171, 112–117. doi: 10.1016/j.seppur.2016.07.016

Mosquera-Corral, A., González, F., Campos, J., and Méndez, R. (2005). Partial nitrification in a SHARON reactor in the presence of salts and organic carbon compounds. *Process Biochem.* 40, 3109–3118. doi: 10.1016/j.procbio.2005.03.042

Ouyang, C. F., Her, M. C., and Liaw, S. L. (1994). Optimization of modified single continuous flow batch reactor for activated sludge treatment. *J. Chin. Inst. Environ. Eng.* 4, 143–150.

Pan, M., Henry, L. G., Liu, R., and Huang, X. M. (2014a). Nitrogen removal from slaughterhouse wastewater through partial nitrification followed by denitrification in intermittently aerated sequencing batch reactors at 11°C. *Environ. Technol.* 35, 470–477. doi: 10.1080/09593330.2013.832336

Pan, M., Wen, X., Wu, G., Zhang, M., and Zhan, X. (2014b). Characteristics of nitrous oxide (N_2O) emission from intermittently aerated sequencing batch reactors (IASBRs) treating slaughterhouse wastewater at low temperature. *Biochem. Eng. J.* 86, 62–68. doi: 10.1007/s11270-011-0998-z

Qiu, S., Hu, Y., Liu, R., Sheng, X., Chen, L., Wu, G., et al. (2019). Startup of partial nitritation-anammox process using intermittently aerated sequencing batch reactor: performance and microbial community dynamics. *Sci. Total Environ.* 647, 1188–1198. doi: 10.1016/j.scitotenv.2018.08.098

Rajagopal, R., Rousseau, P., Bernet, N., Girault, R., and Béline, F. (2011). Combined anaerobic and activated sludge anoxic/oxic treatment for piggery wastewater. *Bioresour. Technol.* 102, 2185–2192. doi: 10.1016/j.biortech.2010.09.112

Renou, S., Givaudan, J. G., Poulain, S., Dirassouyan, F., and Moulin, P. (2008). Landfill leachate treatment: review and opportunity. *J. Hazard. Mater.* 150, 468–493. doi: 10.1016/j.jhazmat.2007.09.077

Richardson, S. D., and Ternes, T. A. (2011). Water analysis: emerging contaminants and current issues. *Anal. Chem.* 83, 4614–4648. doi: 10.1021/ac200915r

Sakar, S., Yetilmezsoy, K., and Kocak, E. (2009). Anaerobic digestion technology in poultry and livestock waste treatment a literature review. *Waste Manag. Res.* 27, 3–18. doi: 10.1177/0734242X07079060

Sanchez, F., Rey, H., Viedma, A., Nicolas-Pérez, F., Kaiser, S. A., and Martínez, M. (2018). CFD simulation of fluid dynamic and biokinetic processes within activated sludge reactors under intermittent aeration regime. *Water Res.* 139, 47–57. doi: 10.1016/j.watres.2018.03.067

Sheng, X., Liu, R., Song, X., Chen, L., and Tomoki, K. (2017). Comparative study on microbial community in intermittently aerated sequencing batch reactors (SBR) and a traditional SBR treating digested piggery wastewater. *Front. Environ. Sci. Eng.* 11:8. doi: 10.1007/s11783-017-0929-3

Shin, J. H., Lee, S. M., Jung, Y. J., Chung, C. Y., and Noh, H. S. (2005). Enhanced COD and nitrogen removals for the treatment of swine wastewater by combining submerged membrane bioreactor (MBR) and anaerobic upflow bed filter (AUBF) reactor. *Process Biochem.* 40, 3769–3776. doi: 10.1016/j.procbio.2005.06.012

Shoukat, R., Khan, J. S., and Jamal, Y. (2019). Hybrid anaerobic-aerobic biological treatment for real textile wastewater. *J. Water Proc. Eng.* 29:100804. doi: 10.1016/j.jwpe.2019.100804

Singh, R., Bhunia, P., and Dash, R. R. (2019). Impact of organic loading rate and earthworms on dissolved oxygen and vermifiltration. *J. Hazard. Toxic Radio. Waste* 23:04019001. doi: 10.1061/(ASCE)HZ.2153-5515.0000435

Song, X., Liu, R., Chen, L., Dong, B., and Kawagishi, T. (2017). Advantages of intermittently aerated SBR over conventional SBR on nitrogen removal for the treatment of digested piggery wastewater. *Front. Environ. Sci. Eng.* 11:13. doi: 10.1007/s11783-017-0941-7

Spagni, A., and Marsili-Libelli, S. (2009). Nitrogen removal via nitrite in a sequencing batch reactor treating sanitary landfill leachate. *Bioresour. Technol.* 100, 609–614. doi: 10.1016/j.biortech.2008.06.064

Sui, Q., Liu, C., Dong, H., and Zhu, Z. (2014). Effect of ammonium nitrogen concentration on the ammonia-oxidizing bacteria community in a membrane bioreactor for the treatment of anaerobically digested swine wastewater. *J. Biosci. Bioeng.* 118, 277–283. doi: 10.1016/j.jbiosc.2014.02.017

Tien, T. T., and Luu, L. T. (2020). Electrooxidation of tannery wastewater with continuous flow system: role of electrode materials. *Environ. Eng. Res.* 25, 324–334. doi: 10.4491/eer.2018.349

Wang, Y., Gong, B., Lin, Z., Wang, J., Zhang, J., and Zhou, J. (2018). Robustness and microbial consortia succession of simultaneous partial nitrification, ANAMMOX and denitrification (SNAD) process for mature landfill leachate treatment under low temperature. *Biochem. Eng. J.* 132, 112–121. doi: 10.1016/j.bej.2018.01.009

Wang, H., Guan, Y., Pan, M., and Wu, G. (2015). Aerobic N_2O emission for activated sludge acclimated under different aeration rates in the multiple anoxic and aerobic process. *Am. J. Environ. Sci.* 43, 70–79. doi: 10.1016/j.jes.2015.08.010

Wegst-Uhrich, S. R., Navarro, D. A., Zimmerman, L., and Aga, D. S. (2014). Assessing antibiotic sorption in soil: a literature review and new case studies on sulfonamides and macrolides. *Chem. Cent. J.* 8, 1–12. doi: 10.1186/1752-153X-8-5

Wen, S., Liu, H., He, H., Luo, L., Li, X., Zeng, G., et al. (2016). Treatment of anaerobically digested swine wastewater by *Rhodobacter blasticus* and *Rhodobacter capsulatus*. *Bioresour. Technol.* 222, 33–38. doi: 10.1016/j.biortech.2016.09.102

Xu, Z., Zhang, L., Gao, X., and Peng, Y. (2020). Optimization of the intermittent aeration to improve the stability and flexibility of a mainstream hybrid partial nitrification-anammox system. *Chemosphere* 261:127670. doi: 10.1016/j.chemosphere.2020.127670

Yamamoto, T., Takaki, K., Koyama, T., and Furukawa, K. (2008). Long-term stability of partial nitritation of swine wastewater digester liquor and its subsequent treatment by Anammox. *Bioresour. Technol.* 99, 6419–6425. doi: 10.1016/j.biortech.2007.11.052

Yang, L., Ren, X. Y., Chen, N., Cui, S., Wang, H. X., and Xiao, Q. (2018). Organic loading rate shock impact on extracellular polymeric substances and physicochemical characteristics of nitrifying sludge treating high strength ammonia wastewater under unsteady state conditions. *RSC Adv.* 8, 41681–41691. doi: 10.1039/c8ra08357f

Yang, J., Trela, J., Zubrowska-Sudol, M., and Plaza, E. (2015). Intermittent aeration in one stage partial nitritation/anammox process. *Ecol. Eng.* 75, 413–420. doi: 10.1016/j.ecoleng.2014.11.016

Yoong, E. T., Lant, P. A., and Greenfield, P. F. (2000). In situ respirometry in an SBR treating wastewater with high phenol concentrations. *Water Res.* 34, 239–245. doi: 10.1016/S0043-1354(99)00142-6

Zeinaddine, H. R., Ebrahimi, A., Alipour, V., and Rezaei, L. (2013). Removal of nitrogen and phosphorous from wastewater of seafood market by intermittent cycle extended aeration system (ICEAS). *J. Health Sci. Surveillance Sys.* 1, 89–93.

Zhang, M., Lawlor, P. G., Wu, G., Lynch, B., and Zhan, X. (2011). Partial nitrification and nutrient removal in intermittently aerated sequencing batch reactors treating separated digestate liquid after anaerobic digestion of pig manure. *Bioprocess Biosyst. Eng.* 34, 1049–1056. doi: 10.1007/s00449-011-0556-5

Zhang, M., Peadar, G., Li, J., and Zhan, X. (2012). Characteristics of nitrous oxide (N_2O) emissions from intermittently-aerated sequencing batch reactors treating the separated liquid fraction of anaerobically digested pig manure. *Water Air Soil Pollut.* 223, 1973–1981. doi: 10.1007/s11270-011-0998-z

Zheng, W., Zhenya, Z., Liu, R., and Zhongfang, L. (2017). Removal of veterinary antibiotics from anaerobically digested swine wastewater using an intermittently aerated sequencing batch reactor. *Am. J. Environ. Sci.* 65, 8–17. doi: 10.1016/j.jes.2017.04.011

Zhou, Q. X., Luo, Y., and Wang, M. E. (2007). Environmental residues and ecotoxicity of antibiotics and their resistance gene pollution: a review. *Asian J. Ecotoxicol.* 82, 243–251.

Conflict of Interest: The authors declare that the research was conducted in the absence of any commercial or financial relationships that could be construed as a potential conflict of interest.

frontiers in Microbiology

ORIGINAL RESEARCH
published: 03 November 2020
doi: 10.3389/fmicb.2020.584020

Biodegradation of Doxylamine From Wastewater by a Green Microalga, *Scenedesmus obliquus*

Jiu-Qiang Xiong, Pengfei Cui and Shaoguo Ru**

College of Marine Life Sciences, Ocean University of China, Qingdao, China

Pharmaceutical contaminants (PCs) have been recognized as emerging contaminants causing unexpected consequences to environment and humans. There is an urgent need for development of efficient technologies to treat these PCs from water. The current study has investigated the removal capacity of a green microalgal species, *Scenedesmus obliquus*, for doxylamine, chemical oxygen demand (COD), and nutrients from real wastewater. Results have indicated that *S. obliquus* can grow well in the doxylamine-polluted wastewater with the achievement of 56, 78.5, 100, and 89% removal of doxylamine, COD, total nitrogen (TN), and total phosphorus (TP). Addition of 2 g L^{-1} bicarbonate enhanced the removal of doxylamine up to 63% and slightly inhibited the removal of COD. Decreased carbohydrate (28–26%) and increased protein content (30–33%) of the harvested biomass have been observed after cultivation in the wastewater. The current study has shown the feasibility of using microalgae-based biotechnologies for PC-contaminated wastewater.

Keywords: pharmaceutical contaminants, microalgae, doxylamine, wastewater, bioremediation, biodegradation

OPEN ACCESS

Edited by:
Dayanand Kalyani,
Royal Institute of Technology, Sweden

Reviewed by:
Yin Ye,
Northwestern Polytechnical University, China
Hu Zhenhu,
Hefei University of Technology, China

****Correspondence:***
Pengfei Cui
cuipengfei@ouc.edu.cn
Shaoguo Ru
rusg@ouc.edu.cn

Specialty section:
This article was submitted to Microbiotechnology, a section of the journal Frontiers in Microbiology

Received: *16 July 2020*
Accepted: *22 September 2020*
Published: *03 November 2020*

Citation:
Xiong J-Q, Cui P and Ru S (2020) Biodegradation of Doxylamine From Wastewater by a Green Microalga, Scenedesmus obliquus. Front. Microbiol. 11:584020. doi: 10.3389/fmicb.2020.584020

INTRODUCTION

Pharmaceuticals have been extensively used in human, and culturing of livestock, poultry, and fish to help and facilitate their lives. These high-biologically activated compounds cannot be efficiently degraded, and >70% of the uptaken drugs can be excreted into environment with urine and feces (Tran et al., 2018). Numerous countries including United States, China, Canada, Europeans, South Korea, and Japan have found their frequent occurrence in surface water, groundwater, wastewater, seawater, and soil with levels of ng L^{-1} to μg L^{-1} (Patel et al., 2019). These pharmaceutical contaminants (PCs) have been recognized as emerging contaminants since increasing evidences have demonstrated their unexpected consequences on ecological systems and health of humans. For example, PCs at environmental concentrations extended the lag phase of benthic microorganisms, inhibited bacterial denitrification, and reduced microbial diversity (Underwood et al., 2011). Potential permanent damage and consequent effects on coming generations can be induced by PCs demonstrated by their significant influence on uterus [Commission European (CE), 2016]. Existence of the PCs in environment also can generate drug-tolerant bacteria and antibiotic-resistant genes, which can be biomagnificated through food web and finally reach higher consumers (Martínez, 2008). There is an urgent need for effective treatment of such PCs from environments.

Traditional conventional technologies for wastewater treatment are highly effective for removal of chemical oxygen demand (COD); however, it shows limited performance to remove persistent PCs, total nitrogen (TN) and total phosphorus (TP; Matamoros et al., 2015). Different strategies such as advanced oxidation processes (AOPs), adsorption, bacterial degradation, and electrolysis have shown highly efficient performance of PC treatment (Patel et al., 2019). There are unexpected disadvantages with use of these advanced approaches. For example, more hazardous intermediates can be formed during AOPs and electrolysis (Yang et al., 2019); organic matrixes of the wastewater can significantly decrease the adsorption capacity (Ersan et al., 2017); and drug-resistant bacteria can be easily acclimated during degradation of PCs (Xiong et al., 2018). Microalgae-based biotechnologies have shown potential applications for advanced treatment of different wastewaters such as municipal wastewater, swine wastewater, poultry litter anaerobic digestate, industrial wastewater, and aquaculture wastewater (Yu et al., 2015; Zhuang et al., 2020). Additionally, microalgae can utilize the nutrients and carbon sources of wastewaters for their cellular metabolisms with generating biomass for production of bioenergy and high value-added compounds (Perez-Garcia et al., 2011; Fernandes et al., 2017). Microalgal treatment of PCs needs further exploration to achieve potential application under current scenario; in particular, more attention should be paid on the development in the performance for removal of nutrients and PCs from real wastewaters.

In this study, the microalgal degradation of a frequently found PC, doxylamine from real wastewater, has been investigated. Doxylamine has been frequently detected in different water sources with concentrations of ng L^{-1} to μg L^{-1}. Earlier studies mainly investigated the formation dynamics of N-nitrosodimethylamine (NDMA) from doxylamine since NDMA is a highly carcinogenic product and can be easily formed during oxidation of amine-based PCs (Shen and Andrews, 2011). Rare investigations have focused on microalgal removal of doxylamine from real wastewater. Therefore, the current study aims to investigate the removal efficiencies of doxylamine by microalgae from municipal wastewater, the effect of doxylamine on the growth of microalgae, and the effect of doxylamine on the microalgal performance for treatment of COD, TN, and TP.

MATERIALS AND METHODS

Chemicals

Doxylamine succinate salt with a molecular weight 338.46 g mol^{-1} has been obtained from Sigma-Aldrich (St. Louis, USA). Compositions of mobile phase were acetonitrile, water, and formic acid, which are at HPLC-grade and were purchased from Thermo Fisher Scientific and Mallinckrodt Baker Inc. (USA).

Removal of Doxylamine by *Scenedesmus obliquus* From Real Wastewater

The removal capability of a widely distributed freshwater microalgal species, *S. obliquus*, for doxylamine from real wastewater has been investigated. The microalgal inoculum has been cultivated in Erlenmeyer flasks containing sterilized Bold's Basal Medium (BBM, 150 ml) under a continuous light source with an intensity of 45–50 μmol photons m^{-2} s^{-1} for 7 days in a shaking incubator (150 rpm). The temperature was 27°C. The microalgal cells were harvested by centrifugation (4,000 rpm), and the biomass was washed three times with distilled water before its further use.

Batch experiments to investigate the removal of doxylamine (1 mg L^{-1}) from real wastewater by *S. obliquus* were conducted in 250-ml Erlenmeyer flasks containing 150 ml of raw wastewater inoculated with 1.5% of microalgal suspension with an optical density at 680 nm (OD_{680}) of 1.0. The reduction of doxylamine in wastewater was examined by supplying the culture flasks with the same amount of doxylamine without inoculum of microalgae. The effect of sodium bicarbonate ($NaHCO_3$, 2 g L^{-1}) was also investigated since biocarbonate has been found to be an enhancement strategy not only for microalgal growth but also for promoting the nutritional treatment efficiency (Pancha et al., 2015; Zhai et al., 2020). On the other aspect, high cost of carbon dioxide (CO_2) capture and transportation and CO_2 loss for microalgal cultivation have enabled people for searching alternative solutions to CO_2 fixation (Chi et al., 2011). The bicarbonate-carbon cycling system has been proposed as an advanced approach (Song et al., 2019). All the experiments were conducted in triplicate.

Determination of Microalgal Growth and Biochemical Characteristics

Growth of *S. obliquus* was determined according to the changes of the microalgal culture at OD_{680} (Xiong et al., 2020). In a brief, the cell numbers of the microalgal cultures with different absorbance were counted using a Countess II Automated Cell Counter (Thermo Fisher Scientific, USA). A linear relationship between microalgal cell numbers and OD_{680} has been found as follows:

$$\text{Cell numbers of } S.obliquus\left(10^7\ \text{ml}^{-1}\right) = 1.3914 \times \text{OD}_{680} + 0.0038\left(R^2 = 0.999\right) \quad (1)$$

The specific growth rate (μ) was calculated using the following equation:

$$\mu = \frac{\ln N_2 - \ln N_0}{t_2 - t_0} \quad (2)$$

where N_2 is the dry cell weight at time t_2 and N_0 is the dry cell weight at time t_0 (day 0).

Total chlorophyll and carotenoid content of *S. obliquus* were measured according to an earlier reported protocol (Kurade et al., 2016). Carbohydrate of microalgal biomass was analyzed using phenol-sulfuric acid method with glucose as a standard, and amount of the protein was measured using Bradford assay (Xiong et al., 2019).

Analytical Measurement of Doxylamine, COD, and Nutrients

Samples for analysis of doxylamine have been taken at regular intervals of 0, 2, 4, 6, 8 and 10 days, which were firstly centrifuged

and then filtered using 0.45-μm membrane filters (Pall Life Sciences, USA). Twenty-microliter solution has been injected into a high-performance liquid chromatography (HPLC) equipped with a UV-visible detector (Waters 2695, USA). The running mobile phase consisted of acetonitrile, water, and formic acid at a ratio of 10:90:0.1 (v/v/v), and the flow rate was 0.8 ml min^{-1}.

Kinetics analyses of doxylamine removal have been conducted using zero-order model, first-order model, and second-order model based on the following equations:

$$C_t = -kt + C_0 \quad (3)$$

$$\ln C_t = -kt + \ln C_0 \quad (4)$$

$$\frac{1}{C_t} = kt + \frac{1}{C_0} \quad (5)$$

where C_0 is the initial amount of doxylamine, C_t is the residual concentration at time t, k is the removal rate constant (day^{-1}), and t refers to the sampling time. Equation (3) presents zero-order kinetic reaction; Eq. (4) is for first-order kinetic reaction; and Eq. (5) is for calculation of second-order kinetic reaction parameters.

COD of wastewater was determined with a reference to the guideline of APHA 5220D, which uses potassium hydrogen phthalate for standard curve. TN and TP were measured using the kits named Test N Tube Total Nitrogen Reagent Set (2–150 mg L^{-1}) and the phosphorus (total) TNT Reagent Set (0.06–3.5 mg L^{-1}). All the kits were purchased from Hach (USA), and the analysis was done according to the manufacturer's protocol. pH of the samples was determined using an Orion Star A321 pH portable meter (Thermo Fisher Scientific, USA).

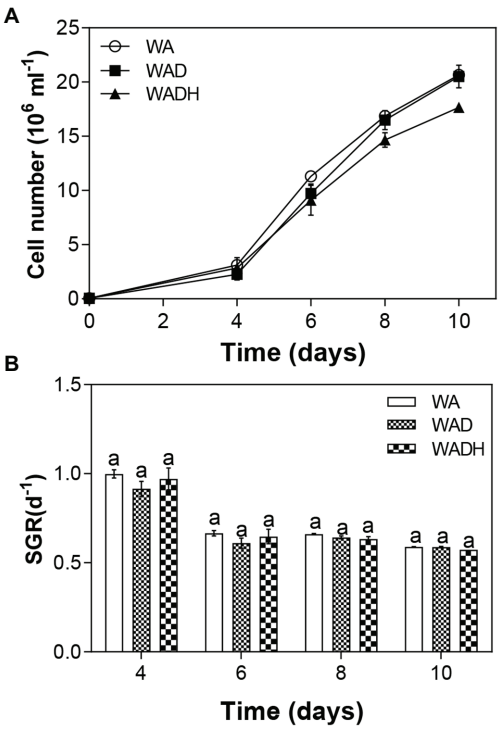

FIGURE 1 | Cell numbers **(A)** and specific growth rate **(B)** of *Scenedesmus obliquus* in wastewater (WA), wastewater with doxylamine (WAD), and wastewater with addition of doxylamine and biocarbonate (WADH) during 10 days of cultivation.

RESULTS AND DISCUSSION

Growth Pattern of *Scenedesmus obliquus*

The growth rate of *S. obliquus* with and without doxylamine in wastewater is shown in **Figure 1**. The density of microalgal cells have been calculated from Eq. (1), and were 20.67×10^6 ml^{-1}, 20.51×10^6 ml^{-1}, and 17.65×10^6 ml^{-1} for WA (wastewater with inoculum of microalgae), WAD (wastewater with addition of microalgae and doxylamine), and WADH (wastewater with addition of microalgae, doxylamine, and bicarbonate), respectively (**Figure 1A**). The results indicated that the exposed amount of doxylamine in wastewater negligibly influenced the growth of *S. obliquus*. Specific growth rate (SGR) of *S. obliquus* in different experimental conditions was calculated form Eq. (2), and have been shown in **Figure 1B**. There was no observable difference of SGR with the effect of either doxylamine or the combination of doxylamine and bicarbonate during 10 days of cultivation. The negligible difference of microalgal growth and SGR influenced by doxylamine indicated that *S. obliquus* is a tolerant species toward the treatment of doxylamine-polluted wastewater. Earlier studies also demonstrated low concentrations of levofloxacin, amoxicillin, and ciprofloxacin (Xiong et al., 2017; Xie et al., 2020). For example, the growth of a green microalga, *Chlorella vulgaris*, was not influenced with exposure up to 5 mg L^{-1} levofloxacin (Xiong et al., 2017). Xie et al. (2020) investigate the effect of ciprofloxacin on a *Chlamydomonas* sp., which showed that there was no significant alteration of microalgal growth under 10 mg L^{-1} ciprofloxacin. Liu et al. (2016) demonstrated that there was a hermetic effect of amoxicillin on the growth of a cyanobacteria, *Microcystis aeruginosa*. All these results indicated the engineering feasibility of microalgae in different conditions. However, there are many studies showing the inhibitory effect of various PCs on microalgal growth. For example, Li et al. (2020) found that the growth of *Chlorella pyrenoidosa* was significantly inhibited by roxithromycin from 0.25 mg L^{-1} to 2 mg L^{-1} (Li et al., 2020). A mixture of sulfamethazine and sulfamethoxazole significantly inhibited the growth of *S. obliquus* at concentrations from 0.05 mg L^{-1} to 0.5 mg L^{-1} (Xiong et al., 2019). Transcriptomic analysis of the microalgal cells exposed to high concentrations of PCs indicated that PCs downregulated the expressions of genes involved in DNA replication and repair process, biosynthesis of biochemicals (steroids, sesquiterpenoid, fatty acids, triterpenoid), and photosynthesis, thus causing toxicity to microalgal cells (Wei et al., 2019; Guo et al., 2020).

Changes of Microalgal Pigments Influenced by Doxylamine

Photosynthesis of microalgae mediated by chlorophyll and carotenoid plays essential roles to convert light energy, carbon

dioxide, and water into microalgal biomass. Thus, evaluation of pigment production helps to understand the overall cellular metabolic activities (Blossom et al., 2019; Stock et al., 2020). As shown in **Figure 2**, total chlorophyll of *S. obliquus* was 27.21, 26.68, and 16.81 mg g^{-1} in wastewater, doxylamine polluted wastewater, and wastewater with doxylamine and sodium biocarbonate, respectively, whereas the amount of carotenoid showed a similar trend with a final production of 5.62, 5.15, and 3.35 mg g^{-1}. The result agreed with the microalgal growth pattern, which indicated that there was no significant effect of doxylamine (1 mg L^{-1}) on the microalgal photosynthesis. The decreased content of microalgal chlorophyll is consistent with earlier studies. For example, phytoplankton photosystem II (PSII) efficiency (*Fv*/*Fm*) of a marine microalga, *Nannochloropsis salina*, was slightly inhibited with the addition of 2 g L^{-1} bicarbonate (White et al., 2013). *Fv*/*Fm* of a marine green microalga *Tetraselmis subcordiformis* was significantly inhibited with 5 g L^{-1} bicarbonate (Qi et al., 2019). Sampathkumar and Gothandam (2019) demonstrated that chlorophyll and carotenoid content of a green microalga, *C. vulgaris*, increased at low concentration of bicarbonate (0–150 mM) and decreased at 200 mM bicarbonate (Sampathkumar and Gothandam, 2019). High concentrations of bicarbonate induced adverse effects on photosynthetic pigments, which can be due to energy interactions for photosynthetic carbon dioxide fixation and energy-consuming metabolic pathways since assimilation of bicarbonate involves an active transport (Srinivasan et al., 2018; Qi et al., 2019).

Removal of Doxylamine by *Scenedesmus obliquus* From Real Wastewater

Figure 3 showed the removal of doxylamine from real wastewater by *S. obliquus*. There was 15% decrease of the exposed doxylamine concentrations in the wastewater without inoculum of microalgae, while growth of *S. obliquus* removed 56% doxylamine (1 mg L^{-1}) after 10 days of cultivation, and addition of sodium bicarbonate increased the removal up to 63%. Removal kinetics of doxylamine removal at different experimental conditions were analyzed using zero-order, first-order, and second-order reaction models (**Table 1**). The removal kinetic constant (k, day^{-1}) of doxylamine from wastewater was 0.057, 0.064 and 0.014 day^{-1} for wastewater with microalgae, wastewater without microalgae and bicarbonate, and wastewater without microalgae, respectively, and half-lives ($T_{1/2}$, day) increased from 8.31 days to 36.3 days, which were calculated by zero-order kinetic reaction (r^2 = 0.87–0.99). First-order kinetic analysis showed the removal kinetic constant (k, day^{-1}) of doxylamine were 0.12, 0.16, and 0.02 day^{-1} with half-lives ($T_{1/2}$, day) of 5.56, 4.33, and 34.15 (r^2 = 0.86–0.99). Second-order kinetic reaction constant (k, day^{-1}) was 0.1224, 0.1675, and 0.0166 with half-lives ($T_{1/2}$, day) of 10.26, 8.34, and 59.79 (r^2 = 0.94–0.95) for WAD, WADH, and WD, respectively. Removal of doxylamine using microalgae from

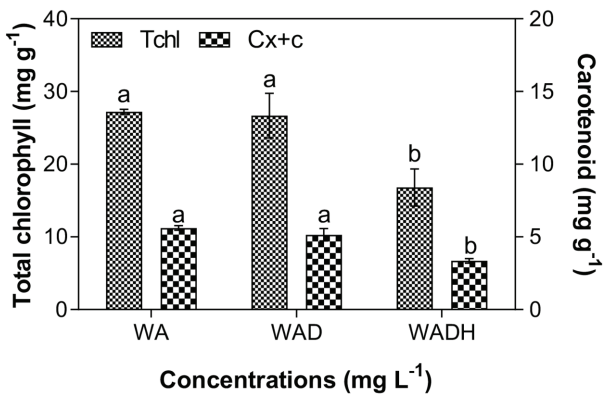

FIGURE 2 | Total chlorophyll and carotenoid content of *Scenedesmus obliquus* after cultivation in wastewater (WA), wastewater with doxylamine (WAD), and wastewater with addition of doxylamine and biocarbonate (WADH).

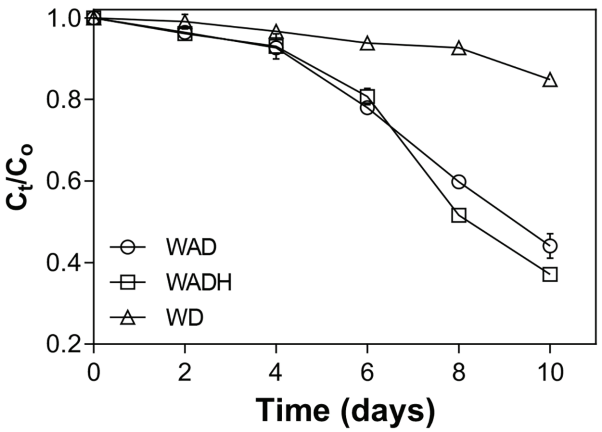

FIGURE 3 | Removal of doxylamine by *Scenedesmus obliquus* in wastewater (WAD), wastewater with addition of bicarbonate (WADH), and wastewater without inoculation of microalgae (WD).

TABLE 1 | Kinetic parameters of doxylamine (1 mg L^{-1}) degradation by *Scenedesmus obliquus* in different experimental conditions.

Experiments	Zero-order kinetic reaction		
	k (day^{-1})	$T_{1/2}$ (day)	r^2
WAD	0.057	9.30	0.99
WADH	0.064	8.31	0.97
WD	0.014	36.30	0.87
Experiments	**First-order kinetic reaction**		
	k (day^{-1})	$T_{1/2}$ (day)	r^2
WAD	0.1247	5.56	0.99
WADH	0.1601	4.33	0.97
WD	0.020	34.15	0.86
Experiments	**Second-order kinetic reaction**		
	k (day^{-1})	$T_{1/2}$ (day)	r^2
WAD	0.1224	10.26	0.95
WADH	0.1675	8.34	0.94
WD	0.0166	59.79	0.94

k, kinetic removal rate constant (day^{-1}); $T_{1/2}$, removal half-life (day); r^2, correlation coefficient; WAD, wastewater with doxylamine and microalgae; WADH, wastewater with doxylamine, microalgae, and biocarbonate; WD, wastewater with doxylamine.

real wastewater has been rarely reported. However, numerous studies have demonstrated the removal capacity of microalgae for various PCs. Microalgae-based biotechnologies have been proven as a promising tool toward effective treatment of diverse organic and inorganic pollutants (Villar-Navarro et al., 2018; Sutherland and Ralph, 2019). For example, Vo et al. (2020) found that *Chlorella* sp., can remove 16–58% of tetracycline, sulfamethoxazole, and bisphenol A, and the removal efficiency was enhanced up to 99% with a cometabolic mechanism (Vo et al., 2020). It has demonstrated that the high-rate algal ponds (HRAPs) removed 22–90% of 26 PCs including acetaminophen, ibuprofen, and oxybenzone from urban wastewater (Matamoros et al., 2015). Instead of upflow anaerobic sludge blanket in the wastewater treatment plant, high-rate algae ponds have been used as a tertiary treatment for nutrients and other contaminants from wastewater, which showed 15 and 50% higher removal of diclofenac and some specific antibiotics and diuretics (Villar-Navarro et al., 2018).

Removal of COD and Nutrients by *Scenedesmus obliquus*

Figure 4 showed the changes of pH, and removal of COD, TN, and TP in different experimental sets. Investigation of the microalgal capacity for elimination of various contaminants is essential since it can help to screen a robust species. The pH of the raw wastewater (WD) increased from 6.4 to 8.70 after 10 days of cultivation, and pH of wastewaters with cultivation of microalgae (WA), doxylamine (WAD), and/or bicarbonate (WADH) increased up to 10.85 (**Figure 4A**). Growth of microalgae can increase pH as uptake of inorganic carbon (e.g., HCO_3^-) in photosynthesis induces release of hydroxyl ions. Nitrate reduction also causes an increase in pH since denitrification process will consume hydrogen ions. Concentrations of COD decreased from 235.67 mg L^{-1} to 45.67, 47.33, 50.67, and 57.33 mg L^{-1} for WD, WA, WAD, and WADH, respectively. Initial amount of TN was 33.5 mg L^{-1}, which achieved 23.9, 94, 100, and 98.5% removal in WD, WA, WAD, and WADH. In case of TP, it was observed that the doses declined from 6.67 mg L^{-1} to 5.72, 1.10, 0.75, and 1.05 mg L^{-1}, which equaled to 14.2, 83.5, 88.8, and 84.3% removal, respectively. Microalgae are able to assimilate different nitrogen sources (ammonium, nitrate, and nitrite) from wastewater using different enzymes such as glutamate synthase, glutamine synthetase, glutamate dehydrogenase, nitrite reductase, and nitrate reductase (Perez-Garcia et al., 2011). A microalgal species, *Chlorella* sp., decreased the TN and TP of municipal wastewater from 19.1 to 1.5 mg L^{-1} and from 3 to 0.2 mg L^{-1}, respectively, after 9 days of cultivation (Cho et al., 2011; Ji et al., 2013). On the other hand, the presence of other environmental factors such as PCs and heavy metals in wastewaters has significant effect on the removal efficiency of TN and TP. For example, concentrations of 150 μM Cd^{2+}, Cu^{2+}, or Zn^{2+} inhibited 75% removal of nitrate in *Chlamydomonas mexicana* due to the downregulated activity of glutamine synthetase (Devriese et al., 2001). In the current study, there was no observable effect of doxylamine on the removal efficiency of COD, TN, and TP, indicating the feasibility of *S. obliquus* toward an advanced treatment of wastewater.

Carbohydrate and Protein Content of *Scenedesmus obliquus* Cultivated in Wastewater

Advantages of microalgae-based wastewater treatment technologies include the high value-added by-products such as carbohydrate and protein-rich microalgal biomass. The effect

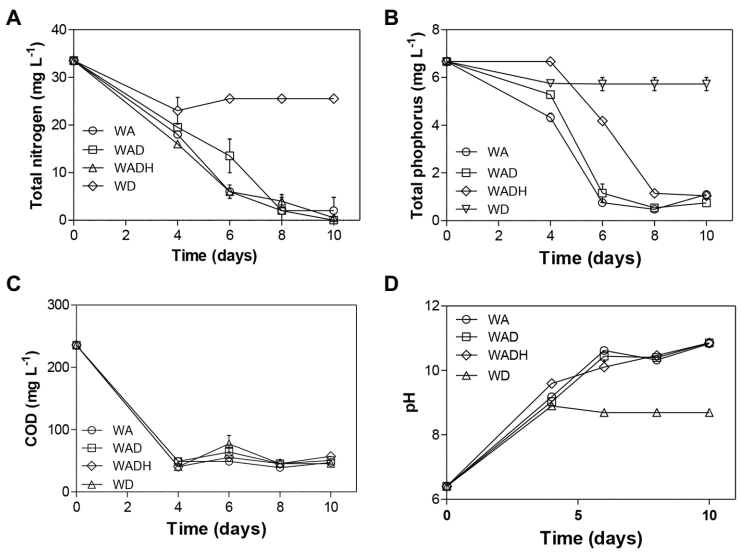

FIGURE 4 | Removal of **(A)** total nitrogen (TN), **(B)** total phosphorus (TP), **(C)** chemical oxygen demand (COD), and **(D)** change of pH in wastewater without microalgae (WD), wastewater with microalgae (WA), wastewater with microalgae and doxylamine (WAD), and wastewater with microalgae, doxylamine, and bicarbonate (WADH).

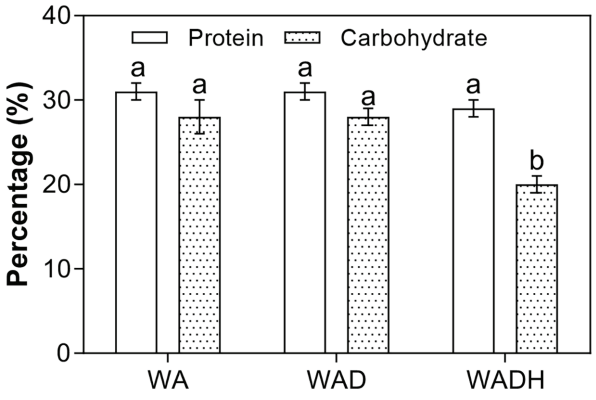

FIGURE 5 | Carbohydrate and protein content of *Scenedesmus obliquus* after cultivation in wastewater (WA), wastewater with doxylamine (WAD), and wastewater with addition of doxylamine and biocarbonate (WADH).

of doxylamine and bicarbonate on the carbohydrate and protein compositions of the harvested biomass of *S. obliquus* is shown in **Figure 5**. There were 27, 28, and 26% carbohydrate, and 30, 31, and 33% protein in the microalgal biomass cultivated in WA, WAD, and WADH, respectively, after 10 days of cultivation. Carbohydrate, protein, and lipid are the three main components of microalgal biomass, and changes of their contents can indicate the overall metabolic activities induced by different environments. Earlier studies demonstrated that the PCs such as sulfamethazine and sulfamethoxazole decreased the carbohydrate content of *S. obliquus* since the pollutants disrupted the photosynthesis for carbon fixation and conversion for formation of starch and lignin (Xiong et al., 2019). There was a slight increase in the protein percentage, which is consistent with other studies (Sampathkumar and Gothandam, 2019; Li et al., 2020). Elevated protein content can be caused by the increased synthesis of metabolic and protective enzymes such as degradation and antioxidant enzymes to help in detoxification.

CONCLUSION

The treatment capacity of a green microalga, *S. obliquus*, for doxylamine-contaminated wastewater was investigated in this study, and the results showed that *S. obliquus* can grow well under current experimental conditions. There was negligible effect of doxylamine on *S. obliquus* and its biochemical characteristics including chlorophyll, carotenoid, and carbohydrate. In contrast, doxylamine slightly increased the protein content. *S. obliquus* showed high removal capacity toward doxylamine, COD, TN, and TP, indicating its feasibility for the remediation of doxylamine-polluted wastewater. Further studies should be conducted in pilot-scale plants to investigate the engineering application of microalgae-based biotechnology.

DATA AVAILABILITY STATEMENT

All datasets presented in this study are included in the article/supplementary material.

AUTHOR CONTRIBUTIONS

J-QX: conceptualization, funding acquisition, resources, methodology, validation, formal analysis, investigation, visualization, writing – original draft, and writing – review and editing. PC: writing – review and editing. SR: funding acquisition, resources, and writing – review and editing. All authors contributed to the article and approved the submitted version.

FUNDING

This work was supported by the National Key Research and Development Program of China (2019YFC1605704), and startup funds provided by Ocean University of China for highly talented young researchers (862001013135).

REFERENCES

Blossom, H. E., Markussen, B., Daugbjerg, N., Krock, B., Norlin, A., and Hansen, P. J. (2019). The cost of toxicity in microalgae: direct evidence from the dinoflagellate *Alexandrium*. *Front. Microbiol.* 10:1056. doi: 10.3389/fmicb.2019.01065

Chi, Z., O'Fallon, J. V., and Chen, S. (2011). Bicarbonate produced from carbon capture for algae culture. *Trends Biotechnol.* 29, 537–541. doi: 10.1016/j.tibtech.2011.06.006

Cho, S., Luong, T. T., Lee, D., Oh, U. K., and Lee, T. (2011). Reuse of effluent water from a municipal wastewater treatment plant in microalgae cultivation for biofuel production. *Bioresour. Technol.* 102, 8639–8645. doi: 10.1016/j.biortech.2011.03.037

Commission European (CE) (2016). Communication from the Commission to the European Parliament, the Council, the European Economic and Social Committee and the Committee of the Regions. A European Agenda for the Collaborative Economy (2016).

Devriese, M., Tsakaloudi, V., Garbayo, I., León, R., Vílchez, C., and Vigara, J. (2001). Effect of heavy metals on nitrate assimilation in the eukaryotic microalga *Chlamydomonas reinhardtii*. *Plant Physiol. Biochem.* 39, 443–448. doi: 10.1016/S0981-9428(01)01257-8

Ersan, G., Apul, O. G., Perreault, F., and Karanfil, T. (2017). Adsorption of organic contaminants by graphene nanosheets: a review. *Water Res.* 126, 385–398. doi: 10.1016/j.watres.2017.08.010

Fernandes, T., Suárez-Muñoz, M., Trebuch, L. M., Verbraak, P. J., and de Waal, D. B. V. (2017). Toward an ecologically optimized N:P recovery from wastewater by microalgae. *Front. Microbiol.* 8:1742. doi: 10.3389/fmicb.2017.01742

Guo, J., Bai, Y., Chen, Z., Mo, J., Li, Q., Sun, H., et al. (2020). Transcriptomic analysis suggests the inhibition of DNA damage repair in green alga *Raphidocelis subcapitata* exposed to roxithromycin. *Ecotoxicol. Environ. Saf.* 201:110737. doi: 10.1016/j.ecoenv.2020.110737

Ji, M. K., Abou-Shanab, R. A. I., Kim, S. H., Salama, E. S., Lee, S. H., Kabra, A. N., et al. (2013). Cultivation of microalgae species in tertiary municipal wastewater supplemented with CO_2 for nutrient removal and biomass production. *Ecol. Eng.* 58, 142–148. doi: 10.1016/j.ecoleng.2013.06.020

Kurade, M. B., Kim, J. R., Govindwar, S. P., and Jeon, B. H. (2016). Insights into microalgae mediated biodegradation of diazinon by *Chlorella vulgaris*: microalgal tolerance to xenobiotic pollutants and metabolism. *Algal Res.* 20, 126–134. doi: 10.1016/j.algal.2016.10.003

Li, J., Min, Z., Li, W., Xu, L., Han, J., and Li, P. (2020). Interactive effects of roxithromycin and freshwater microalgae, *Chlorella pyrenoidosa*: toxicity and

removal mechanism. *Ecotoxicol. Environ. Saf.* 191:110156. doi: 10.1016/j.ecoenv.2019.110156

Liu, Y., Chen, S., Zhang, J., and Gao, B. (2016). Growth, microcystin-production and proteomic responses of *Microcystis aeruginosa* under long-term exposure to amoxicillin. *Water Res.* 93, 141–152. doi: 10.1016/j.watres.2016.01.060

Martínez, J. L. (2008). Antibiotics and antibiotic resistance genes in natural environments. *Science* 321, 365–367. doi: 10.1126/science.1159483

Matamoros, V., Gutiérrez, R., Ferrer, I., García, J., and Bayona, J. M. (2015). Capability of microalgae-based wastewater treatment systems to remove emerging organic contaminants: a pilot-scale study. *J. Hazard. Mater.* 288, 34–42. doi: 10.1016/j.jhazmat.2015.02.002

Pancha, I., Chokshi, K., Ghosh, T., Paliwal, C., Maurya, R., and Mishra, S. (2015). Bicarbonate supplementation enhanced biofuel production potential as well as nutritional stress mitigation in the microalgae *Scenedesmus* sp. CCNM 1077. *Bioresour. Technol.* 193, 315–323. doi: 10.1016/j.biortech.2015.06.107

Patel, M., Kumar, R., Kishor, K., Misna, T., Pittman, C. U., and Mohan, D. (2019). Pharmaceuticals of emerging concern in aquatic systems: chemistry, occurrence, effects, and removal methods. *Chem. Rev.* 119, 3510–3673. doi: 10.1021/acs.chemrev.8b00299

Perez-Garcia, O., Escalante, F. M. E., de-Bashan, L. E., and Bashan, Y. (2011). Heterotrophic cultures of microalgae: metabolism and potential products. *Water Res.* 45, 11–36. doi: 10.1016/j.watres.2010.08.037

Qi, M., Yao, C., Sun, B., Cao, X., Fei, Q., Liang, B., et al. (2019). Application of an in situ CO_2–bicarbonate system under nitrogen depletion to improve photosynthetic biomass and starch production and regulate amylose accumulation in a marine green microalga *Tetraselmis subcordiformis*. *Biotechnol. Biofuels* 12:184. doi: 10.1186/s13068-019-1523-7

Sampathkumar, S. J., and Gothandam, K. M. (2019). Sodium bicarbonate augmentation enhances lutein biosynthesis in green microalgae *Chlorella pyrenoidosa*. *Biocatal. Agric. Biotechnol.* 22:101406. doi: 10.1016/j.bcab.2019.101406

Shen, R., and Andrews, S. A. (2011). NDMA formation kinetics from three pharmaceuticals in four water matrices. *Water Res.* 45:5687–5694. doi: 10.1016/j.watres.2011.08.034

Song, C., Qiu, Y., Li, S., Liu, Z., Chen, G., Sun, L., et al. (2019). A novel concept of bicarbonate-carbon utilization via an absorption-microalgae hybrid process assisted with nutrient recycling from soybean wastewater. *J. Clean. Prod.* 237:117864. doi: 10.1016/j.jclepro.2019.117864

Srinivasan, R., Mageswari, A., Subramanian, P., Suganthi, C., Chaitanyakumar, A., Aswini, V., et al. (2018). Bicarbonate supplementation enhances growth and biochemical composition of *Dunaliella salina* V-101 by reducing oxidative stress induced during macronutrient deficit conditions. *Sci. Rep.* 8:6972. doi: 10.1038/s41598-018-25417-5

Stock, F., Bilcke, G., Decker, S. D., Osuna-Cruz, C. M., den Berge, K. V., Vancaester, E., et al. (2020). Distinctive growth and transcriptional changes of the diatom *Seminavis robusta* in response to quorum sensing related compounds. *Front. Microbiol.* 11:1240. doi: 10.3389/fmicb.2020.01240

Sutherland, D. L., and Ralph, P. J. (2019). Microalgal bioremediation of emerging contaminants - opportunities and challenges. *Water Res.* 164:114921. doi: 10.1016/j.watres.2019.114921

Tran, N. H., Reinhard, M., and Gin, K. Y. H. (2018). Occurrence and fate of emerging contaminants in municipal wastewater treatment plants from different geographical regions-a review. *Water Res.* 133, 182–207. doi: 10.1016/j.watres.2017.12.029

Underwood, J. C., Harvey, R. W., Metge, D. W., Repert, D. A., Baumgarter, L. K., Smith, R. L., et al. (2011). Effects of the antimicrobial sulfamethoxazole on groundwater bacterial enrichment. *Environ. Sci. Technol.* 45, 3096–3101. doi: 10.1021/es103605e

Villar-Navarro, E., Baena-Nogueras, R. M., Paniw, M., Perales, J. A., and Lara-Martín, P. A. (2018). Removal of pharmaceuticals in urban wastewater: high rate algae pond (HRAP) based technologies as an alternative to activated sludge based processes. *Water Res.* 139, 19–29. doi: 10.1016/j.watres.2018.03.072

Vo, H. N. P., Ngo, H. H., Guo, W., Nguyen, K. H., Chang, S. W., Nguyen, D. D., et al. (2020). Micropollutants cometabolism of microalgae for wastewater remediation: effect of carbon sources to cometabolism and degradation products. *Water Res.* 183:115974. doi: 10.1016/j.watres.2020.115974

Wei, L., Hajjami, M. E., Shen, C., You, W., Lu, Y., Li, J., et al. (2019). Transcriptomic and proteomic responses to very low CO_2 suggest multiple carbon concentrating mechanisms in *Nannochloropsis oceanica*. *Biotechnol. Biofuels* 12:168. doi: 10.1186/s13068-019-1506-8

White, D. A., Pagarette, A., Rooks, P., and Ali, S. T. (2013). The effect of sodium bicarbonate supplementation on growth and biochemical composition of marine microalgae cultures. *J. Appl. Phycol.* 25, 153–165. doi: 10.1007/s10811-012-9849-6

Xie, P., Chen, C., Zhang, C., Su, G., Ren, N., and Ho, S. H. (2020). Revealing the role of adsorption in ciprofloxacin and sulfadiazine elimination routes in microalgae. *Water Res.* 172:115475. doi: 10.1016/j.watres.2020.115475

Xiong, J. Q., Govindwar, S. P., Kurade, M. B., Paeng, K. J., Roh, H. S., Khan, M. A., et al. (2019). Toxicity of sulfamethazine and sulfamethoxazole and their removal by a green microalga, *Scenedesmus obliquus*. *Chemosphere* 218, 551–558. doi: 10.1016/j.chemosphere.2018.11.146

Xiong, J. Q., Kurade, M. B., and Jeon, B. H. (2017). Biodegradation of levofloxacin by an acclimated freshwater microalga, *Chlorella vulgaris*. *Chem. Eng. J.* 313, 1251–1257. doi: 10.1016/j.cej.2016.11.017

Xiong, J. Q., Kurade, M. B., and Jeon, B. H. (2018). Can microalgae remove pharmaceutical contaminants from water? *Trends Biotechnol.* 36, 30–44. doi: 10.1016/j.tibtech.2017.09.003

Xiong, J. Q., Ru, S., Zhang, Q., Jang, M., Kurade, M. B., Kim, S. H., et al. (2020). Insights into the effect of cerium oxide nanoparticle on microalgal degradation of sulfonamides. *Bioresour. Technol.* 309:123452. doi: 10.1016/j.biortech.2020.123452

Yang, Q., Ma, Y., Chen, F., Yao, F., Sun, J., Wang, S., et al. (2019). Recent advances in photo-activated sulfate radical-advanced oxidation process (SR-AOP) for refractory organic pollutants removal in water. *Chem. Eng. J.* 378:122149. doi: 10.1016/j.cej.2019.122149

Yu, X., Chen, L., and Zhang, W. (2015). Chemicals to enhance microalgal growth and accumulation of high-value bioproducts. *Front. Microbiol.* 6:56. doi: 10.3389/fmicb.2015.00056

Zhai, X., Zhu, C., Zhang, Y., Pang, H., Kong, F., Wang, J., et al. (2020). Seawater supplemented with bicarbonate for efficient marine microalgae production in floating photobioreactor on ocean: a case study of *Chlorella* sp. *Sci. Total Environ.* 738:139439. doi: 10.1016/j.scitotenv.2020.139439

Zhuang, L. L., Li, M., and Ngo, H. H. (2020). Non-suspended microalgae cultivation for wastewater refinery and biomass production. *Bioresour. Technol.* 308:123320. doi: 10.1016/j.biortech.2020.123320

Conflict of Interest: The authors declare that the research was conducted in the absence of any commercial or financial relationships that could be construed as a potential conflict of interest.

Advantages of publishing in Frontiers

OPEN ACCESS
Articles are free to read for greatest visibility and readership

FAST PUBLICATION
Around 90 days from submission to decision

HIGH QUALITY PEER-REVIEW
Rigorous, collaborative, and constructive peer-review

TRANSPARENT PEER-REVIEW
Editors and reviewers acknowledged by name on published articles

Frontiers
Avenue du Tribunal-Fédéral 34
1005 Lausanne | Switzerland

Visit us: www.frontiersin.org
Contact us: frontiersin.org/about/contact

REPRODUCIBILITY OF RESEARCH
Support open data and methods to enhance research reproducibility

DIGITAL PUBLISHING
Articles designed for optimal readership across devices

FOLLOW US
@frontiersin

IMPACT METRICS
Advanced article metrics track visibility across digital media

EXTENSIVE PROMOTION
Marketing and promotion of impactful research

LOOP RESEARCH NETWORK
Our network increases your article's readership